DEVELOPMENT OF CLINICALLY RELEVANT TESTING METHODS FOR THE FATIGUE PERFORMANCE OF TIBIAL TRAYS

By

SUNITA PREM AHIR

SUBMITTED FOR THE DEGREE OF DOCTOR OF PHILOSOPHY
DEPARTMENT OF MECHANICAL ENGINEERING
UNIVERSITY OF LONDON

FEBRUARY 2004

THE CENTRE FOR BIOMEDICAL ENGINEERING
INSTITUTE OF ORTHOPAEDICS AND MUSCULO-SKELETAL RESEARCH
UNIVERSITY COLLEGE LONDON
ROYAL NATIONAL ORTHOPAEDIC HOSPITAL TRUST
STANMORE
MIDDLESEX
UNITED KINGDOM

ProQuest LLC
789 East Eisenhower Parkway
P.O. Box 1346
Ann Arbor, MI 48106-1346

CONTENTS

Abstract

This thesis investigates whether the testing method proposed by the International Standards Organisation (ISO) for determining the fatigue performance of total knee tibial trays is clinically relevant, and if so what would be the appropriate load for testing.

Fracture of tibial trays occurs for a number of reasons. These include poor design, insufficient support beneath the tray, inadequate manufacturing and material properties, malalignment, incomplete coverage of the tibial plateau, and overloading due to patient weight and/or activity level.

The literature identified a number of trays that had a propensity for fracture. These tray designs are now no longer used. A survey was conducted of current designs from manufacturers' data. Examples of trays that had a history of clinical failure and those that are regarded as clinically successful were analysed using finite element analysis (FEA) and mechanical testing under the ISO test conditions for a range of load values.

The results showed that using a physiological value of 2000N (peak force during the normal walking cycle) all trays that had some history of failure and some of the clinically successful trays failed. Further analysis revealed that a load level of 900N distinguished between clinically successful and unsuccessful trays. The ISO test also showed that trays always failed with a crack propagating in the anteroposterior direction (across the length of the tray).

Examination of retrieved trays using light microscopy and scanning electron microscopy revealed that crack propagation occurred in a number of other ways as well as across the length of the tray. FEA of a tibial tray placed in a realistic bone model showed that support conditions play a large part in the way in which crack propagation occurs and the likelihood of fatigue fracture. Further fatigue testing with a variety of support conditions validated this result.

Hence an alternative testing method was developed based on clinical findings. This showed that multiple crack formation occurred for a tray that had some history of clinical failure due to fatigue. Using this method, a load of 2000N can be used to distinguish between clinically successful and unsuccessful trays. The test was also repeatable. However the results of this testing method always revealed the same design faults as those predicted by the ISO test protocol. Based on these factors, it is the final conclusion of this study that the ISO test protocol is clinically relevant when using a load level of 900N.

Acknowledgements

I would like to thank my supervisor, Professor Peter Walker for giving me the opportunity to learn and grow both professionally and personally; for his invaluable contribution to this work, his support and encouragement throughout. I thank Dr. Mike Dewar for his help, support and encouragement particularly towards achieving completion.

I am grateful to Professor Gordon Blunn for his immense contribution to this project, for his guidance and support.

This project was funded by the Department of Trade and Industry and a consortium of orthopaedic companies. I acknowledge their financial contribution and donation of tibial trays.

My very special thanks go to Dr. Carol Bell for proof reading this thesis and for her support and encouragement.

I consider myself very fortunate to have worked at the Centre for Biomedical Engineering where I have met some wonderful people, past and present, who have contributed to this work and to me personally. I particularly would like to thank the following: to Mark Harrison for listening and being there for me; to the technicians, Mark, Keith and Bob for their technical expertise with fatigue testing but especially for the fun, jokes, laughter and tea; to Jay Meswania, John Wray and Alan Watkins for all their technical assistance but also for their support and friendship; to Mary Wait for all her help with the SEM and photography, her support and encouragement.

To Dr Martin Brown, for making the stressful times so much more enjoyable.

To my family for their unfailing commitment and support: to my parents for believing in me.

And finally to Brian.....words will never be enough .....thank you for dispersing the dark clouds and showing me the silver linings.

LIST OF FIGURES

4.5.5	(a-b) FEA models show that the peak stress for the IB2 model at 2000N is 635 MPa on the upper surface. This is below the fatigue limit of the material. (c-d) Survival of the IB2 trays at 2000N at 5 million cycles under the ISO test.	172
4.5.6	(a-b) FEA models show that the peak stress for the MBK model at 2000N is 163MPa. This is below the fatigue limit of cast CoCrMo alloy. (c-d) Survival of the MBK trays at 2000N at 5 million cycles under the ISO test.	173
4.5.7	(a-b) FEA models show that the peak stress for the Kinemax model at 2000N is 1000MPa. This is much higher than the fatigue limit for solution treated CoCrMo alloy. (c) Only one sample was used. Failure of the Kinemax tray occurred at 594,600 cycles using 5Hz. The tray shows crack formation in areas predicted by the FEA model.	174
4.5.8	(a-b) FEA models show peak stresses at 910.6 MPa at a load level of 2000N, which are above the fatigue limit for cast CoCrMo alloy. (c & d) Failure of first baseplate showing crack formation at 69,830 cycles (e) this component was allowed to continue under the test conditions. Final fracture occurred at 782,000 cycles. Fracture of second baseplate at 1,290,000 cycle (e) main and inset: Crack formation on third baseplate at 1,716,220 cycles (h) Fracture of fourth baseplate at 3,133,190 cycles (i & j): No crack formation at 5 million cycles for the fifth and sixth baseplates using a load level of 2000N.	175 176 177
4.5.9	(a-b) FEA models show that the peak stress for the MG2 model at 2000N is 1500MPa. This is much higher than the fatigue lim for titanium alloy. (c & d) Failure of both MG2 trays occurred within 29,060 cycles.	178
4.5.10	(a-b) FEA models show that the peak stress for the Kinemax model at 1500N is 750 MPa. This is above the highest limit for solution heat-treated CoCrMo alloy. (c & d) Survival of both Kinemax trays at 5 million cycles.	179

4.5.11	(a-b) FEA models show that the peak stress for the AGC model at 1500N is 682.9 MPa. This is higher than the fatigue limit for cast CoCrMo alloy. (c & d) Failure of one of the two AGC trays at 1,310600 and survival of the other. (e) Undersurface of the porous coated AGC tray. (f & g) Survival of both porous coated trays at 5 million cycles.	180
4.5.12	(a-b) FEA models show that the peak stress for the Rotaglide model at 1500N is 433 MPa. This is higher than the fatigue limit for cast CoCrMo alloy. (c & d) Survival of the two uncoated Rotaglide trays. (e & f) Failure of one of the two porous coated occurred at 1,698,000 cycles and survival of the other at 5 million cycles. (g & h) Failure of one of the two HA-coated trays at 4,058,100 and survival of the other at 5 million cycles.	181
4.5.13	FEA models show that the peak stress for the MG2 model at 1500N is 1124 MPa. This is higher than the fatigue limit for titanium alloy. (c & d) Failure of both MG2 trays at 22,900 and 52,600 cycles.	182
4.5.14	(a-b) FEA models show that the peak stress for the Kinemax model at 900N is 450 MPa. This is within the fatigue limit for solution heat-treated CoCrMo alloy. (c & d) Survival of both Kinemax trays at 5 million cycles.	183
4.5.15	(a-b) FEA models show that the peak stress for the AGC model at 900N is 421 MPa. This is higher than the fatigue limit for cast CoCrMo alloy. (c & d) Survival of both AGC trays at 5 million cycles. (e) the undersurface of the porous AGC tray. (f & g) Survival of both porous coated trays at 5 million cycles.	184
4.5.16	(a-b) FEA models show that the peak stress for the Rotaglide model at 900N is 260 MPa. This is below the fatigue limit for cast CoCrMo alloy. Upper and lower surfaces of the Rotaglide trays showing survival of (c & d) uncoated (e & f) porous coated (g & h) HA- coated at 5 million cycles.	185

4.5.17	(a-b) FEA models show that the peak stress for the MG2 model at 900N is 675 MPa. This is higher than the fatigue limit for titanium alloy. (c & d) Survival of both MG2 trays at 5 million cycles.	186
4.5.18	(a-b) FEA models show that the peak stress for the Kinematic model at 900N is 2.05GPa. This is significantly higher than the fatigue limit for cast CoCrMo alloy. (c & d) Failure of both Kinematic trays occurred at 154,300 and 485,700 cycles.	187
4.5.19	(a-b) FEA models show that the peak stress for the PCA model at 900N is 1019 MPa. This is significantly higher than the fatigue limit for cast CoCrMo alloy. (c & d) Failure of both trays at 336,100 and 413,100 cycles.	188
4.5.20	(a-b) FEA models show that the peak stress for the Total Condylar (type 2) tray at 900N is 1917MPa. This is significantly higher than the fatigue limit for cast CoCrMo alloy. (c & d) Failure of both trays at 527,500 and 848,700 cycles.	189
4.5.21	(a-b) FEA models show that the peak stress for the Total Condylar (type 1) tray at 900N is 1016 MPa. This stress level is significantly higher than the fatigue limit for cast CoCrMo alloy. There were no samples to test of this component.	190
4.5.22	(a-b) FEA models show that the peak stress for the revision PCA tray at 900N is 1462 MPa. This is significantly higher than the fatigue limit for cast CoCrMo alloy. For both tray designs no samples were available for testing. There were no samples to test of this component.	190
4.5.23	Dye penetrant tests for (a) the IB2 and (b) the Kinemax trays tested at 2000N and 1500N respectively.	191
5.1	The five regions of the tibia: (1) the medial, (2) paramedical, (3) intercondylar or central, (4) paralateral, (5) lateral.	202

6.2.1	FEA model of the Kinematic. The point of load application is based on the shiny surface indicated in (b). The shiny surface represents rubbing of the femoral component against the tibial tray *in vivo* (c) The highlighted green nodes are the area of the tray that is fully supported. The remainder of the tray receives no support. d) FEA results showing that the areas of maximum stress occur at the boundary of the supported and unsupported areas. (e) Retrieved tray, showing crack formation in the posteromedial part of the tray, consistent with (d).	230 231
6.2.2	FEA model of the Kinematic. (b) The highlighted green nodes are the area of the tray that is fully supported. The remainder of the tray receives no support. (c) FEA results showing that the areas of maximum stress occur at the boundary of the supported and unsupported areas. (d) Retrieved tray showing crack formation in the posteromedial part of the tray.	231 232
6.2.3	(a) FEA model of the Kinematic. The highlighted green nodes are the area of the tray that is fully supported. The remainder of the tray receives no support. The point of load application is on the unsupported area (b) FEA results showing that the areas of maximum stress occur at the boundary of the supported and unsupported areas. (c) Mechanical test performed where the supported region is modelled using cement. The point of load application is on the unsupported side. (d) Fatigue test results of the component showing crack formation at the border of the supported and unsupported region. (e) Retrieved tray showing crack formation that is similar to the FEA and fatigue testing results. (f) FEA study showing that if the point of load application is on the supported region then peak stresses are well below the fatigue limit of the material.	232 233

6.2.4	(a) Fatigue test results using the 1996 contact position for the ISO support conditions (b) Fatigue test results using the 1997 contact position for the ISO support conditions. This shows that using the same support conditions (from the ISO test method) but two different contact positions there is a slight variation in crack propagation with (a) showing a more lateral crack path.	234
6.2.5	Contact position is affected by (a) design of the tibial insert and (b) wear degradation of the tibial insert.	234
6.3.1	Fibrous tissue layers observed *in vivo* resulting in greater displacement of the plate of the tray.	236
6.3.2	Alternative testing method: the stem is well-fixed and the plate is not cemented to the supporting block allowing greater displacement of the plate of the tibial tray.	237
6.3.3	Support blocks made from (a) titanium (b) aluminium (c) Delrin (d) polyurethane.	239
6.3.4	Frequency of 1mm radiolucency in 7 zones averaged for 616 cases of Kinematic knees followed for mean follow-up of 2.2 years, minimum 6 months.	239
6.3.5	(a & b): Aluminium support blocks with cut-outs to show varying partial support.	239
6.3.6	Contact locations: (a) first contact position defined in the 1996 draft standard, (b) second contact position defined in the 1997 draft standard (zero degrees flexion), (c) third contact position medio-laterally in the same position at zero degrees flexion but anteriorly in line with the cruciate cut-out.	240
6.3.7	(a) Stress distribution for the Kinematic component supported on titanium blocks. (b) Close–up view showing high stresses in the notch of the Kinematic component. (c) Fatigue test results of the Kinematic component using titanium support blocks.	246

C1.1	COMPONENT C: A retrieved Kinematic in a left knee showing medial compartment failure at 6 years and 6 months	294
C1.2	COMPONENT D: Failure of a Kinematic knee in the medial compartment of a left knee at 5 years 2 months.	294
C1.3	COMPONENT E: Failure of a Kinematic knee in one of the compartments as a result of polyethylene wear and malalignment. Fractured tibial tray (a) top view (b) from below (c) tibial baseplate (d) fractured portion showing shiny surface (e) tibial insert with wear more marked in same location as fracture of the baseplate.	295
C1.4	COMPONENT F: Medial compartment fracture of a Kinematic tibial tray of a right knee in a patient two years post-operatively.	296
C1.5	COMPONENT G: No records were available for this fractured Kinematic tibial tray	296
C1.6	COMPONENT H: Medial compartment failure in a left knee for a Kinematic tray. The tray was retrieved at 13 years.	296
C1.7	(a & b): COMPONENT I: Lateral compartment fracture of a Kinematic tibial tray for the right knee of a male patient. The tray was retrieved 4 years after implantation.	297
C1.8	COMPONENT J: No records were available for this tray.	297
C1.9	COMPONENT K: No records were available for this tray.	298
C2.1	COMPONENT M: (a-f): No records were available for fracture of this Total Condylar design.	299
C2.2	COMPONENT N(a-d): Fracture of a Total Condylar design. The fracture began at the anterior side at one of the grooves within the design. The tray was removed prior to the fracture reaching the other side of the tray.	300
C3.1	COMPONENT 0: (a –b): Fracture of a PCA tray design. (c-d): The fracture surfaces of both parts of the tray (e-f): close up views of (c).	301

LIST OF TABLES

CHAPTER ONE:
FAILURE MODES AND TESTING METHODS FOR ARTIFICAL KNEE JOINTS

1.1 INTRODUCTION

For patients with advanced degenerative arthritis of the knee it is now evident that a Total Knee Replacement (TKR) is a successful method of treatment (Scuderi et al., 1989). An ideal total knee replacement should reproduce the normal knee anatomy and kinematics, alleviate pain, restore stability and correct deformity. It must be relatively easy to insert with a range of sizes to account for dimensional variations of the natural tibia, have precision instrumentation, provide life-long fixation have an acceptable wear pattern and be biologically compatible (Baldwin et al., 1996; Woods et al., 1983). The choice of prosthesis design depends on a number of factors including patient characteristics (age, weight, gender), amount of bone stock available and the condition of the ligament structures.

A typical condylar knee prosthesis consists of both a femoral and tibial surface replacement. The femoral component is generally made from cobalt-chrome alloy and resurfaces the natural femoral condyles. The tibial component can consist of a one piece, Ultra High Molecular Weight Polyethylene (UHMWPE), all-polyethylene, component that is fixed to the natural tibial providing a bearing surface for the femoral components to articulate against. Alternatively, the tibial component can consist of a metal-backed polyethylene component. Depending on the condition of the natural patella, it may or may not be resurfaced. There are many different total knee products available but they are mostly based on a small number of different types (Walker and Sathasivam, 2000). Walker and Sathasivam (2000) classified knee prostheses according to functional aspects and design. Designs varied to cater for the preservation or sacrifice of the natural collateral and cruciate ligaments. They also differed by the way in which different designs achieved motion. Total knee replacements can be subdivided into those knees that have a fixed or mobile bearing insert and those that have guided motion, using intercondylar cams or specially shaped or additional bearing surfaces between the femoral and tibial component.

In fixed bearing knees articulation only occurs between the upper surface of the tibial insert and the femoral component. These designs are created to either retain or sacrifice both the anterior and posterior cruciate ligaments, or only sacrifice the anterior cruciate ligament. In those tray designs that sacrificed both ligaments the insert had a posteriorly stabilized tibial insert. For this type of insert the bottom of the dish was more posterior and the anterior upsweep was higher preventing excessively anterior contact points (Walker and Sathasivam, 2000). An intercondylar cam was also added to control the anterior position of the femur on the tibia and provide posterior rollback of the femur increasing the range of flexion. Mobile bearing designs, where the plastic bearing is interposed between the femoral condyle and the tibial plate, maintain a large contact area throughout all or much of the flexion range. The advantages of these types of design are low wear volume and freedom of rotational and/or anterior-posterior (A-P) position (Walker, 2000). Guided motion knees aim to provide some control or guidance to A-P translation and/or internal-external rotation during flexion-extension. This has produced designs that provide a much higher range of flexion and therefore has increased the types of activities that can be performed.

For those patients where the collateral ligaments have been compromised, designs that provide varus-valgus stability exist. These prostheses can be unlinked as in the superstabiliser or linked as in fixed or rotating hinges. The former has an elevated plastic post for additional stability. Fixed hinges use an axle to connect the femoral and tibial components, usually with plastic bushings to act as the bearing. For rotating platform designs, rotation can be achieved by a flat polished metal surface pivoted on a flat plastic surface or by a convex metal surface in a dished plastic surface.

These different design forms have been used clinically over the past 30 years since TKRs were first introduced. Due to the accumulated experience, most modern designs can be expected to provide equally successful results. In terms of longevity, several TKR designs have been reported to give at least 90% survivorship at 10 years (Knutson et al., 1986; Scuderi et al., 1989;

Nelissen et al., 1992; Lewis et al., 1994; Nafei et al., 1996; Schai et al., 1998). Ranawat et al. (1993) reported a 94% survivorship at 15 years for the Total Condylar prosthesis. Buechel (1998) reported survivorship data for the cemented Rotating Platform LCS of 97.9% at 18 years and for the cementless LCS Rotating Platform of 98.1% at 15 years. However, every new design especially those of a non-standard type requires rigorous pre-clinical testing and clinical follow-up in order to identify possible failure modes. These failure modes include instability, loosening, component fracture, wear, patellar problems and pain (Woods et al., 1983; Rorabeck, 1995). This introduction will focus primarily on failure modes and their possible causes, together with testing and evaluation methods.

1.2 MALALIGNMENT AND INSTABILITY

Malalignment and instability are two problems that affect the overall performance of a total knee replacement. These two problems are inter-related and surgical technique has a large part to play in these factors (Moreland, 1988). Achieving correct alignment of the prosthesis is critical (Elloy et al., 1992; Callaghan and Dennis, 1995). Correct alignment requires the implants to be aligned correctly in flexion and extension as well as in the sagittal and frontal planes. If the knee is reconstructed so that the patient is left with genu varum or genu valgum, the line of action of the weight bearing force will be off centre. Such loading on the tibial component causes subsidence on one side of the component and lift-off on the other side. This can lead to loosening and instability of the prostheses.

The mechanical axis is defined as being from the centre of the femoral head to the centre of the ankle (refer to figure 1.1). It is generally thought that this line passes slightly medial to the centre of the knee (Townley, 1988). Although some authors believe that the mechanical axis should pass over the center of the knee (Hungerford and Kenna, 1983) and others slightly lateral to the center of the knee (Insall et al., 1985). In terms of placement of the

artificial prosthesis, preservation of the dense subchondral bone in the upper regions of the tibia is important for anchorage of the tibial component (Insall et al., 1985). The tibial component should lie central to the mechanical axis in the frontal plane (Elloy et al., 1992; Cates et al., 1993). In the sagittal plane the tibial component is placed at an angle so that it slopes posteriorly. This angle can vary from 5-7° degrees although some knee designs such as the Rotaglide (Corin (UK) Ltd.) advocate an angle of 10°. The femoral component is placed parallel to the tibial component.

Ligamentous balance is also a requirement to ensure correct alignment. If malalignment is created at the time of surgery even minor degrees of ligament imbalance can become a major problem. Yet if the knee is aligned properly at the time of surgery, mild degrees of ligament imbalance can be tolerated (Moreland, 1988). If ligament balancing in the varus/valgus plane is not performed correctly, polyethylene wear and relative ligament laxity can result. In addition to ligament balancing and malalignment, the integrity of the posterior cruciate ligament (PCL) has been implicated as a cause for instability. Some designs require a deeply sloping posterior cut of the proximal tibia and this has caused the PCL to dysfunction. The PCL may also be incompetent at the time of surgery, and the surgeon may not have detected this.

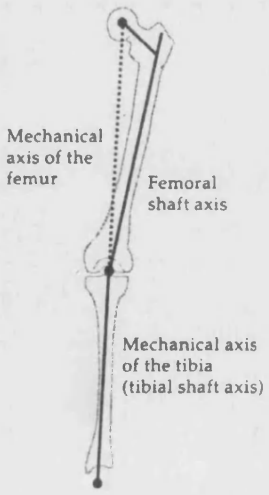

Figure 1.1: Normal alignment of the knee
(Reproduced from Callaghan and Dennis, 1995)

1.3 LOOSENING

Femoral component loosening is reported to be less than 1% (Windsor et al., 1989). Tibial components have experienced loosening on a much wider scale (Insall et al., 1979). The mechanism for loosening is generally accepted as tilting of the tibial component in response to eccentric loads, causing subsidence on one side. The prosthesis may sink as a result of compressive forces crushing the supporting bone, with lift-off on the other side, as a result of tensile or shear forces at the interface (Walker et al., 1976; Vince et al., 1986). The component can tilt in an anterior-posterior (A-P) or medial-lateral (M-L) direction and obliquely (Cameron and Hunter, 1982). In addition, due to the unequal resultant compressive force on the medial and lateral plateaus, there is a tendency for the prosthesis to rotate about its central axis (Ducheyne, 1978). Fixation of a total knee arthroplasty is critical (Albrektsson, 1990; Hofmann et al., 1991) both initially and in the long-term. A loss of fixation inherently leads to loosening.

During the 1970s and 1980s, loosening of the tibial components was considered to be the most common mechanism of failure, but it is now only occasionally seen (Insall, 1995; Walker, 1994; Rorabeck, 1995). This is attributed to improvements in surgical procedures such as minimal bone resection, which preserves dense and strong cancellous bone (Insall, 1988), increased cement penetration into the cancellous bone, metal-backing of the tibial component, and the emphasis placed on achieving good axial alignment to evenly distribute the loads transmitted through the prosthesis. This has reduced the likelihood of tibial component migration (Brach del Prever et al., 1987; Johnson et al., 1993). Design changes, in particular with respect to constraint and conformity, have restricted high stresses being transferred to the cement-bone interface (Moreland, 1988). Highly conforming designs such as the hinged knees, experienced failure from loosening (Insall and Dethmers, 1982). These designs do not permit rotational movement and led to the transmission of high shear stresses at the bone-cement interface resulting in loosening. Rotating hinge devices are

considered to be more successful with clinical follow-up studies demonstrating improved performance compared with fixed hinges (Steinbrink, 1999; Unwin et al., 1999). Problems have however, occurred with rotating hinge devices. These include component breakage and fracture at the junction of the stem and baseplate, bearing axle and the baseplate itself (Scott et al., 1996).

1.3.1 METAL-BACKING OF TIBIAL COMPONENTS

Metal backing of tibial trays was introduced as a result of excessive deformation of all-polyethylene components (Skolnick et al., 1976; Chillag & Barth, 1991). A number of researchers (Bartel et al., 1982; Lewis et al., 1982) showed that metal backing provided better force transmission across the bone-implant interface and resisted bending forces. Walker et al. (1982) showed that cement strains around the central stem and the upper surface in the medial-lateral direction were much reduced for a metal tray compared with an all-polyethylene tibial component. This reduction in strain in the cement and the underlying trabecular bone addressed the problem of high stresses that contributed to loosening, which was a feature of early designs with thin plastic components (Walker et al., 1981; Bartel et al., 1982; Lewis et al., 1982).

Metal backing also provided a number of other options/advantages. These are the use of supplemental screw fixation and porous surfaces (Miura et al., 1990), modular plastics allowing soft tissue balancing, ease of matching the femoral component size to tibial component size, simple modular tibial stem extensions and potential for simplifying revision in the event of polyethylene wear (Chillag & Barth, 1991). However, there are a number of disadvantages. These include the decrease in polyethylene insert thickness, stress shielding in designs with a central stem, difficulty in removal at revision and fracture of the baseplate.

1.3.1.1 DESIGN OF THE TIBIAL BASEPLATE

Various studies have documented that the use of intramedullary stems, pegs and screws reduce micromotion, subsidence and lift-off (Miura et al., 1990; Cadambi et al., 1994; Kraemer et al., 1995; Whiteside, 1994). However cancellous screws have been implicated with a host of problems: penetration and damage to nerves and vessels (Rubash et al., 1993; Whiteside, 1994), debris formation arising from migration of polyethylene particles through screwholes leading to osteolysis and massive bone loss; fretting at the screw-plate junction causing third body abrasive wear and corrosion between the cobalt-chrome alloy baseplate and the titanium alloy screws (Whiteside, 1994; Ezzet et al., 1995; Lewis et al., 1995; Silverton et al., 1996). Pegs, screws, posts and keels are also subject to fracture, bending or buckling due to asymmetric forces.

The shape and size of the tray is also important. Coverage of both cortical and cancellous bone reduces rocking in the transverse plane about the anteroposterior and mediolateral axes, preventing subsidence and allowing uniform load transfer for both cemented and cementless designs (Incavo et al., 1994; Wevers et al., 1994). Walker et al. (1982) stated that complete coverage of the upper surface considerably reduced the peripheral deflections compared with incomplete coverage. Insall (1996) reported that symmetric components are more likely to overhang posterolaterally and in this respect, asymmetric components can be fitted to provide better coverage of the entire surface because prosthesis that extend beyond the natural tibial could interfere with soft tissues. Incavo et al. (1994) defined best coverage, as an implant that achieved multiple contact points with cortical bone. They found that symmetric components offered slightly greater coverage than their asymmetric components. They also found that products with a greater number of sizes in their range were more able to provide a better fit to the cut surface.

At the present time there is a range of tibial designs both asymmetric and symmetric with fixation achieved by pegs, stems and screws. A detailed description of this range is given in chapter 4.

1.3.1.2 POROUS SURFACES

Cementless implants were introduced for younger and more active patients to provide more durable fixation. The early methods of achieving a porous surface consisted of sintering metal beads onto a solid metal substrate (Pilliar, 1983). The metal beading aimed to provide a surface for bony ingrowth. The porous coating (figure 1.2) was formed by high temperature sintering of metal alloy powders on the substrate surfaces. This increased temperature changed the microstructure of the metal substrate.

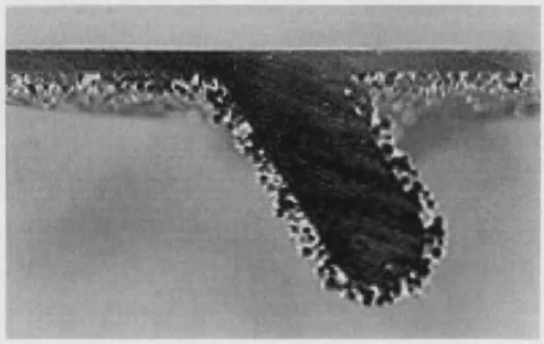

Figure 1.2: The double beaded porous layer bonded to the core structure. (Hungerford and Kenna, 1983)

Follow-up studies (Kavolus et al., 1991) showed separation of metal beads from the porous coating (Cheng and Gross, 1988; Cooke et al., 1990), metal fatigue, a high incidence of pain, poor evidence of bony ingrowth and increased incidence of failure when contrasted to the cemented version. The loose beads led to third body wear of the polyethylene resulting in severe wear. This then led to the formation of an interfacial membrane resulting in micromotion and loosening of the implant (Cooke et al., 1990). Excessive micromotion of the implant relative to the bone can prevent bone ingrowth (Volz et al., 1988; Bloebaum et al., 1992).

Improvements in the results using porous surfaces were reported by Bloebaum et al. (1992). They advocated the use of autograft bone chips when using a cementless implant. Other methods have been developed for achieving bone ingrowth. These are the use of a cancellous structure titanium or fiber mesh titanium. Both are considered to have about 60% porosity as opposed to a beaded surface, which has about 35% porosity (Hofmann, 1996). In addition, titanium is considered to have a more favourable ingrowth when compared to cobalt-chrome alloy. A study by Bloebaum et al. (1991) compared the PCA (Stryker Ltd., UK) which had a beaded porous coating with the Natural knee (Intermedics Orthopaedics Inc, USA) which had a cancellous structured titanium and found that there were was more bone ingrowth and less fibrous tissue in the titanium surface.

Hofmann (1996) found that the design of the tibial tray was an important parameter with regards to bone ingrowth. He found that with a pegged design there was a 'starburst' bone ingrowth pattern around the lower part of the peg. In other areas of the tray, particularly immediately below the plate and upper parts of the peg, there was evidence of stress-shielding resulting in fibrous tissue formation. For this reason he advocated avoiding porous coated pegs and stems. A case study by Ranawat et al. (1986) showed fracture of a PCA metal baseplate as a result of extensive but inhomogenous adherence of bone. They showed that bone growth was non-uniform and had occurred only on the posterior surface of the pegs with no bone growth on the porous coated tibial plateau, which compromised fixation.

Hydroxyapatite (HA) is the main component of normal bone and has been developed synthetically as a ceramic material that promotes bone growth. It has attracted widespread interest and use because of its success. Oonishi et al. (1989) examined the effect of hydroxyapatite coating on bone growth into porous titanium alloy implants. They compared an uncoated group with a plasma-sprayed HA group. The results showed that the HA coated implant had earlier and stronger fixation compared to the uncoated implants. A study by Regner et al. (1998) compared the use of a titanium mesh that was either

uncoated or coated with hydroxyapatite on an MG2 tibial tray. They found that there was less migration of tray in the coated group. Therefore the use of HA ceramic coating may be beneficial in the long term. Cementless implants are still a viable solution but long-term follow up studies still require evaluation.

1.4 WEAR

The early designs of total knee replacements consisted of an all-polyethylene tibial component. These early designs rarely suffered failure as a result of polyethylene wear (Engh et al., 1992). This may have been due to the design of the tibial component, which was relatively thick and moderately conforming in both the anterior-posterior (A-P) and medio-lateral (M-L) planes. These features minimized contact stresses and allowed functional laxity and stability. However, the problems of loosening and deformation of all-polyethylene designs led to the introduction of metal backing (Bryan and Rand, 1982). Since the introduction of metal backing, the problem of loosening has reduced significantly, but in order to minimise the amount of bone resection on the tibial surface, thinner polyethylene components have been used. Some tibial inserts were only 4mm thick (Engh et al., 1992). As a consequence, wear through of the plastic insert was a major problem in many cases. Wear is an important issue because wear debris can result in severe femoral bone loss even in the presence of rigidly fixed implants (Cadambi et al., 1994). The loss of height of the polyethylene due to wear can be detrimental to stability. In particular, severe wear (delamination) results in loss of some areas of the polyethylene insert and can impair function. There are a number of contributing factors to the problem of wear. Patient characteristics including size, gender and level of activity have a direct effect on wear (Bauer et al., 1993). Alignment of the prostheses affects pressure distribution (Tsao et al., 1993). Other factors can be discussed in two groups: design of the tibial insert and quality of the polyethylene.

1.4.1 DESIGN OF THE TIBIAL INSERT

Tibial insert design can be grouped into those that use a fixed bearing insert and those that use a mobile bearing insert. These two groups are discussed below.

1.4.1.1 FIXED BEARING KNEES

At the time of the introduction of metal backing, design changes were also made to the tibial insert. Products such as the PCA (Stryker Inc, USA) were designed to simulate the anatomic form and the kinematics of the natural knee by relying on balanced soft tissues and retention of the posterior cruciate ligament (Wright et al., 1992). This geometry, described as being flat on flat, was designed to reduce the stresses on the bone-cement interfaces and allowed greater flexibility for sizing between the femoral and tibial component. However, these flat on flat designs including the Microloc (Depuy Inc, USA), PCA (Stryker Inc, USA) and Tricon M (Smith and Nephew Inc, USA) have been particularly prone to failure as a result of their lack of conformity (Feng et al., 1994; Lewis et al., 1994; Ritter et al., 1995). All these designs exhibited cold flow in the posteromedial part of the insert leading to severe wear and exposure of the baseplate. One study (Lewis et al., 1994) showed wear of the baseplate with marked scoring of the femoral component caused by abrasion with the rim of the tibial baseplate. These non-conforming surfaces allowed variable contact areas during motion and increased stresses on the collateral and cruciate ligaments. If the ligaments became weak or improperly balanced the translational and rotational movements became excessive, moving the contact points to the edge of the inserts, resulting in excessive polyethylene wear and deformation. Edge loading substantially increased the stresses associated with fracture of the polyethylene and failure of the underlying cancellous bone (Bartel et al., 1982).

Varus-valgus moments, which occur during normal gait and as a result of malalignment, have been reported to lead to localised contact stresses resulting in delamination and fracture of the insert particularly with unicompartmental designs (Engh et al., 1992; Wright et al., 1992; Tsao et al., 1993; Feng et al., 1994; Lewis et al., 1994; Walker and Blunn, 1997). Other design issues such as screw holes in the metal tibial baseplates resulted in cold flow of the polyethylene (Engh et al., 1992; Cadambi et al., 1994). If the polyethylene insert was thin, as in the case of the PCA design (< 6mm) then the contact stress increased further (Engh et al., 1992; Wright et al., 1992; Cadambi et al., 1994; Wasielewski et al., 1994). Bartel et al. (1986) showed that as the polyethylene became thinner, the contact stresses increased exponentially, especially for thicknesses less than 6mm. On the other hand, highly conforming designs were created to reduce contact stresses but they have been associated with cement particle entrapment resulting in abrasion of the plastic (Landy and Walker, 1988).

The optimium design of the plastic tibial insert described by Walker and Blunn (1997) was a double dished surface to reproduce functional laxity and stability, minimising contact stresses. They concluded that articulating surfaces require a curvature that is smooth with no abrupt changes in radii, hence reducing stress concentration effects. A study conducted by Blunn et al. (1997) comparing different design types found that delamination wear occurred on both conforming and non-conforming designs and that the likelihood of delamination wear depended on a number of factors. These factors included the degree of conformity and supported the view that the optimal type of congruency for a fixed bearing knee arthroplasty is probably one of intermediate conformity that possesses advantages of both low and high conformity.

The importance of securing the tibial insert to its metal-backing is paramount and where this has not taken place, relative motion between the two surfaces has led to wear. In particular in cases where the tray was not smooth or sufficiently rigid, a complete breaking up of the polyethylene occurred (Engh

et al., 1992; Hailey et al., 1994). For example in the PCA designs, error during the fitting of the insert to the tray resulted in the insert lifting off from the tray as well as damage to the locking mechanism (Davis et al., 1991). Wear of thin polyethylene inserts leading to abrasion of the locking mechanism on the femoral component, have also been reported in other designs. Also, metallic debris from the locking mechanism has contributed to third body abrasion at the articulating surfaces (Tsao et al., 1993; Cadambi et al., 1994; Engh et al., 1994; Ezzet et al., 1995; Knight et al., 1995).

1.4.1.2 MOBILE BEARING KNEES

A new concept for knee replacements introduced in the 1970s focussed on reducing the incidence of fixation failure, by increasing the congruency but allowing rotations and translations through mobile bearing knees (Goodfellow and O'Connor, 1978; Buechel and Pappas, 1986). A mobile bearing design can reduce wear by maximising the tibiofemoral contact area throughout the entire range of knee motion. Mobile bearings reduce constraint by allowing freedom of motion between the plastic and tibial component. In the Oxford unicompartmental design, the plastic tibial insert slides freely on the polished surface of the metal tibial baseplate. In the LCS (Depuy Inc, USA) rotating platform design, the plastic bearing component rotates about a central pivot in the metal tibial baseplate. Long-term follow-up studies have been conducted on both of these designs showing excellent long-term survivorship. However, a number of failure mechanisms have been reported with mobile bearing designs. Loosening of unicompartmental designs has occurred in particular with knees where the anterior cruciate ligament was resected (Goodfellow et al., 1988). Dislocation of the polyethylene resulted in the two metal components articulating against each other resulting in a large amount of wear debris (Hailey et al., 1994; Williams et al., 1999). Dislocation has also led to fracture for both unicompartmental and total knee designs (Carr et al., 1993; Weaver et al., 1993). Fracture and excessive

wear of the insert has also occurred as a result of the polyethylene insert overhanging the metal baseplate in extremes of motion (Walker et al., 1996).

A study by Williams et al. (1999) compared a series of 206 retrieved mobile bearing knees with a series of 619 fixed bearing knees. They found that the mobile bearings had a lower incidence of delamination, abrasive wear and cold flow. Argenson and O'Connor (1992) in a long-term follow up of the Oxford meniscal knee reported a wear rate of 0.028mm/year and showed no evidence of structural failure. This compares with a wear rate of 0.046mm/year (Polyzoides et al., 1999) for the Rotaglide, a fully conforming total knee mobile bearing design. This was reported in a ten year survivorship study and showed that a fully conforming mobile bearing knee can reduce polyethylene wear.

Wear on the undersurface (backside wear) of the insert is considered an important source of wear debris with one study showing evidence of fretting wear readily apparent with relatively large insert motions and rougher surface finishes (Gabriel and Dennis, 1997). However, Williams et al. (1999) found that visible wear on the backside surface occurred with similar frequency in both the fixed and mobile bearings indicating that both designs are susceptible to backside fretting and third body wear. Backside wear of fixed bearing knees was also reported by Engh et al. (2001) who compared the security of the locking mechanism in fixed and mobile bearing knees.

Williams et al. (1999) indicated that the advantages offered by mobile bearing knees are that they are less likely to experience loosening; they have a reduced incidence of abrasive wear (which in the absence of fatigue is the dominant long term wear mechanism); and that concerns about greater debris generation due to dual articulation have been shown to be unfounded.

1.4.2 QUALITY OF POLYETHYLENE

The quality of UHMWPE is regarded as one of the main factors that contribute to wear (Wright et al., 1992; Hailey et al., 1994). Fusion defects, material properties, manufacturing process and post manufacture treatments of the polyethylene are considered as important parameters affecting the wear characteristics of tibial inserts (Engh et al., 1992; Wright et al., 1992; Cadambi et al., 1994; Wasielewski et al., 1994; Knight et al., 1995).

Fusion defects are considered to be sites for crack propagation leading to subsurface failure and delamination. However, a study conducted by Blunn et al. (1997) showed some components retrieved after long duration (>10 years) were observed to have no defects but they still delaminated.

The method of manufacture has a direct effect on the amount of wear debris. Bell (1999) compared directly moulded polyethylene (Biomet Merck Ltd., UK) with a modified polyethylene known as Hylamer (Depuy Inc, USA) and a stabilized polyethylene (Stryker Inc, USA). This study showed that directly moulded polyethylene had greater oxidation resistance and lower wear rates compared to other materials. Furman et al. (1997a) compared the tibial inserts of the Insall-Burstein 1 (IB1) and Insall-Burstein 2 (IB2) both made by Zimmer Inc (USA). The designs of both inserts are essentially the same, but the IB1 insert was made from directly moulded polyethylene and the IB2 was machined to its final shape. Furman et al. (1997a) showed that the machined polyethylene from the IB2 exhibited higher levels of wear in comparison to the directly moulded polyethylene from the IB1.

Post manufacture treatments such as heat pressing and sterilisation techniques also affect wear properties. Heat pressing was used by some manufacturers of polyethylene inserts most notably the PCA design. This technique was intended to remove machine marks and create a smooth surface finish. However, heat pressing created a subsurface zone of demarcation that contributed to delamination and particle generation (Wright

et al., 1992; Knight et al., 1995) as determined from clinically retrieved PCA components.

Sterilisation techniques are important as they kill any bacteria prior to insertion of a prostheses and hence reduce the risk of infection. There are two main types of sterilisation techniques. These are gamma irradiation and gas sterilisation in ethylene oxide.

Gamma irradiation is the preferred method due to ease of mass sterilisation and components can be stored until they are required for *in vivo* usage. The disadvantages of this technique are deterioration in material properties due to chemical reactions within the polymer, which result in oxidation. The changes which oxidation cause have been reported as reduction in static strength, elongation and fatigue properties (Collier et al., 1996). Other authors (Ries et al., 1995; Sun et al., 1994; Kurtz et al., 1994) have also found that as oxidation increases, fatigue strength decreases and modulus increases. An increase in stiffness leads to a consequent increase in contact stresses *in vivo*, a decrease in fatigue strength and a decrease in wear resistance.

Alternatives to gamma irradiation are gas sterilisation in Ethylene Oxide (EtO). The advantage of this method is low cost investment for a sterilisation unit. Jahan et al. (1996) found minimal to no free radicals in the surface and core regions of EtO sterilised samples and this has been reported to lead to prevention of oxidation on the shelf *in vivo*. Trieu et al. (1997) found significant reduction in the fatigue wear resistance of gamma irradiated sterilized polyethylene compared to EtO. However, Wang et al. (1996) found much lower wear rates in air irradiated material than nonsterile or EtO sterilised material. Polineni et al. (1996) found a 60% reduction in wear rate for gamma in air over EtO.

The time after sterilisation to implantation is variable and is called the shelf age. Furman et al. (1996) found that oxidation of UHMWPE on the shelf is

more extensive, severe and rapid than oxidation *in vivo*. Trieu and Paxson (1995) found the oxidized surface layer became more oxidized and grew thicker with time during shelf aging. In contrast, other researchers found that bearings, which were gamma irradiated in air, did not fail prematurely (Wang et al., 1997). Interestingly, Bell (1999) found that there was no oxidation of directly moulded polyethylene after gamma irradiation. Furman et al. (1997b) found that compression moulded components appeared to be more resistant to 'on the shelf' aging than other types of UHMWPE.

It is important to determine the effects of sterilisation techniques on the material properties of different types of UHMWPE and manufacturing process with respect to shelf-life and *in vivo* life (Furman, 1997b)

1.5 PATELLOFEMORAL JOINT

Patellofemoral complications are the most common postoperative problem in total knee arthroplasty and represent the most frequent cause of reoperation. (Harwin, 1999). The reported incidence of failure varies considerably from 5 to 50% (Stulberg, 1995; Churchill et al., 1997; Harwin, 1999). Most early designs of TKR did not include patella resurfacing, and the reported incidence of anterior knee pain associated with these early implants dominated. The introduction of a patella replacement led to significant reduction in anterior knee pain and improved knee function (Johnson and Eastwood, 1992) but other complications with the patellofemoral joint remain significant (Dennis, 1992; Bindeglass et al., 1993; Kitsugi et al., 1994; Doerr and Eckhoff, 1995; Churchill et al., 1997). As a result considerable controversy exists regarding the necessity for patellar resurfacing in TKR (Levitsky et al., 1993).

There have been a number of problems associated with patella replacement. These include loosening, subluxation, dislocation, patella fracture, osteonecrosis, stiffness, instability, weakness, inappropriate patellar bone

resection, malalignment of the quadriceps mechanism, oversized femoral component, patella tilt and displacement causing eccentric loads resulting in cold flow and wear of the polyethylene, devascularisation by excessive lateral release, soft-tissue impingement (patella clunk), patellar fractures, extensor mechanism disruption and residual anterior knee pain. Patellar fracture with significant displacement will result in extensor mechanism power loss. Extensor mechanism power loss after TKR is a serious complication since without extensor muscle power the knee will collapse when flexed. Other factors such as patella thickness, patella height, and joint line position have been implicated in patellofemoral function (Moreland, 1988; Johnson and Eastwood, 1992; Berry and Rand, 1993; Kitsugi et al., 1994; Dennis, 1995; Healy et al., 1995; Hsu et al., 1996; Insall, 1996; Shoji and Shimozaki, 1996; Harwin, 1999).

In general problems with patella replacement can be categorized by patient selection, surgical technique and design of the component.

1.5.1 PATIENT SELECTION

Soudry et al. (1986) reported comparable results between patients who were treated with TKR with or without patella resurfacing, but noted diminished stair-climbing ability in the unresurfaced knees compared with their historical controls. They recommended against patellar resurfacing in patients with relatively normal patellar cartilage or relatively young or active patients. Picetti et al. (1990) in a retrospective view of 100 TKRs without patellar resurfacing, recommended resurfacing in selected circumstances. These were patients with preoperative patellofemoral pain, height greater than 160cm, weight more than 60kg or advanced changes in the patella observed intraoperatively. Abraham et al. (1988) compared rest pain, walking pain, walking distance, stair climbing, chair rising, active arc of motion, or extensor lag and concluded that resurfacing the patella resulted in no clear advantage in the final result. However, choice of treatment is age dependent, with patellar preservation procedures favoured in the younger patient (Levitsky et

al., 1993; Dennis, 1995). An important point is that conversion of an unresurfaced patella is far less complicated than revision of a resurfaced patella with a complication.

1.5.2 SURGICAL TECHNIQUE

Different surgical techniques for proper patella positioning have been proposed (Grace and Rand, 1988; Rhoads et al., 1990; Yoshii et al., 1992a; Doerr and Eckhoff, 1995). An important factor is how much bone is resected from the natural patella. If too little is removed, there is an excessive total thickness resulting in high patella-femoral forces. If too much bone is removed there is a risk of fracture of the remaining bone. As an illustration of the importance of technique, Insall (1996) stated: "The most important observation that can be made about extensor mechanism complications is that they are avoidable. All these can be avoided by attention to the details of surgical technique."

Insall (1996) advocated unequal posterior femoral condyle resection, which results in the femoral component being externally rotated with respect to the tibia. This results in better patellofemoral stability because the femoral groove is placed more laterally. Others advocate equal amounts of resection on the posterior femoral condyles (Hungerford and Kenna, 1983). Figgie et al. (1986) suggested that most patella complications could be managed by aligning the tibial prosthesis in neutral rotational and varus-valgus alignment, aligning the femoral component in neutral rotational alignment and central positioning of the patella component.

Moreland (1988) said that the method used by Insall (1996) described above would provide the anatomically correct result. Correct positioning of the patella is important because if the patella is forced excessively anteriorly, flexion may be limited and the tendency for lateral patella subluxation or dislocation may increase. In addition, malalignment may increase the stress

at the patellofemoral articular surface and cause abnormal patella kinematics and wear (Nagamine et al., 1996). Figgie et al. (1986) have demonstrated a correlation between major malalignments of the tibial and femoral components and patella fractures in posteriorly stabilised prostheses. They found that three of the five patients with patellar fractures in their series had 3-5° of varus tibial component alignment. They felt that the criteria for neutral alignment developed for cruciate sacrificing prostheses may not necessarily be transferable to cruciate–sparing prostheses. In their study, proper positioning of the patella led to good or excellent results in 94.3% of cases with a low rate of complication (5.7%) at the 5-7 year follow-up evaluation.

1.5.3 PATELLA DESIGN

The design of the patella and the femoral trochlea play an important role with regards to function and performance. Metal-backed patella components were introduced to reduce the strains in the bone but in some designs the metal-backing increased the stress on the polyethylene at the metal-plastic interface. This often led to premature wear through of the polyethylene. Fracture and separation of the polyethylene also occurred at the metal-backing. Other failure modes were due to increased tilt, malposition and wear. Even for cementless metal-backed patellas, significantly higher rates of patellofemoral complications including loosening occurred. All-polyethylene patella components and patella components implanted with cement are reported to avoid such problems (Healy et al., 1995).

Concerning design there are three different profile shapes of patella components. These are the dome, cone and Gaussian as shown in figure 1.3 (Walker, 2000). Of the three profile shapes, the dome is the most widely used. The problems that are associated with the patella design refer to deformation and the ability of the femoral flange to function well whether it has a natural patella or an artificial one. With reference to deformation, the dome is associated with increased deformation because it has thinner sides

whereas the cone and the Gaussian profile are thicker at the sides as shown in figure 1.3 (Walker, 2000). However, Harwin (1999) who reported the use of a three peg all-polyethylene offset-dome oval patella, implanted with a symmetrical patellofemoral TKR, found that the design concept had few patellofemoral complications and reoperations.

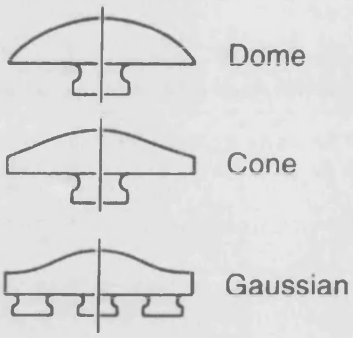

Figure 1.3: Patella Profiles
(Walker, 2000)

1.6 FRACTURE OF METAL PROSTHESES

Fracture of the femoral component is an extremely rare occurrence (Whiteside et al., 1993). In the case reported by Whiteside et al. (1993) the femoral component was cementless and the porous coating was achieved by sintering. Failure of the Ortholoc II (Dow Corning Wright, USA) femoral component occurred in the smaller sizes of the product and was attributed to thin sections and the porous coating weakening the fatigue properties of the material. Fracture of the tibial baseplate has been reported and is discussed in detail in Chapter 2.

1.7 TESTING METHODS

In the past many prostheses have been designed, developed and used in patients without any preclinical tests being conducted. This greatly increased the risk of premature failure of the device. Clinical success was then assessed upon survivorship data. In these situations, a number of years has to pass with the prosthesis *in vivo* before it can be said to what extent it is a success. Based on clinical performance, failure modes were determined and then subsequent design modifications were made. We are now in an era where the least that is expected from a knee prosthesis design is over 90% survivorship at 10 years. In this regard, pre-clinical testing methods are important particularly to identify possible failure modes that occur and to meet the standards required by regulating bodies such as the Food and Drug Administration (FDA). By using pre-clinical tests, unsuitable designs can be identified in an objective way and modifications made as a result of a series of test procedures before actual clinical trials. However, it is recognised that complete and final evaluation of prosthetic devices is impossible in the laboratory for three reasons. The first is that the environment within the human body can only be approximated experimentally, secondly pain cannot be measured and finally the response of the tissue to the materials of the implant and wear debris produced cannot be ascertained.

The success of prostheses is dependent upon good design and construction as much as it is on the materials. Hence the need for tests which can evaluate both these aspects. Pre-clinical testing can determine the range of motion, stability, component strength and long-term wear. There are a number of different physical testing methods examining particular functions of a knee prosthesis. Static tests have included fixation tests to determine the likelihood of loosening, tests for the security of locking mechanisms and strength testing of plastic posts. Pin-on-plate tests are used for evaluating new materials and knee simulator tests have been used for long term wear testing. Each of these methods is discussed in more detail in the following sections.

1.7.1 FIXATION TESTS

Fixation tests have been devised to address the problems of loosening of the tibial component that had dominated in the 1970s and 1980s.

1.7.1.1 Axial load test

In axial load tests the tibial component is mounted in a materials testing machine such as Instron or MTS and a cyclic sinusoidal load is applied perpendicular to the tibial surface (figure 1.4). The load is applied through one condyle to represent eccentric loading using a matching femoral component or spherical indentor. Linear Variable Displacement Transformers (LVDTs) are most commonly mounted, one placed on both condyles to measure subsidence and lift-off (Walker et al., 1982; Bargren et al., 1983; Volz et al., 1988; Lee et al., 1991; Kraemer et al., 1995). Alternatively three LVDTs have been used to measure vertical displacements (Yoshii et al., 1992b) as well as six LVDTs to measure micromotion in the three translatory directions and 3 rotationary positions (Bourgeault et al., 1997).

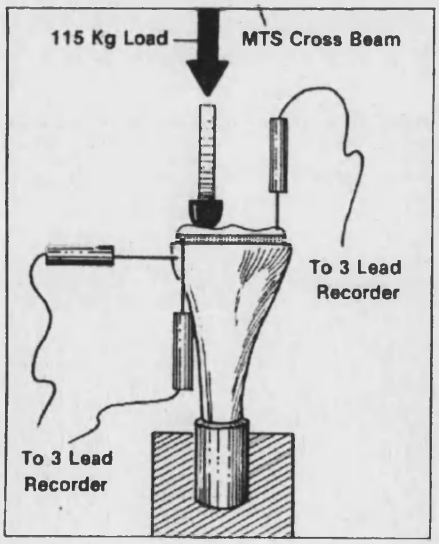

Figure 1.4: Test equipment to measure lift-off and subsidence during axial load testing. (Volz et al., 1988)

1.7.1.2 Shear load test

Shear load tests have been conducted by mounting the tibial tray parallel to the direction of load application (refer to figure 1.5) in a materials testing machine such as Instron or MTS (Yoshii et al., 1992b). The load was applied to the central tibial notch between the medial and lateral condyles of the tray with an LVDT placed symmetrically on both the medial and lateral posterior rims, measuring micromovement of the tibial tray relative to the proximal tibia in the posteroanterior direction.

However, Kraemer et al. (1995) state that pure shear loading does not occur physiologically and in their study mounted the tibial tray at 15 degrees to the vertical (figure 1.6), representing a flexed knee. This prevents lift-off of the component during testing. A cyclic load was applied to the posterior part of the component to create a combined shear and axial load. Two LVDTs were again used to measure micromovement.

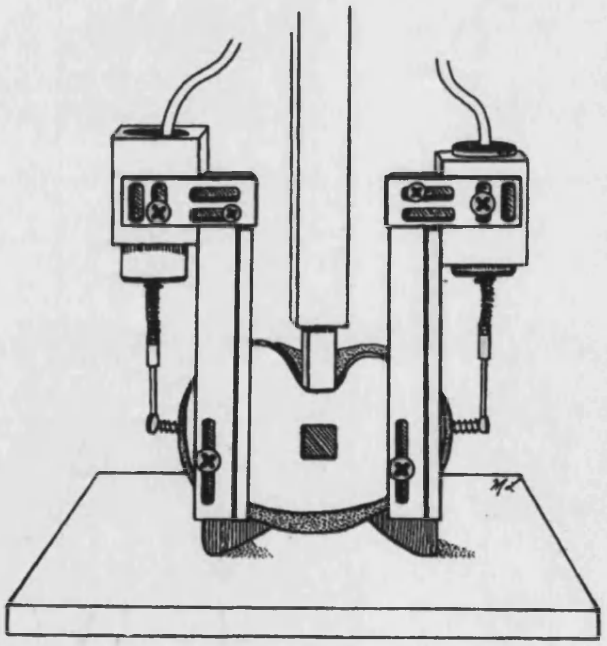

Figure 1.5: Anteroposterior view showing loading of the tibial tray. (Kraemer et al., 1995)

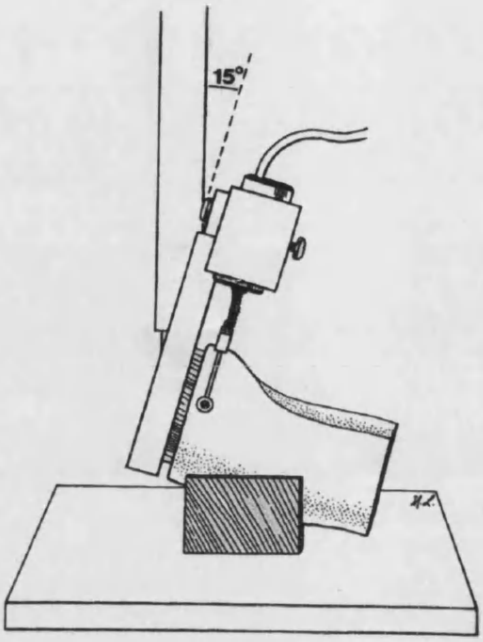

Figure 1.6: Lateral view showing flexed knee during shear test. (Kraemer et al., 1995)

1.7.1.3 Torsional test

Various testing configurations have been constructed to measure torque transmitted across the knee. Werner et al. (1978) calculated the transmitted torque, using a torsion load cell, by rotating the prosthesis through a known angle. Bargren et al. (1978) mounted both tibia and femoral shafts in a torsion test rig, which was placed in a compression testing rig. A turning moment as well as compressive loading was applied. Rotation and vertical displacement of the femur relative to the tibia were measured as the turning moment was increased. The tests were continued until the femur rotated out of the tibial component. More recently, Kraemer et al. (1995) conducted torsional loading tests by machining a square or circular slot into the surface of the tibial component and applying both torsional and compressive loading through a shaft which fits blindly into the slot. Two LVDTs, one placed on the medial side and the other on the lateral measured horizontal micromotion from reference points.

1.7.1.4 Intra-operative micromovement test

Yoshida et al. (1993) have used a test to measure micromovement for cementless tibial components during the surgical procedure. The basis for the test procedure is that micromovements greater than 150 μm inhibit bone ingrowth and increases the likelihood of loosening. Figure 1.7 shows the configuration used to measure the micromotion. A manual load of 200N is applied in the four quadrants of the component. The accuracy of the test equipment is 10 μm. If the micromotion is greater than 100 μm then cement is used to improve the quality of fixation. However, the long-term stability has not been assessed. Limitations of this testing procedure are the time taken to fix the test equipment and the time taken to obtain the measurements. The authors state a time of 10-15 minutes during the operation. The loading is not representative of a walking cycle as this is extremely difficult to achieve using manual loads.

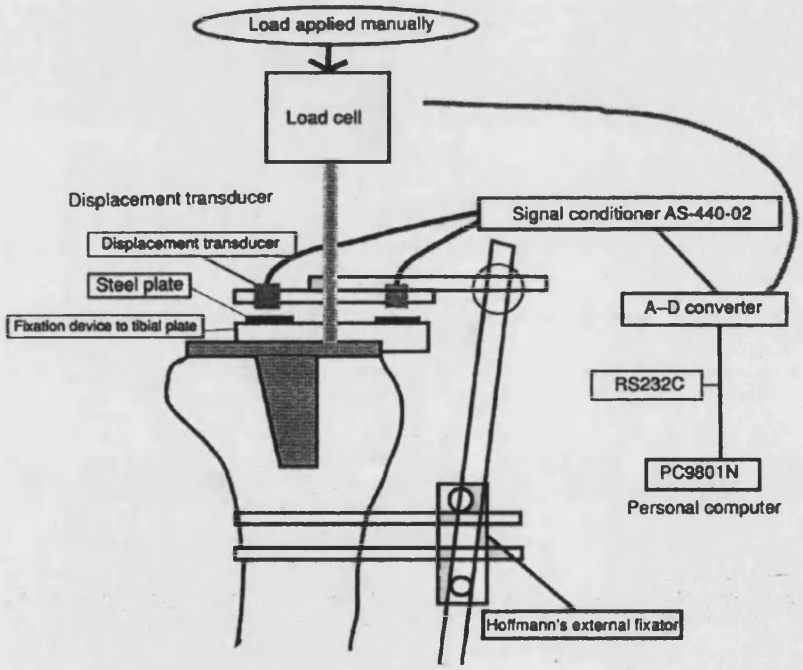

Figure 1.7: Test equipment for measuring micromovement intra-operatively
(Yoshida et al., 1993)

1.7.2 EFFECTIVENESS OF THE LOCKING MECHANISM

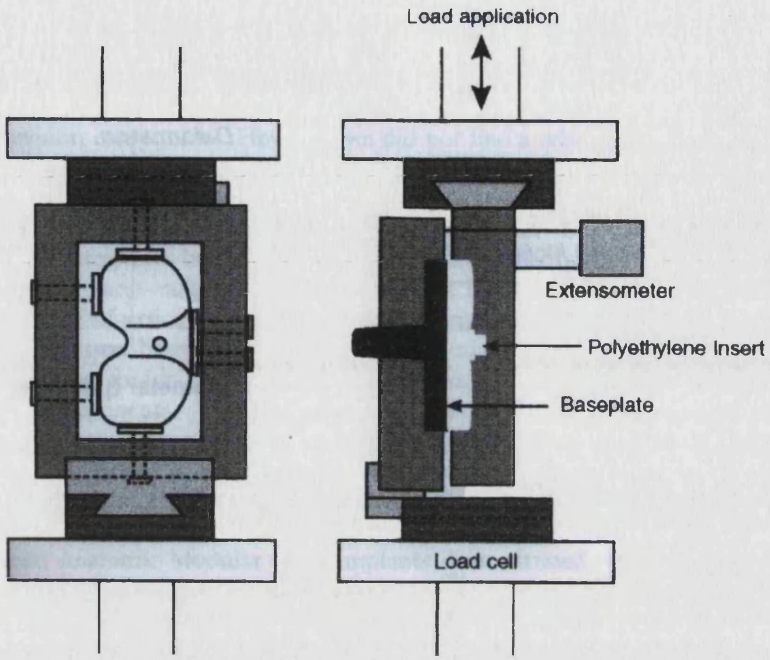

Figure 1.8: Test set-up to measure the security of the locking mechanism. (Engh et al., 2001)

A method of comparing the effectiveness of the locking mechanism, for fixed and mobile bearing knees, was described by Engh et al. (2001). In their test both the metal and polyethylene components were mounted separately in metal frames as shown in figure 1.8. The test was conducted in a materials testing machine. A cyclic load of 100N at a rate of 10N/second, was applied vertically to the metal frame so that the polyethylene insert experiences compression followed by tension. This moved the polyethylene insert downwards followed by upwards with respect to the fixed tibial baseplate. Both the metal plate and the insert are rotated 90° and the procedure repeated. In this way, the polyethylene insert was subjected to motion along both axes. The displacements from motion in both planes was recorded. The results obtained between the fixed and mobile bearing knees, were compared. Walker (2000) proposed that for testing the security of fixation of the plastic in the metal tray and the security of mobile bearing components a

cyclic shear force possibly accompanied by a compressive force could be applied to the tibial tray and plastic insert configuration. He proposed that a shear force of 750N could be applied for 10 million cycles representing vigourous walking. This could be interspersed with a force of 1250N applied for a total of 0.5 million cycles, representing the extreme forces that could be applied in rapid ascending or descending.

1.7.3 SUPERSTABILISER TESTING

For those patients where the collateral ligaments may be compromised, superstabilisers are used. Superstabilisers have a large central post that provide stability against varus–valgus loading. To test the ability of the post to resist varus-valgus loading, a superstabiliser insert is rigidly fixed to the tibial tray, which may be fixed to rigid supports in some way (figure 1.9). A cyclic force, C, is applied through a bar clamped to the stem of a femoral component. The force is offset from the centreline and medial to the femerotibial contact point. The value of the force is 1000N, applied at a point 45mm from the center of the knee. By applying a load in this way, a moment is induced, which causes the femoral component to shift onto one component of the tibial insert. This results in the post being subjected to a bending moment. Deformation of the post can then be measured and compared with other designs (Walker, 2000).

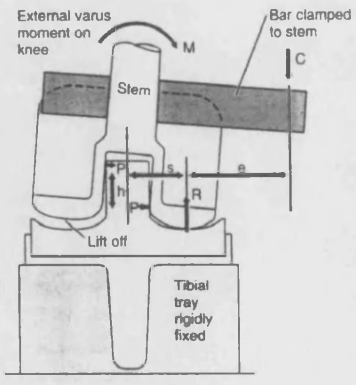

Figure 1.9: Superstabiliser test set-up (Walker, 2000)

1.7.4 TESTING FOR ALL FAILURE MODES

The testing methods described above are used to evaluate the effect of certain features of tibial components or to demonstrate the likelihood of a particular mode of failure. A more comprehensive test is required to address known failure modes and reveal possible failure modes for new designs. Such a test to assess the durability of tibial components has been proposed by Walker (1994).

The rationale for this test is that the forces and moments that act on a tibial component at any instant in a given activity cycle, can be applied as a single resultant force inclined in three dimensions to the test specimen. The components of the force then represent the shearing forces in the medial-lateral direction, antero-posterior direction and a vertical force. If the resultant applied force is offset from the centre of the tray, then the induced moments, at the centre, will represent internal-external torque, the varus-valgus moment and the flexion-extension moment.

Following from this, by orienting the component so that it is tilted about the three axes at the centre of the tray and applying a vertical force offset from the centre, the same forces and moments will be generated (figure 1.10). The component can then be mounted in this configuration, in a uniaxial test machine and a cyclic vertical force applied. To allow elastic and progressive deformation the components have to be mounted so that the medial-lateral, antero-posterior, internal-external torque are unconstrained. It may also be necessary to move the force applicator during the activity cycle, if the position of high stress varies with contact location. Although the aim of the test is to represent the forces and moments experienced *in vivo* it is not without its limitations (Walker et al., 1996). If the forces acting at the centre of both condyles are equal, the resultant force will act at the mid-line of the tray - this will not induce any bending moments on either side of the tray. If only the largest force is selected, then the bending moment on that side will be correct but overall the forces and moments for the component will be incorrect.

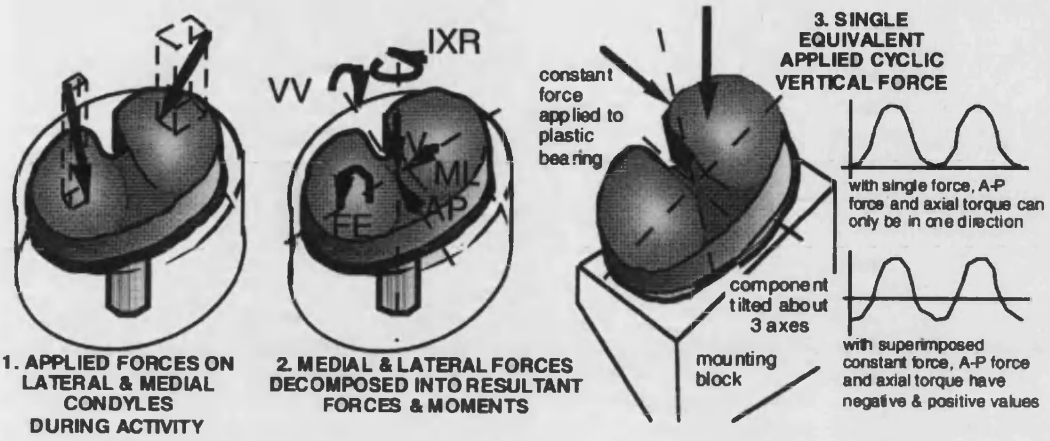

Figure 1.10: Diagram representing the forces and moments generated by applying a vertical force to a component tilted about three axis. (Walker et al., 1996)

Walker et al. (1996) proposed that a vertical force three times body weight should be used with the majority of cycles representing walking but with time periods representing stair climbing or rising from a chair should be included and that the test should apply 20 million cycles at 3-5 Hz for a continuous testing time of 46-77 days to provide a simulation representing 10 years.

This test addresses failure modes in addition to fracture. By including shear components and moments and varying the location of the point of load application this test proposes a baseline for predicting the behaviour of tibial component with respect to the range of known failure modes. Validation of this test using designs that have failed *in vivo* will reveal to what extent the test fulfils its aims, from which progress can be made.

1.7.5 PIN-ON-PLATE TESTING

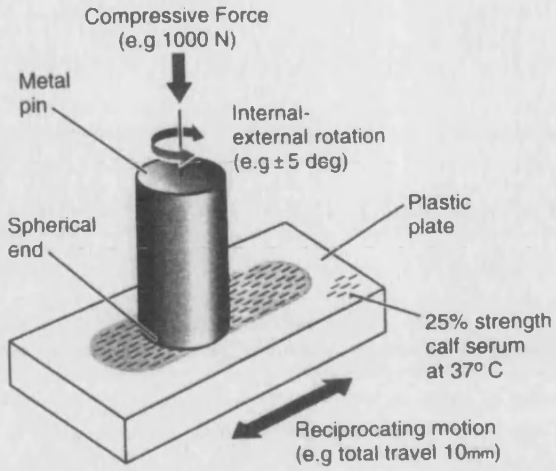

Figure 1.11: Pin-on-plate testing
(Walker, 2000)

Pin on plate testing is used to evaluate a new material for a total knee bearing surface. A metal pin with a spherical surface at the end representing the femoral component is made to slide across a flat plate (figure 1.11). The plate is made from the new material. The pin moves forwards and back by a total of 10mm at a rate of 1Hz. The test is conducted in a medium consisting of 25% to 50% serum at 37° C. A compressive load of 1000N is applied, representing the force applied to one condyle. The pin can be rotated to represent internal-external rotation. The medium is changed every two days to prevent degradation. Particle analysis is conducted every million cycles by taking samples of the medium (Walker, 2000).

1.7.6 KNEE SIMULATORS

A knee simulator is a complex machine that is intended to represent the functional loads and motions of activities. It provides a method of long-term durability testing that allows comparisons to be made between designs. These tests are validated, by comparing simulator wear patterns with those from retrievals.

The design of a joint simulator requires a compromise between the ideal degree of sophistication desired and the time and money for development and construction. There are basically two types of simulator: the force-input and the displacement-input designs (figure 1.12). For the force-input approach, waveforms representing the compression force, AP shear force and torque are applied. Each knee then moves according to its inherent constraint. The displacement-input machine is less complex mechanically, applies an AP displacement and internal-external rotation rather than forces and torque. However, the magnitude of the displacements, applied to each knee design have to be determined by some other means. Also the fixed displacements and rotations can change over time due to deformation and wear. Knee simulator tests are usually carried out to 10 million cycles, representative of 5 to 7 years of *in vivo* life.

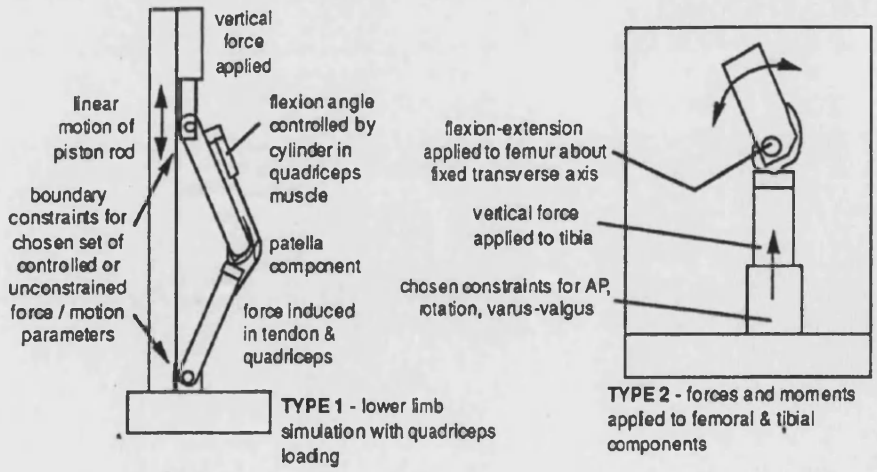

Figure 1.12: The two types of knee simulators (Walker et al., 1996)

As well as long-term wear testing (Walker et al., 2000) simulators have been used for kinematic studies. The kinematics of different designs have been compared and the dependance on ligamentous restraints assessed (Des Jardins et al., 2000a & b). Haider et al. (2001) evaluated the effects of different patient and surgical variables on the kinematics of different designs. Each of these different tests is important. For example, it is important to assess what effect slight variations in implant orientation would have on fixation and function of the knee as any variation in the angle can produce large variations in the loading patterns. Any shift of this mechanical axis from the centre of the knee due to variation of the angle between the femur and the tibia will result in increased loading of the compartment toward which the axis is shifted, and increased stress on the collateral structures of the opposite compartment. Accelerated wear of the prosthesis with accompanying increases in lateral deformity will result if the prosthesis cannot tolerate the abnormal loading (Shaw and Murray, 1973). Also, it is important to determine the wear characteristics and functional behaviour in each different design so that appropriate selection can be made by surgeons for their patients.

1.7.7 FATIGUE TESTING

Fatigue testing of the tibial component has been devised and is the subject of chapter 2.

1.7.8 CONCLUSION

Total knee replacement (TKR) was initially used in older patients with degenerative diseases. However its success had led to calls for design improvements that allow its applications to increase. This has included more durable usage for younger patients with the ability to cope with higher levels of function. To address this issue, improved cementless techniques have been developed with osteoconductive coatings that enable longer fixation and service life. Reductions in length of surgery and recovery time for patients post-operatively has resulted in minimally invasive techniques using unicompartmental prostheses. This has aroused much interest and in some cases is a viable option. Some cultural expectations require deep knee bends to be performed routinely and this has led to the development of knee designs such as the Bi-Surface (Kyocera, Japan) that allow a high range of flexion. Other designs such as the Medial Pivot knee (Wright Medical Inc, USA) are intended to provide more natural kinematics.

Testing methods have been a major factor in the development of the design of artificial joints. Fixation testing on tibial components of different designs showed that one piece designs with one or two posts had far smaller levels of loosening than others (Walker et al., 1981). Over time this has led to the widespread usage of one-piece tibial components. The failure of plastic posts (McPherson et al., 1993) in superstabilised designs and subsequent static testing of the tray design in varus has led to metal reinforcement which has led to the frequency of failure diminishing (Walker, 2000). Hence, in the development of more advanced artificial designs, appropriate testing methods have to be specified and further developed. This is important especially with regards to the patients need and to prevent unnecessary revision operations. It also might prove useful to the surgeon in selecting an appropriate and safe device for their patient. With these requirements in mind, regulating bodies have set stringent standards that have to be met. Testing methods play an important role in meeting these goals and have to be continually advanced to meet new designs and more exacting requirements.

CHAPTER TWO:
INTRODUCTION TO FRACTURE OF TIBIAL TRAYS AND PRE-CLINICAL TESTING METHODS

2.1 FRACTURE OF TIBIAL TRAYS

Fracture of metallic tibial trays is commonly reported as a rare occurrence but nonetheless leads to catastrophic failure of the artificial joint, resulting in pain and loss of function for the patient. Incidences of fatigue fracture have been reported in the literature and are associated with a number of factors. These include:

(i) poor design (Skinner et al., 1987; Gradisar et al., 1989; Flivik et al., 1990; Maruyama et al., 1994);

(ii) manufacturing process and material properties (Morrey and Chao, 1988; Gradisar et al., 1989; Flivik et al., 1990; Maruyama et al., 1994);

(iii) patient weight and activity levels (Scott et al., 1984; Morrey and Chao, 1988; Gradisar et al., 1989);

(iv) lack of bony support especially under either the medial or lateral portion of the tray (Mendes et al., 1984; Scott et al., 1984; Morrey and Chao, 1988; Gradisar et al., 1989; Flivik et al., 1990; Maruyama et al., 1994; Abernethy et al., 1996; Altintas et al., 1999; Clarke and Trousdale, 1999);

(v) malalignment (Mendes et al., 1984; Scott et al., 1984; Morrey and Chao, 1988; Gradisar et al., 1989; Abernethy et al., 1996; Altintas et al., 1999; Clarke and Trousdale, 1999);

(vi) incomplete coverage of the tibial plateau (Morrey and Chao, 1988; Altintas et al., 1999).

These factors are discussed in more detail in the following sections.

2.1.1 TRAY DESIGN

The design of the tibial tray has been implicated as a contributing factor to the process of fracture. Mendes et al. (1984) reported failure of a metal-backed Total Condylar (Stryker Inc, USA) prosthesis due to the formation of cracks within the groove based in the rim of the tray (figure 2.1). They concluded that the groove reduced the cross-section of the tray, thus

reducing the maximum tolerable load. The tray failed by brittle cleavage fracture characteristic of fatigue in cobalt-chrome (CoCrMo) alloys, and this caused fracture across the medial side of the baseplate (figure 2.2).

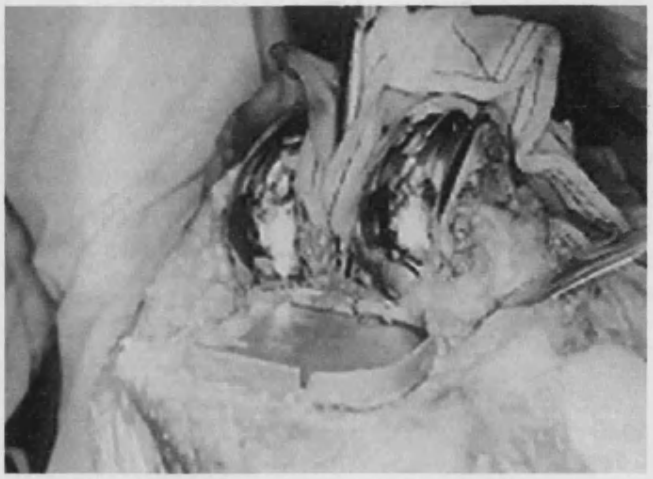

Figure 2.1: Total Condylar prosthesis showing the groove in the rim. (Mendes et al., 1984)

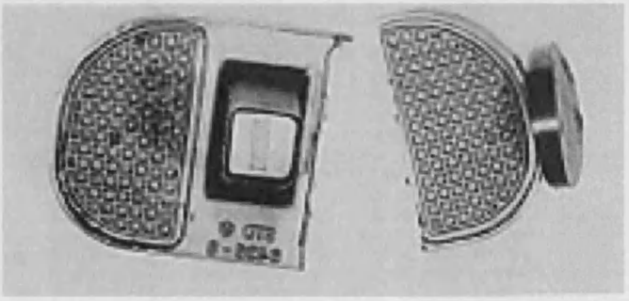

Figure 2.2: Fracture of the medial portion of the Total Condylar tibial tray. (Mendes et al., 1984)

Scott et al. (1984) reported failure of a Kinematic (Stryker Inc, USA) tibial tray where the cracks propagated from the cruciate cut-out (figure. 2.3). Abernethy et al. (1996) also reported that in the seventeen cases they examined, fracture occurred close to the central stem on the medial side, passing forwards from the cut-out in the tray for the posterior cruciate ligament. It resulted in a sagittal split close to the central stem with a second coronal fracture of the posteromedial part of the plate or a single oblique fracture (figure 2.4).

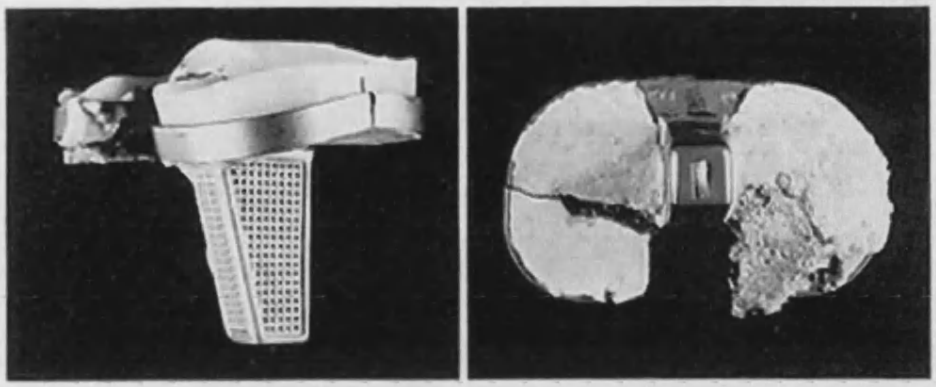

(a) (b)

Figure 2.3: Fracture of the Kinematic component: (a) shows the medial to lateral crack (b) crack emanating from the PCL cut-out (Scott et al., 1984).

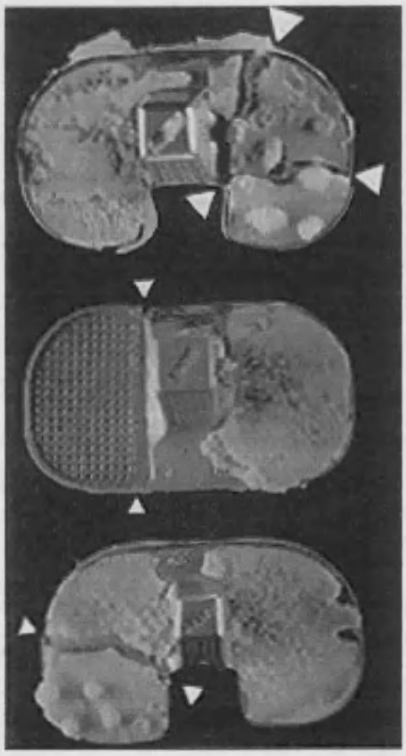

Figure 2.4 (top to bottom): Fracture of the Kinematic component: (top) anterior-posterior and medio-lateral crack formation; (middle) anterior-posterior crack formation; (bottom) medio-lateral crack formation (Abernethy et al., 1996).

Gradisar et al. (1989), Flivik et al. (1990) and Maruyama et al. (1994) all reported fatigue failure of the PCA revision (Stryker Inc, USA) tibial tray. Figure 2.5a shows a top view of this component. In all reported cases, fracture of this design emerged at, or near the fenestration slots surrounding the posts (the aim of which was to aid in removal of the stem at revision) as shown in figures 2.5b-e.

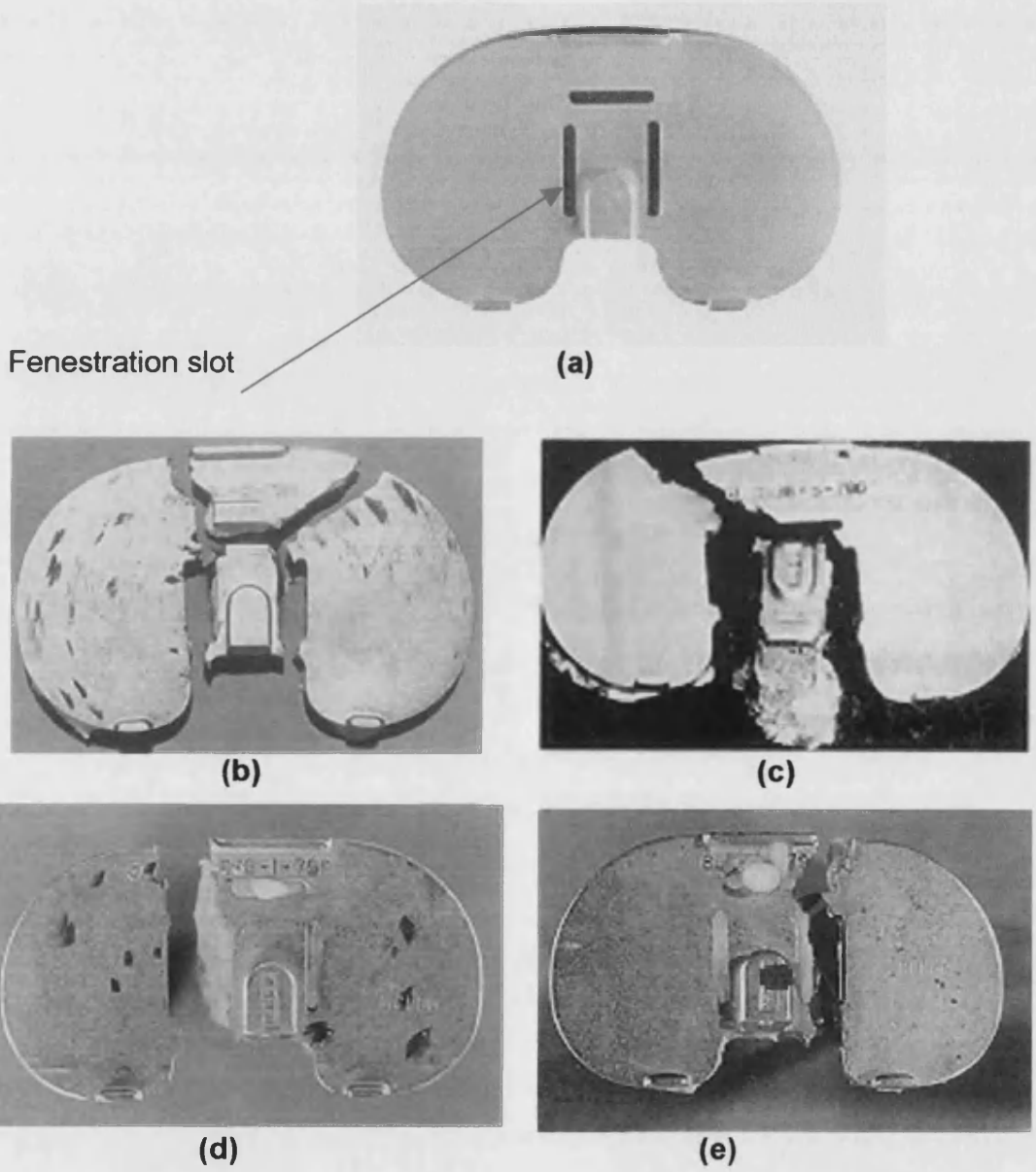

Figure 2.5 (a) top view of the PCA revision design;
(b) fractured tray (Gradisar et al., 1989);
(c) fractured tray (Flivik et al., 1990);
(d & e) fractured trays (Maruyama et al., 1994).

Clarke and Trousdale (1999) reviewed the incidence of fracture among the Total Condylar, Kinematic (cruciate sparing and retaining), PCA, and PCA revision trays and found that the locations of fracture occurred at positions of design related to high stress concentrations. Koeneman et al. (1986) also recommended that stress concentrating notches in the tray lip should be avoided in metal trays as they were often a position for the initiation of cracks. Other researchers (Morrey and Chao, 1988; Altintas et al., 1999) have reported fracture of the baseplate but they considered design not to be a factor in their cases (see figure 2.6).

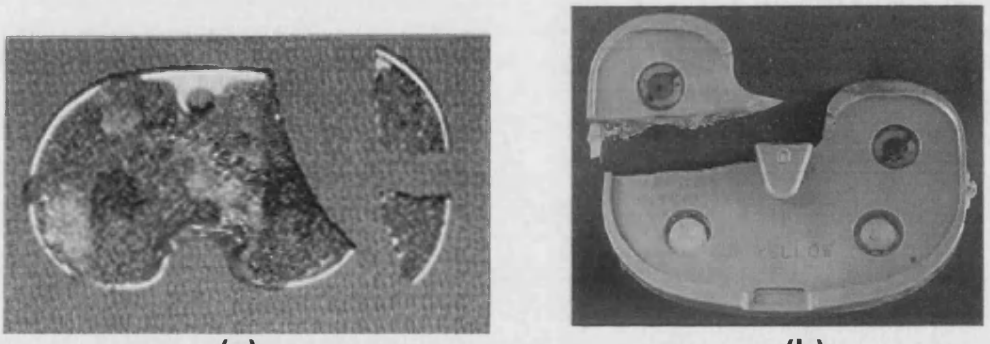

(a) (b)

Figure 2.6: (a) Fracture of the sintered two pegged PCA tray (Morrey and Chao, 1988); (b) Fracture of the MG2 baseplate (Altintas et al., 1999)

2.1.2 MATERIAL PROPERTIES AND MANUFACTURING PROCESS

There are two metals used for artificial knee joints. These are Cobalt-Chrome (CoCrMo) alloy and Titanium (Ti6Al4V) alloy. Cast CoCrMo alloy has a limited ductility (8%) and is prone to fracture in the presence of notches, fillets or other stress risers (Mendes et al., 1984; Gradisar et al., 1989). The fatigue limit of the material in this state is approximately 250MPa (Weinstein & Clemow, 1990) but during the casting process, defects in the form of voids or inclusions, become present in the cast material. These can further reduce the fatigue properties of the material. Fatigue properties of CoCrMo alloy, however, can be improved by processes such as Hot Isostatic Pressing (HIPing) and solution heat-treatment (Georgette and Davidson, 1986).

Ti6Al4V alloy has a higher fatigue limit than cast CoCrMo alloy but it is notch sensitive (Gradisar et al., 1989) and there have been reported failures of titanium alloy baseplates (Scott et al., 1984; Cook et al., 1991; Altintas et al., 1999).

Achievement of a porous surface by using a sintering process reduced the fatigue properties of the PCA revision tibial tray (Gradisar et al., 1989; Flivik et al., 1990; Maruyama et al., 1994). Pilliar (1983) estimated that a 16% decrease in strength for CoCrMo alloys occurred from the sintering process. Morrey and Chao (1988) examined the surfaces of a fractured PCA tibial baseplate that had been sintered and showed that there were multiple cracks across the sintered beads of the porous surface, between the beads and the surface of the solid tray, as well as between individual beads. These cracks may have propagated across the thickness of the metal tray under high repetitive loading. Morrey and Chao (1988) stated that the porous surface caused stress concentrations at the junction of the solid substrate and porous layer, and that the irregular surface caused notch sensitivity. Cook et al. (1991) reported failure of two PFC (Depuy Inc, USA) titanium alloy components that were porous coated. Cook et al. (1991) said that in porous-coated prostheses, bone ingrowth was not uniform and generally occurred only in isolated areas creating regions of stress concentration due to enhanced stress transfer in the areas of bone ingrowth. As a result, porous-coated bone ingrowth prostheses were generally found to be much weaker than contemporary cemented devices (Moreland, 1988; Miller, 1984; Callaghan et al., 1988). Hence, material properties and manufacturing processes have affected the fatigue performance of tibial trays.

2.1.3 PATIENT WEIGHT AND ACTIVITY LEVEL

Patient weight and activity levels have been considered by some researchers to be factors leading to failure of tibial baseplates. However examining these cases revealed that a range of patient weights and activity levels were reported.

Average body weight is regarded as 75-80kg. Scott et al. (1984) reported fatigue fracture in two patients that weighed 96kg and 105kg; Gradisar et al. (1989) reported fracture for a patient who weighed 100kg and Morrey and Chao (1988) reported fracture for a 34 year old man who weighed 97.7kg. Flivik et al. (1990) reported fracture for an 83kg patient and Altintas et al. (1999) reported failure in an 80kg patient. Clarke and Trousdale (1999) reported a mean weight of 87kg (55-105) at the time of fracture for 24 patients; Maruyama et al. (1994) reported fracture for two female patients that weighed 67kg and 53kg and Abernethy et al. (1999) reported fracture for 6 female patients that were of average weight and height. From this analysis of patient weights it is clear that it is possible for baseplates to fracture even in those patients that had below average weight and therefore patient weight cannot be regarded as a primary cause for fracture.

Morrey and Chao (1988) and Flivik et al. (1990) presented two cases where they considered their patients to be active. Altintas et al. (1999) stated that their patient had average activity levels. Abernethy et al. (1996) reported that six of their seventeen cases had polyarticular rheumatoid arthritis which restricted activity. Clarke and Trousdale (1999) defined ambulatory ability as an indicator of overall activity level. They found, in their study of twenty-four patients, that preoperative activity levels were 2 blocks (range 0 –10), where a block is the distance around buildings in the United States. Postoperatively the patients' activity levels increased to 3.5 blocks. Again it is clear that fracture has occurred in patients with high, moderate and low activity levels. Therefore fracture can occur with all levels of activity.

2.1.4 LACK OF BONE SUPPORT

In all of the reported cases for fracture of the baseplate, lack of bone support has been cited as one of the main factors leading to fracture. Bone loss in patients can occur as a result of large defects prior to surgery as a result of diseases such as osteoporosis and bone tumours. They can also occur after

surgery where bone loss occurs due to resorption. Skinner et al. (1987) conducted a finite element analysis on the revision PCA design and predicted that if the support beneath the fenestration slots was inadequate then the tray would fail due to fatigue. Maruyama et al. (1994) fully supported this view. They reported that the most significant problem in the two cases they examined was the poor proximal bone support especially beneath the medial portion of the tray that led to fracture of an improper design. Gradisar et al. (1989) and Flivik et al. (1990) also reported poor bone support beneath the tray as a factor in PCA revision failure. Abernethy et al. (1996) also reported marked tibial bone loss especially on the medial side of their cases of fracture of the Kinematic baseplate. A finite element analysis study on a generic metal tray, conducted by Koeneman et al. (1986), showed that lack of support under the tray compromised its strength.

The following sections discuss the reasons for poor bone support:

2.1.4.1 Pre-existing poor bone stock

This can arise from depressions of either the lateral or medial tibial bone plateau due to severe valgus and varus deformities (Chen and Krackow, 1994). There are several methods for correcting deformities. These include bone resection or osteotomy, filling with cement, cement with reinforcing screws or wire mesh, shifting the component off the defect, bone grafting, modular wedges and custom components (Brand et al., 1989; Rand, 1995; Scott, 1995; Fehring et al., 1996). Osteotomy is often used for correction of deformity and in the cases reported by Morrey and Chao (1988) and Gradisar et al. (1989) it preceded the arthroplasty. Another method utilised bone grafts. Morrey and Chao (1988) showed that the bone graft had incorporated but it was depressed and had become cystic leading to poor structural strength. Abernethy et al. (1996) reported three cases requiring bone graft but in each case the bone did not incorporate and collapsed. They pointed out that the poor incorporation of bone grafts might have compromised the strength of the supporting bone, leading to subsequent fracture of the tray.

2.1.4.2 Bone resorption due to foreign body reaction

In the histological study conducted by Maruyama et al. (1994), of two fractured baseplates, they found that numerous wear particles were present, which induced osteolysis. Radiographs showed evidence of lucency with fibrous tissue beneath the fractured portions of the tray. Altintas et al. (1999) found that the polyethylene insert had severe degradative wear and the bony area had diffuse metallosis. There was an extensive lytic bone reaction to the polyethylene and metal debris. Abernethy et al. (1996) found that there was considerable wear of the plastic insert on the medial side of the trays they studied. They also found marked synovial reaction to the resultant debris.

2.1.4.3 Bone resorption due to stress shielding

Clarke and Trousdale (1999) found that only two of their twenty-five cases had developed lucencies about the tibial stem on either the A-P or lateral radiographs, indicating that the other cases had well-fixed stems. Only one implant from the twenty-five case studies had no lucency beneath the condyles of the tray. In all the other reported cases of fracture, the stem was reported to be well fixed (with considerable difficulty reported at revision for removal of the stem) and in some cases the lateral portion was also rigidly fixed (Abernethy et al., 1996; Flivik et al., 1990; Gradisar et al., 1989; Maruyama et al., 1994; Mendes et al., 1988). Scott et al. (1984), Mendes et al. (1988) and Gradisar et al. (1989), stated that the well-fixed stem resulted in stress shielding with subsequent bone resorption beneath the unsupported tray, resulting in fracture. Abernethy et al. (1996) also discussed the evidence of patchy osteoporosis due to stress shielding beneath the fractured portions of the tray and the difficulty of removing the stem at revision. However, Gradisar et al. (1989) acknowledged that it was possible for fracture to occur even if the stem was not well–fixed.

2.1.5 METHODS OF DEALING WITH BONE LOSS USING CEMENT

Cement has been used to build-up the deficient area. Scott et al. (1984) reported two cases of fractured tibial trays; one was built up with cement reinforced with cancellous screws and in the other, cement with reinforced CoCrMo alloy wire mesh, which resulted in fracture of the baseplate. Mendes et al. (1984) also reported fracture where the deficient area had been built up with cement. A study carried out by Brooks et al. (1984) examined different methods for treating bony deficiencies and concluded that the greatest deflection of the metal tray occurred when using cement alone to fill the defect, followed by using cement reinforced with screws. The clinical evidence shows that using cement to fill large defects (greater than 5mm) can provide less than optimal support to the metal tray. This is as a result of shrinkage of the methylmethacrylate during polymerisation, which is thought to be in the region of 1-4% and is not enhanced, even when using a reinforcing screw (Mendes et al., 1984). Fracture of the cement mantle may also occur, resulting in it separating from the tibial component (Jeffery et al., 1994).

Brooks et al. (1984) also examined alternative methods of treating bony deficiencies. They found that the use of spacers made of plexiglass or metal were an improvement, but custom-made tibial components provided the most secure support. They also found that the use of a central stem, 70mm long, provided a means for dissipating more of the axial load. Abernethy et al. (1996) now use longer stemmed prosthesis in young individuals as an alternative to the grafts and metal wedges used in elderly patients. The study by Brooks et al. (1984) concluded that modular metal wedges might provide an acceptable alternative to custom-made tibial components.

It is now regarded that for small defects, suitable treatments are either bone resection or filling with cement or cement with screws (Pagnano et al., 1995). Bone grafting is recommended for contained defects and for younger patients but the possibility of resorption or collapse of the graft exists (Brand et al.,

1989). For larger defects (greater than 5mm) bone resection is not recommended, as the strength of the cancellous bone reduces distally and hence can affect the integrity of the tibial plateau. However, the durability of metal wedges also needs to be assessed for both wedge-cement-bone and wedge-prosthesis configurations (Pagnano et al., 1995). The performance of wedges at the junction with the tibial baseplate where they may be susceptible to fretting and fracture also has to be examined (Rand, 1995; Walker, 1994).

The evidence shows that poor bone support is a significant factor in the fracture process. Therefore tibial tray designs should to some extent cater for any possible bone loss in the lifetime of a patient. This may mean that tibial tray designs may have to be thicker or have superior material properties that would not result in a substantial increase in thickness. The difficulty being that to accommodate a thicker tibial baseplate will result in removal of more subchondral bone and this maybe detrimental to the overall success of a TKR. In any case, tibial tray designs should be subjected to a testing method that mimics bone loss and to determine what load levels a tray is able to sustain under such conditions.

2.1.6 MALALIGNMENT

Many of the reported cases of fracture have cited malalignment as a contributing factor. The authors of these studies showed that fracture occurred when the mechanical axis of the knee was placed in varus. This increased the loading on the medial side of the tibial baseplate causing subsidence, loosening or fracture. Abernethy et al. (1996) discussed the findings of seventeen cases of Kinematic tibial tray fracture and reported that nine out of seventeen patients had varus deformity pre-operatively. Of these only three were fully corrected at surgery but radiographs showed that post-operatively and over time they all showed an increase in varus. Of the remaining eight patients, six had pre-operative varus deformity but all were

corrected to at least 4° of valgus. However subsequent radiographs showed a gradual shift into varus with subsequent fracture on the medial side. Overall, the amount of varus alignment varies with each case. Reported cases range from 1-2° (Mendes et al., 1984), 5° (Gradisar et al., 1989); Morrey and Chao, 1988), and 10° (Scott et al., 1984; Maruyama et al., 1994).

The study conducted by Clarke and Trousdale (1999) showed the importance that alignment and load bearing through the prosthesis play in the development of tibial component fracture. Their study consisted of twenty-five cases of tibial component fracture. Preoperatively, only twenty-four patient x-rays were available. This showed that eighteen knees were in varus alignment, five were in valgus alignment and one was in neutral alignment. Postoperatively all twenty-five patients had available x-rays. Of these, eleven were in valgus (mean 7.8°; range 1-12°), twelve in varus (mean 5°; range 1-12°) and two in neutral alignment. At fracture, twenty-three patients had available x-rays. These showed that fifteen were in varus (mean 11°; range 1-22°) and eight were in valgus (mean 12.4°; range 6-21°) alignment. Of the fifteen cases in varus alignment at fracture, post-operatively twelve were in varus, one was in valgus and two were in neutral. All fifteen cases in varus failed through the medial portion of the tray. Of the eight cases in valgus, four failed through the lateral portion of the tray and the remaining four failed through the medial portion. In the latter four cases, all were noted to have greater than 2mm lucencies beneath both medial zones of the component. The authors concluded that the relationship between alignment and component fracture was statistically significant. Altintas et al. (1999) also highlighted the significance of alignment and load bearing. They reported that the patient had 12° of varus deformity pre-operatively and this had been corrected to 3° valgus post-operatively. However at the time of the operation the femur had been placed in a neutral anatomic rotation, which caused posteromedial tightness in flexion and increased the loading on the medial compartment with subsequent fracture.

In conclusion, severe malalignment alone does not lead to failure of tibial trays although it has been prevalent in many cases. Other factors such as the extent of lucency beneath the tray can affect the way in which a component fractures. This is evident from the study by Clarke and Trousdale (1999), which showed that those trays that had a varus alignment fractured on medial side. Four out of eight trays with a valgus alignment failed on the lateral side. The other four had fibrous tissue formation beneath the medial side and in spite of valgus alignment fractured through the medial side.

2.1.7 COVERAGE OF TIBIAL PLATEAU

A number of reports have discussed fracture of baseplates where the tray was a smaller size than the natural tibia leading to little or no support from cortical bone (Flivik et al., 1990; Morrey and Chao, 1988; Altintas et al., 1999). These cases reported anterior tilting, poor structural support, subsidence, and formation of fibrous tissue and eventual fracture of the tray. This is an important consideration for designers with regards to the shape of the tray; manufacturers in providing enough sizes; and surgeons for appropriate selection of size of tray at the time of operation.

2.1.8 THE TIME AT WHICH FRACTURE OCCURS

Differences in the time to fracture depend on a number of factors. In those cases where there is poor bone support, fracture occurs early. For a well-supported tibial tray, load is transmitted though the tray and the bone. If the stem is well fixed, the tray is unable to subside and therefore cannot get any support from the bone. The tray is then subjected to a greater part of the load compared to a well-supported tray. This situation would result in early fracture. In those situations where at the time of surgery there are no bony defects or adequate provision is made for them, the time for a sufficient layer of fibrous tissue to form results in late fracture. Altintas et al. (1999) stated

that the process of fracture in the MG2 tibial tray design took place as a result of posteromedial tightness, which increased the loading on that side of the tibial component causing subsidence. This led to increased degradation wear of the polyethylene on that side. The wear debris associated with this induced osteolysis caused bone resorption and the formation of fibrous tissue. The fibrous tissue layer provided little support to the tray. The tray subsequently experienced greater amounts of load and the increased stresses led to fracture. Dannenmeier et al. (1985) also believe that the formation of fibrous tissue coincided with the likelihood of fracture in their case.

Clarke and Trousdale (1999) conducted a detailed study of twenty-five cases of baseplate fracture. From the twenty-five cases, only twenty-three sets of x-rays were available to determine the process of development of radiolucency. This study showed that seventeen had developed progressive lucencies measuring 2mm or more in at least two consecutive zones beneath the tibial trays. One patient had 1-2mm in all four zones; four had 2mm in at least one zone and only one had no lucency.

Clarke and Trousdale (1999) also noted that gross subsidence of the component only occurred in three cases. These included two uncemented components without stems and one case that developed lucencies about the entire component. In the remaining twenty-two cases of their study, subsidence only occurred beneath the fractured portion of the component. Subsidence beneath the fractured portion of the tray was also noted reported in other case studies (Mendes et al., 1984; Morrey and Chao, 1988; Maruyama et al., 1994; Abernethy et al., 1996; Altintas et al., 1999). This indicates that the whole of the tray was unable to subside because the stem was well fixed. Only the fractured part of the tray subsided.

Clearly the time at which fracture occurs depends on a number of factors. Early fracture was noted by some researchers (Scott et al., 1984; Mendes et al., 1988; Gradisar et al., 1989; Abernethy et al., 1996). The factors relating

to these cases were poor design, alignment, condition of bone, and the method of correcting bone deformity. For late fracture, the development of fibrous tissue and severe malalignment were prevalent factors (Maruyama et al., 1994; Abernethy et al., 1996; Clarke and Trousdale, 1999).

Weir et al. (1996) reported revision of a Kinematic baseplate at 6 months due to fracture. Scott et al. (1984) reported revision of a fractured Kinematic baseplate at 1 year. Cook et al. (1991) reported failure of two titanium alloy PFC tibial components that had been porous coated. Failure was reported after 28 months and 35 months. Mendes et al. (1988) reported failure of a Total Condylar baseplate at 2 years; whilst Gradisar et al. (1989), Flivik et al. (1990) and Maruyama et al. (1994) reported failure of the PCA tray at 2,4,5 years 4 months and 6 years respectively. Morrey and Chao (1988) reported failure of an unstemmed PCA at 3 years and Altintas et al. (1999) reported failure of the unstemmed MG2 baseplate at 6 years and 6 months. Abernethy et al. (1996) divided their cases into two groups: those that required early fracture at a mean of 29 months (23 to 48 months) and those that required late fracture at a mean of 84 months (60 to 105 months).

2.1.9 CONCLUSION

Fracture is an infrequent occurrence and this is evident from long-term survivorship data. Scuderi et al. (1989) reviewed 917 metal backed Total Condylar baseplates and reported no cases of fracture of tibial trays at 7 years. Malkani et al. (1995) reviewed 168 Kinematic replacements and reported no baseplate fractures at 10 years. Emmerson et al. (1996) reviewed 95 Kinematic stabiliser (no cruciate cut-out) cases and reported no baseplate fractures. Moran et al. (1991) reported fracture, on the medial side, for one PCA baseplate due to the patient falling down the stairs. This was in a 5 year follow-up study of 108 PCA total knee replacements. Weir et al. (1996) reported 5 Kinematic baseplate fractures from 208 cases at 14 years. Khaw et al. (1999) reported failure of one PFC baseplate on the

medial side from a follow-up study at 11 years for 277 cases. Hamelynck (1999) also reported failure of one LCS (Depuy Inc, USA) baseplate out of 783 primary cases at 15 years.

This study has shown that lack of bone support particularly beneath the medial portion of the tray or eventual formation of fibrous tissue was apparent in all cases. A well-fixed central stem was also observed in those tray designs with a central fixation post. These factors led to increased stresses on one side of the tray with subsequent fracture. Tray design is an important issue. Stress concentrations in the design, thickness of the baseplate and porous coatings have been implicated as potential hazards. These design features have resulted in a higher incidence of fracture for some tibial baseplates especially when there has been poor bone support. Other factors have been identified that have also played a part. These include material properties, manufacturing processes, patient weight, activity levels and malalignment. It can be concluded that baseplate failure is multi-factorial.

In order to reduce the incidence of fracture of baseplates it is imperative to consider the design, manufacture and selection prior to surgery. Removal of stress concentrations from designs, improvement of manufacturing processes and material properties, and attention to the quality of bone are important factors. In particular bony deformities must be addressed, as well as ensuring that the component is properly aligned.

2.2 TESTING METHODS

Pre-clinical testing of joint replacements is necessary to assess the likelihood of a particular failure mode or the overall performance of the implant to prevent failures *in vivo*. A standardised protocol has the purpose of ensuring that implants are rigorously tested in a valid and appropriate manner that represents failures seen *in vivo*. In this regard the testing method has to be

relatively inexpensive, easily set-up and carried out. The results must also be highly repeatable so that the same tests can be carried out by different laboratories revealing the same results. The ideal test would be one that cyclically simulates the three-dimensional movements and forces that an implant experiences *in vivo* (Paul, 1997). Testing methods should therefore be based on clinical experience and the total testing time has to be a reflection of *in vivo* experience. A number of mechanical testing methods have been proposed. These are discussed in sections 2.2.1-2.2.3.

2.2.1 TESTS FOR MODULAR SYSTEMS

Modular systems are increasingly designed and used today to provide the surgeon with flexibility and to address a host of issues associated with the patients' condition during surgery without having to use a custom-made prosthesis. Modular systems include the use of wedges, spacers and stem extensions. These modular systems are often used for patients where there is inadequate stability of the tray due to loss of bone or bony defects. Areas of concern with a tray requiring a stem extension (tray-stem) configuration are the structural integrity of the tibial tray itself as well as the stem extension, disengagement of the stem and tray connection and fretting at the stem and tray connection. The safety and performance of this type of constructed device has to be ascertained because there is greater opportunity for possible failure compared with a component without accessories. Cooper et al. (1997) proposed three different testing methods for modular tibial trays with stem extensions. These tests are representative of worst case conditions and in each case they identify the advantages and limitations.

2.2.1.1 Cantilever Test

The first of the tests described is the cantilever test. This test is based on the occurrence of an over-reamed tibia allowing the tibial stem to move within the canal so that it impacts against one of the endosteal surfaces, generating a bending load on the tibial stem. The tibial tray and stem are positioned so that the stem is horizontal and the superior surface of the tray is fixed as shown in figure 2.7.

A compressive sinusoidal fatigue load is then applied to the distal part of the stem. The stem then experiences bending and the tray-stem connection undergoes severe bending loads. One method, to determine a suitable magnitude for the fatigue load, would be to strain gauge a cadaver and load it as *in vivo*. The strain levels recorded are then matched to a load that would create the same level of strain in the Cantilever Test position. To determine the position of high strain, finite element analysis could be used.

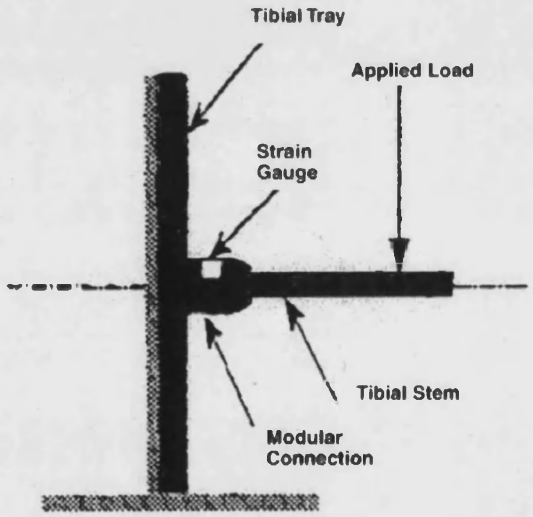

Figure 2.7: The Cantilever Test
(Cooper et al., 1997)

2.2.1.2 Unsupported stem test

The second test is the unsupported stem test which aims to test the tibial tray-stem construct under conditions where there is complete bone loss from the tray and stem. In this configuration only the most distal part of the stem is rigidly fixed. The tray is loaded eccentrically using a compressive sinusoidal fatigue load (refer to figure 2.8). The tray, stem and tray-stem connection all undergo extreme bending loads and hence any or all of the modular parts are subject to failure. The tray-stem connection can be examined for fretting and corrosion.

However, if the stem undergoes extreme elastic deformation the loading point may slip from its intended area and this may mean that the position of loading may require constant adjustment during the running of the test. Overall, Cooper et al. (1997) concluded that the condition upon which the test is based rarely occurs *in vivo*. This is because the patient would experience high levels of pain and would undergo a revision operation prior to implant failure and so this test configuration may be an exaggerated representation of bone loss.

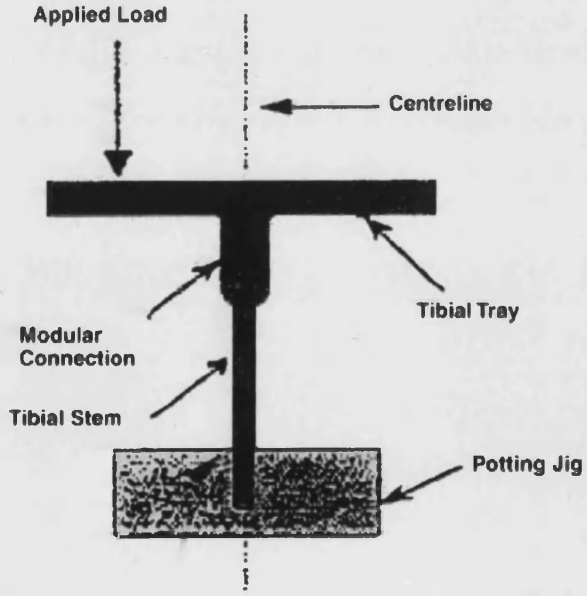

Figure 2.8: Unsupported stem test
(Cooper et al., 1997)

2.2.1.3 Partial Support Test

The final test method proposed is called the partial bone support. This is similar to the unsupported stem test but a smaller amount of bone loss under the tray is represented. This provides more support to the stem extension and reduces the stress distribution through the tray-stem connection and the tibial tray and thus may be more representative of *in vivo* conditions. The requirements of this test are that the stem is rigidly fixed at some point below the tray-stem connection (i.e. 25mm) thus representing only a small amount of bone loss. The tray is then eccentrically loaded at a defined position from the anteroposterior and mediolateral centreline (refer to figure 2.9). A compressive sinusoidal fatigue load is then applied to the structure from which a load versus cycle to fatigue curve can be developed to determine the fatigue integrity of the tray-stem configuration.

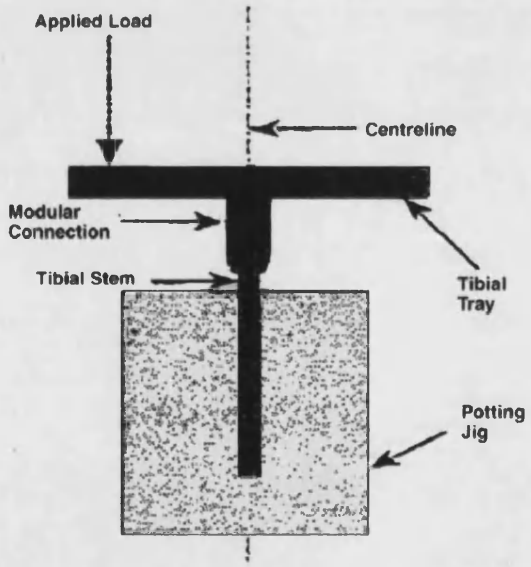

Figure 2.9: Partial bone support test
(Cooper et al., 1997)

2.2.2 THE SULZER MEDICA TEST

Sulzer Medica (Zurich, Switzerland) has developed an alternative testing method to the International Standards Organisation (ISO) and American Standards for Testing and Materials (ASTM) protocols. They began developing a testing method to eliminate the incidence of fracture of their own tibial tray designs, prior to the establishment of the ISO test protocol.

This testing method examines not only the fatigue strength of the tibial tray but also the stem and the connection between the stem and the tibial tray (figure 2.10). This test is also based on a worst case *in vivo* loading situation, characterised by a varus alignment and collapse of the medial compartment (figure 2.11). Two polyurethane blocks placed underneath the medial and lateral compartments of the tibial component support the tray. The Young's modulus of the lateral block is higher than that of the medial. This reflects the poor medial support often found in cases of fracture and a stronger lateral support. Only the medial compartment is loaded at 4000N. In addition, the stem receives a load by a reaction force acting at the distal part of the stem. The test is carried out in an environment of Ringer's Solution, at a frequency of 6 Hz and 37°C.

Only Sulzer Medica has validated this test method. They used designs of their own trays that had failed *in vivo* due to fracture. They concluded that the test is more physiological than the proposed ISO test because high load values above the peak force during the normal walking cycle (2000N) can be used. Tray fractures patterns produced during their fatigue tests mimicked those found *in vivo* (2.12). However, the fracture pattern varied each time the test was performed for the same tray. Using such a method, there is no repeatability of the test results and hence does not allow tray comparisons to be made between laboratories. In addition, the rationale of the test is that the distal part of the stem becomes in contact with the cortical shell. From retrieval studies discussed in detail in sections 2.1.4, 2.1.6 and 2.1.8, it is commonly reported that for fractured trays the stem was well fixed with

difficulty in removal at the time of revision. Clarke and Trousdale (1999) reported that radiolucency about the stem was minimal in the majority of the cases they studied. It would be expected that in the Sulzer Medica rationale, micromovements would occur at the position where the stem came into contact with the cortex (figure 2.11). If this was the case then fibrous tissue would be more prevalent in these areas of the stem. The clinical evidence does not suggest this.

The disadvantages of this test method are the increased complexity of the test set-up (when compared with the ISO test method) and reduced reproducibility of the test results. The test method uses very specific material properties for the supporting blocks. The availability and reproducibility of these blocks may also be difficult.

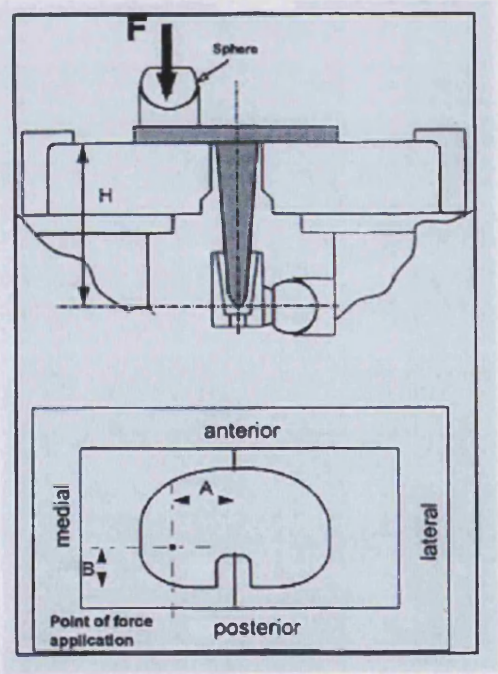

Figure 2.10: The Sulzer Medica test set up.
(courtesy of Sulzer Medica)

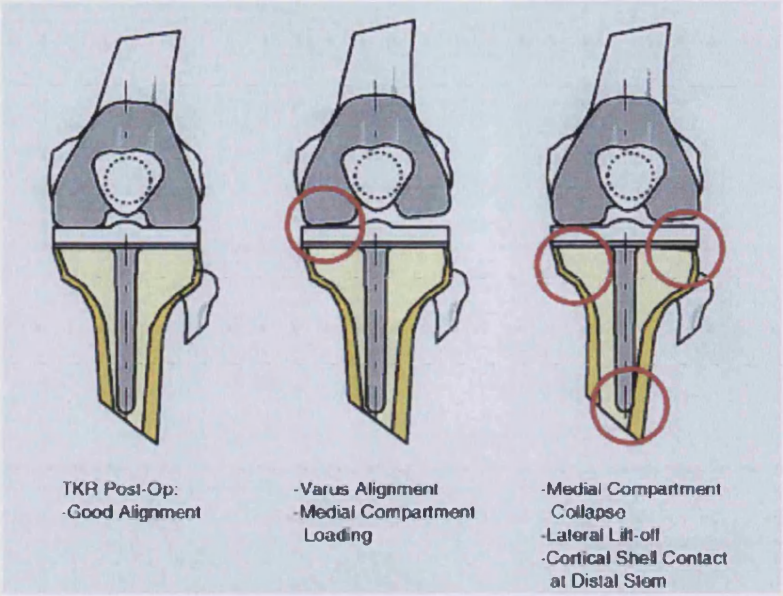

Figure 2.11: The rationale behind the Sulzer Medica testing method.

(courtesy of Sulzer Medica)

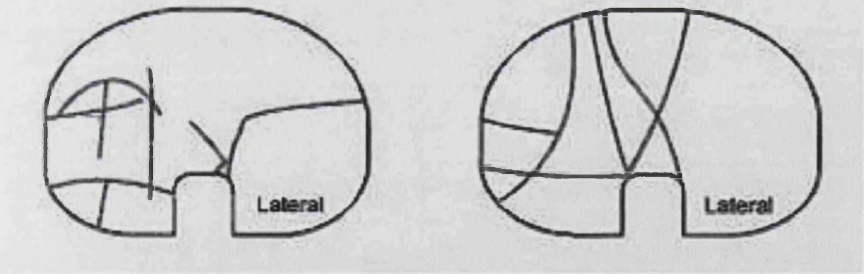

(a) **(b)**

Figure 2.12 (a) fracture lines produced from the Sulzer Medica test;

(b) fracture lines produced *in vivo*.

(courtesy of Sulzer Medica)

2.2.3 INTERNATIONAL STANDARDS ORGANISATION TEST

A test has been proposed by the International Standards Organisation (ISO), which aims to determine the endurance properties of tibial trays with respect to materials, manufacturing and design variables. The types of trays considered are metallic, covering both the medial and lateral plateaus of the tibia. The test method is based on the most commonly reported mechanism for fracture. The literature on this subject revealed that fracture has occurred when the central stem is firmly anchored and support of the lateral or medial condyle is absent (Mendes et al., 1984; Gradisar et al., 1989; Flivik et al., 1990; Maruyama et al., 1994; Abernethy et al., 1996; Clarke and Trousdale, 1999).

In this test, the tibial tray is mounted as a cantilever beam such that the medial condyle is completely unsupported. Only the unsupported condyle is loaded because during varus alignment of the knee the majority of the loading occurs through the medial portion of the tray. The tray is loaded through a polyethylene (UHMWPE) spacer, using a metal spherical indentor with a cyclic constant amplitude force, perpendicular to the undeflected superior surface. The polyethylene spacer is attached to the tibial tray using epoxy resin adhesive. The load is applied using a sinusoidal waveform with an R ratio of 0.1 (maximum load to minimum load). The environment in which the test takes place is not defined. The load is positioned at a predefined location relative to the tray. This contact location was defined as being at a known distance from the anteroposterior centreline, $d_{ml} = {}^1/_3 w$ and from the mediolateral centreline, $d_{ap} = {}^1/_4 d$ where w and d are the maximum anteroposterior and mediolateral dimensions of the tray respectively. In 1997 the draft standard was modified and the location for load application was redefined as being the femorotibial contact position at 0 degrees flexion. To date (February, 2002) the ISO committee has not defined the magnitude of the applied load.

The tibial component is fixed in such a manner that it takes into account the tray design including support features such as keels. If the tray is asymmetrical then it is fixed so that maximum bending moments occur about the tray centre-line. Figure 2.13 shows the test configuration for a tray without central support. Figure 2.14 shows the test configuration with central support.

The load is applied until the test specimen exhibits failure or until 5 million cycles is achieved. The tray is examined for crack formation or fracture throughout the test.

The draft ASTM standard (Draft H – January 1997), which shares the same reasoning as the proposed ISO test method, has a number of variations. The test specimen is set-up as in the ISO test but tray size is accounted for (the greater the size the larger the bending moments); the test is also run for 10 million cycles. In addition they propose an alternative method for loading the tray. Rather than use a spherical indentor, loading can be achieved using a matching femoral component to apply the load with a greater distribution on the medial condyle. Researchers specify that the load distribution is larger on the medial condyle but differ between a ratio of 60/40 or 80/20. To date (February 2000) the magnitude of the load has not been defined.

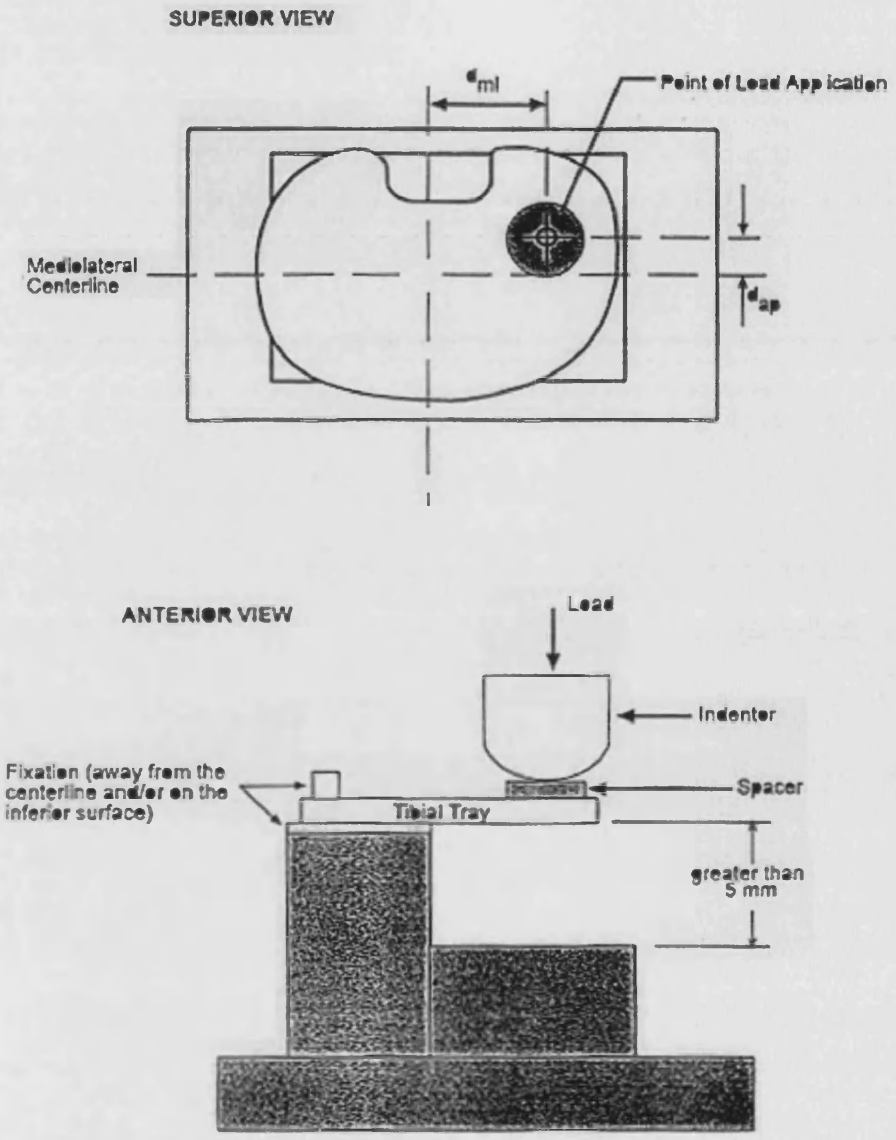

Figure 2.13: The test set-up for a tray without central support (ISO/CD 14879-1)

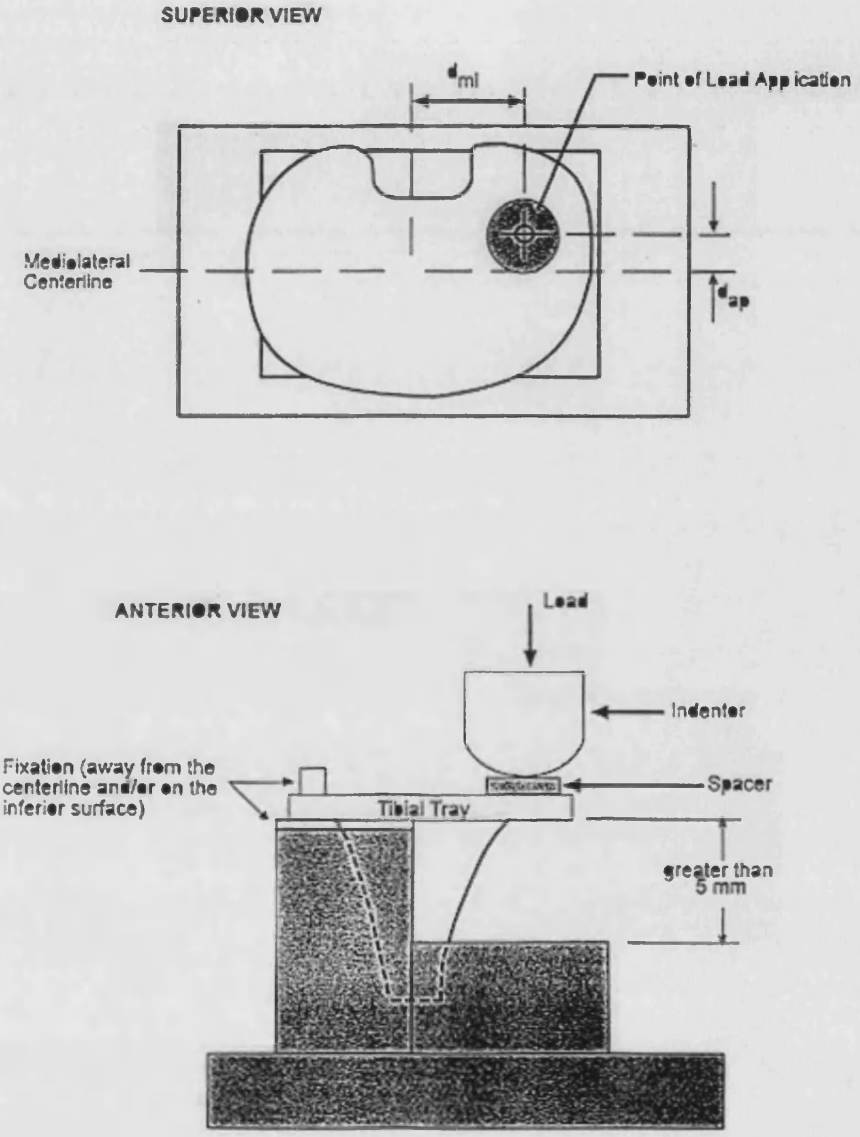

Figure 2.14: The test set-up for a tray with central support (ISO/CD 14879-1)

2.3 HYPOTHESIS AND AIMS

The hypothesis investigated by this study is that the testing method proposed by the ISO committee for determining the fatigue performance of tibial trays is clinically relevant.

In the context of this project clinical relevance is defined as "being representative of failures seen *in vivo*". The study carried out to determine if this hypothesis is correct comprised a number of steps.

1. establish a specific load for the ISO test for defined contact positions;
2. determine whether the stress patterns of tibial trays under the ISO test are representative of clinical findings by comparing with:
    a. fracture patterns from retrieved trays that have fractured,
    b. stress patterns predicted by an FEA model of tibial trays implanted in bone.
3. develop alternative testing methods and compare test results with clinical retrievals of tibial trays.
4. make a final recommendation for the testing of tibial trays.

CHAPTER THREE:
INTRODUCTION TO THE THEORY OF FRACTURE

3.1 FRACTURE

Fracture of solid components arises from a combination of factors including mechanical stresses, thermal and chemical influences, improper choice of material, conditions of services and manufacturing technique. Fracture results in separation of the component into composite parts.

Under static loading, ductile materials exhibit characteristic behaviour shown in figure 3.1a. Brittle materials, however, show very little extensions prior to fracture with little or no necking. Hence, the partially plastic region of the graph is much reduced (figure 3.1b).

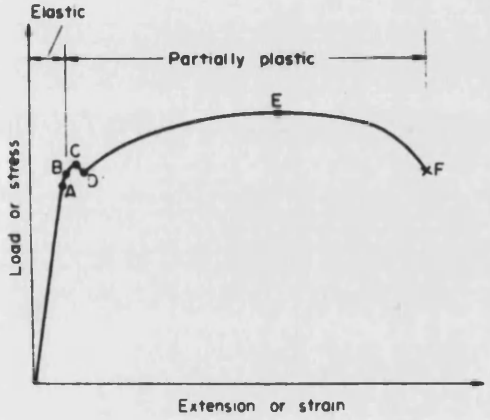

A = Limit of proportionality
B = Elastic limit
C = Upper Yield Point
D = Lower Yield Point
E = Ultimate tensile strength
F = Fracture

(a)

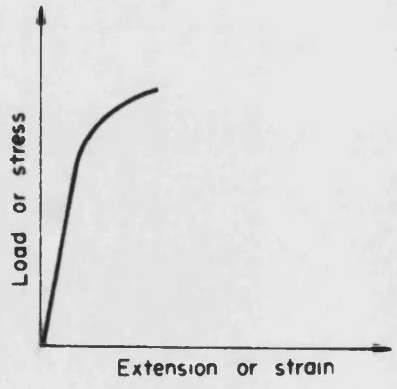

(b)

Figure 3.1: The behaviour of (a) ductile material (b) brittle material under static loading. (reproduced from Hearn, 1985)

3.1.1 METALLIC STRUCTURE

Metals are crystalline in structure. The external shape of each individual crystal is irregular (although the particles within these crystals are arranged in some regular pattern). The irregular outer surfaces of the crystals interface directly with neighbouring crystals, with few voids between individual crystals. These irregularly shaped crystals are called grains and the borders between adjacent grains are called grain boundaries. Grains can vary in size from a few microns to several millimetres.

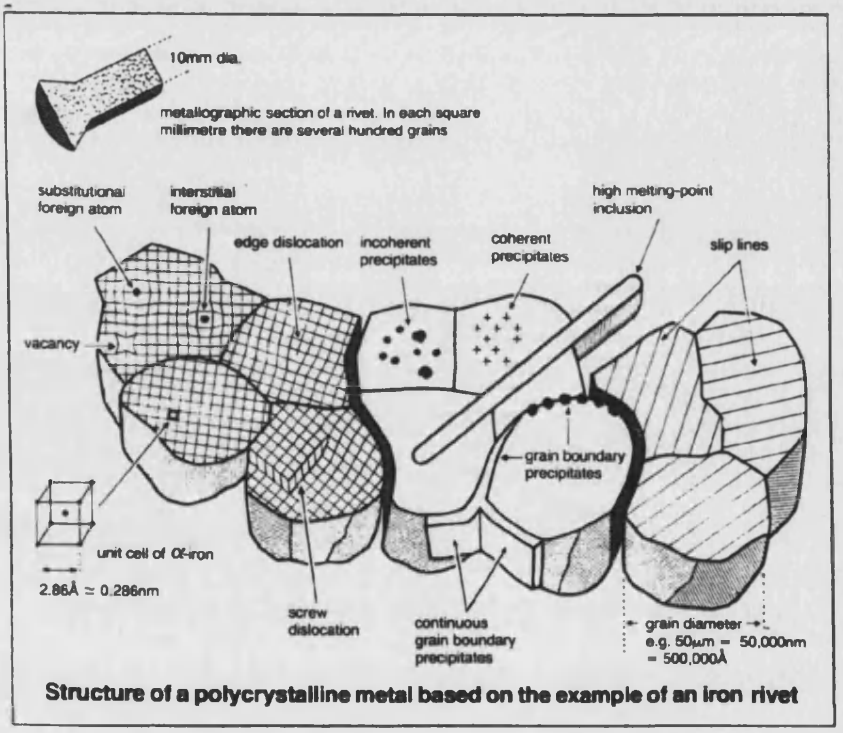

Figure 3.2: Grain structures in metals.
(reproduced from Engel and Klingele, 1981)

In a pure metal all atoms are of the same kind and size. The atoms arrange themselves in the closest possible packing patterns that are associated with positions of minimum potential energy. Metals, in general, crystallise in one of three principal types of structure:

(i) close-packed hexagonal structure (CPH)

(ii) face-centred cubic (FCC)

(iii) body-centred cubic (BCC)

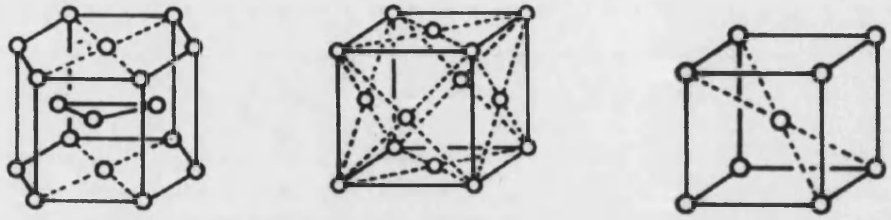

(a) (b) (c)

Figure 3.3: Metallic structures: (a) close-packed hexagonal (CPH) (b) face-centred cubic (FCC) (c) body-centred cubic (BCC) (reproduced from Higgins, 1977)

The face centred cubic and hexagonally close packed crystal structures of metals may be regarded as the stacking layers of hexagonally arranged atoms. These structures may be represented by the stacking sequences of ABCABC and ABABAB respectively. These layers indicate the position of the nearest neighbours in adjacent layers. For some metals the stacking sequences may be broken and this is called a stacking fault. The stacking sequence may become CABC|BCAB where | denotes a symmetry plane of the resulting fault sequence. The stacking fault affects crystal growth, dislocation motion and deformation processes. A low stacking fault energy (SFE) indicates that the energy cost of forming the fault is small compared to the energy gained by moving different layers apart.

Metals posses the ability to deform under the influence of externally applied forces. Stresses are relieved by means of slip processes. Slip is the movement of atoms sliding over each other. However, slip is not a simultaneous process of displacement of many atoms in the same direction for the same distance. Depending on the type of metal lattice the crystal possesses a variable number of slip systems involving a combination of slip direction and slip planes. The movement of dislocations will eventually be halted by such obstacles as grain boundaries, other groups of dislocations

and imperfections along the slip plane. If the acting stress is increased, new dislocations will be initiated in the structure and slip will continue until all available slip planes have been used up, so that the movement of dislocations is no longer possible. As deformation proceeds, the metal becomes harder and stronger and a stage is reached when further deformation is impossible. At this stage, when tensile stress and hardness are at a maximum and ductility is at a minimum, the material is said to be work-hardened. Any further increase in stress will lead to fracture.

The result of the slip process can be seen in the light microscope or the SEM as slip lines or slip steps that delineate the regions of the grain that have been moved relative to one another. In each successive grain, slip must be reinitiated by the stresses produced by the surrounding grains. Slip takes place on specific crystallographic planes in a given metal. Generally these slip planes are the atomic planes of greatest interplanar spacing since the forces between the sliding planes will be at a minimum. Within the planes the greatest density of packing is present. In the CPH structure such slip is limited since it will occur mainly along basal planes of the hexagon. Thus most metals with a CPH structure are much less ductile than those with a face centred cubic structure. Body-centred cubic structures are also less ductile than FCC structures.

Sometimes it is important to describe a particular plane upon which dislocation occurs. Miller indices were set-up to define crystallographic planes and crystal faces relative to crystallographic axes. Miller indices are proportional to the reciprocals of the intercepts, which the plane makes with the three principal axes (x, y, and z) of the system (refer to figure 3.4). In this example the intercepts are 3,1,and 2 in x, y ,and z respectively. The reciprocals of these are taken $(\frac{1}{3}, 1, \frac{1}{2})$ and then these numbers are then converted to the smallest integers in the same ratio (i.e. 2,6,3). So the plane described in figure 3.4a is represented by the Miller indices (263). Other examples are given in figure 3.4(b-d).

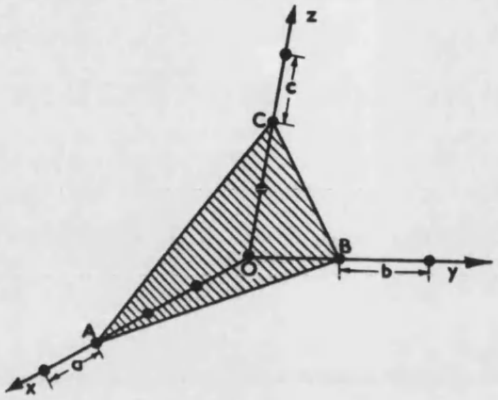

(a)

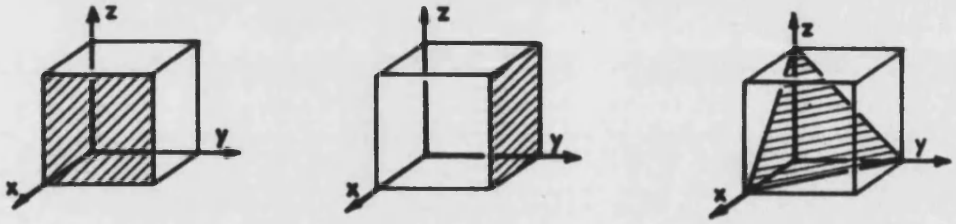

(b) (c) (d)

Figure 3.4: (a) plane 263 (b) plane (100) (c) plane (001) (d) plane (111)

(reproduced from Higgins, 1977)

3.1.2 FATIGUE FRACTURE

Fatigue fracture is a particular case of fracture that occurs in components that are subjected to alternating loads. Fracture occurs at stress levels below both the yield and ultimate tensile stress of the material. Experimental data conducted by Fairbairn (1861) and later Wohler (1870) showed that there was a relationship between the amplitude of the alternating load and the number of cycles at which a material fails due to fatigue fracture. From this relationship the fatigue limit was defined. This is the stress condition which a

material may endure an infinite number of cycles prior to failure. However, very few materials exhibit a fatigue limit. A more realistic criteria for fatigue is the endurance limit or fatigue strength. This is the stress condition under which a specimen would have a fatigue life of N cycles.

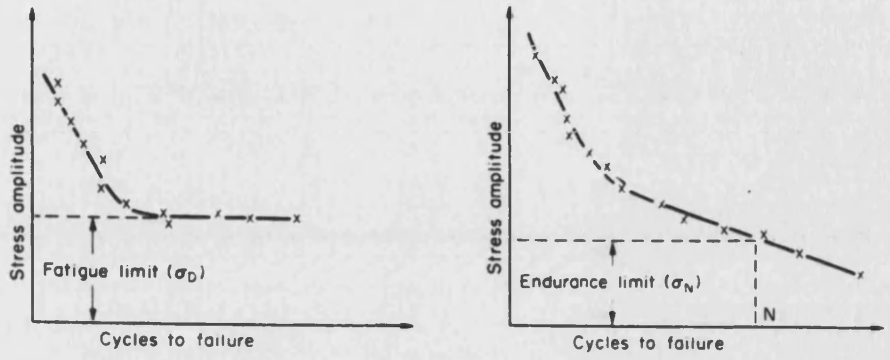

(a) (b)

Figure 3.5: S/N curve showing (a) fatigue limit (b) endurance limit (reproduced from Hearn, 1989)

Fatigue is characterised as either low cycle or high cycle. Low cycle fatigue is caused by high fluctuating stresses and strains that result in a lifespan ranging from 1 to 10,000 cycles as opposed to high cycle fatigue (HCF) where the lifespan is more than 10,000 cycles. Low cycle fatigue experiences larger plastic deformation prior to failure whereas high cycle fatigue has only macroscopic zones of plasticity very close to the crack tip. The process by which fatigue fracture occurs is complicated. It is characterised by three stages (figure 3.3). Stage I is the initiation of a crack from points of high stress concentration (such as defects, sharp changes in cross-section slag inclusions and tool marks). The crack then grows along some favourably oriented direction in the microstructure. Eventually the crack will become sufficiently large so that the microstructure has little effect on the direction of growth of the crack. The crack then proceeds to propagate on average in a plane normal to the maximum principal stress direction. This is stage II. When the crack reaches a critical value it accelerates more rapidly and catastrophic failure occurs. This accelerated growth is classified as stage III.

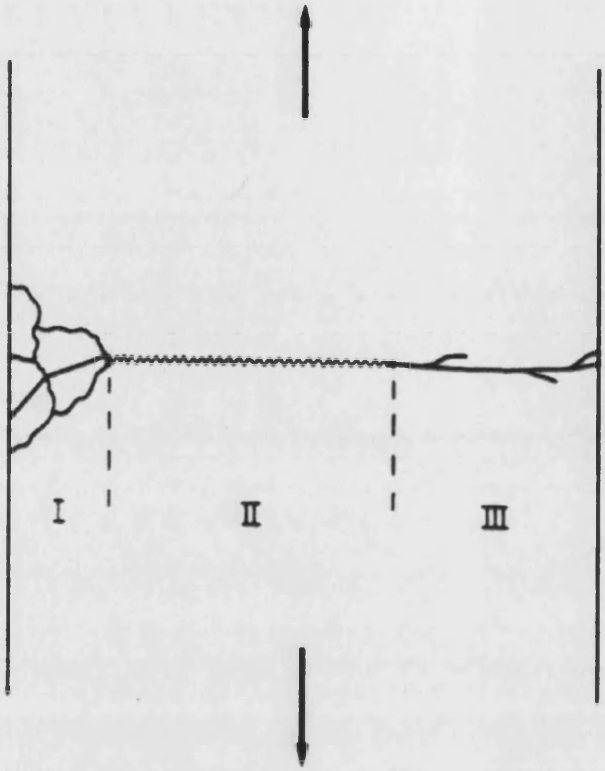

Figure 3.6: The three stages (I, II, III) of fatigue crack growth. (reproduced from Hearn, 1989)

3.1.3 STAGE ONE

Cracks normally initiate at a free surface. This free surface may be perfectly smooth but crack initiation is considerably facilitated by irregularities in the surface. Notches, grooves, scratches, surface finish, and cracks formed by sandblasting or surface damage caused by fretting can be initiation sites for fracture. Microstructural features such as brittle intermetallic particles, second phases and grain boundaries are often suspected of causing crack initiation. However, defects within the structure can act as stress-raisers that initiate the growth of the cracks. In addition, the design of the component, in particular changes in cross-section and stress concentrations as well as the environment within which it operates can also severely reduce its fatigue life.

Scanning Electron Microscope (SEM) micrographs of intrusions and extrusions have shown that the process is associated with the formation of micronotches and microcracks. The cracks propagate at an angle of approximately 45° to the tensile stress and the surface. These 45° cracks can also be identified as the narrow initiation zone on fracture surfaces after failure. The most important difference between slip bands formed by steady stress and those formed by cyclic stress is that the latter produces a slip band groove. The groove deepens with continued cyclic stress to form a crevice or intrusion.

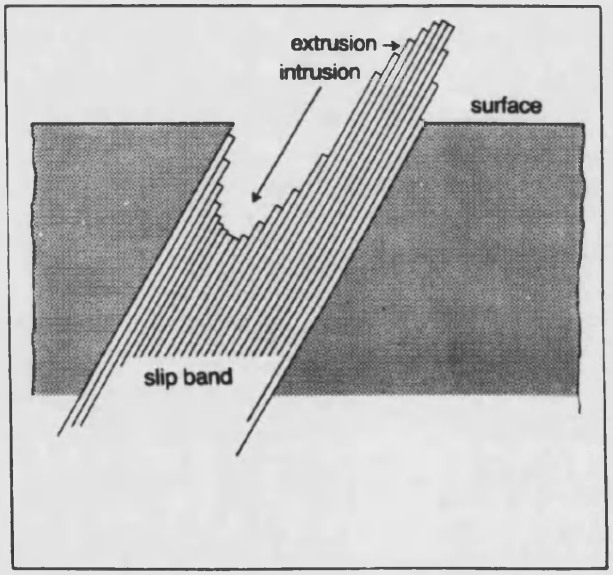

Figure 3.7: A slip band groove.
(reproduced from Engel and Klingele., 1981)

3.1.4 STAGE TWO

At some point, usually when the crack encounters a grain boundary Stage I is replaced by Stage II growth in which the crack is normal to the maximum principal tensile stress. Close examination of the fractured surface shows that over that part associated with stage II, there are a number of fine lines called striations (figure 3.8). The striations are ridges in the fracture surface. Each line being produced by one fatigue cycle and the spacing of the striations represents the local crack growth during a stress cycle.

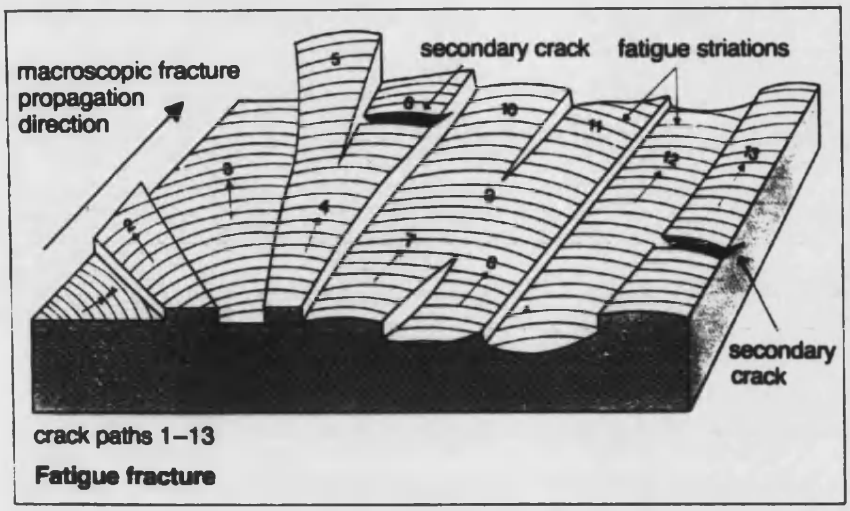

Figure 3.8: Characteristics of Stage two crack propagation (reproduced from Engle and Klingele, 1981)

Crack fronts do not extend at a constant rate over their whole length. Differences in the material locally may cause the growth rate to change in different regions of the structure. The material adjacent to the crack tip is subjected to alternating plastic strains, which lead to cumulative plastic damage and a weakening of the structure so that the crack can propagate.

Macroscopically crack propagation in Stage II shows characteristic propagation patterns. These are indicated by the beach marks (figure 3.9) on the fatigue fracture surface and also by the crack front at the transition to final catastrophic fracture. The beach marks lying parallel to the fatigue striations form due to changes in loading and/or due to changes in the crack tip environment and the surface layers that subsequently form.

(a)

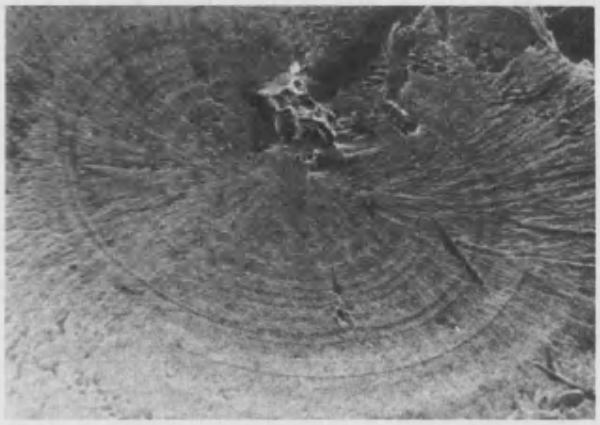

(b)

Figure 3.9: Characteristics of stage two crack propagation.
(a) Beach marks observed in the PCA tray (Maruyama et al., 1994).
(b) A fatigue crack, which initiated at shrinkage porosity inside the material, showing beach marks (Engel and Klingele, 1981).

3.1.5 STAGE THREE

Once the fatigue crack has reached some critical length such that the energy for further growth can be obtained from the elastic energy of the surrounding metal, catastrophic failure takes place. This accelerated growth is classified as Stage III. The final fracture area is frequently rougher than the fatigue growth area. Sometimes it may show evidence of plastic deformation before final separation. Stage III growth is usually a small fraction of the total lifetime of a fatigue crack and often neglected in the assessment of the maximum number of load cycles.

3.1.6 FRACTURE MECHANICS

The relationships involved in the process of fracture are termed fracture mechanics. Griffith (Parton, 1982) made an important contribution to this field in 1920. He established that a crack would propagate in a body if work were done which causes the formation of new surfaces in a material. He concluded that the work done is proportional to the crack length. His study was limited to only brittle materials such as glass.

Professor George Irwin (Parton, 1982) working on ships in 1948 studied fracture from a different perspective. He was particularly interested in the vicinity around the crack tip. He showed that the only parameter determining the stressed state of the tip zone is the stress intensity factor, K. For a two dimensional geometry shown in figure 3.10, the stress intensity factor is defined as

$$K = f\sigma\sqrt{\pi a}$$

where **K** = stress intensity factor
f = compliance function that describes the geometry of the part
σ = applied stress
a = length of the crack

The stress intensity factor can be calculated for different loading modes and these formulations can be obtained from standard fracture textbooks.

A theory was then developed called the Griffith-Irwin theory, which was designed to compute the crack propagation based on the fundamental assumption that the material was linearly elastic and the fracture was brittle. This method basically approaches the crack propagation problem in two-dimensional space.

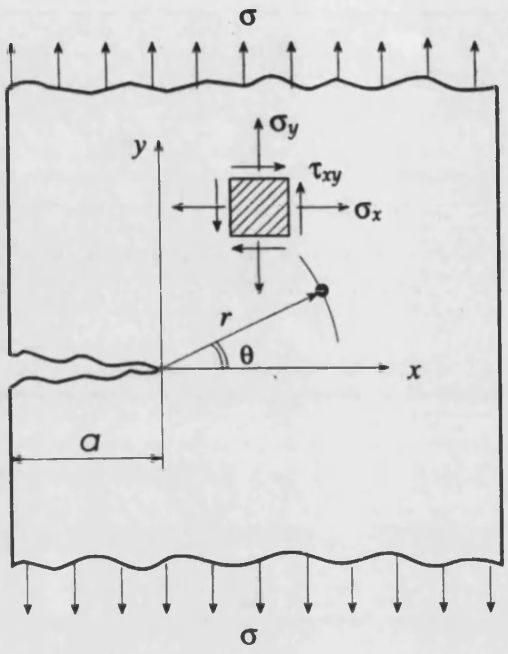

Figure 3.10: A two- dimensional body subjected to a crack (reproduced from Zahavi, 1996)

3.1.7 CRACK GROWTH RATES

The rate at which cracks grow is an important phenomenon. There is a minimum value of ΔK below, which the crack will not propagate. This is termed the threshold value or ΔK_{th} and is usually determined when the growth rate falls between 10^{-7}mm/cycle, or roughly, one atomic spacing. Growth rates of 10^{-9} mm/cycle can be detected but at this point measurement is being made only in a few areas of localised growth, over the whole crack front.

Stage Two growth is described by the Paris-Erdogan Law

$$\frac{da}{dn} = C(\Delta K)^m$$

where c and m are material coefficient

In this stage, the rate of growth of a fatigue crack is described in terms of the increase in crack length per load cycle, $\frac{da}{dn}$ where *a* describes crack length and *n* is the number of load cycles. This is related to the amplitude of the stress intensity factor ΔK. If the criterion for fracture is based on the stresses near the crack tip then the value of ΔK determines whether or not the crack will propagate. If the amplitude of the applied stress remains constant then as the crack grows, ΔK will increase. Such conditions produce growth-rate curves of the type shown in figure 3.11.

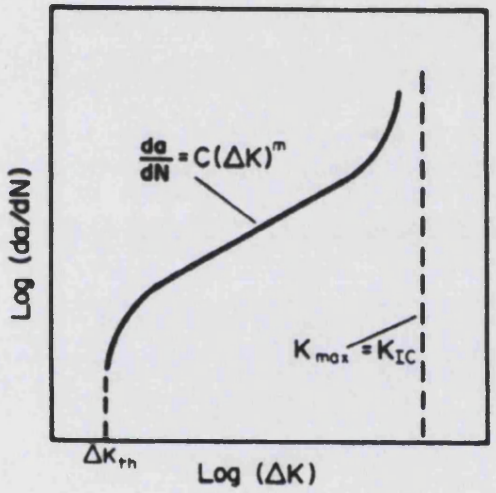

Figure 3.11: Crack growth rate curve. (reproduced from Hearn, 1989)

When K reaches a critical value the crack will become unstable. Thus when $K=K_{ic}$, stage III growth occurs.

This method of assessing crack behaviour can only be used for brittle materials or those with well-contained plasticity. If the plastic zone becomes extensive alternative methods have to be used to express the material's non-linearity.

3.1.8 PROBABILITY CURVES

The fatigue limit of a component is determined at a particular stress level. However, seemingly identical specimens may give widely different results. The scatter arises from many sources including variations in material composition, and heterogenity, variations in size, surface finish and axiality of loading as well as the presence of defects.

Probability curves (as shown in figure 3.12) can be created by testing a number of test pieces, at a variety of stress levels. The fatigue life of a material or component can then be estimated and the probability of failure at different stress levels can be assessed.

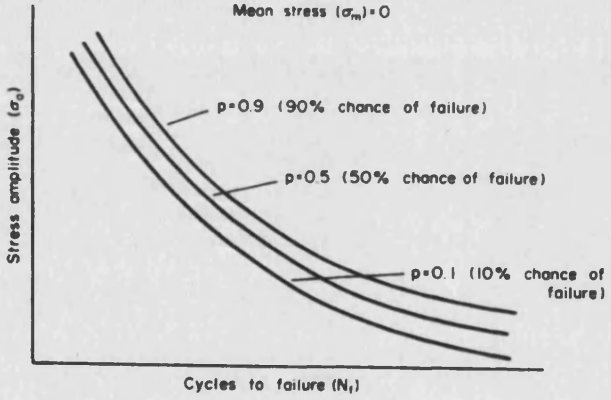

Figure 3.12: Probability curves.
(reproduced from Hearn, 1989)

3.1.9 CHARACTERISTICS OF COBALT-CHROME

CoCrMo alloy is a superalloy with excellent biocompatibility, wear behaviour, corrosion resistance, high strength and low ductility. In the cast form this alloy shows a cored cobalt-rich face centred cubic matrix with interdendritic precipitates and grain boundary precipitates including carbides and non-metallic oxide inclusions (Zhuang and Langer, 1990; Dobbs and Robertson, 1983).

In the cast form, CoCrMo alloy suffers from wide variability in mechanical properties and generally low mechanical integrity. This is because of random casting defects such as shrinkage cavities and a non uniform grain size which tends to reduce the alloy's tensile and fatigue properties (Zhuang and Langer, 1990).

Faceted fractures have been found to be the dominant feature of fatigue fractures in cast CoCrMo alloy (Zhuang and Langer, 1990). Faceted fracture features are indications of low fatigue strength of the alloy. Comparing the fatigue strength of alloys prone to faceted fatigue fractures with that of non faceted fracture alloys, the latter normally have a fatigue limit higher that their yield strength while faceted fracture alloys have a fatigue limit much lower than their yield strength.

Faceted fracture surfaces have a crystallography oriented fracture structure with cracks running in specific directions on the fracture planes (Zhuang and Langer, 1989a). Cast CoCrMo alloy also has a low Stacking Fault Energy (SFE). Alloys with a low ratio of fatigue strength to yield strength together with a low SFE are prone to faceted fatigue fracture because when a high stress or strain reaches a crack tip, slip on specific crystal planes, cannot be accommodated by appropriate deformation processes. This is because slip on specific crystal planes is restricted by some fine microstructural defects such as stacking faults. This results in critical cleavage stresses at the fatigue crack tip under a low applied load resulting in faceted fractures. The fine microstructural defects also affect the fatigue fracture characteristics of the alloy, leading to a brittle fracture mode (Zhuang and Langer, 1989a). This brittle fatigue fracture appearance in which crystallographically $\{111\}_{fcc}$ faceted fractures are found to be the dominant fatigue fracture feature and is characteristic of stage I fatigue growth. A number of investigators (Rostoker et al., 1978; Dobbs and Robertson, 1983) have shown extensive stage I fatigue behaviour in this alloy. The brittle fracture feature is very important for the application of this material to surgical implants as sudden and premature failure can occur (Rostoker et al., 1978).

Zhuang and Langer's (1989a) investigations of cast CoCrMo alloy show that the low stacking fault energy is considered to be the dominant factor for the development of faceted fatigue features in this alloy which affects the strain hardening behaviour and facilitates the formation of dense dislocations, stacking faults and twins.

Further investigations into the characteristics of cast CoCrMo alloy showed that near the crack tip there was a plastic zone (Zhuang and Langer, 1989c). Zhuang and Langer (1989c) found that within the plastic zone, local cyclic strain induced FCC to CPH transformation was taking place. This resulted in work hardening of the cast CoCrMo alloy. They suggested that the FCC to CPH transformations take place mainly in the plastic zone where the plastic strain amplitudes are large. They reported that strain induced FCC to CPH transformation normally takes place at or near precipitate particles and grain boundaries because a higher concentrated stress exists at the precipitate particles and grain boundaries. A TEM study (Zhuang and Langer, 1989a) also revealed the fact that the FCC to CPH transformation takes place and that a much higher density of dissociated dislocations, stacking faults and twins than that seen in the specimens before fatigue testing exists in the specimens, close to the fatigue fracture surfaces.

Investigations into other factors that affect the fatigue properties of cast CoCrMo alloy are:

(1) grain size

Zhuang and Langer (1989a) compared the behaviour of a coarse grain size with a fine equiaxed grain structure (produced by casting in a metallic mould) for a range of stress intensity values. They found that with both the fine and coarse grain structure there was little difference in the fracture characteristics of cast CoCrMo alloy.

(2) alloy additions

Zhuang and Langer (1990) showed that adding nickel improves the mechanical properties due to changes in the stacking fault energy (SFE). Adding minor additions of elements such as aluminium, titanium and boron as well as nickel results in improvements of the fatigue crack growth resistance. This is because the minor additions of these elements result in the elimination of some of the microstructural casting defects. Escobedo et al. (1996) showed that increasing the nitrogen content of the cast alloy produced fine carbides. This resulted in improvements of the yield, tensile and fatigue strength but a decrease in ductility.

(3) Stress intensity

Zhuang and Langer (1988) studied the effect of a range of stress intensity factors (25, 35 and 45 MPa$\sqrt{m}$). They found that there was no significant difference between the three ΔK values for stage I fatigue. They found that faceted fractures were the main features of the fracture surface. They measured that angles between facets and found them to be consistently within 5 to 10 degrees with $\{111\}_{fcc}$ plane orientations. At low Δk values the fracture surfaces show a rock like cleavage $\{111\}_{fcc}$ plane faceted fatigue fracture (refer to figure 3.13). At Δk values above 35 MPa$\sqrt{m}$ well developed block structures with steps, large facets with three plane orientation and abrupt height changes are observed (refer to figure 3.13a, b & c). A grain boundary is included in this region. A cluster-like facet fracture morphology is seen near the grain boundary and changes the orientation of facets at grain boundaries is also evident. High Δk values, 45 MPa$\sqrt{m}$ fatigue fracture surfaces still show faceted fracture characteristics with signs of normal fatigue striations (refer to figure 3.15a&b). Well-developed block structures with steps, large facets with three or four plane orientations and abrupt height changes are also observed. In the fine scale regions, tetrahedral as well as stair step morphology are clearly seen.

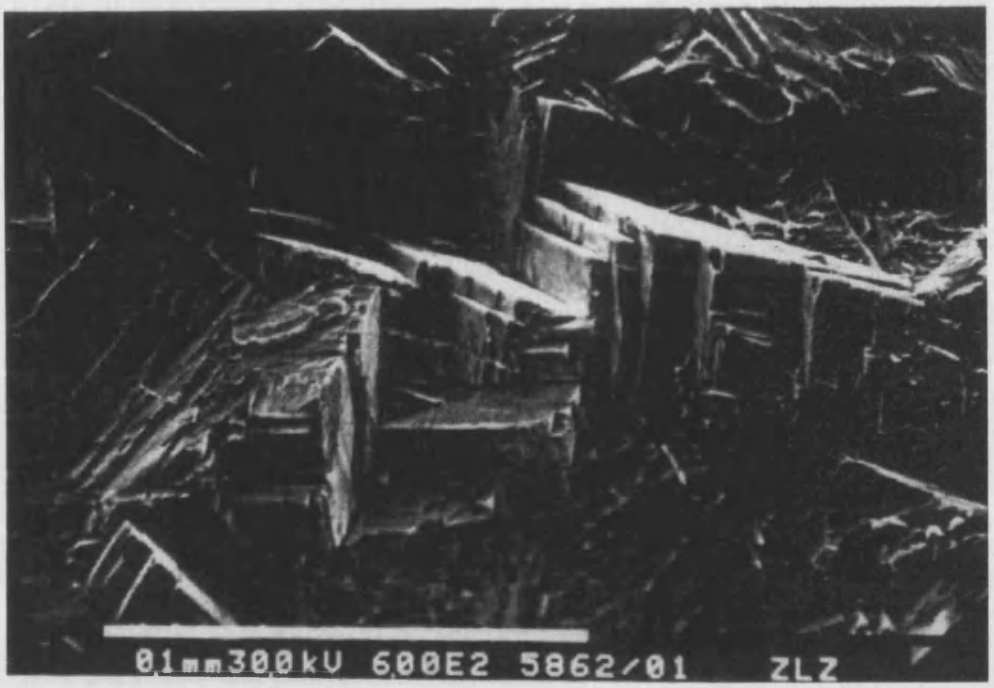

Figure 3.13: Fracture morphology at 25MPa $\sqrt{m}$.
(reproduced from Zhuang and Langer, 1989a)

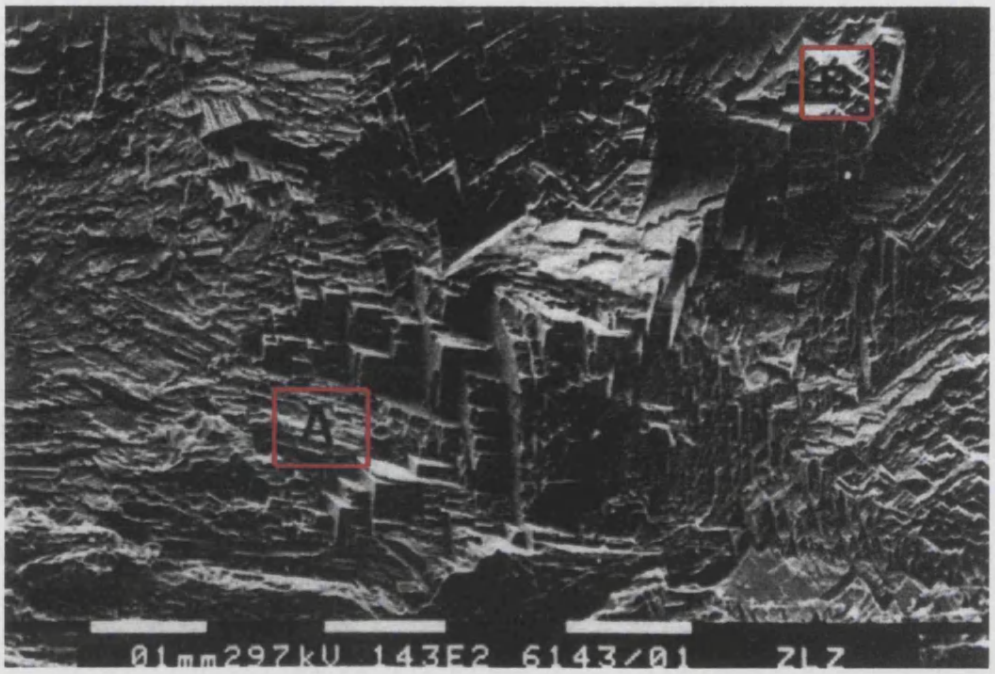

(a)

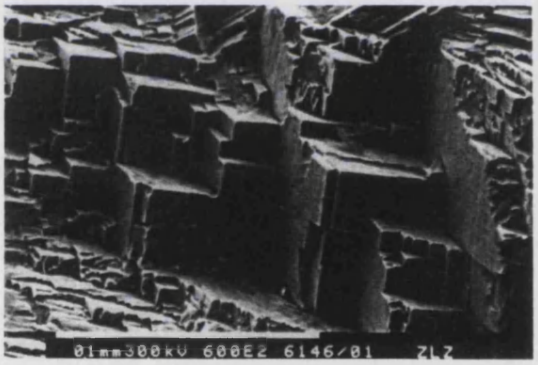

(b)

(c)

Figure 3.14: Fracture morphology at 35MPa $\sqrt{m}$
(a) general view (b & c) details of regions A and B in (a)
(reproduced from Zhuang and Langer, 1989a)

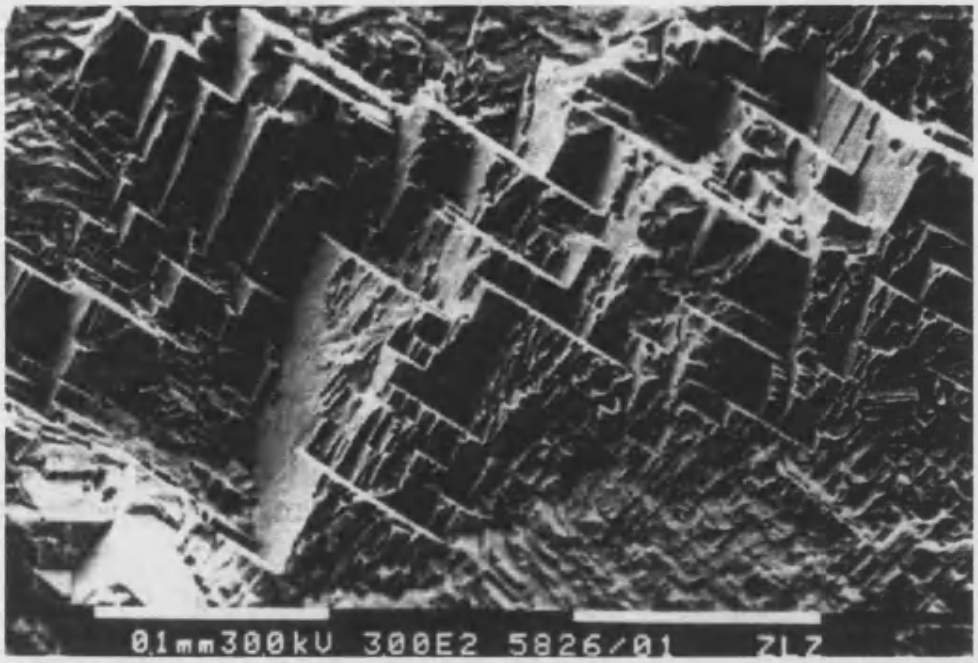

(a)

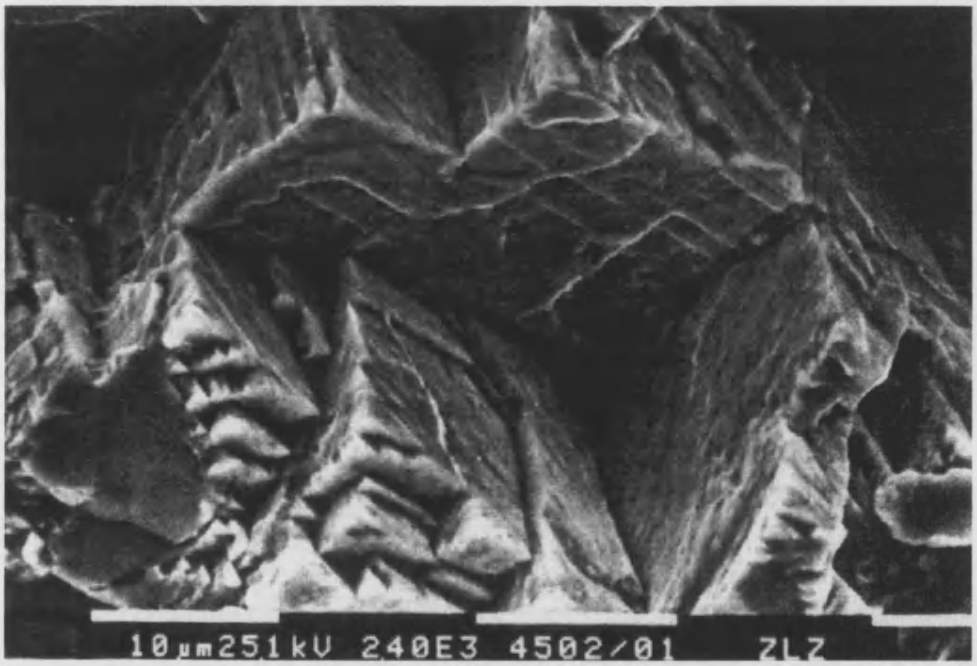

(b)

Figure 3.15: Fracture morphology at 45 MPa $\sqrt{m}$

(a) general view (b) high magnification

(reproduced from Zhuang and Langer, 1989a)

Brown and Gregson (2001) carried out studies to investigate the fatigue performance of cast CoCrMo alloy. They investigated the effect of environment, loading frequency, R-ratio (ratio of maximum to minimum load), effect of constant amplitude loading, and the effect of incorporating overloads into a baseline spectrum. Cast keel bars of CoCrMo alloy were obtained and subject to three point bend tests. The R ratio was varied from 0.1 to 0.7; frequency was varied from 5Hz to 20Hz; the environments used were air and Ringer's solution at 37°C. Their results showed that there was extensive stage I behaviour and this was characterised by large scale facetting appearing on the fracture surface. Stage II type growth was not observed until significant crack growth had occurred, and the crack began to propagate in a direction normal to the maximum applied load. Stage III was characterised by the presence of dimpling of the fracture surface and inter-dendritic growth.

They found that the effect of a change in R-ratio had a minor effect for the material. The physiological environment had little effect on crack growth behaviour for the majority of the component lifetime. A change in the test frequency from 5 to 20Hz had minimal effect on the fatigue crack growth of CoCrMo alloy. They found that under a constant amplitude loading, the fracture characteristics showed an extensive stage I fatigue crack growth with $\{111\}_{fcc}$ faceting. However, with a variable amplitude loading, the fracture surface was almost featureless with smaller facets at higher ΔK values and there was a reduction in crack growth rate compared to the constant amplitude loading test. They attributed this reduction in growth rate to crack closure. Hence they concluded that constant amplitude loading was more damaging than variable amplitude loading.

A number of heat treatment and alloy addition methods have been used to improve the tensile properties of CoCrMo alloy (Dobbs and Robertson, 1983; Kilner et al., 1986; Zhuang and Langer, 1989a & b). These include solution heat-treatment for 1 hour at temperatures of 1473K to dissolve any interdendritic material remaining after casting and to homogenise the

microstructure. This increases ductility when compared with the as cast alloy (Kilner et al., 1986). These researchers have found that when examining the effect of heat treatments on cast CoCrMo alloy, improvements in ductility, yield and tensile strength could be achieved. They found that improving fatigue strength was difficult due to porosity. However Dobbs and Robertson, (1983) found that the fatigue strength could be improved if the grain boundary was removed. In their study they found that a partial solution treatment resulted in a significant improvement of the fatigue properties of the alloy. They also noted, however, that although this heat treatment improved the mean fatigue life, scatter in the results remained. They attributed this variability to minor casting defects such as porosity.

3.1.10 CHARACTERISTICS OF TITANIUM

Titanium alloy (Ti6Al4V) is used in orthopaedics because of its superior biocompatibility, low toxicity and it is well tolerated by bone and soft tissue. It also has good mechanical properties, in particular a low elastic modulus.

Titanium (in its elemental form) has a hexagonal close packed crystal structure, α, up to the beta transus (882.5°C) transforming to a body centred cubic (BCC) β above this temperature (Long and Rack, 1998). Titanium alloy is a two phase transus α-β material where alloy additions contribute to increased strength by solid solution strengthening mechanisms. Aluminium (Al) has a much greater solubility in α titanium and tends to increase the transformation between α and β phases. Vanadium (V) decreases the transformation between the α and β phases, stabilising the β phase. The combination of both Al and V enables both α and β phases to co-exist at room temperature.

Fatigue in titanium alloys (in the absence of defects and gross flaws) is controlled by the size, shape and texture of the primary α grains and the

amount and shape of the transformed β phase. The initiation of cracks involves slip bands that traverse α grains (Grosskreutz and Shaw, 1972; Stubbington and Bowen, 1974; Gerdes et al., 1979), α/β interface decohesion (Grosskreutz and Shaw, 1972; Stubbington and Bowen, 1974; Gerdes et al., 1979), α/β interface cracking (Grosskreutz and Shaw, 1972; Stubbington and Bowen, 1974; Gerdes et al., 1979), α/α grain boundary cracking (Grosskreutz and Shaw, 1972) or subsurface cracking of α grains (Gilbert and Piehler, 1989; Gilbert and Piehler, 1993).

The sensitivity of Ti alloy to fatigue depends on its surface condition. Gilbert and Piehler (1993) observed subsurface crack initiation in Ti6Al4V hip joint prostheses. Subsurface cracking was thought to be associated with compressive surface residual stresses (350-500MPa). Crack initiation occurred by damage accumulation on the pyramidal planes of primary α grains, which linked to form a fatigue crack. It was suggested that fracture of pyramidal planes was due to their higher slip directions causing higher damage accumulation/dislocation interactions. Fracture surfaces exhibited failure traversing several α grains with little change in fracture path orientation.

Leverant at el. (1994) explored the effect of surface residual stresses and topography on the fatigue properties of Ti6Al4V. Crack initiation was observed at machine grooves and the bottom of shot peening pits with the most important factors being sharpness (root radius) rather than depth. Shot peened samples exhibited improved fatigue lives. Sharp peening defects were found to initiate cracks at a low number of fatigue cycles but improved fatigue lifetimes resulted from the retardation of small crack growth by compressive surface residual stresses.

Another factor to consider is titanium's sensitivity to notching. Notch sensitivity is defined as being:

$$q = \frac{\text{effective increase of stress due to notch}}{\text{theoretical increase of stress due to notch}}$$

Notch sensitivity is a complex factor depending not only upon the material but also upon the grain size with a finer grain size resulting in a higher value of q than a coarse grain size.

The notch sensitivity of α/β titanium alloys is a critical factor in the performance of porous-coated implants for cementless prostheses, where the application of a bead or wire coated prostheses produces preferential crack initiation sites at the porous coating/substrate interface. Porous coated Ti6Al4V hip stems show a large reduction in the fatigue limit as compared to the smooth condition (Long and Rack, 1998).

Messersmith and Cooke (1990) investigated the effect of porous coatings on the fatigue life of Ti6Al4V. The coating consisted of one or more layers of metal beads that were sintered to the metal surface. These materials were found to possess fatigue limits one-third of that exhibited by the uncoated, polished material. It was suggested that detrimental microstructural changes during sintering and the sinter neck (where the beads joins the metal surface) acts as a stress raiser. Control of sintering time/temperature was found to greatly reduce the neck stress concentration.

3.2 RETRIEVAL STUDIES OF TIBIAL TRAYS

3.2.1 INTRODUCTION

A collection of retrieved tibial trays is held by the Centre for Biomedical Engineering (BME). These retrieved trays were sent to the department from a number of surgeons. It was important to examine these trays to ascertain initiation points, crack patterns and other features that may have affected the fatigue behaviour of the material as well as that of the tray designs. The purpose of this study was to characterise the crack patterns for each of the tray designs. Thereby obtaining data from clinical cases to compare with stress patterns generated from finite element models. Light microscopy and Scanning Electron Microscopy (SEM) were used to determine the initiation sites for these fractures. The aim was to ascertain if the crack patterns obtained under the ISO test conditions are clinically relevant and to develop a new method for testing tibial baseplates that would account for the manner in which fractures were initiated in trays that failed *in vivo*.

3.2.2 MATERIALS AND METHOD

Samples were booked in and labelled. Each sample was then photographed, including the fractured surfaces. Samples were cleaned prior to examination by light microscopy and SEM. If a sample had either cement particles or a cement mantle around the tibial tray, soaking in chloroform (BDH, UK) overnight dissolved the cement. This could take up to 2-3 changes of chloroform. Alcohol (Genta, UK) was used to remove traces of chloroform (as chloroform is not miscible with water). Each component was then placed in an ultrasonic bath with 5-10% quadraline (BDH, UK) in an appropriate glass receptacle. The samples were rinsed thoroughly in tap water followed by 2-3 rinses in distilled water. They were allowed to dry in air and then stored in a dust-free environment. Each sample was then examined using a light microscope and interesting areas were photographed. Areas were then selected for further examination using SEM. A Jeol 35C (JSM, UK) SEM was

used and the specimens were held in an appropriate holder and silver taped to provide good contact between the specimen and holder. Photographs were taken and developed. Eleven samples were examined under SEM. Representative samples of each type of tibial tray are presented in the results section.

3.2.3 RESULTS

The results show that a range of crack patterns was observed for both the Kinematic (refer to figures 3.16-3.18) and PCA (refer to figures 3.21-3.22) samples whereas crack patterns in the Total Condylar (refer to figures 3.19-3.20) developed in the anterior-posterior direction only.

3.2.3.1 The Kinematic Tray

Figure 3.16a shows all the components that had cracks that occurred across the surface of the tray. Figure 3.16b shows the two Kinematic trays that had cracks that grew into the depth of the tray. For both sets of fractures, secondary fractures were also present. Figure 3.17 shows an SEM of the fracture surface, which shows characteristic initiation points at the root of the notch. This was the only sample from the collection that showed evidence of beach marks. Other samples did not show this pattern. Using SEM, figure 3.18 shows another Kinematic retrieval. In this example, however, there was no evidence of beach marks. The SEM for this sample and all the other samples examined showed evidence of porosity, with characteristic stair step cracks and secondary cracks.

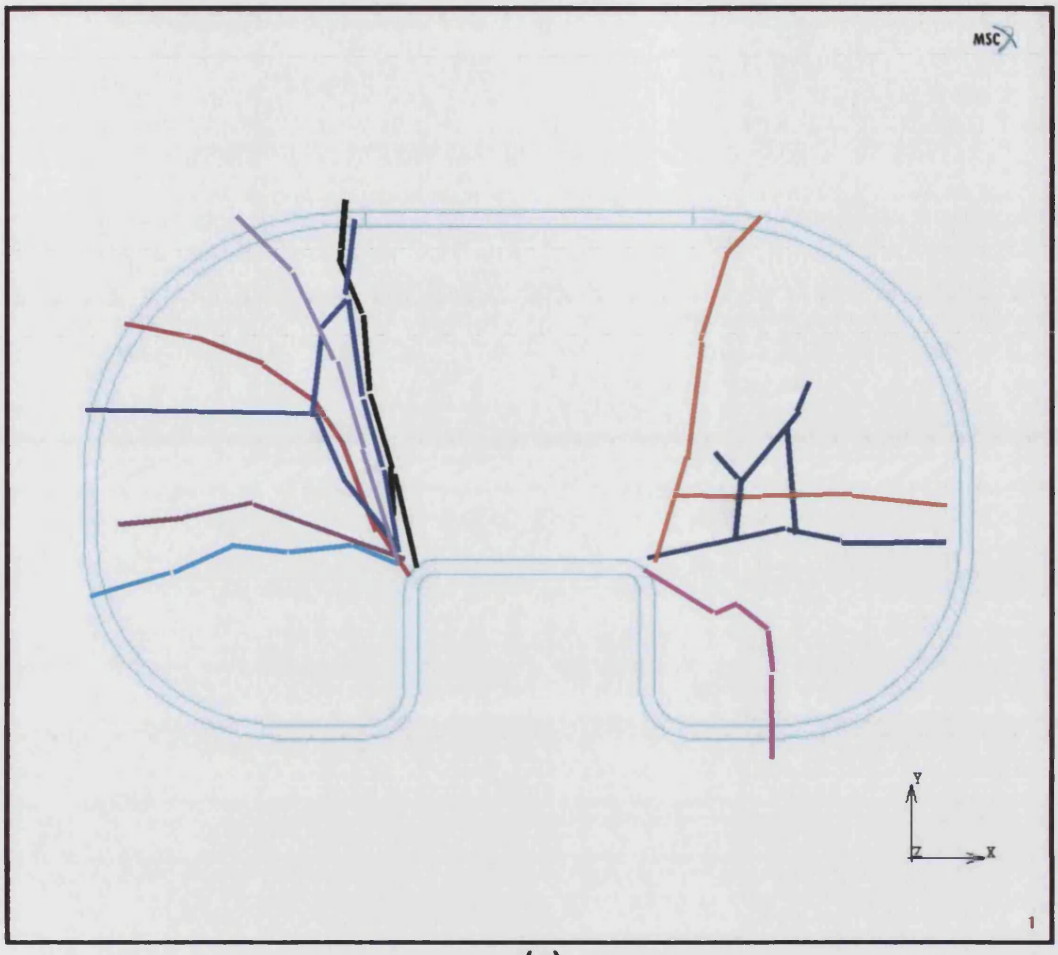

(a)

Figure 3.16a: Kinematic fracture patterns

Fracture line colour	Component Label	Figure Number
	A	3.16
	B	3.17
	C	Appendix C 1.1
	D	Appendix C 1.2
	E	Appendix C 1.3
	F	Appendix C 1.4
	G	Appendix C 1.5
	H	Appendix C 1.6
	J	Appendix C 1.8

Table 3.1: Table showing the relationship between the fractured line colours shown in Figure 3.16a, the component label and where the picture of the actual tray can be found.

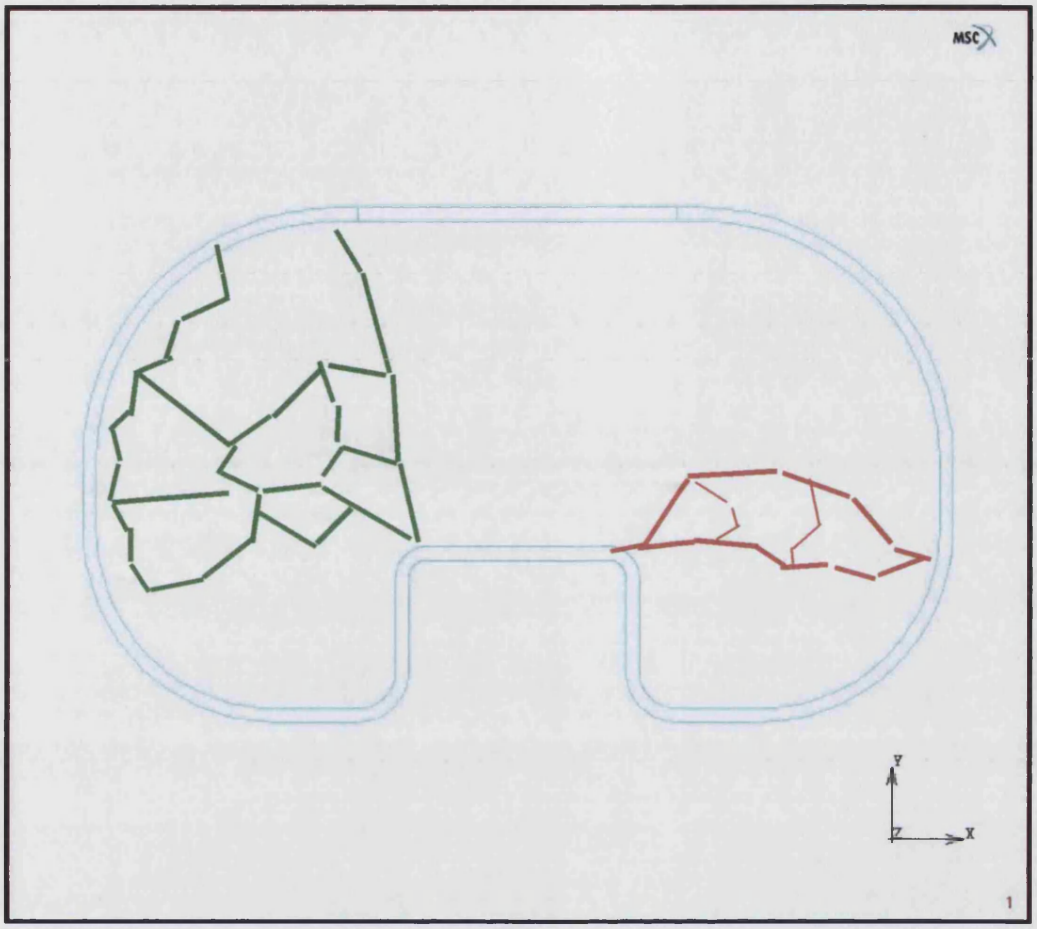

(b)

Figure 3.16b: Kinematic fracture patterns

Fracture line colour	Component Label	Figure Number
	I	Appendix C 1.7
	K	Appendix C 1.9

Table 3.2: Table showing the relationship between the fractured line colours shown in Figure 3.16b, the component label and where the picture of the actual tray can be found.

Comp. Label	Medial/ Lateral	Fracture characteristics	Porosity	Facetted fracture	Other
A	Medial	Initiation site found at root of notch, beach marks observed	Yes	Yes	
B	Medial	No initiation sites found using SEM	Yes	Yes	Shiny surface on rim
C	Medial	No initiation sites found using SEM	Yes	Yes	Shiny surface indicative of poly. insert wear through to metal tray
D	Medial	Fractured piece	not sent.	No SEM	carried out.
E	No record	No initiation sites found under SEM	Yes	Yes	Shiny surface indicative of poly. Insert wear through to metal tray
F	Medial	Incomplete fracture	unable	to view	using SEM
G	No record	No initiation sites found using SEM	Yes	Yes	
H	Medial	Fractured piece	not sent.	No SEM	carried out.
I	Lateral	Fractured piece	not sent.	No SEM	carried out.
J	No record	No initiation sites found using SEM	Yes	Yes	
K	No record	No initiation sites found using SEM			Shiny surface indicative of poly. Insert wear through to metal tray

Table 3.3: The main features found for the Kinematic Tray

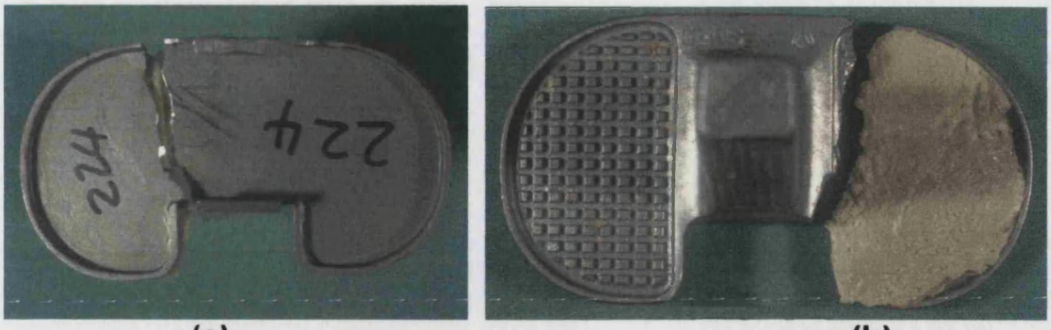

(a) (b)

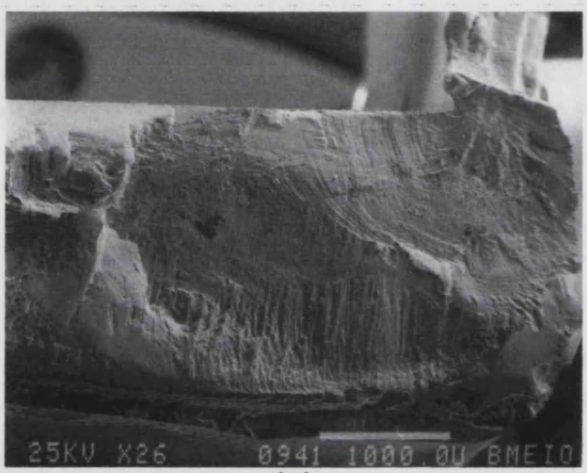

(c)

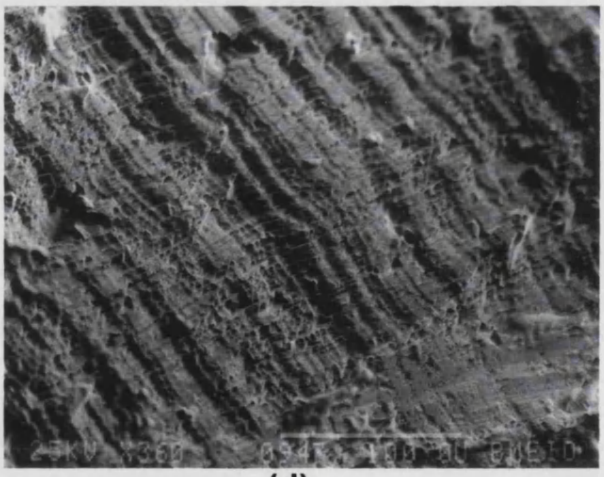

(d)

Figure 3.17: COMPONENT A (a & b) Medial compartment fracture of a Kinematic tibial tray in a right knee of a female patient. The tray was removed four years and eleven months post-operatively. (c & d,) SEM photographs of the fracture surface. (c) General view of the notch area (bar represents 1000 microns) (d) Close up view showing characteristic beach marks (bar represents 100 microns).

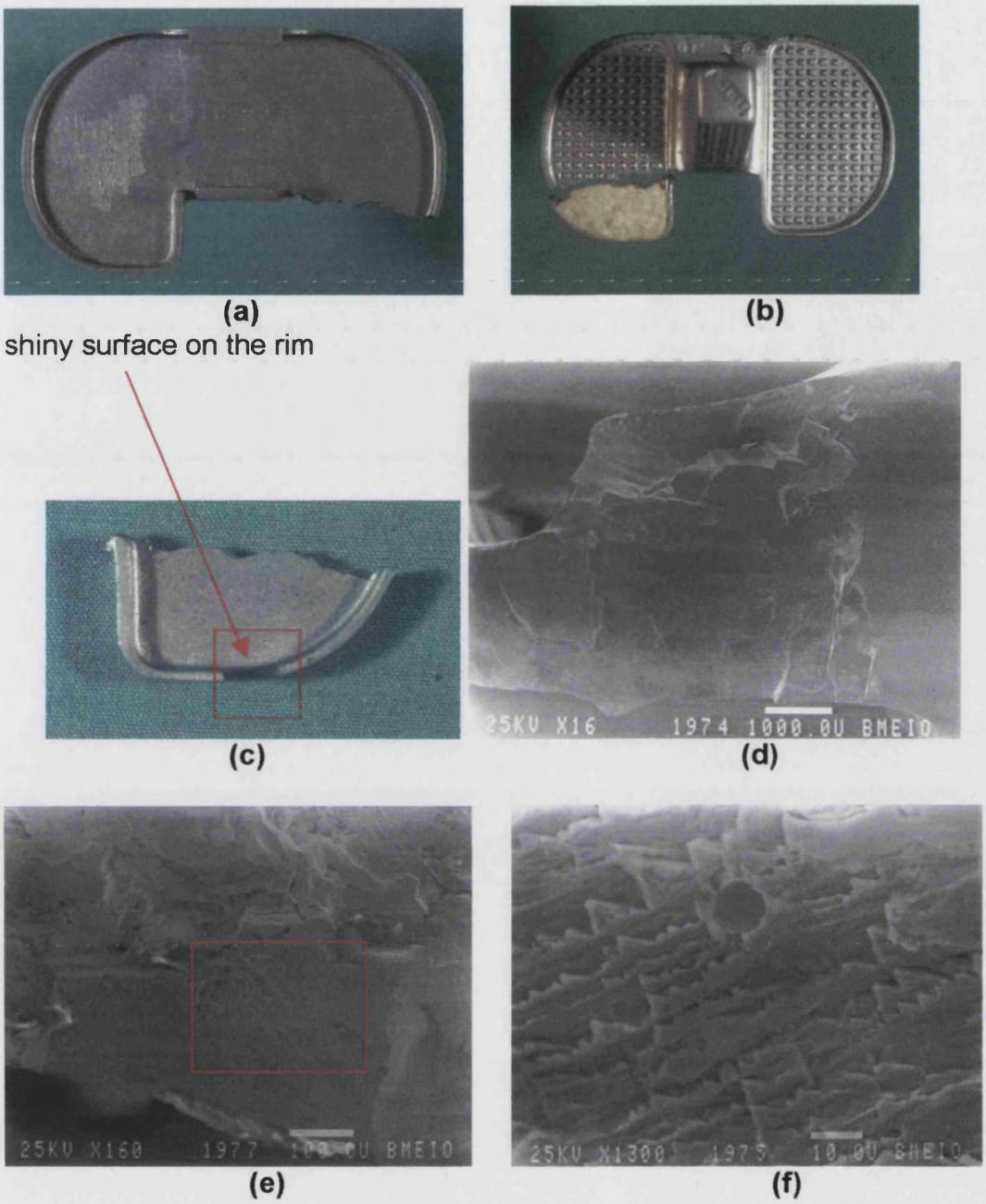

Figure 3.18: COMPONENT B (a, b & c) Medial compartment fracture of a Kinematic tray in a left knee 5 years post-operatively. (d, e, f, g): SEM photographs of the fracture surface (d) The notch area where initiation was expected. However no characteristic beach marks were observed (bar represents 1000 microns). (e) Lower part of the notch area (bar represents 100 microns). (f) Higher magnification view within the red box of (e) Showing porosity and stair–step facets (bar represents 10 microns).

3.2.3.2 The Total Condylar Tray

Figures 3.19 show the fracture patterns for the Total Condylar. The crack path always occurred in an anterior-posterior direction. SEM of the fracture surface (Figure 3.20) showed evidence of porosity and as with the Kinematic, stair step cracks and secondary cracks, consistent with fatigue failure of CoCrMo alloys (Brown and Gregson. 1999).

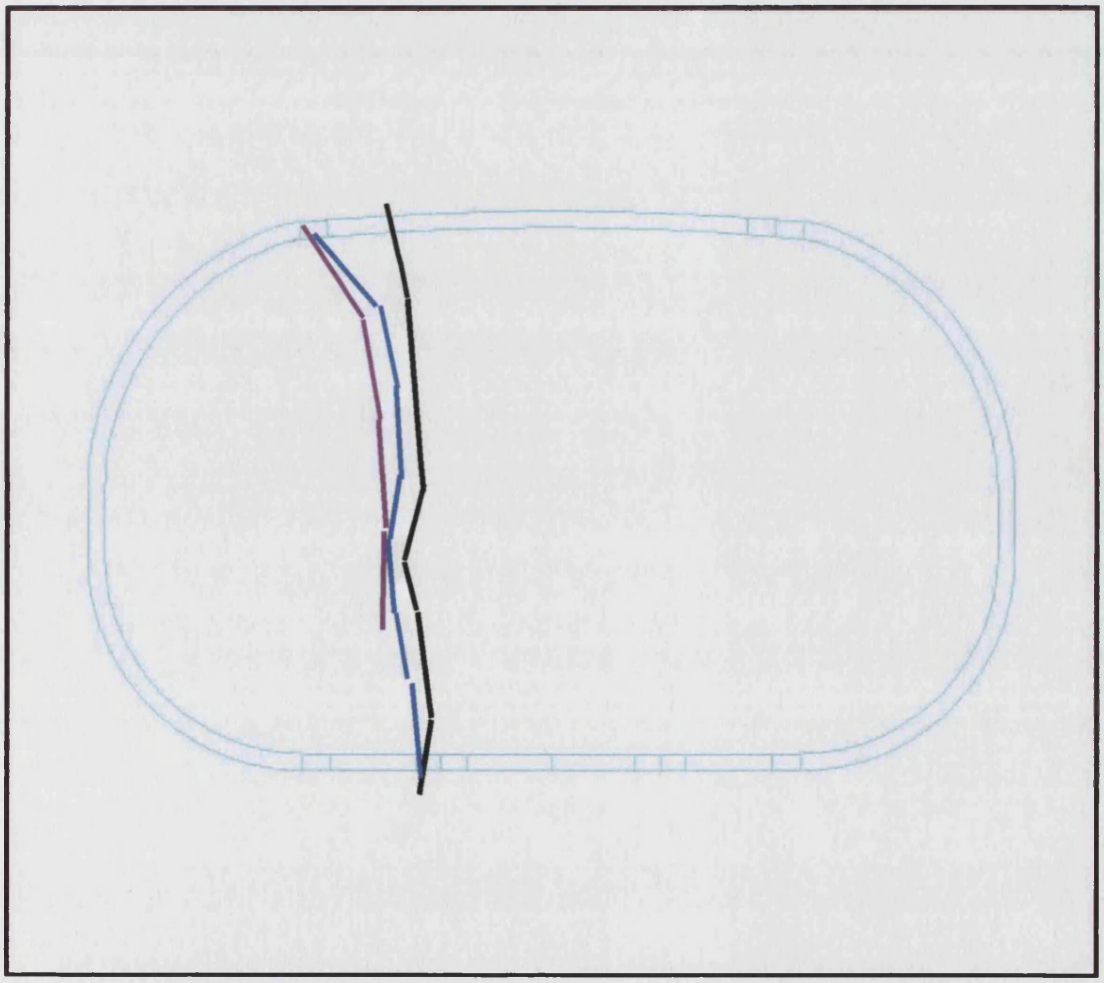

Figure 3.19: Total Condylar patterns

Fracture line colour	Component Label	Figure Number
———	L	3.20
———	M	Appendix C 2.1
———	N	Appendix C 2.2

Table 3.4: Table showing the relationship between the fractured line colours shown in Figure 3.19, the component label and where the actual picture can be found.

Comp. Label	Medial/ Lateral side	Fracture characteristics	Porosity	Facetted fracture	Other
L	Medial	No initiation sites found using SEM	Yes	Yes	
M	No record	No initiation sites found using SEM	Yes	Yes	
N	No record	Incomplete fracture	unable	to view	under SEM

Table 3.5: The main features found for the Total Condylar Tray

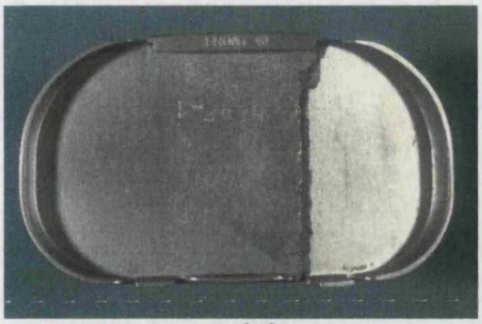

(a)

(b)

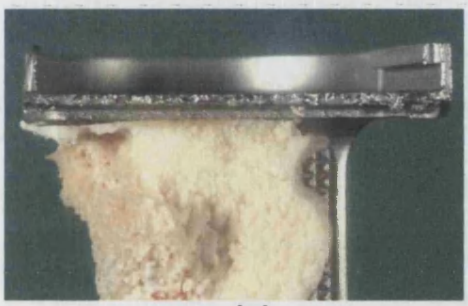

(c)

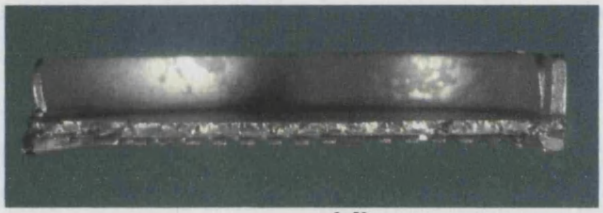

(d)

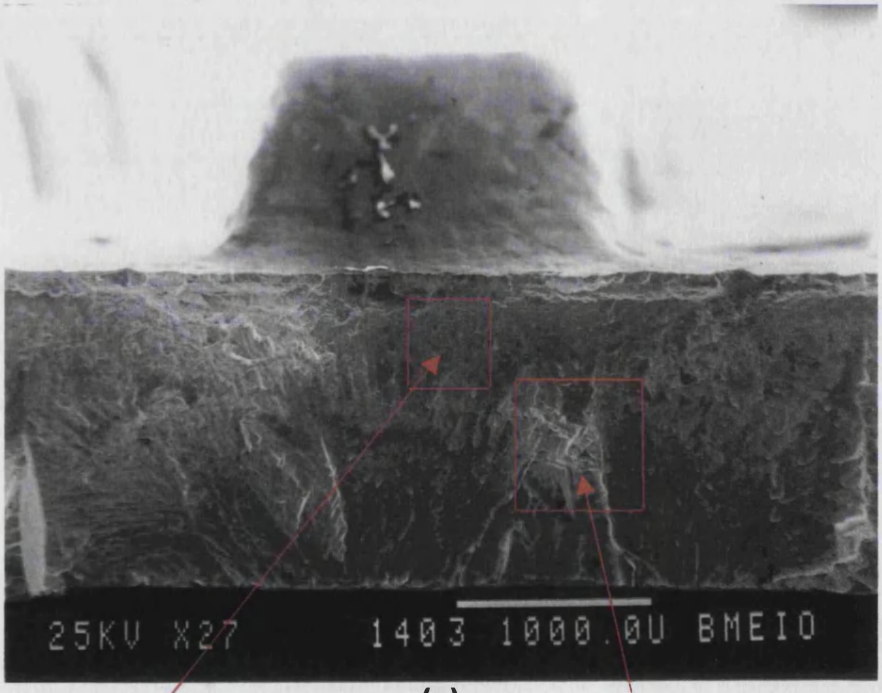

(e)

Further examination under SEM seen in figure (f and g)

Further examination under SEM seen in figure (h and i)

Figure 3.20 (a-d): COMPONENT L: Medial compartment failure of a Total Condylar tibial tray in a left knee 7 years and 3 months after implantation. (e) Lower magnification SEM photograph of the Total Condylar fracture surface (bar represents 1000 microns).

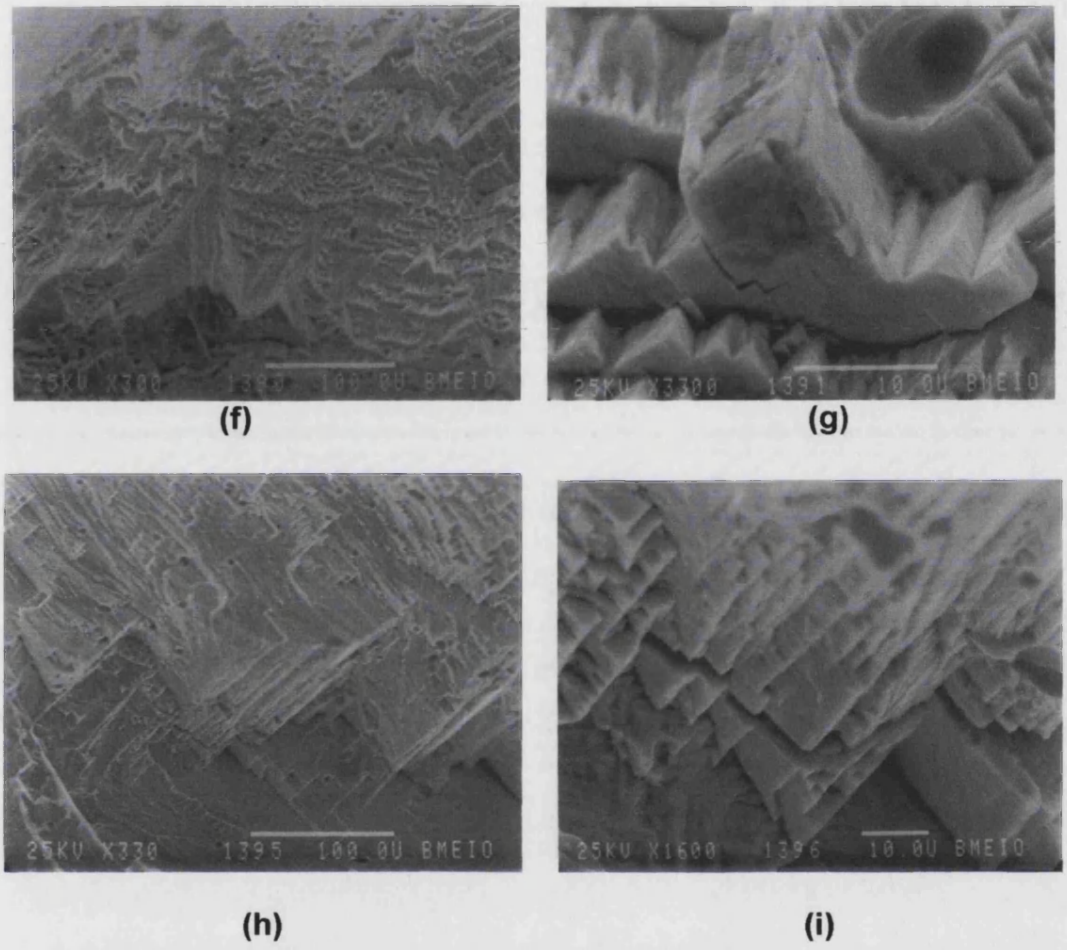

Figure 3.20 (f) and (h) lower power magnification of different parts of the fracture surface represented in the red squares for (e). (g), (i), high power magnification of (f) and (h) respectively. Bar represents 100 microns in (f) and (h); bar represents 10 microns in (g) and (i).

3.2.3.3 The PCA Tray

Figures 3.21 shows two types of fracture path for the PCA. Component 0 (refer to appendix C3.1) had a shiny surface in the anterior section of the fractured portion of the tibial tray. SEM of both trays showed evidence of fatigue fracture and porosity.

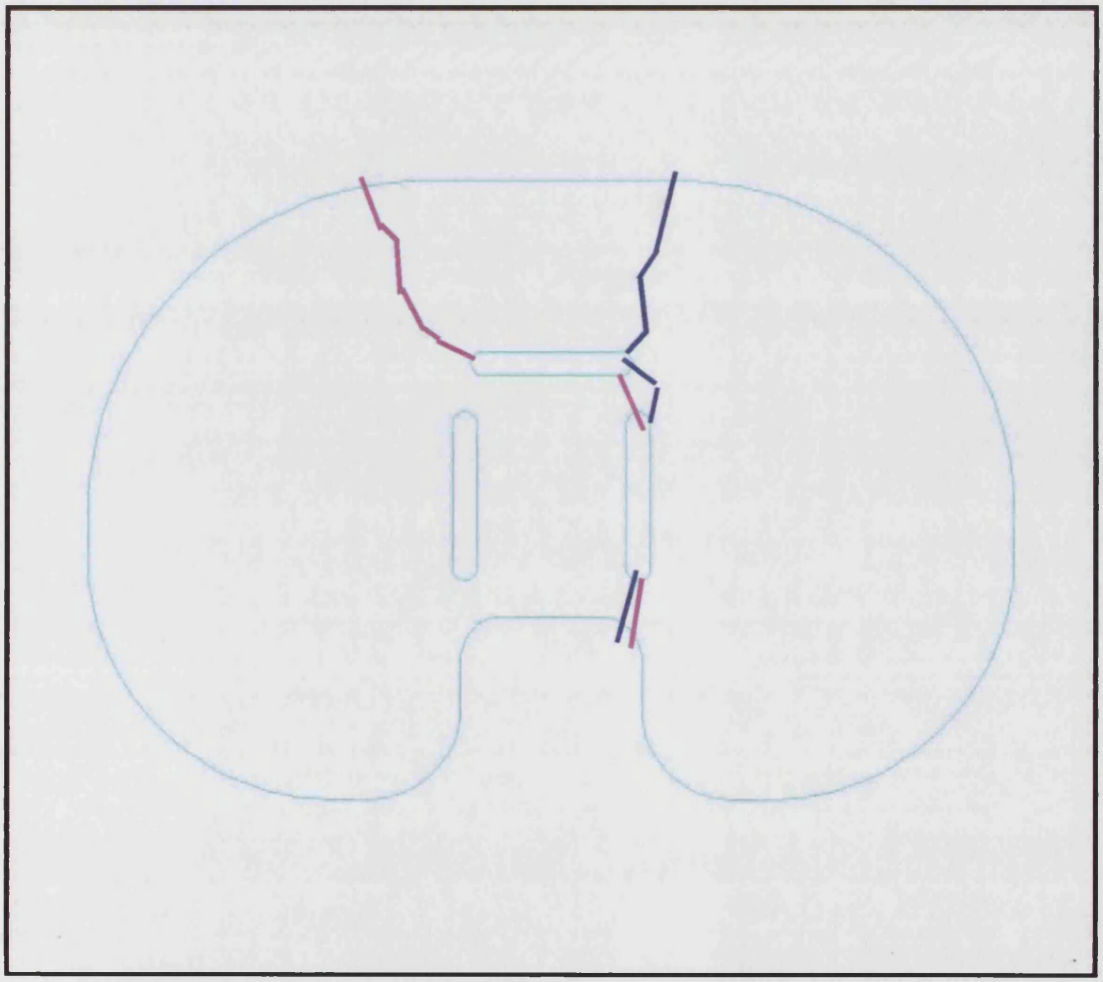

Figure 3.21: PCA fracture patterns

Fracture line colour	Component Label	Figure Number
———	O	Appendix C 3.1
———	P	3.22

Table 3.6: Table showing the relationship beteen the fractured line colours shown in Figure 3.21, the component label and where the picture can be found.

Comp Label	Medial/ Lateral side	Fracture characteristics	Porosity	Facetted fracture	Other
O	No record	No initiation sites found under SEM	Yes	Yes	Shiny surface indicative of polyethylene insert wear through to metal tray
P	No record	No initiation sites found under SEM	Yes	Yes	Fractures observed of the beaded surface

Table 3.7: The main features found for the PCA Tray.

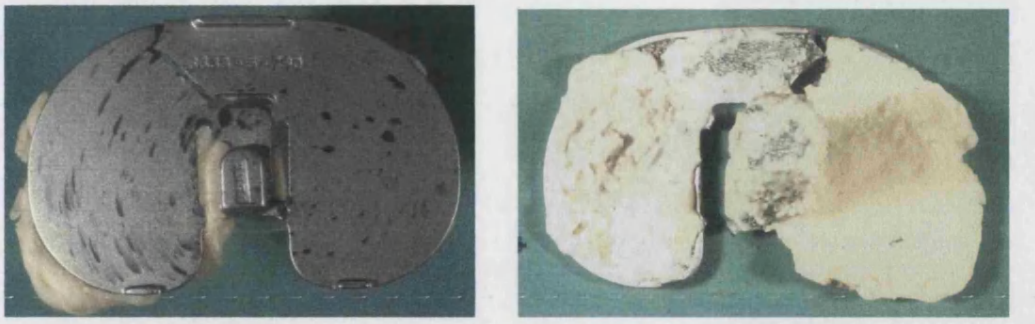

(a) (b)

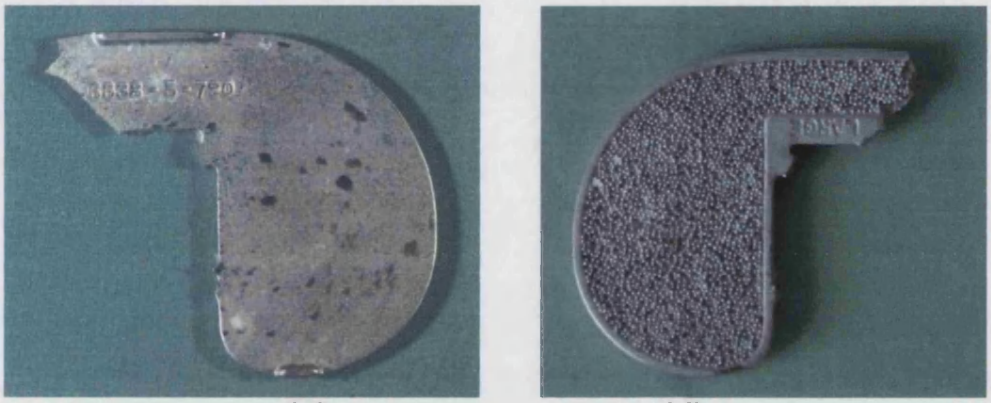

(c) (d)

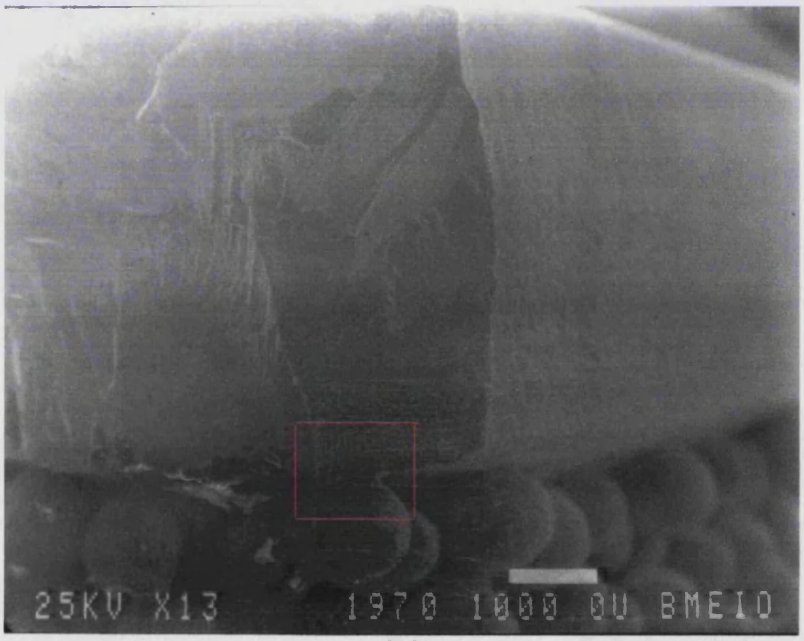

(e)

Figure 3.22 COMPONENT P (a-d): Fracture of a PCA knee tibial tray at 5 years. (e) Low power magnification of the fracture surface of the PCA knee (bar represents 1000 microns). Red square inidicates magnified SEM in (f)

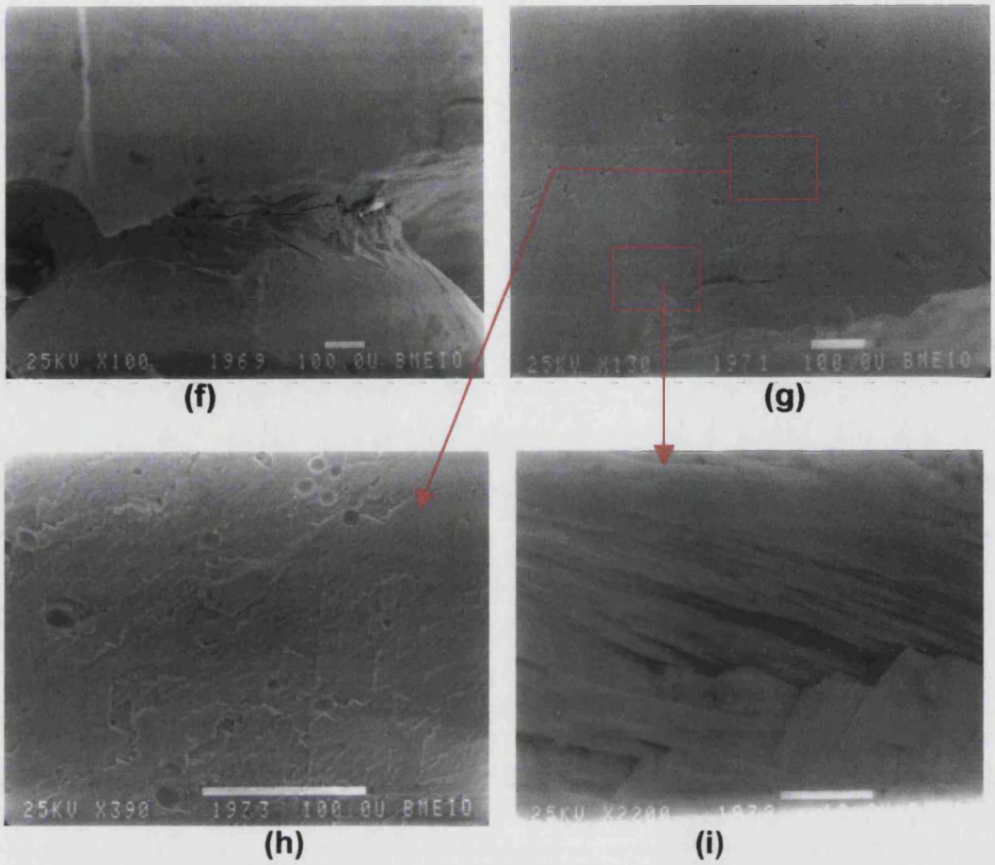

Figure 3.22 (f) Fracture of the sintered bead on the surface of the tray (bar represents 100 microns) (g & h) evidence of porosity and faceting of the fracture surface (bar represents 100 microns), (i) evidence of facetting (bar represents 10 microns).

3.2.4 DISCUSSION

The results show that the Kinematic and PCA (refer to fig. 3.16 and 3.21) have fractured with different crack paths. Only one sample of the Kinematic showed the initiation stage of fracture exhibiting characteristic beach marks (refer to fig 3.17). All other samples of fractured trays, using SEM, showed evidence of porosity and facetted fractures along the fractured surfaces. Examining each of the SEM photographs, features of the fractured surfaces showed variations. There may have been a number of reasons why this occurred. There may have been possible batch differences in manufacturing and casting quality. Brown and Gregson (1998) compared two failed identical Kinematic trays. One of the trays had a coarse grained structure and the other had a finer grain structure. They found that both trays showed crack growth along the plane of maximum bending but the coarse grained structure exhibited crack branching, deflection and growth at an angle to the plane of maximum opening. In a separate study, Brown and Gregson (1999), found that the type of loading also affected the features of the fractured surfaces for cobalt-chromium alloy. Changes from a high load to a low load as a result of different activities (or this may occur in regions of the tray that are well-supported compared to unsupported areas where no load transfer occurs) may affect how a crack grows and how it initiates. They found that overloading resulted in crack retardation and with a variable amplitude loading regime (incorporating overloading) the fractured surfaces were almost featureless with some areas of small facets. A constant amplitude loading regime showed a large degree of faceting. Another factor that can affect fracture in CoCrMo alloys is heat treatment. Hot Isostatic Pressing (HIPing) results in a reduced grain size for CoCrMo alloys and the fractured surfaces have finer faceting.

Porosity was another feature for all the trays examined under SEM. Porosity may develop within a casting due to (i) shrinkage of the metal (ii) gas porosity (iii) interdendritic porosity (iv) the composition of the alloy. The pores act as stress raisers, and from these areas microcracks can originate, reducing the

fatigue strength of the structure. Differences in results between studies can also be attributed to heat treatments applied to the metal after casting. For example, Zhuang and Langer (1988, 1989a,b,&c, 1990) did not report porosity in their studies. They had employed either a fast cool or a slow cool to promote a fine grained and coarse grained structure after casting. Brown and Gregson (1999) in their studies of CoCrMo alloy employed a solutionising treatment for 4 hours which resulted in a homogenous distribution of carbides resulting in reduced porosity and an increase in resistance to crack retardation. Georgette and Davidson (1986) found that HIPing removed porosity. In this study, porosity was evident in every tray examined using SEM. It is possible that at the time of the casting of these trays (late 1970s–mid-1980s) further heat treatments were not employed and knowledge about the manufacturing process was limited. However, there are similarities between the findings of two other studies and this one. Zhuang and Langer (1999), figures 3.15 and this study 3.20(g) show very similar features of the fractured surface. Brown and Gregson (1999) reported extensive porosity of the Kinematic trays that they examined.

Another interesting feature of the fractured trays was the presence of patches of shiny surfaces on the tibial baseplate. Engh et al. (1992) reported wear through of the polyethylene insert to the metal baseplate, with rubbing of the femoral component against the metal tibial tray. They reported that often the femoral component would get stuck in the cavity within the polyethylene insert. Figure 3.18c shows a shiny surface on the rim of the tray. Figures C1.1, C1.3, C1.9, and C3.0 all show patches of shiny surfaces. Figure C1.3 clearly shows that the polyethylene insert has worn through so exposing the metal baseplate to the femoral component.

If the bone supporting the tray was absent then this may cause an indention form of crack (refer to Figure C3.0) leading into the depth of the tray. These differences support and contact locations may also explain why the crack paths vary so much with the Kinematic tray. Further work was carried out to investigate this, which is reported in Chapter 6.

CHAPTER FOUR:
A STUDY OF THE PERFORMANCE OF TIBIAL TRAYS USING THE EXISTING ISO TESTING METHOD

4.1 INTRODUCTION

This chapter identifies current tray designs and previous designs that have failed due to fracture. These tray designs are then tested under the ISO test conditions using Finite Element Analysis and fatigue testing. The objective of this study is to identify a test load that distinguishes between clinically successful and unsuccessful tray designs. Study One compared the performance of one clinically successful design with one design that has a history of some clinical failure for the first and second contact positions (defined in the 1996 and 1997 draft ISO standards, refer to Appendix A1 and A2 or chapter 2, figure 2.2.7 and 2.2.8). Study Two established the peak load that can be used using the second contact position. Appendix B contains two studies that examine the effect of cement layers, and peak stress for the first contact position.

4.2 CURRENT TRAY DESIGNS

A survey was conducted of current tibial tray designs by approaching manufacturers of artificial knee replacements. Forty different tray designs were identified from twenty-six product ranges. These are reviewed below.

4.2.1 TRAY MATERIAL

Twenty tray designs were made from cobalt-chrome (CoCrMo) alloy, fourteen from titanium (Ti6Al4V) alloy and six were made from UHMWPE (all-polyethylene).

4.2.2 TRAY SHAPE

Tray shape was categorised into four types. Fifteen had a square cruciate cut-out (figure 4.1a); sixteen had a rounded cut-out (figure 4.1b); four had no cruciate cut-out (figure 4.1c); five had an asymmetric shaped tray (figure 4.1d).

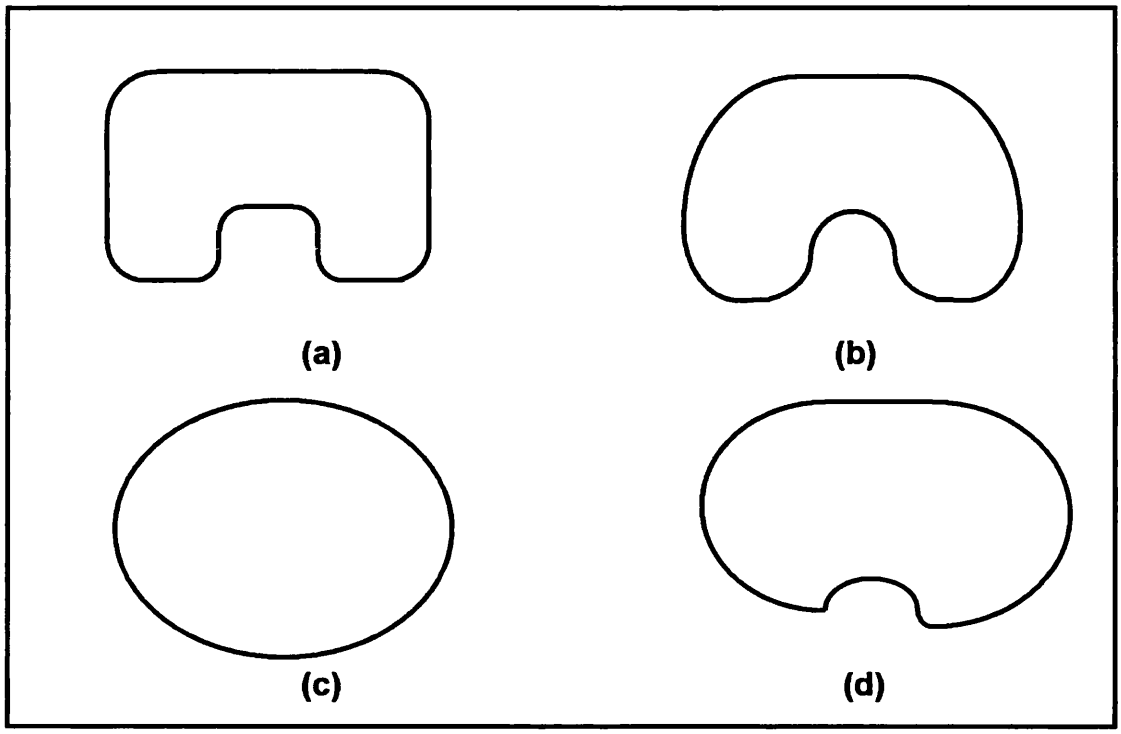

Figure 4.1 (a) 'square' cruciate cut-out; (b) 'round' cruciate cut-out; (c) no cruciate cut-out; (d) asymmetric cruciate cut-out.

4.2.3 FIXATION

One product range offered cemented fixation only - all other products could achieve fixation by cemented and cementless means. For the cemented case four products achieved fixation against smooth surfaces; seven had a rim or struts on the undersurface to form a recess for the cement - two of these offered the option to precoat the tibial surfaces with PMMA; eight had a roughened surface such as grit-blasting, or a non-porous roughened surface treatment; nine had a surface structure to allow cement interdigitation such as cast meshes. The all-polyethylene components had islands on the undersurface of the component to form cement recesses.

Cementless fixation was achieved by using the sintering technique producing a layer of titanium beads (five products) or CoCr beads (six products). Three products offered the option of using a plasma-sprayed CoCr surface or Hydroxyapatite (HA); six products achieved their porous surface by plasma-spraying of titanium and an additional five products used plasma-spraying of HA. Two products used structured cancellous titanium or titanium fiber mesh to produce a porous surface.

A variety of methods are used for fixing the baseplate to the natural bone. Of the forty models, thirty-eight used a central stem for fixation. The stems were simple cylinder or I-beam (five models), or they had fins (fourteen models). The fins were either angled, long (stretching across the baseplate) or of a cruciform type (refer to figure 4.2.1). The remaining nineteen models used a stem with either pegs and/or screws. Eight models used a simple stem with two pegs; five models used a simple stem with four pegs and/or screws. Two models used a finned stem with two pegs; one used a finned stem with three pegs and three used a finned stem with four pegs or screws. Two models used no stem but had four pegs and screw holes. These different configurations are represented in figure 4.2.2.

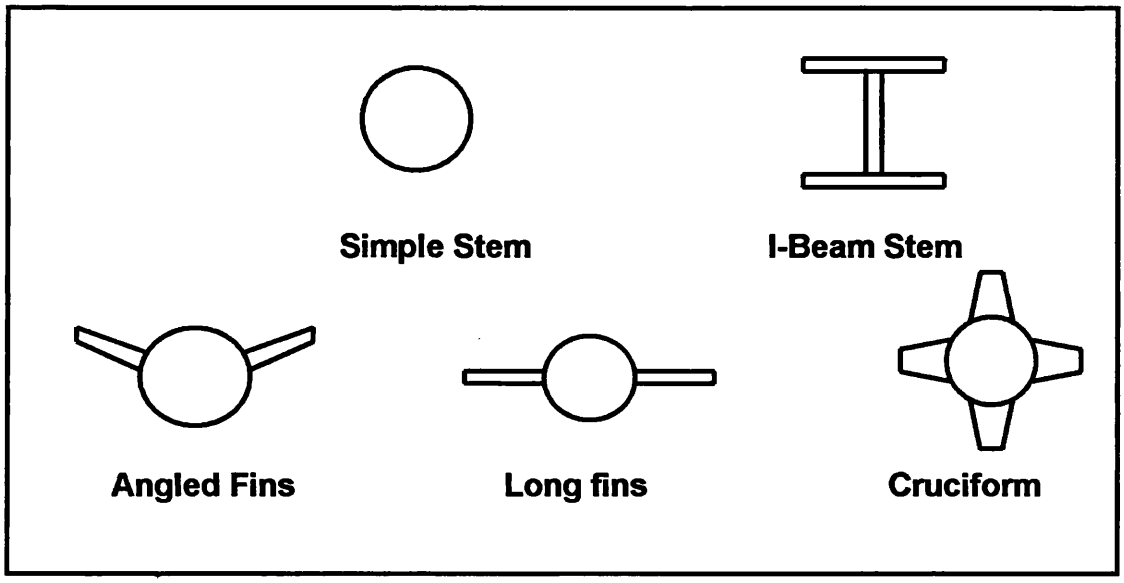

Figure 4.2.1: Stem types

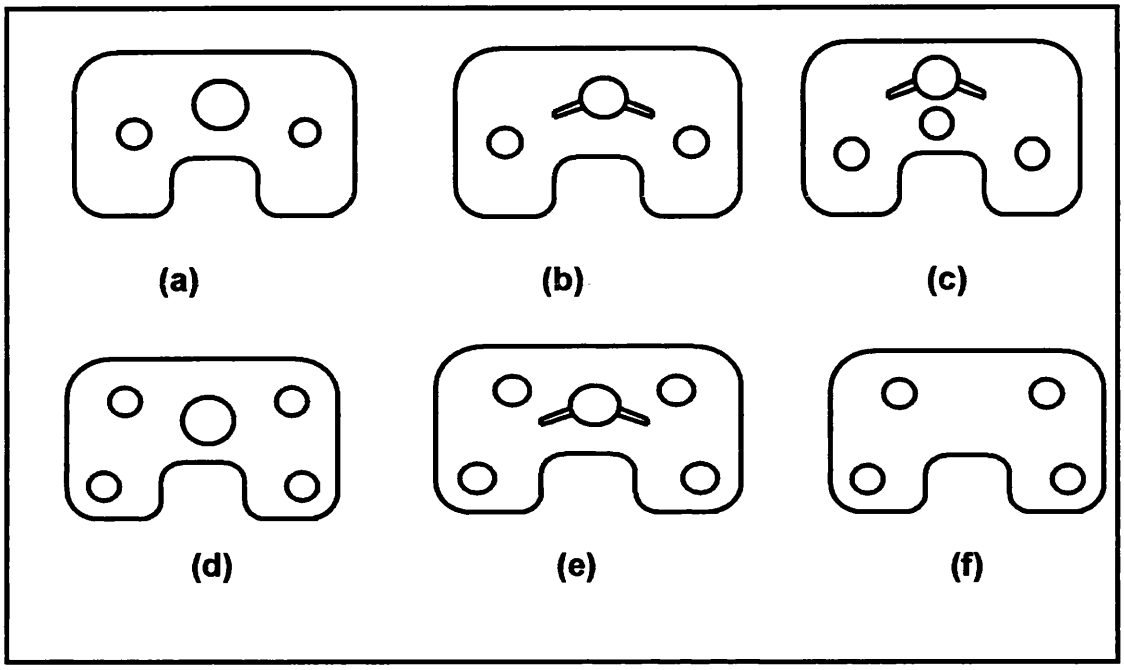

Figure 4.2.2: Tibial baseplate configurations for stems, screw holes and pegs.

4.2.4 TRAY THICKNESS

The smallest tray thickness was 2.5mm for both titanium and cobalt-chrome alloy trays. The thicknesses then ranged upwards with a maximum size of 7.5mm for cobalt-chrome alloy trays.

4.2.5 TRAY SIZE

The number of tray sizes within a product ranged from three to ten, with the smallest width being 60mm and the largest width at 88mm.

4.2.6 BEARING TYPE

Thirty of the models had a fixed bearing insert whilst the remaining ten were of the mobile bearing type.

4.2.7 LOCKING MECHANISM

Secure attachment of the tibial insert to the polyethylene was achieved by locking screws, clips or bars for eleven of the products. Fifteen of the products achieved attachment to the tray by peripheral rims – either a full grooved rim or partial rim segments.

4.2.8 MODULAR PARTS

From the available information, twenty-two of the product ranges offered modular parts taking the form of stems, wedges and blocks. The stem extensions were of a variety of lengths from 40mm to 200mm and of different types such as I-beam, finned, slotted or fluted. The wedges were half or full, fitted by screws or mechanically interlocked, angled from 10 to 26 degrees. Three products offered integral half or full wedges. Block thicknesses ranged from 4 to 12mm.

4.3 TRAYS USED FOR THIS PROJECT

Trays were selected to include as much of the variety of tray design as possible, coupled with availability of the components and total testing time. Three titanium alloy trays and four cobalt-chrome alloy trays were selected. The three titanium alloy trays had a fixed bearing insert. The IB2 (Cremascoli Fry Ltd., UK) tray shown in figure 4.3.1a has no cruciate cut-out, a simple stem with four screw holes. The Profix (Smith and Nephew Inc, USA) tray (figure 4.3.1b) has an asymmetric tray with a medialised stem, four pegs and 4 screwholes. The MG2 (Zimmer Inc, USA) tray (figure 4.3.1c) has a square cruciate cut-out and four pegs with the option of four screwholes. The CoCrMo alloy trays included two fixed bearing designs, the Kinemax (Stryker Inc, USA) and the AGC (Biomet Merck Ltd., UK) (figure 4.3.2a & b respectively), and two mobile bearing designs, the Rotaglide (Corin Ltd., UK) and MBK (Zimmer Inc., USA) trays figure 4.3.2c &d). The Kinemax has a square cruciate cut-out, a simple stem with angled fins. The AGC has a kidney-shaped cruciate cut-out with an I-Beam stem. The MBK has a large

central stem with a small rounded cruciate cut-out. The Rotaglide has a small rounded cruciate cut-out, a simple stem with small fins and two pegs. The Rotaglide has three types of coatings: uncoated, porous coating, and HA-coating. The AGC has two varieties and Interlok finish and a plasma-sprayed titanium coating. The Profix also has two varieties: one without a coating and one that has a triple sintered beading layer of titanium beads. This study examines all types of Rotaglide and AGC tray designs but only the sintered surface for the Profix.

Chapter two reviewed the literature concerning tibial trays that have fractured *in vivo*. The literature revealed that the Kinematic, Total Condylar, PCA and revision PCA tray designs had a propensity for fracture due to their design. These trays are depicted in Figure 4.3.3 (a-d) and are used in the following studies.

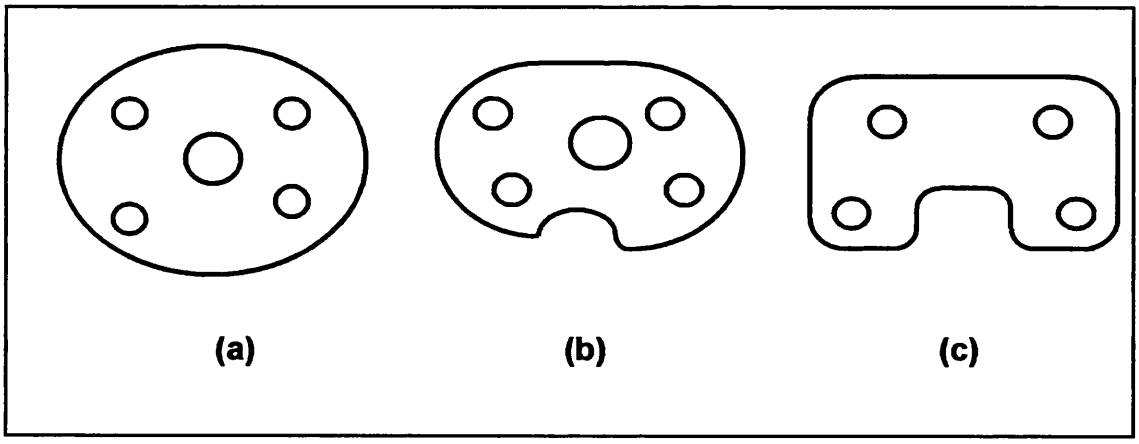

(a) IB2 tray: no cruciate cut-out, central stem and four screwholes
(b) Profix tray: asymmetric tray, medialised central stem, four pegs and four optional screwholes.
(c) MG2 tray: square cruciate cut-out, four pegs with four optional screwholes.

Figure 4.3.1(a-c): Titanium tray designs with fixed bearing insert

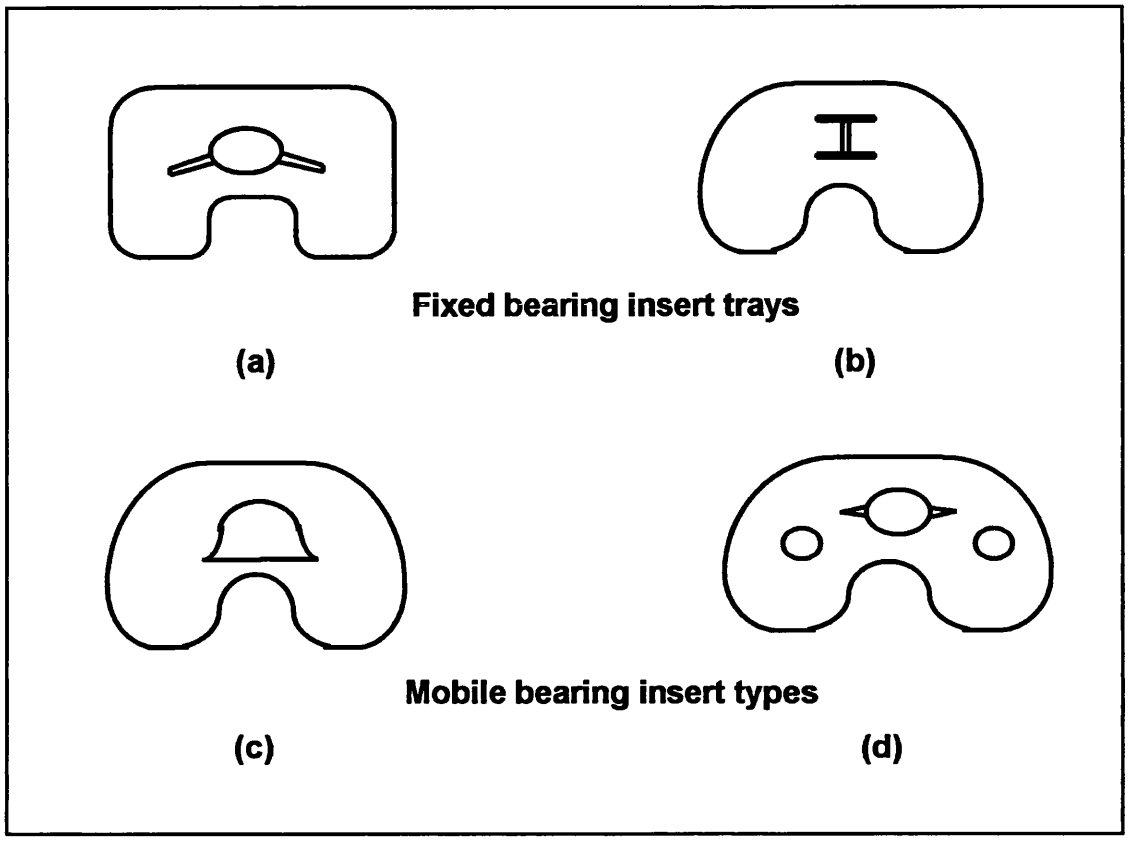

(a) Kinemax tray: square cruciate cut-out, central stem and angled fin. (b) AGC tray: round cruciate cut-out with I-beam stem.
(c) MBK tray: round cruciate cut-out, central stem with small fins.
(d) Rotaglide tray: round cruciate cut-out, central stem with small fins, two pegs.

Figure 4.3.2(a-d): Cobalt-chrome alloy trays.

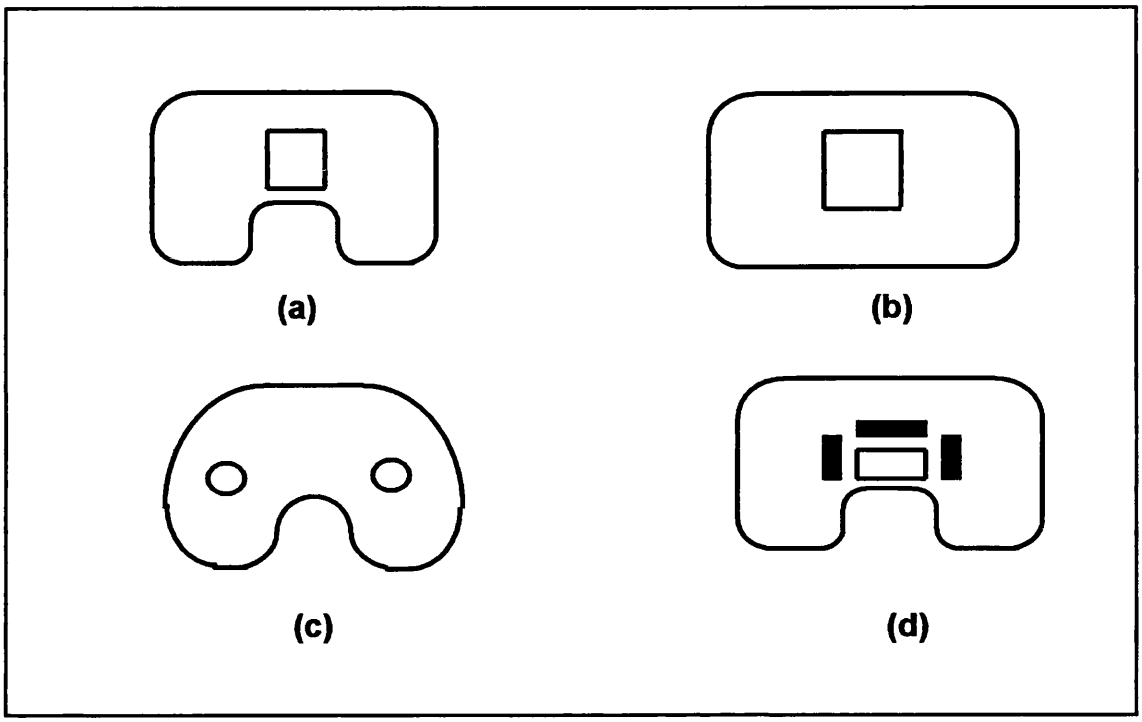

(a) the Kinematic tray with square cruciate cut-out and a central stem.
(b) the Total Condylar with no cruciate cut out, a peripheral rim with slots cut in and a central stem.
(c) the PCA tray with two pegs and sintered beads to form porous surface.
(d) the revision PCA tray with central stem with three slots to aid removal of stem in revision operations.

Figure 4.3.3(a-d): Trays that have failed *in vivo* due to fracture.

4.4 STUDY ONE

The central objective of this study was evaluation of the proposed ISO test by analysing two components, one with a known history of failure by fracture and one that does not have such a record. These components are the Kinematic and the Kinemax (Stryker Ltd., Berkshire, UK) respectively. This study examines the performance of both components, using the two defined contact positions, at a load of 2000N. This is a physiological load value based on theoretical calculation of the peak force during the normal walking cycle (Morrison, 1969). As the test protocol loads only one condyle of the tray, for the purposes of this study it was assumed that this condyle received the total physiological load. It is emphasised that this is an extreme condition which would probably only occur under conditions of severe joint misalignment. However this worst case was chosen as the upper limit for the test.

4.4.1 MATERIALS AND METHOD

4.4.1.1 Finite Element Analysis

Solid models of the Kinematic and Kinemax baseplates were created in Unigraphics (Electronic Data System Corporation, USA) represented in figures 4.4.1a and 4.4.1b respectively. These models were then translated to *iges* format and imported into COSMOS/M (Structural Research and Analysis Corporation, USA) where meshes were generated automatically using higher order tetrahedral elements. A number of mesh sizes were modelled until subsequent mesh sizes showed peak stresses within 3% of each other. The model was then considered to have converged. However, for the Kinematic model a sharp increase in the peak stress was observed when the element size was reduced from 1.1mm to 1.0mm, indicative of high stress concentrations. The convergence curve data results are presented in Figure 4.4.4a. For the Kinemax model, mesh size 1.0mm consisted of 87960

elements and 135696 nodes. The convergence curve is provided in Figure 4.4.4b and shows that meshes have converged showing differences within 3% of subsequent mesh sizes. Material properties for both components were defined as described in Table 4.4.1.

Due to the geometry of the Kinematic model (small notch in the cruciate cut-out area) a further mesh type was used. A parametric solid model was created using volumes to form the geometry of the tray. The volumes were all meshed parametrically with 8 noded hexahedral elements. This model was created in such a way as to give a refinement in areas of peak stress (figure 4.4.1c). Solution checks were then performed on this model to determine the accuracy of the stress field. This was done by comparing the nodal stresses calculated by adjoining elements. The test was performed at various points around the model and showed that in the areas of peak stress the unaveraged stress values were within 2% of each other. At other positions the unaveraged values were within 6% of each other. The resulting mesh consisted of 25099 nodes and 20022 eight noded hexahedral elements. In each of these models one half of the tibial baseplate including the stem was fully restrained in all 6 degrees of freedom (figure 4.4.1d). The test specified applying the load using a spherical indentor impacting on a polyethylene spacer. This would result in a parabolic distribution of the load on the metal tray (figure 4.4.1e). This study modelled two extremes of this loading condition: point and uniform pressure distribution; if the differences in the results for these two types of loading were small, then we would not be required to model a parabolic distribution.

For the two loading positions, (A) defined in 1996 standard (figure 4.4.2a & 4.4.2b) and (B) defined in 1997 standard (taken at 0 degrees flexion), two load cases were used. Position A was determined from the geometry of the tray and position B was determined from data from Sathasivam and Walker (1997). The first case uses a point load of 2000N; the second case uses a uniform pressure of 15.07Nmm^{-2} on a circular area of radius 6.5mm (the area of the spacer. A lower load level was selected based on the FEA results for the Kinemax. This load level was selected as 500N on the basis that the

Kinemax would survive the ISO test. This lower load level of 500N was selected based on the data given by the manufacturer (Howmedica) on the fatigue properties of solution heat-treated CoCrMo alloy. This was a load level that the FEA predicted the Kinematic would fail.

4.4.1.2 Mechanical Testing

A static test was performed for the Kinematic component for both contact positions, using a Hounsfield machine. This was an initial test to determine the accuracy of the FEA results. To determine the performance of the component beyond its yield strength, one half of the component was fixed rigidly using acrylic cement and the other was subjected to a compressive load of 2000N at a rate of 5mm/min.

In the proposed ISO test (14879-1/CD) it is specified that one half of the component should be fully fixed. In our test procedure one half of the component was rigidly held with specifically made fixtures and using acrylic cement. A thin-walled perspex tube was fitted around the set-up to form a container so that the component and indentor were immersed in Phosphate Buffered Saline (PBS) solution (figure 4.4.3a & b). The fixed part of the component was then clamped. A maximum cyclic load was applied vertically at 3Hz through a polyethylene spacer in a multi-channel pneumatically loaded fatigue testing machine until crack formation or 5 million cycles was achieved. The Kinemax component, using two samples for each contact point, was tested so that the tray was subjected to a maximum compressive load of 2000N. Further mechanical testing was performed on the Kinematic and the Kinemax components. Again for each component, two samples were used for each contact point but with a maximum compressive load of 500N.

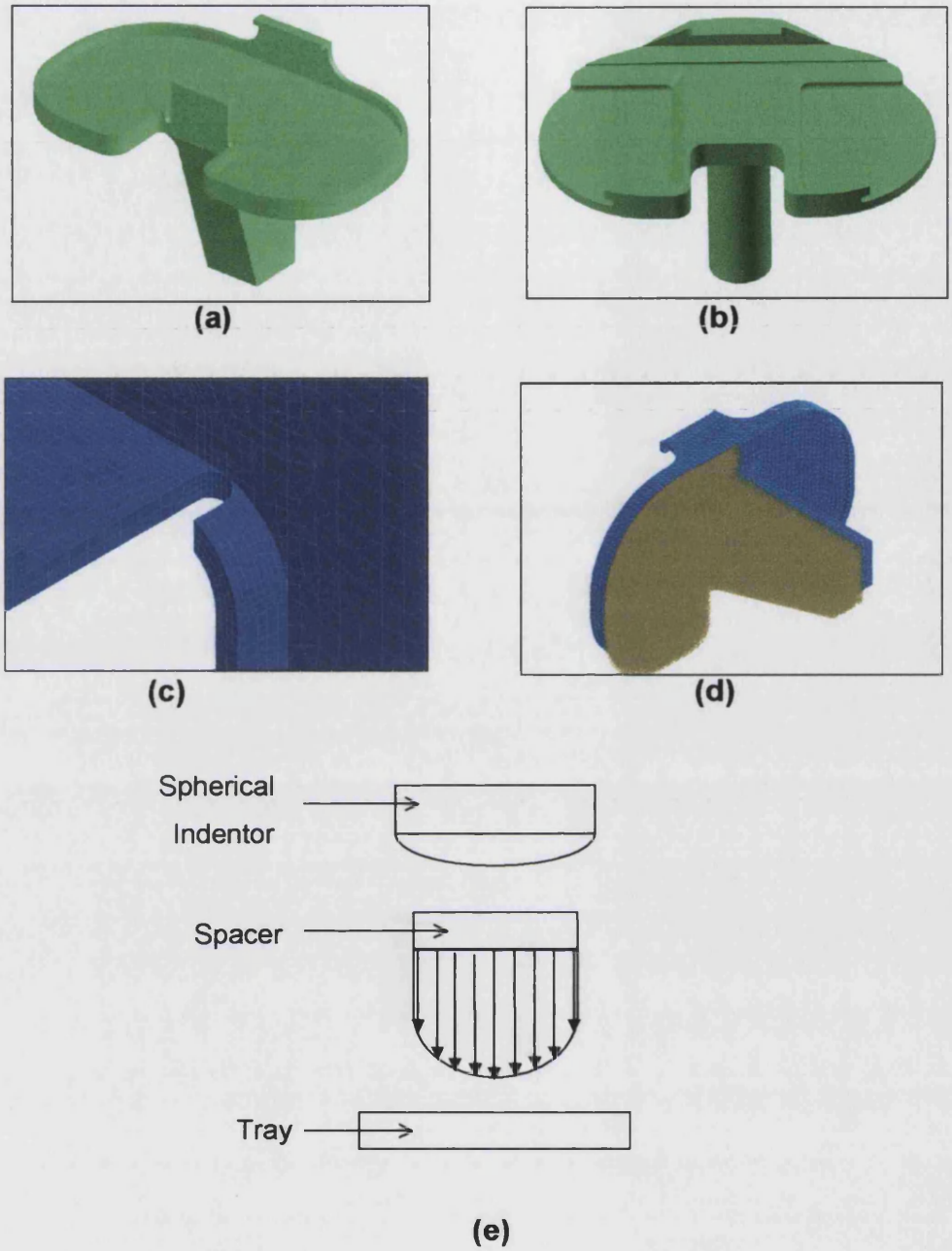

Figure 4.4.1: (a) CAD model of the Kinematic baseplate,

(b) CAD model of the Kinemax baseplate,

(c) Hexahedral mesh of Kinematic baseplate: detailed view,

(d) Boundary conditions applied to one half of the component,

(e) Load distribution experienced by the tray.

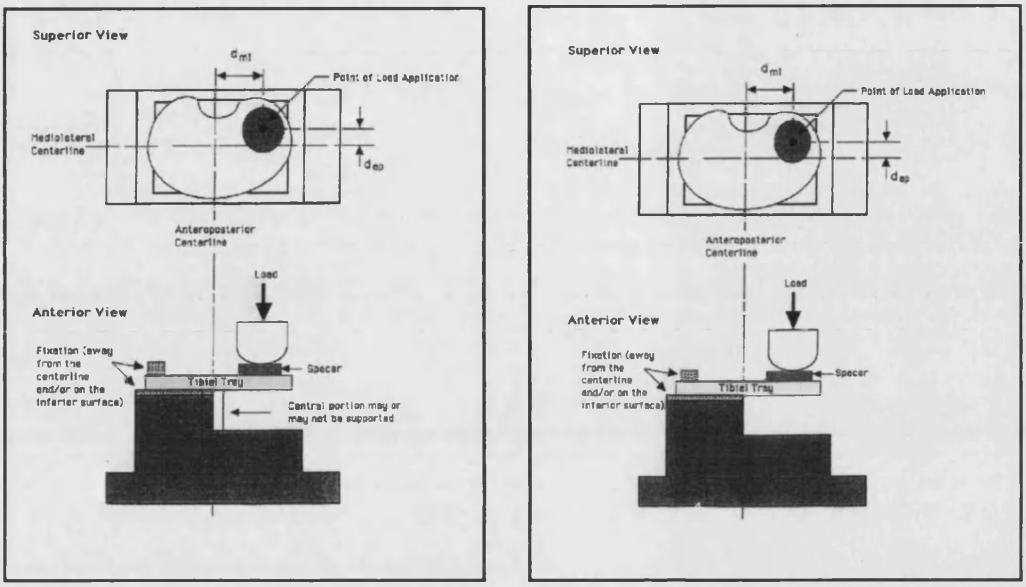

(a) (b)

Figure 4.4.2: The test set up (a) with and (b) without a central stem.

	Young's Modulus (GPa)	Poisson's Ratio	Yield Strength (MPa)	Ultimate Tensile Strength (MPa)	Fatigue Limit (MPa)
Cast CoCrMo	220	0.3	515	725	250 (Weinstow & Clemow, 1990) 300 (Paganelli et al., 1988)
Solution heat-treated CoCrMo	220	0.3	840	1275	400 - 470 (Howmedica)

Table 4.4.1:

Material properties of both cast and solution heat-treated CoCrMo alloy.

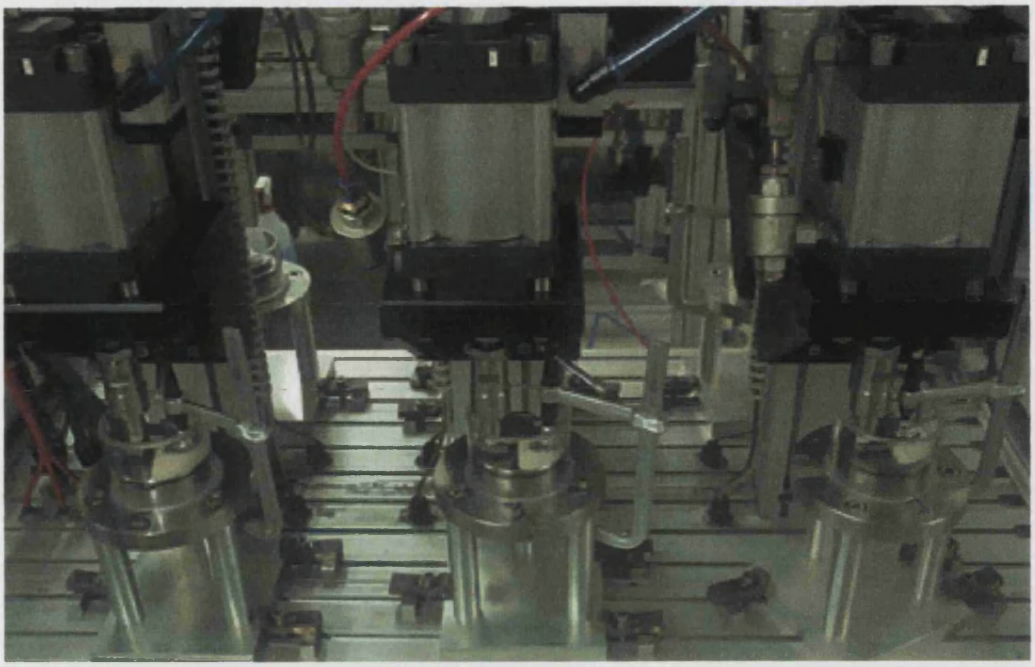

(a)

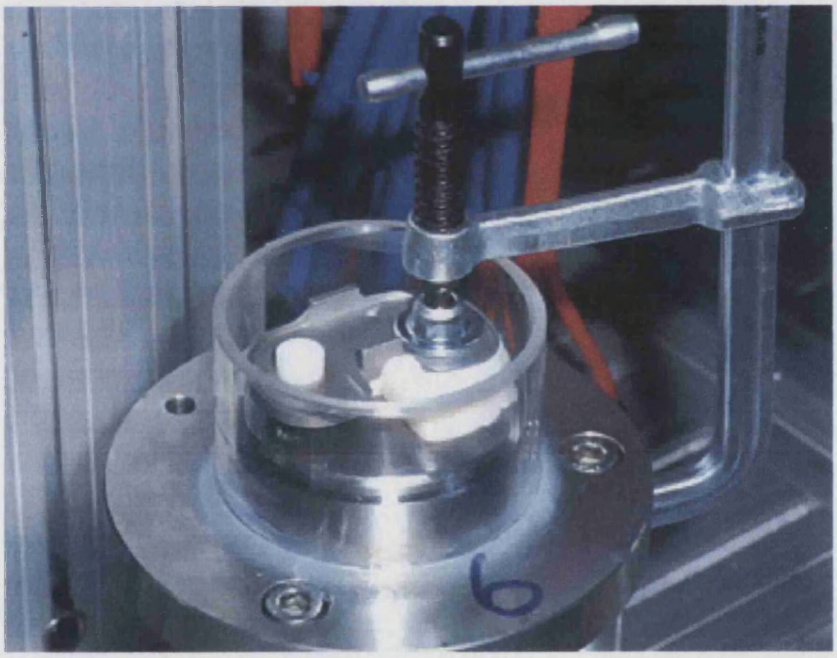

(b)

Figure 4.4.3(a &b): Mechanical test set-up.

4.4.2 RESULTS

4.4.2.1 Using a load level of 2000N

4.4.2.1.1 First Contact Position

The tetrahedral model for the Kinematic component was tested for convergence but this was not obtained, instead sharp increases in peak stress were evident by reducing the element size down to 1.0mm. However, the hexahedral model showed the same stress distribution with the peak maximum principal stress within 3% of the tetrahedral model. Solution checks were performed on the hexahedral model that showed acceptable convergence of the results.

The stress distributions for the Kinematic model (hexahedral) for the first contact position are illustrated in figure 4.4.5a. This shows that the peak maximum principal stress occurred in the gap between the rim and the locking tab. For the Kinematic component the differences for maximum principal stress between point and pressure loading are shown in Table 4.4.2 for tetrahedral and hexahedral meshes. In each case whether point or pressure loading, tetrahedral or hexahedral meshes, the peak stresses were in the region of 9700-10000 MPa which exceeded the yield strength and the fatigue limit of cast CoCrMo alloy (refer to Table 4.4.1). This result predicted plastic flow in the gap on the first load cycle. In the region adjacent to this area, the maximum principal stress remained high (above 500MPa). This part of the tray was unsupported by the stem. Static tests showed permanent deformation of the tibial baseplate as predicted by the finite element results (figure 4.4.5c).

For the Kinemax model the stress distribution indicated peak stresses in the inner edge of the recess (figure 4.4.6a). Also regions of high stress occurred in the corner of the PCL cut-out and in the top corner of the component. The differences between peak stresses for point and pressure loading were within 2% of each other. In the fatigue test of the Kinemax component at 189,000 cycles, crack formation was observed in the inner recess, the PCL cut-out and the top corner of the component (figure 4.4.6b). The areas of stresses

above the fatigue limit of solution heat-treated CoCr alloy predicted by FEA, corresponded with areas of crack formation for the Kinemax under fatigue testing conditions.

4.4.2.1.2 Second Contact Position

The differences in results between point and pressure loading for both Kinematic and Kinemax models were small so for the second contact position only point loading was modelled. For the Kinematic models (tetrahedral and hexahedral) a much lower peak stress was observed. However the overall stress distribution showed regions of high stress in the same areas as the first contact position (figure 4.4.6b). Again, static tests showed permanent deformation as predicted by the finite element results.

For the Kinemax model the peak stress for the second contact position was lower than for the first, but still remained above the fatigue limit and the ultimate tensile strength (refer to Table 4.4.1). The stress distribution showed areas of high stress again in the inner edge of the recess, and the top corner (figure 4.4.6c). The corner of the PCL cut-out also experienced a stress of 563 MPa which was above the fatigue limit for the material. The results from the fatigue testing showed that crack formation and fracture, using the second contact position, occurred before 374,700 cycles. Figure 4.4.6d shows fracture of the component. The inset for figure 4.4.6d shows crack formation at the corner of the PCL cut-out. Again, the areas of stresses above the fatigue limit of solution heat-treated CoCr alloy predicted by FEA, corresponded with areas of crack formation for the Kinemax under fatigue testing conditions.

4.4.2.2 Using a load level of 500N

4.4.2.2.1 First and Second Contact Positions

Table 4.4.4 shows the results for the Kinematic and Kinemax component using a lower load of 500N. Figure 4.4.7(a & c) and figure 4.4.8(a & c) depict the FEA results for the Kinematic and Kinemax components for both contact positions respectively. In each case it shows the same location for high stresses but the magnitude for each is reduced.

For the Kinematic component the areas of high stressses remain above the Ultimate Tensile Strength and the fatigue limit of cast CoCrMo alloy (refer to Table 4.4.1). The results from the mechanical testing (depicted in figures 4.4.7b & d) show failure of the Kinematic component using the first and second contact points at 40,000 and 1.2 million cycles respectively. In each case, crack formation started at the gap between the rim and the locking tab and extended into the flat part of the tray. The rear edge of the back rim also showed crack formation.

FEA results for the Kinemax component showed that the peak stresses for both contact positions were below the fatigue limit for solution heat-treated CoCr alloy. Fatigue testing for the Kinemax component (figure 4.4.8b & d) showed no evidence of crack formation for either contact position for the entire duration of 5 million cycles.

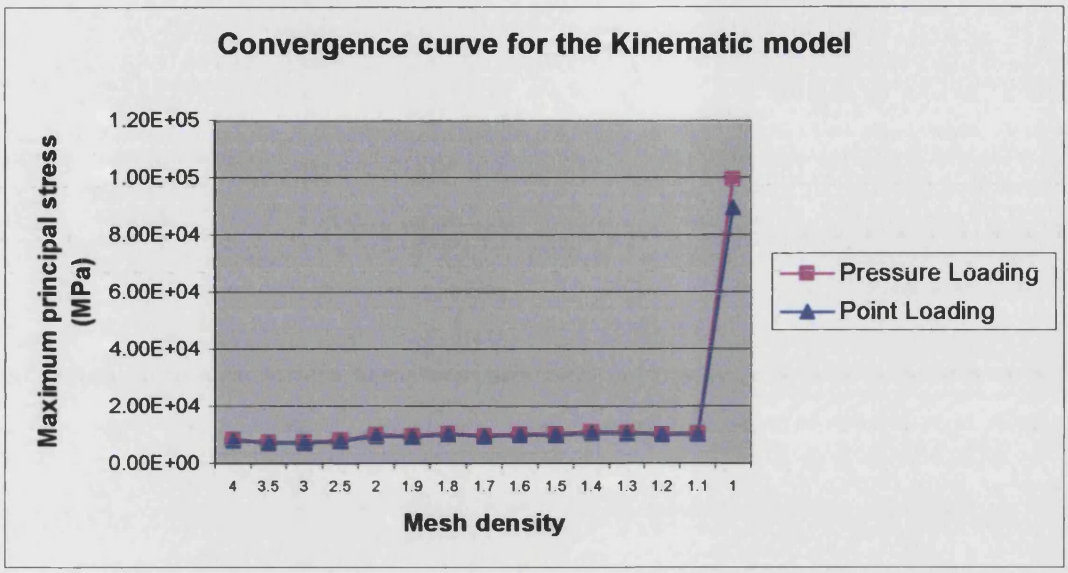

(a)

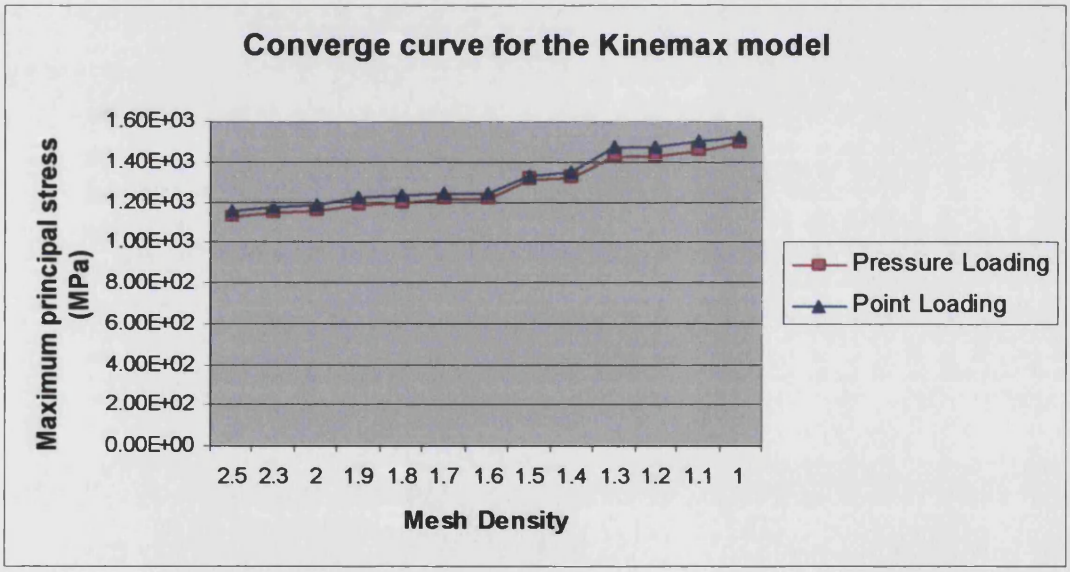

(b)

Figure 4.4.4: Convergence curves for (a) Kinematic (b) Kinemax trays

Model	Pressure Loading Peak Stress (GPa)	Point Loading Peak Stress (GPa)	Difference %
Kinematic (tetrahedral)	10.1	10.6	4.7
Kinematic (hexahedral)	9.8	9.68	1.2
Kinemax (tetrahedral)	1.49	1.52	1.97

Table 4.4.2: Maximum principal stress values for the Kinematic and Kinemax models using the first contact position at 2000N.

Model	Point Loading Peak Stress (GPa)
Kinematic (tetrahedral)	4.45
Kinematic (hexahedral)	4.04
Kinemax (tetrahedral)	1.27

Table 4.4.3: Maximum principal stress values for the Kinematic and Kinemax models using the second contact position at 2000N.

Model	First Contact Point Peak Stress(MPa)	Second Contact Point Peak Stress (MPa)
Kinematic (hexahedral)	2450	1010
Kinemax (tetrahedral)	381	317

Table 4.4.4: Comparison of the peak stresses for the first and second contact positions for the Kinematic and Kinemax components at 500N.

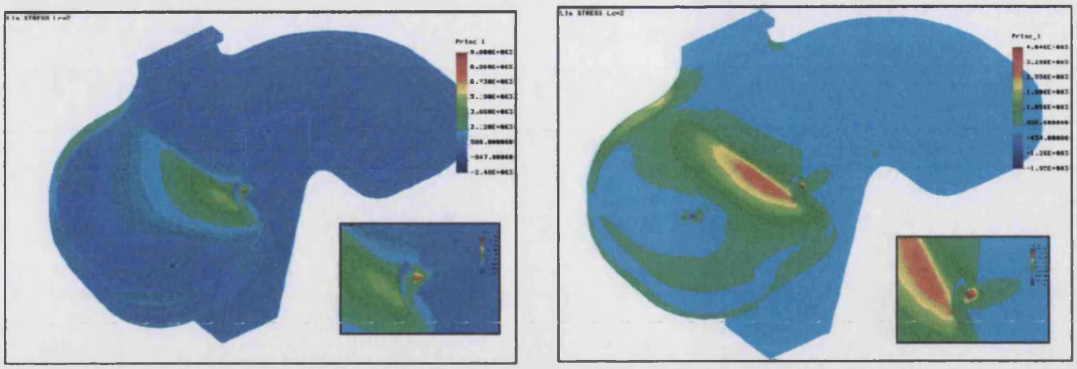

(a) (b)

(c)

Figure 4.4.5: Maximum principal stress distribution for the hexahedral model of the Kinematic tray for (a) the first contact position, (b) the second contact position. (inset : detailed views of stresses in the gap) (c) deformed Kinematic component after being statically loaded.

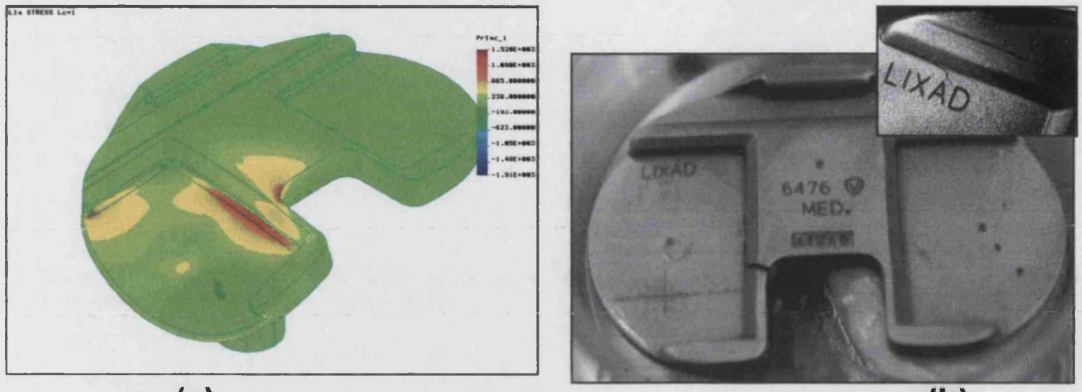

(a) (b)

Figure 4.4.6(a & b): FEA and fatigue test results for Kinemax at 2000N for first contact position. (Inset: crack formation at the top corner of the tray.)

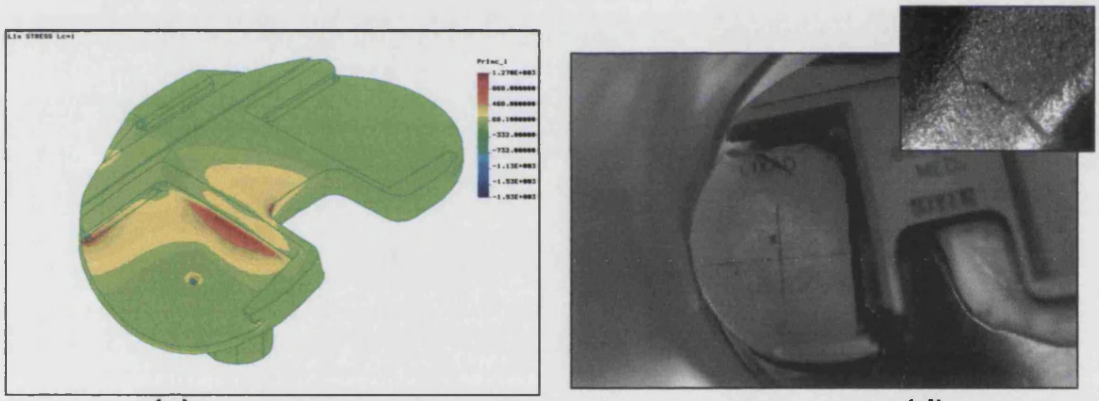

(c) (d)

4.4.6(c &d): FEA and fatigue test results for Kinemax at 2000N for second contact position. (Inset: crack formation at the corner of the posterior cruciate ligament.)

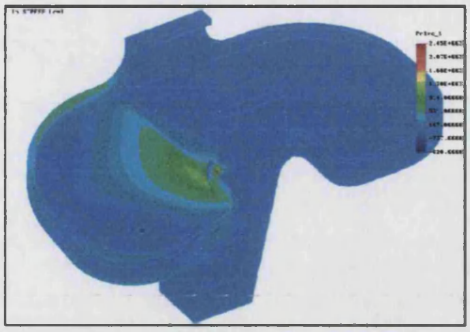

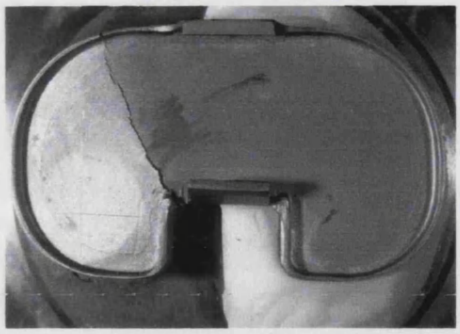

(a) (b)

Figure 4.4.7(a & b): FEA and fatigue test results for Kinematic at 500N for first contact position.

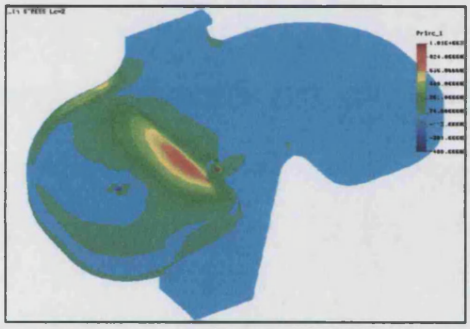

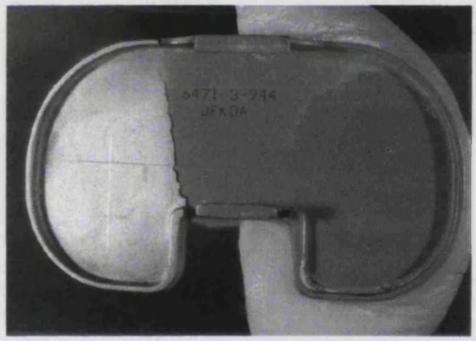

(c) (d)

Figure 4.4.7 (c & d): FEA and fatigue test results for Kinematic at 500N for second contact position.

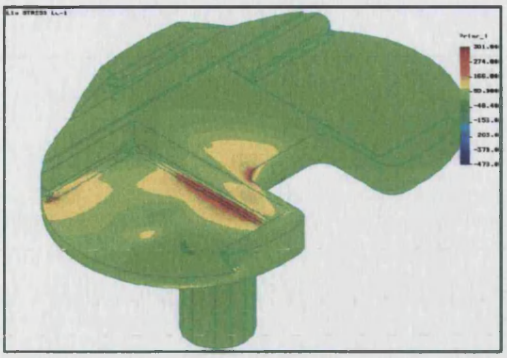

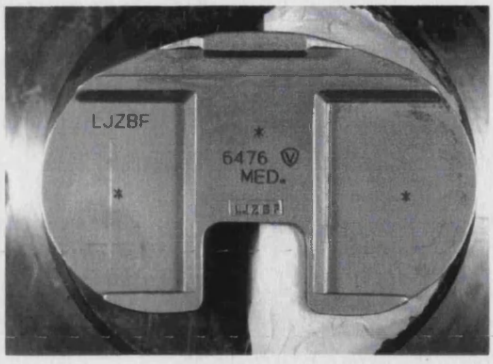

(a) (b)

Figure 4.4.8(a & b): FEA and fatigue test results for Kinemax at 500N for first contact position.

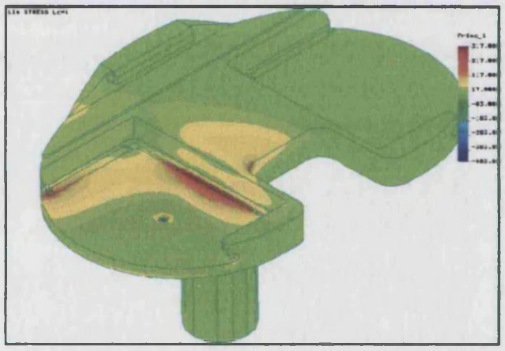

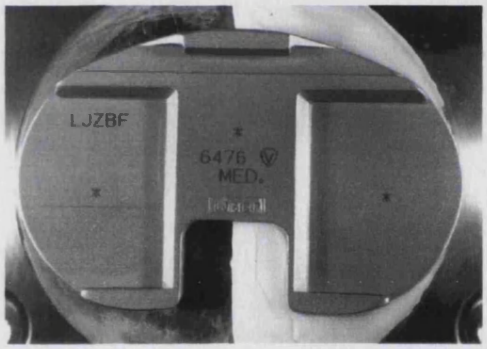

(c) (d)

Figure 4.4.8(c & d): FEA and fatigue test results for Kinemax at 500N for second contact position.

4.4.3 DISCUSSION

For each component using both contact positions, the FEA predictions were confirmed by mechanical testing. This showed that if a physiological load value was used in the test, both the Kinematic and the Kinemax components would rapidly fail.

The Kinematic component was introduced in the late 1970s and withdrawn in the late 1980s during which time, tens of thousands were used. The tray was made from cast CoCrMo alloy and included a cruciate cut out with a gap between the rim and the locking tab. There has been one published report of a series of tray fractures which established failure at a mean of 54 months for early fracture and 7 years for late fracture (Abernethy et al., 1996). However, the evidence is that the actual fatigue failure rate of the tray was only 1-2% of the total at ten years follow-up (Mason et al., 1994). Using FEA and static load testing our study has shown that for the Kinematic tibial baseplate design, plastic flow occurred in the gap on the first load cycle and stresses in this region were well beyond the fatigue limit, indicating early failure. It must be concluded that given the fact that there have been only a limited number of clinical failures that the proposed ISO test represents an extreme situation of *in vivo* conditions. Such conditions are encountered 1-2% of the time clinically. This is enough however to wish to prevent such occurrences.

The Kinemax component was introduced in the late 1980s and is still in widespread clinical use. It is made from CoCrMo alloy that has been solution heat-treated. There are no published reports to the authors' knowledge, of fracture of this baseplate. FEA data and the results from the fatigue testing on the Kinemax tibial baseplate, for both contact positions, using the ISO test conditions predicted failure for this design. Again, it can be concluded that this test is an extreme representation of *in vivo* conditions or is simulating an unrealistic situation.

Further FEA using a load of 500N predicted that the Kinematic tray would still fail due to fatigue for both contact positions but that the Kinemax would survive

using either contact position. In each case the mechanical testing results confirmed the FEA findings. It is therefore concluded that, if the ISO test is to be used as a criteria for clinical failure then a sub-physiological load is required. This study shows that by using a value of 500N, the test would more effectively screen between a component that is liable to fail under physiological conditions and a component that will not fail (Ahir et al., 1999). Further tests on additional tray designs are required to determine whether 500N is the most appropriate dividing line. This is the subject of study two.

4.5 STUDY TWO

The survey of currently available designs categorised tray types according to their features. The trays used for further analyses in this study are shown in Table 4.5.1. Trays that have a history of failure were also included in this study. These were the Kinematic, Total Condylar, and PCA designs.

Tray Design	Material	Tray Shape Insert Type	Fixation	Stem Type
AGC	CoCrMo	Symmetric Fixed	Central stem	I-Beam
AGC porous	CoCrMo	Symmetric Fixed	Central stem	I-Beam
Kinemax	CoCrMo	Symmetric Fixed	Central stem with angled fins	Circular
IB2	Ti6Al4V	Symmetric Fixed	Central stem & 4 screwholes	Square stem
MBK	CoCrMo	Symmetric Mobile	Central stem	Tapered stem
MG2	Ti6Al4V	Symmetric Fixed	4 pegs	No stem
Profix	Ti6Al4V	Asymmetric Fixed	Medialised stem & 4 screwholes	Circular
Rotaglide Uncoated	CoCrMo	Symmetric Mobile	Stem and 2 pegs	Circular
Rotaglide Porous	CoCrMo	Symmetric Mobile	Stem and 2 pegs	Circular
Rotaglide HA coated	CoCrMo	Symmetric Mobile	Stem and 2 pegs	Circular

Table 4.5.1: Tray designs.

4.5.1 Materials and Methods

4.5.1.1 Finite Element Analysis

For this study a different finite element package was used because COSMOS/M (study one) was unable to model more than one material property, or carry out 3D contact analysis. Both these facilities were necessary to conduct studies in appendix B and chapters 5 and 6. Solid models of each design were created in Unigraphics (EDS, USA) and are shown in Figure 4.5.1(a-l). These models were then translated into *iges* format and incorporated into MARC (MSC software, USA) where meshes were generated automatically using higher order tetrahedral elements. For specific features (areas of high stress) the finite element models were refined so that the stress patterns could be accurately obtained. Examples of this refinement are shown in Figure 4.5.2. Material properties of the different types of CoCrMo alloy and titanium alloy are defined in Table 4.5.2. A number of mesh sizes were modelled until subsequent mesh sizes showed peak stresses within 3% of each other for a load of 2000N. (The mesh size depicted in Figure 4.5.2 does not account for the refined areas around stress concentrating features.) The individual models were then considered to have converged. The convergence curve data for each model are shown in Figure 4.5.3. The test specified applying the load using a spherical indentor impacting on a polyethylene spacer. In this study point and pressure loading was applied to the final mesh size. These results are tabulated in Table 4.5.3. These results show that peak differences were 5.5% and this was considered as an acceptable difference. Details of the size of the final mesh size for each component are shown in Table 4.5.4. Finite Element Analysis was conducted on each model to ascertain what load level could be sustained by the component in relation to the material's fatigue limit. A load level was then selected based on FEA results that represented survival of all the clinically successful tray designs. Some tray designs according to the FEA study were able to survive higher load levels. Therefore, three load levels, 900, 1500 and 2000N were then selected to conduct mechanical testing.

4.5.1.2 Mechanical Testing

Two samples of each component were set-up according to the ISO test procedure. One half of the component was rigidly held with specifically made fixtures and using acrylic cement. A gap of at least five millimetres separated the base of the fixture and the undersurface of the tray being tested. The fixed part of the component was then clamped. A maximum cyclic load was then applied at 5Hz through a polyethylene spacer in a multi-channel pneumatically loaded fatigue testing machine until crack formation, or 5 million cycles was achieved (refer to Figure 4.3.3). Tray designs currently available were tested so they were subjected to maximum compressive loads of 900N, 1500N and/or 2000N. Trays that have a history of some clinical failure were subjected to a maximum compressive load of 900N only.

4.5.1.3 Dye Penetrant testing

After the testing regime components were tested for crack formation by using a dye penetrant. This is a method of examining components to detect surface-breaking flaws. The technique is based on the ability of a liquid to be drawn into a "clean" surface breaking flaws by capillary action. The samples were cleaned using a cleaner spray (Flawfinder cleaner, Rocol, UK) to remove any traces of dirt and then wiped with a lint free cloth and placed in a fume cupboard. The dye penetrant (Flawfinder dye penetrant, Rocol, UK) which was a bright pink liquid was then sprayed onto the surfaces of the tibial trays and left for ten minutes to dry. Any excess liquid penetrant was wiped away from the surface. The developer (Flawfinder Developer, Rocol, UK) which was a dry white powder was then sprayed onto the trays and left for ten minutes. The developer draws out the penetrant out of any cracks by reverse capillary action to produce indications on the surface. The trays were then inspected for cracks.

	Young's Modulus (GPa)	Poisson's Ratio	Yield Strength (MPa)	Ultimate Tensile Strength (MPa)	Fatigue Limit (MPa)
Cast CoCrMo	220	0.3	515	725	250 (Weinstow & Clemow, 1990) 300 (Paganelli et al., 1988)
Solution heat-treated CoCrMo	220	0.3	840	1275	410 – 470 (Howmedica)
Ti6Al4V alloy	110	0.3	895	965	515 (Bardos, 1990)
Net forged Ti6Al4V alloy	110	0.3	-	-	724 (Smith & Nephew)

Table 4.5.2: Material Properties of CoCrMo and titanium alloys.

Implant	Point Loading (MPa)	Pressure Loading (MPa)	Difference (%)
Profix	506.6	495.1	2.27
IB2	635	664.3	4.6
MG2	1500	1611	5.2
AGC	910.6	963.5	5.12
KINEMAX	1000	981.4	1.86
ROTAGLIDE	577.3	589.5	2.1
MBK	163	189.2	3.8
KINEMATIC	4553	4732	3.78
PCA	2876.18	2797.8	3.57
Revision PCA	3633	3403.4	2.8
Total Condylar (type 1)	3248	3373	3.85
Total Condylar (type 2)	4260	4436	4.13

Table 4.5.3: Comparison of the difference in stress levels using point and pressure loading

(a) the IB2 tray

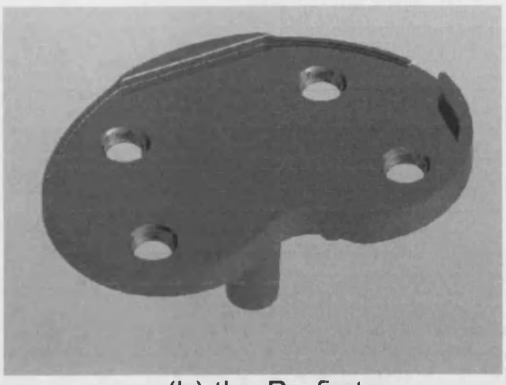

(b) the Profix tray

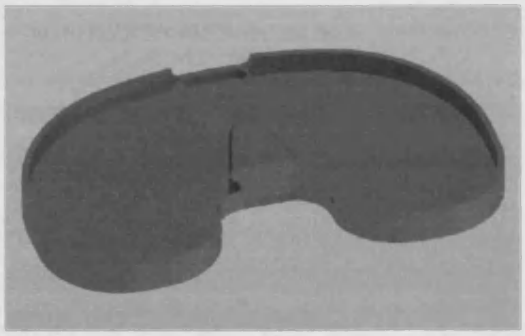

(c) the MG2 tray

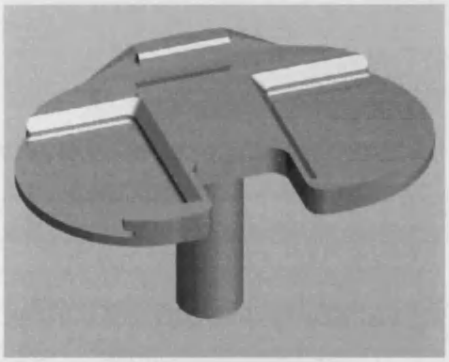

(d) the Kinemax tray

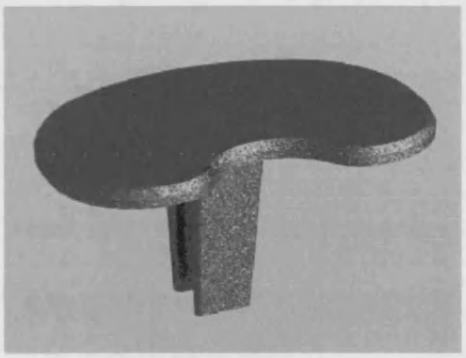

(e) the AGC tray

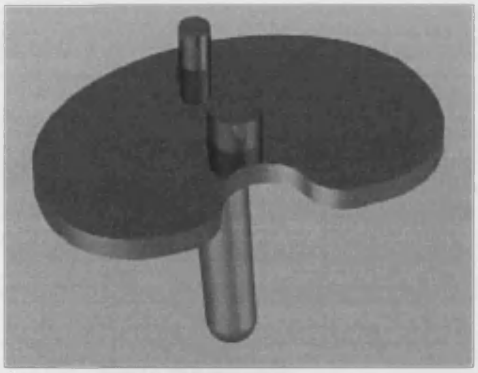

(f) the Rotaglide tray

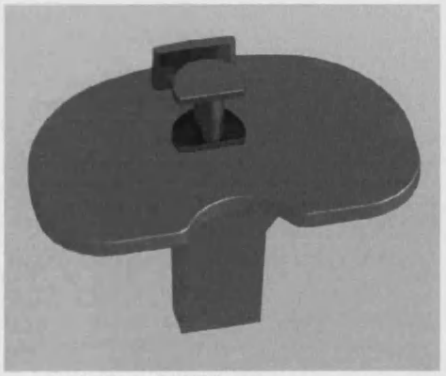

(g) the MBK tray

Figure 4.5.1: Tray designs that are currently available.

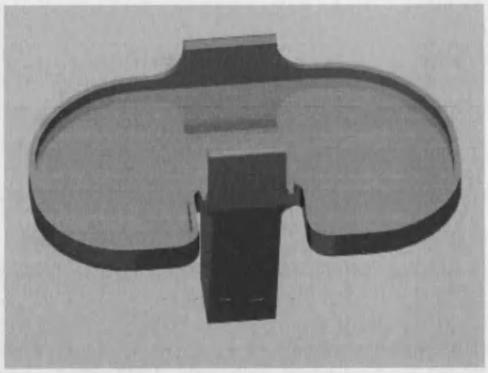

(h) the Kinematic tray

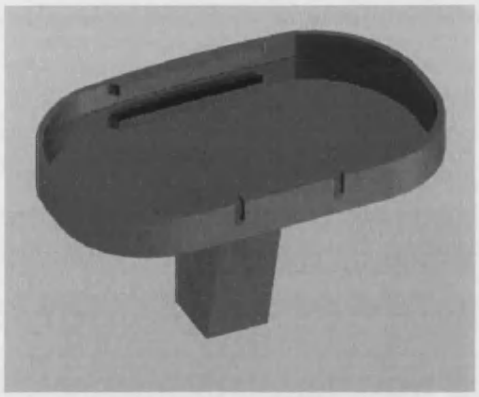

(i) the Total Condylar (type 1)

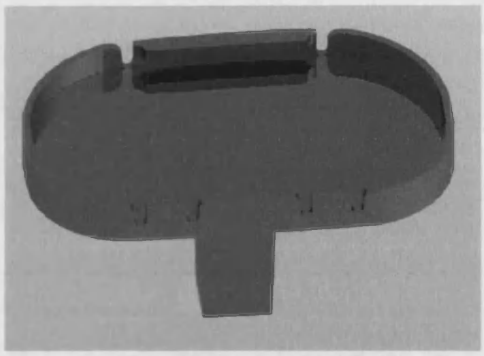

(j) the Total Condylar (type 2)

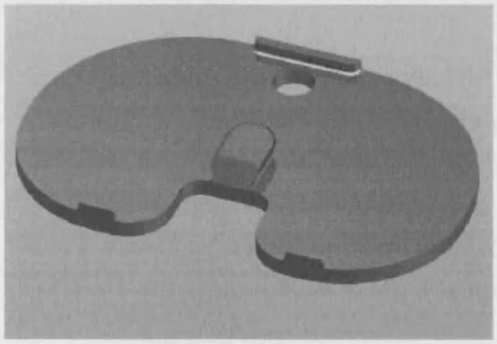

(k) the PCA tray

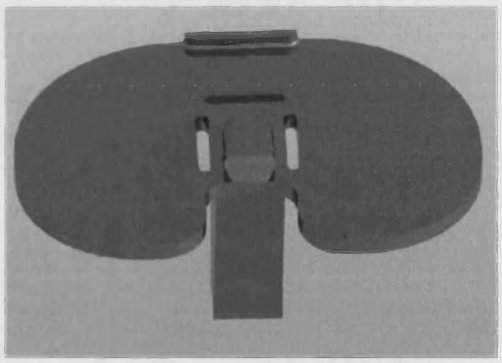

(l) the revision PCA tray

Figure 4.5.1(h)-(l) Tray designs that had a history of clinical failure.

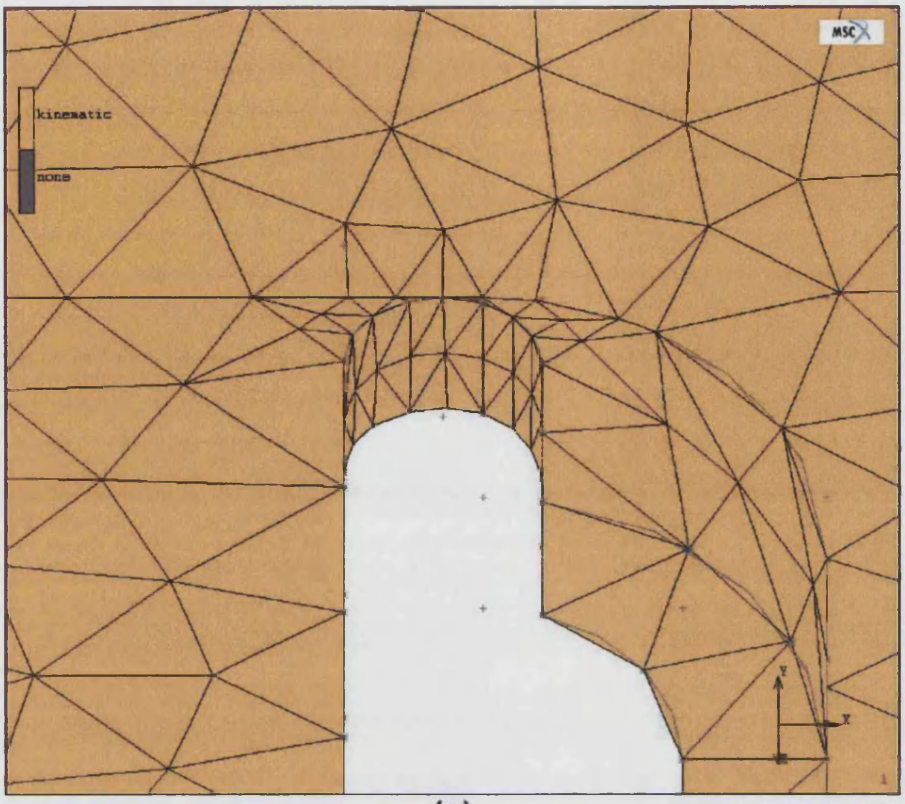

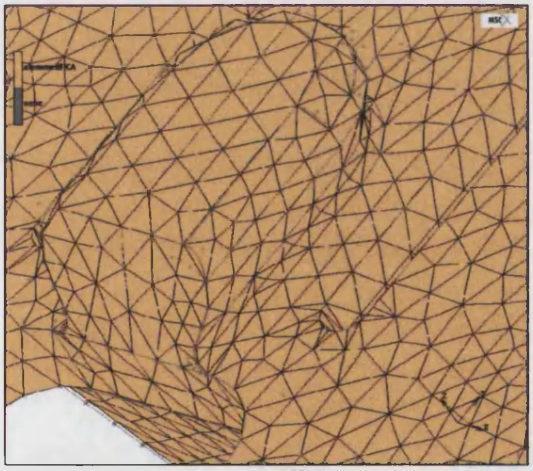

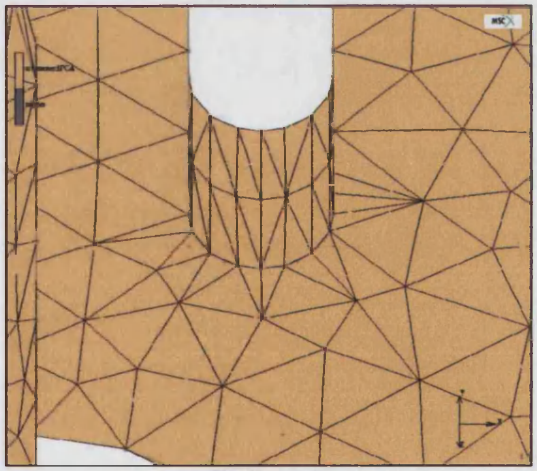

Figure 4.5.2: Refinement of the tetrahedral mesh for (a) kinematic model around the notch adjacent to the locking tab (b) revision PCA model around curved region of the locking tab (c) the fenestration slot.

Implant	Manufacturer	No. of elements	No. of nodes
Profix	Smith & Nephew	30409	49160
IB2	Zimmer	26377	42757
MG2	Zimmer	28814	45822
AGC	Biomet	29767	47071
KINEMAX	Howmedica	30925	48573
ROTAGLIDE	Corin medical	28318	43406
MBK	Zimmer	24954	41350
KINEMATIC	Howmedica	32963	53531
PCA	Howmedica	44287	68299
Revision PCA	Howmedica	27760	43898
Total Condylar (type 1)	Howmedica	32911	52852
Total Condylar (type 2)	Howmedica	27963	45128

Table 4.5.4: FEA models of the components used in this study

Implant	Thickness (mm)
Profix	2.85
IB2	2.5
MG2	3.175
AGC	2.533
KINEMAX	2
ROTAGLIDE	4.75
MBK	3.65
KINEMATIC	1.02
PCA	3
Revision PCA	3
Total Condylar (type 1)	0.85
Total Condylar (type 2)	0.85

Table 4.5.5: Comparison of the thickness of each tray design

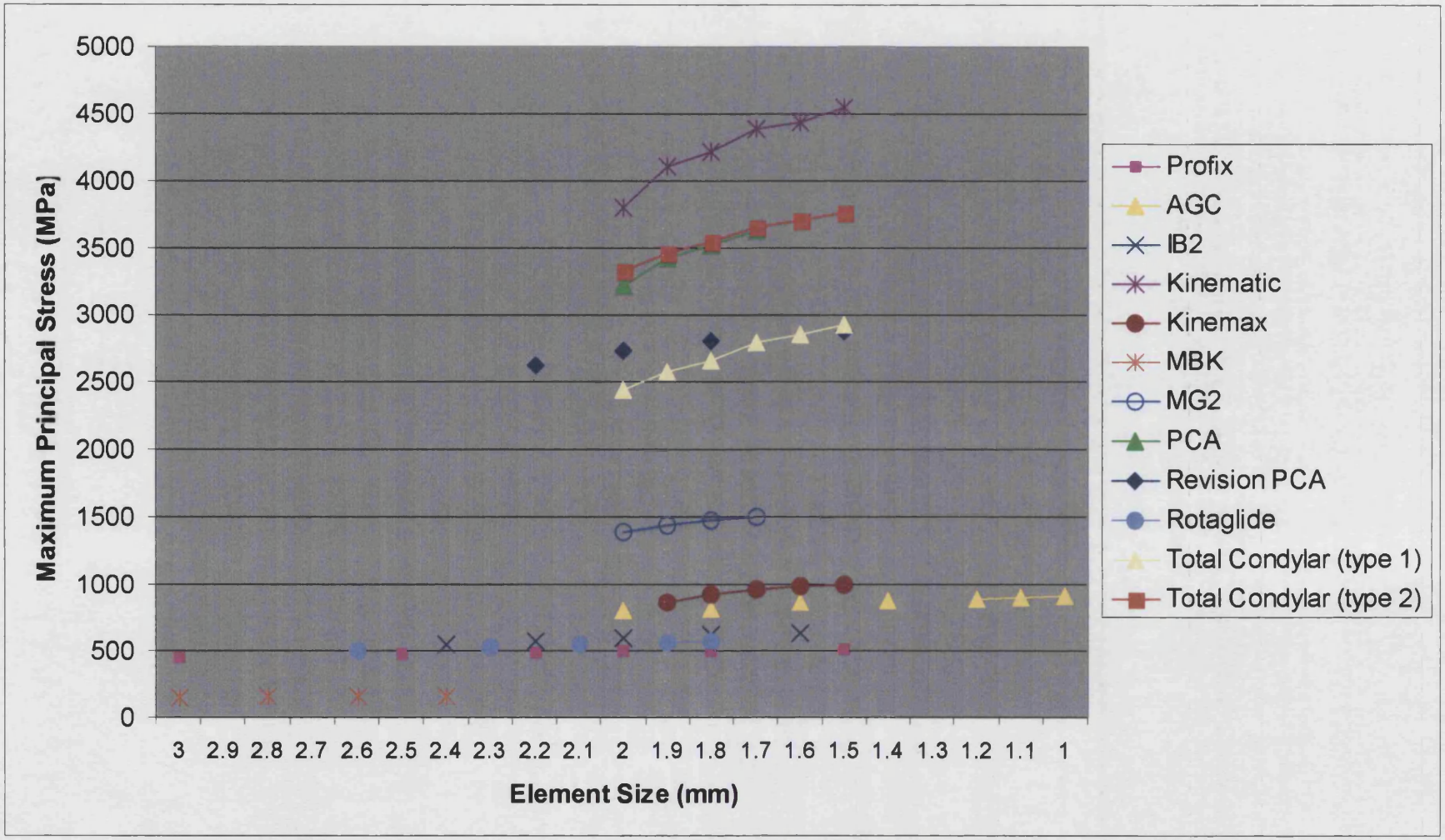

Figure 4.5.3: Convergence curves for all the components used in this study at a load level of 2000N.

4.5.2 RESULTS

4.5.2.1 Using a load level of 2000N

The results of the FEA and mechanical testing carried out on all the tibial tray designs are summarized in Tables 4.5.3 and 4.5.4.

The FEA results predicted that the Profix, IB2 and MBK tray designs would survive a load of 2000N. Fatigue testing of two samples of each component confirmed the FEA results. Each sample of the Profix, IB2 and MBK survived the test to five million cycles (Figures 4.5.4, 4.5.5 and 4.5.6).

From the FEA, it was expected that the Kinemax would fail at 2000N. High regions of stress were predicted in the inner recess and top corner of the component. Fatigue testing of the one Kinemax component showed failure at 594,600 cycles with crack formation consistent with the FEA (Figure 4.5.7).

The AGC tray was predicted to fail using FEA. Six samples were fatigue tested. Four of the samples failed with crack formation in areas consistent with the FEA prediction. However, the results showed a high degree of scatter. Two samples survived the test to five million cycles (Figure 4.5.8).

For the MG2 tray, FEA predicted very high stresses emanating from the notch at the locking mechanism for the tibial insert. Fatigue testing of the two samples showed failure of both components within 29,060 cycles. However, both samples showed failure by crack formation on the supported side of the tray (Figure 4.5.9) due to the whole of the tray and the cement mantle lifting away from the fixture due to insufficient clamp pressure for the applied load.

4.5.2.2 Using a load of 1500N

The FEA for the Kinemax tray loaded at 1500N showed peak stresses above the fatigue limit of solution heat-treated CoCrMo alloy. Under fatigue test conditions, however, both samples tested survived without crack formation to 5 million cycles (Figure 4.5.10).

At 1500N, the AGC and AGC porous were both predicted to fail. Two samples were used, under fatigue test conditions, for both components. The results showed failure of one of the AGC components at 1,310,000 cycles but survival of the other to five million cycles. Both AGC porous components survived to five million cycles (Figure 4.5.11).

The FEA for the Rotaglide tray predicted failure. Under fatigue test conditions, the two uncoated trays survived to five million cycles. One of the porous coated and one of the HA-coated trays failed at 1,698,000 and 4,058,000 cycles respectively in areas consistent with the FEA (Figure 4.5.12).

FEA of the MG2 tray also predicted failure. Two samples of the tray failed under fatigue test conditions at 22,900 and 52,600 cycles. One of the trays had crack formation on the supported side and this was due to insufficient clamp pressure for the applied load (Figure 4.5.13).

4.5.2.3 Using a load of 900N

At 900N, the FEA predicted survival of the Kinemax, AGC, AGC porous, Rotaglide and MG2 tray designs. Under fatigue test conditions, two samples of each tray showed survival to five million cycles (Figure 4.5.14, 4.5.15. 4.5.16 and 4.5.17).

At 900N, the FEA predicted failure of the Kinematic, PCA, PCA revision and Total Condylar (type 1 and 2). Under fatigue testing conditions, two samples

of the Kinematic failed at 154,300 and 485,700 cycles (Figure 4.5.18); the PCA components failed at 336,100 and 413,100 cycles (Figure 4.5.19); the Total Condylar (type 2) failed at 527,500 and 848,700 cycles (Figure 4.5.20). There were no samples available to test for the PCA revision (Figure 4.5.21) or the Total Condylar (type 1) tray (Figure 4.5.22)

4.5.2.4 Dye penetrant testing

All trays that had survived fatigue testing were subjected to dye penetrant testing. The results showed that there were no crack formation which would have resulted in pink dye (the colour of the dye pentrant) emerging through the developer. A representative sample of trays is depicted in Figure 4.5.23.

LOAD LEVEL	2000N	1500N	900N
Tray Design	Peak	Stress	(MPa)
PROFIX	506.6	-	-
IB2	635	-	-
MBK	163	-	-
KINEMAX	1000	750	450
AGC	910.6	682.9	421
MG2	1500	1124	675
ROTAGLIDE	-	433	260
KINEMATIC	-	-	2050
TOTAL CONDYLAR (type 2)	-	-	1917
PCA	-	-	1019
PCA revision	-	-	1061
TOTAL CONDYLAR (type 1)	-	-	1462

Table 4.5.6: FEA results summary.

	Load level		
Tray Design	**2000N**	**1500N**	**900N**
PROFIX	PASS (2 samples)-	-	
IB2	PASS (2 samples)-	-	
MBK	PASS (2 samples)-	-	
KINEMAX	FAIL (2 samples)	PASS (2 samples)	PASS (2 samples)
AGC	4 failures from 6 samples	1 failure from 2 samples	PASS (2 samples)
AGC POROUS	-	PASS (2 samples)	PASS (2 samples)
MG2	-	FAIL (2 samples)	PASS (2 samples)
ROTAGLIDE Uncoated	-	PASS (2 samples)	PASS (2 samples)
ROTAGLIDE Porous	-	1 failure from 2 samples	PASS (2 samples)
ROTAGLIDE HA coated	-	1 failure from 2 samples	PASS (2 samples)
KINEMATIC	-	-	FAIL (2 samples)
TOTAL CONDYLAR (type 2)	-	-	FAIL (2 samples)
PCA	-	-	FAIL (2 samples)
PCA revision	-	-	No samples to test
TOTAL CONDYLAR (type 1)	-	-	No samples to test

Table 4.5.7: Fatigue test results summary.

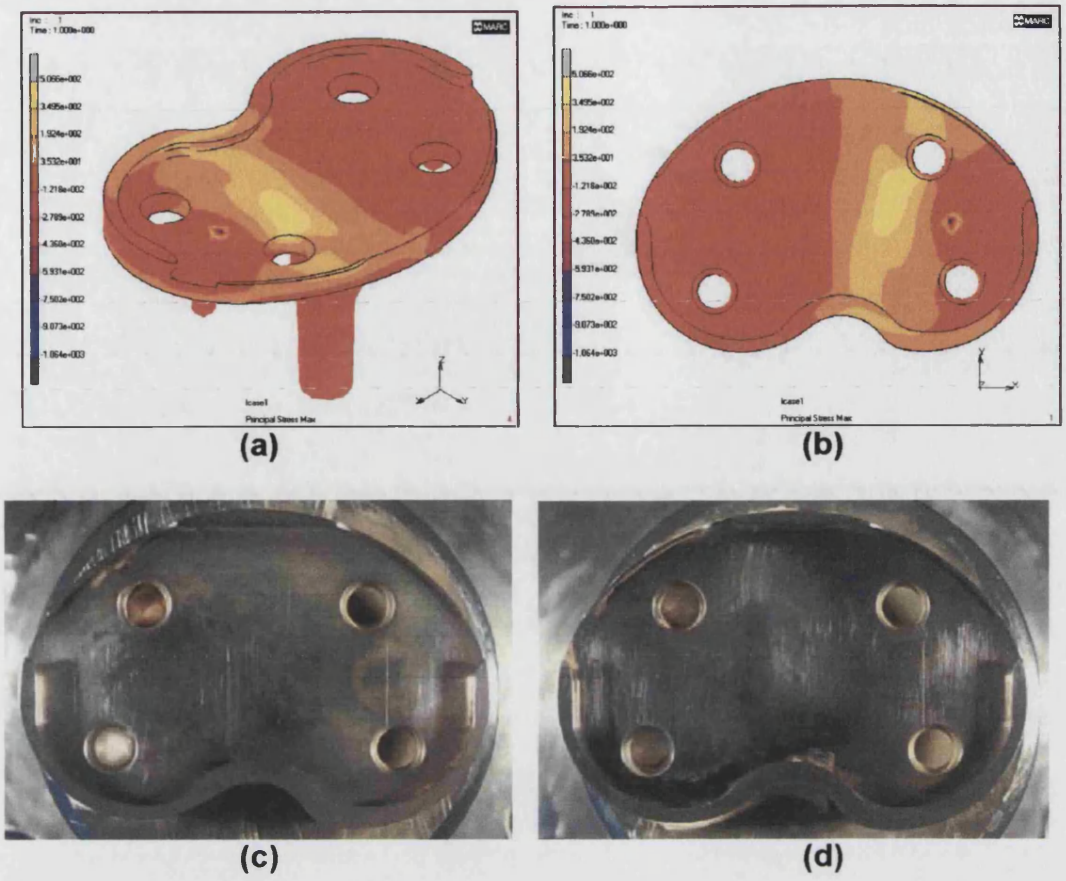

Figure 4.5.4 (a-b) FEA models show that the peak stress for the Profix model at 2000N is 506.6MPa. This is below the fatigue limit of the material. (c & d) Survival of the Profix trays at 2000N at 5 million cycles under the ISO test.

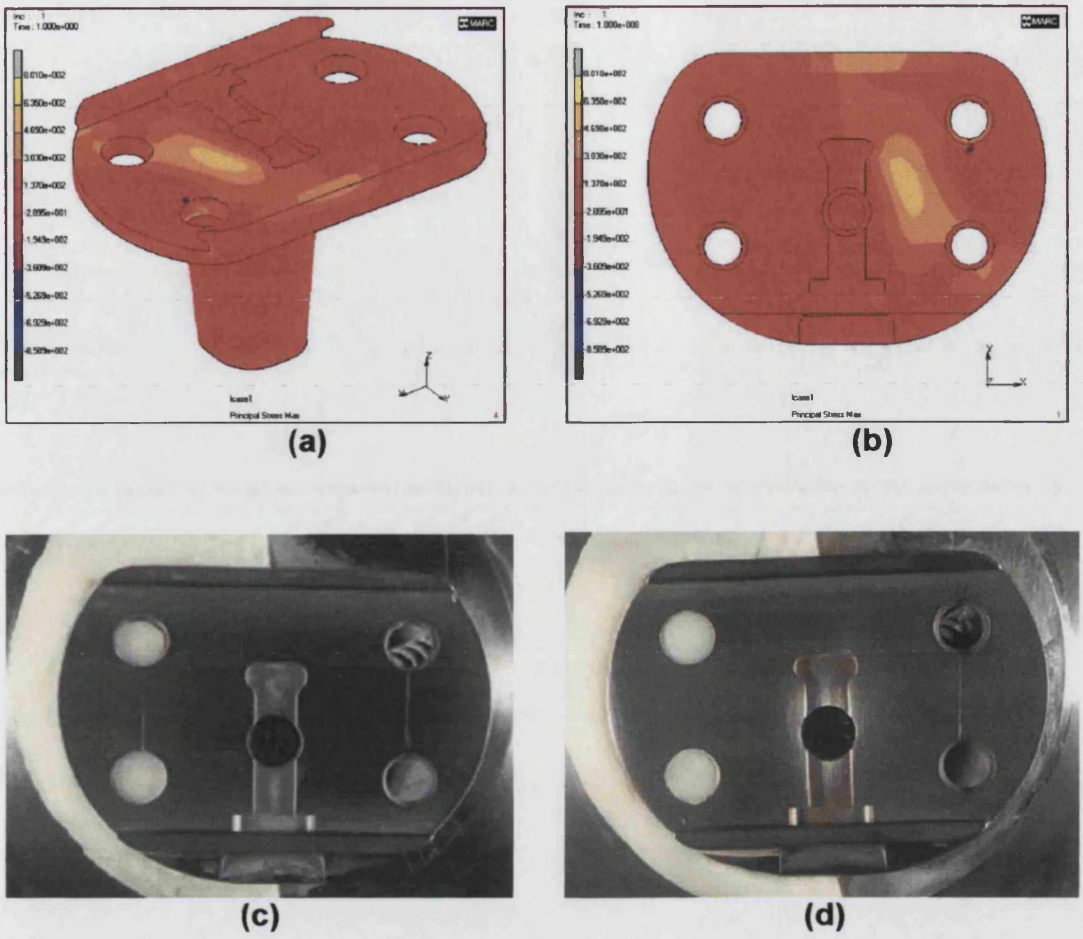

Figure 4.5.5 (a-b) FEA models show that the peak stress for the IB2 model at 2000N is 635 MPa on the upper surface. This is below the fatigue limit of the material. (c-d) Survival of the IB2 trays at 2000N at 5 million cycles under the ISO test.

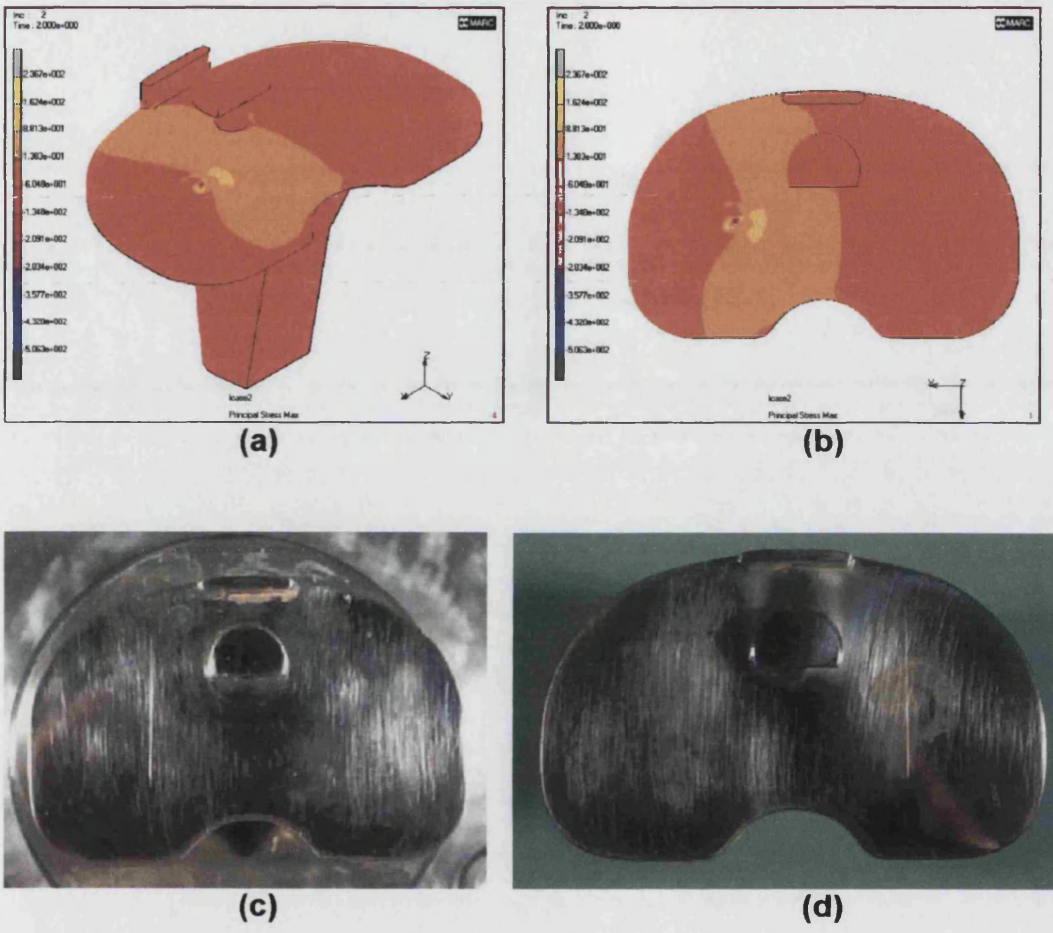

Figure 4.5.6 (a-b) FEA models show that the peak stress for the MBK model at 2000N is 163MPa. This is below the fatigue limit of cast CoCrMo alloy. (c-d) Survival of the MBK trays at 2000N at 5 million cycles under the ISO test.

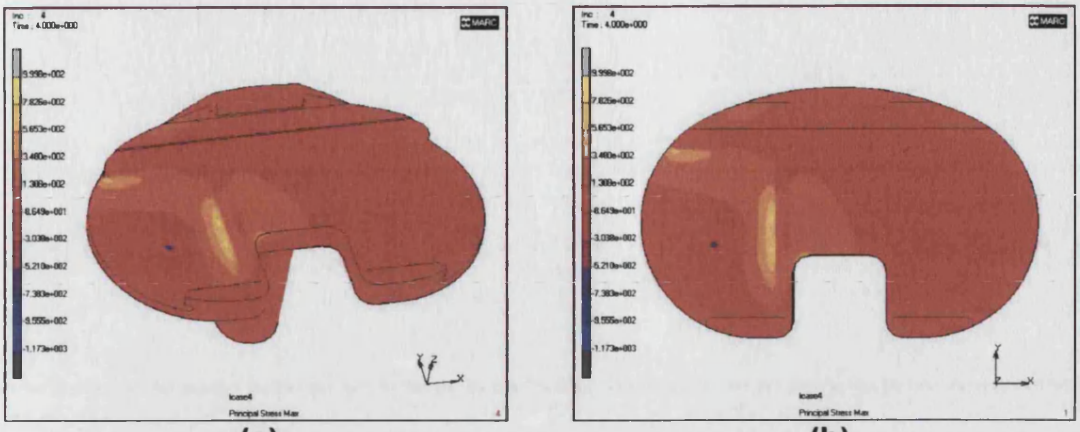

(a) (b)

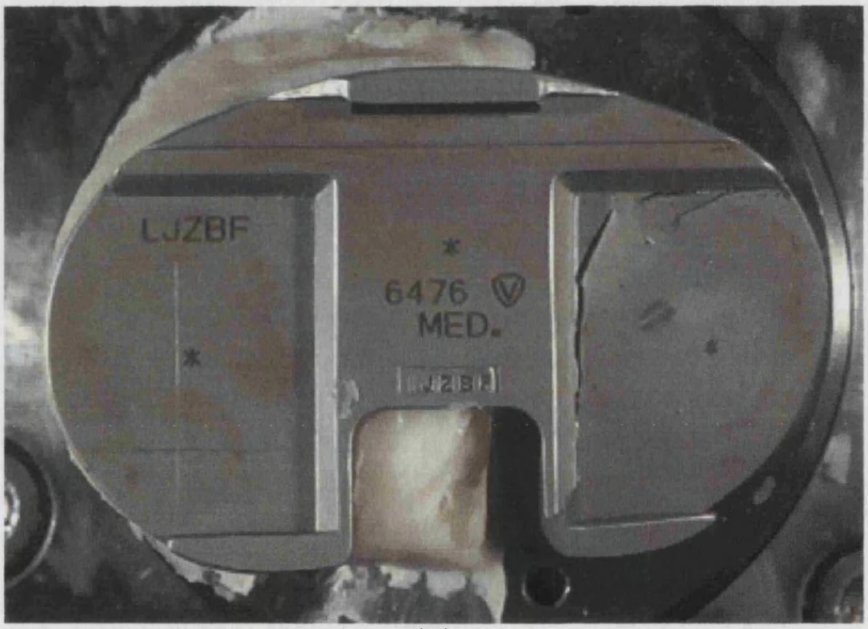

(c)

Figure 4.5.7 (a-b) FEA models show that the peak stress for the Kinemax model at 2000N is 1000MPa. This is much higher than the fatigue limit for solution treated CoCrMo alloy. (c) Only one sample was used. Failure of the Kinemax tray occurred at 594,600 cycles using 5Hz. The tray shows crack formation in areas predicted by the FEA model.

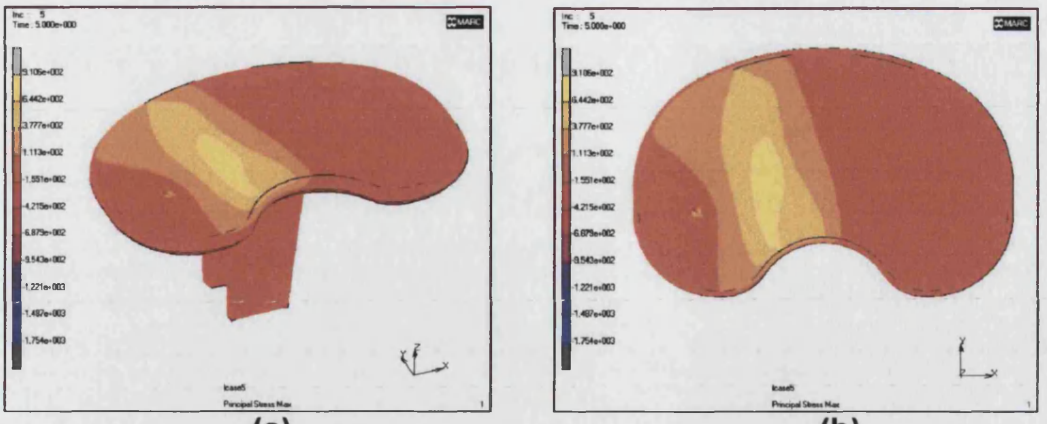

(a) (b)

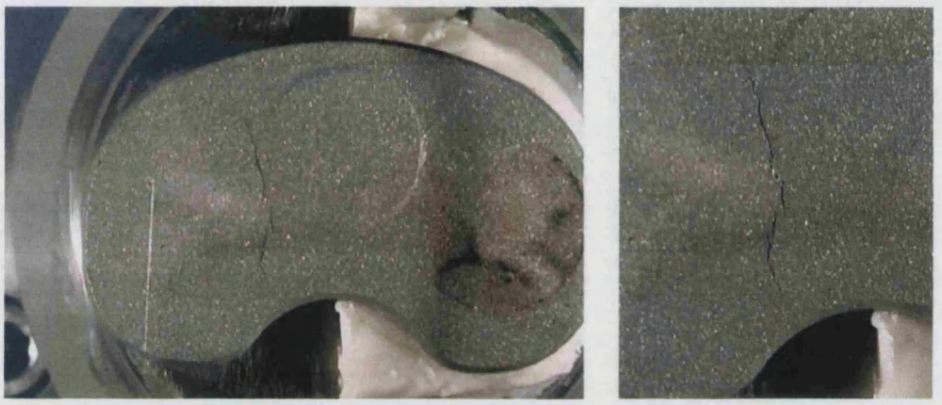

(c) (d)

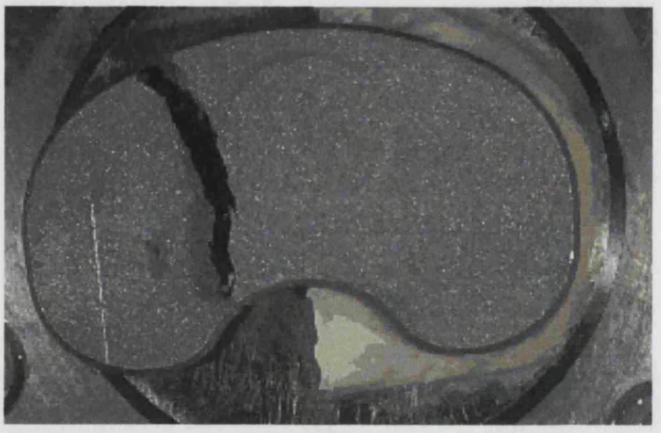

(e)

Figure 4.5.8 (a-b) FEA models show peak stresses at 910.6 MPa at a load level of 2000N, which are above the fatigue limit for cast CoCrMo alloy. (c & d) Failure of first baseplate showing crack formation at 69,830 cycles (e) this component was allowed to continue under the test conditions. Final fracture occurred at 782,000 cycles.

(f) Fracture of second baseplate at 1,290,000 cycles.

(g) main & inset:Crack formation on third baseplate at 1,716,220 cycles

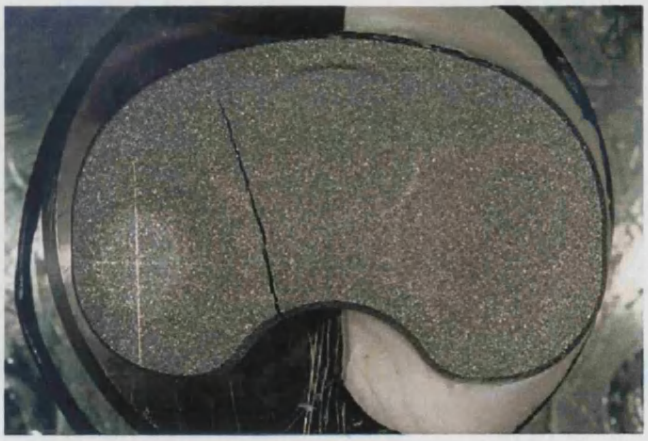

(h) Fracture of fourth baseplate at 3,133,190 cycles.

Figure 4.5.8(cont'd): Fractured baseplates of the AGC.

(i)

(j)

Figure 4.5.8 (cont'd) (i & j): No crack formation at 5 million cycles for the fifth and sixth baseplates using a load level of 2000N.

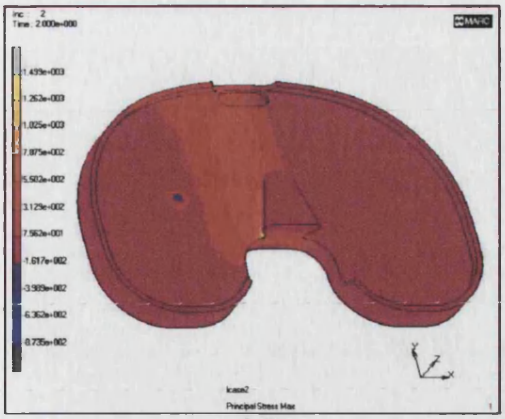

(a)

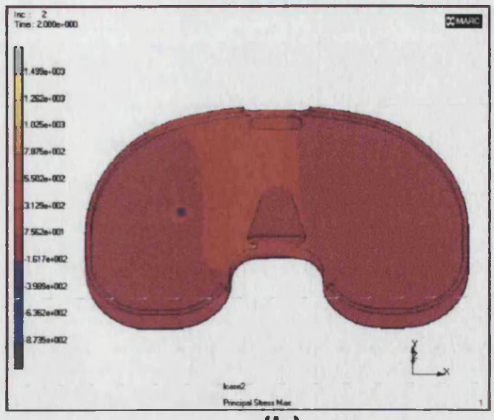

(b)

(c)

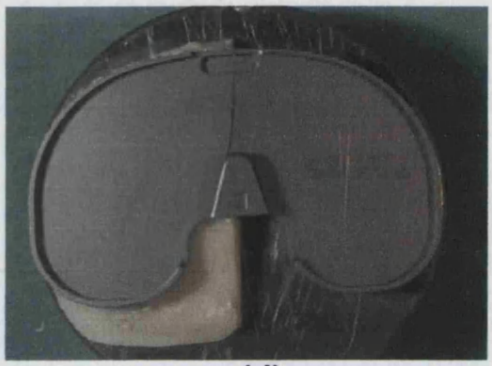

(d)

Figure 4.5.9 (a-b) FEA models show that the peak stress for the MG2 model at 2000N is 1500MPa. This is much higher than the fatigue limit for titanium alloy. (c & d) Failure of both MG2 trays occurred within 29,060 cycles.

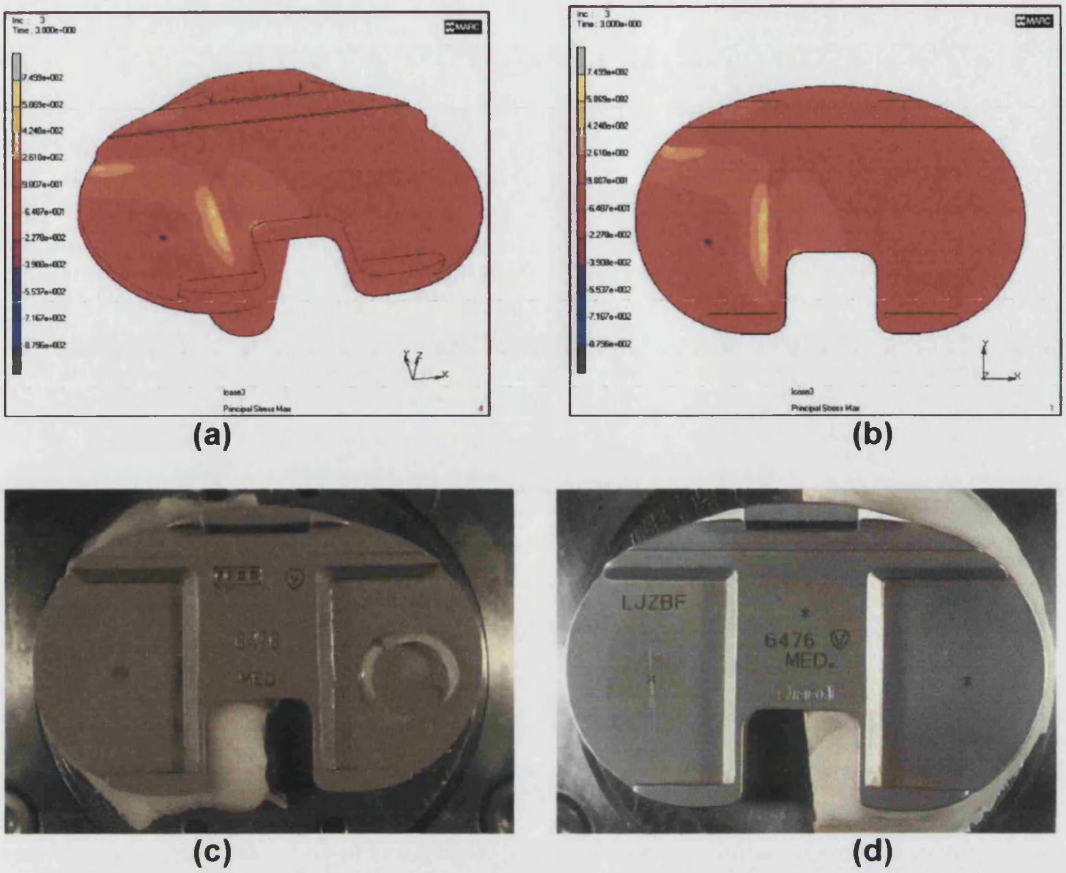

Figure 4.5.10 (a-b) FEA models show that the peak stress for the Kinemax model at 1500N is 750 MPa. This is above the highest limit for solution heat-treated CoCrMo alloy. (c & d) Survival of both Kinemax trays at 5 million cycles.

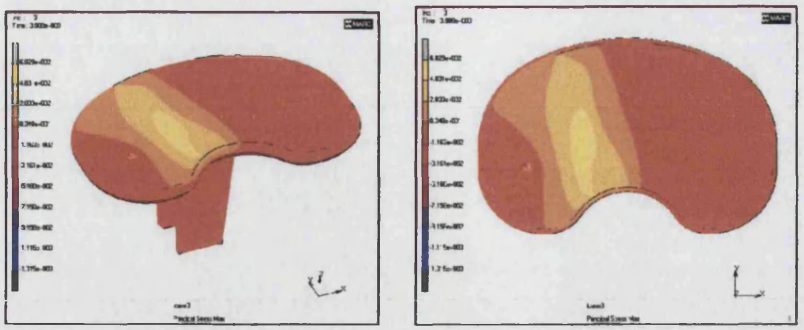

(a) (b)

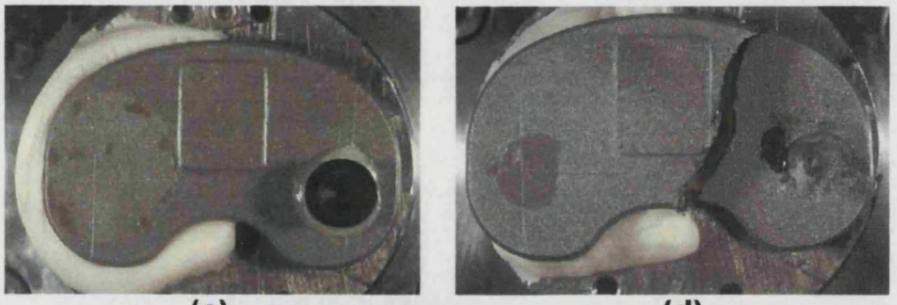

(c) (d)

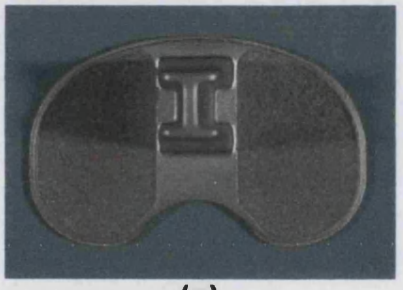

(e)

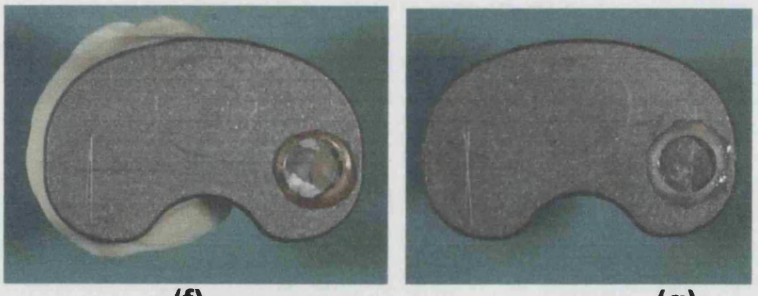

(f) (g)

Figure 4.5.11 (a-b) FEA models show that the peak stress for the AGC model at 1500N is 682.9 MPa. This is higher than the fatigue limit for cast CoCrMo alloy. (c & d) Failure of one of the two AGC trays at 1,310600 and survival of the other. (e) Undersurface of the porous coated AGC tray. (f & g) Survival of both porous coated trays at 5 million cycles.

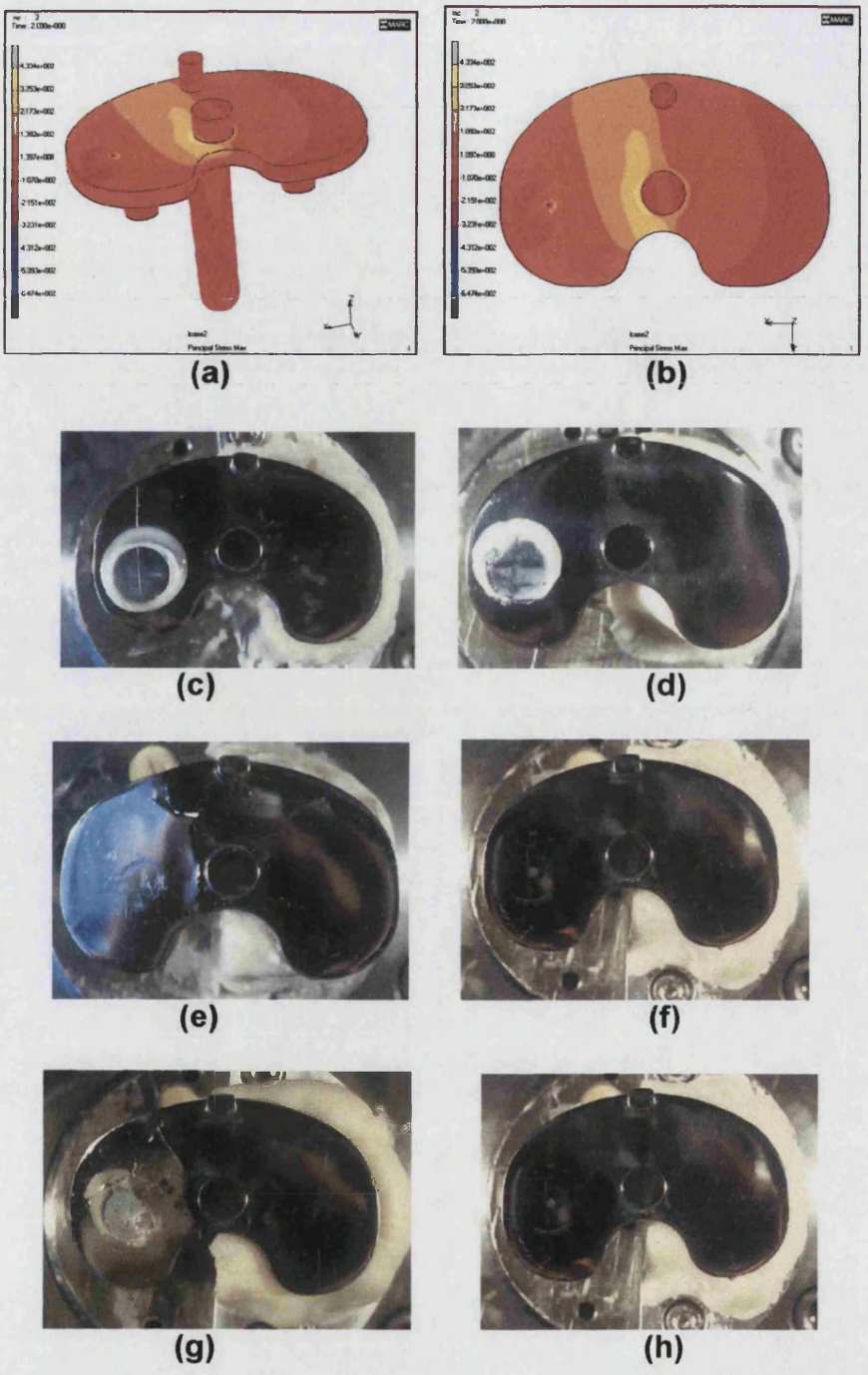

Figure 4.5.12 (a-b) FEA models show that the peak stress for the Rotaglide model at 1500N is 433 MPa. This is higher than the fatigue limit for cast CoCrMo alloy. (c & d) Survival of the two uncoated Rotaglide trays. (e & f) Failure of one of the two porous coated occurred at 1,698,000 cycles and survival of the other at 5 million cycles. (g & h) Failure of one of the two HA-coated trays at 4,058,100 and survival of the other at 5 million cycles.

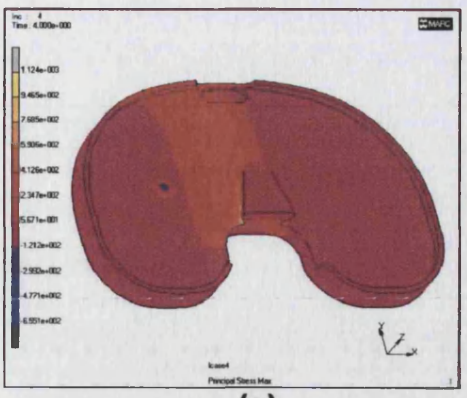

(a)

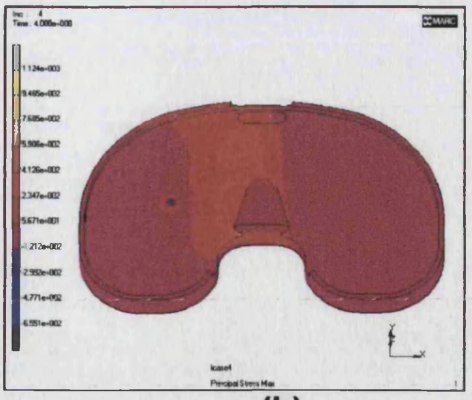

(b)

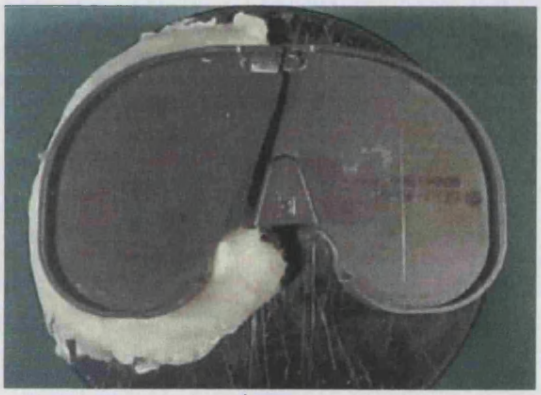

(c)

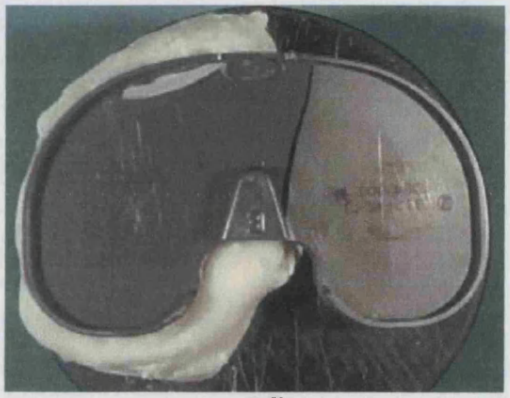

(d)

Figure 4.5.13 (a-b) FEA models show that the peak stress for the MG2 model at 1500N is 1124 MPa. This is higher than the fatigue limit for titanium alloy. (c & d) Failure of both MG2 trays at 22,900 and 52,600 cycles.

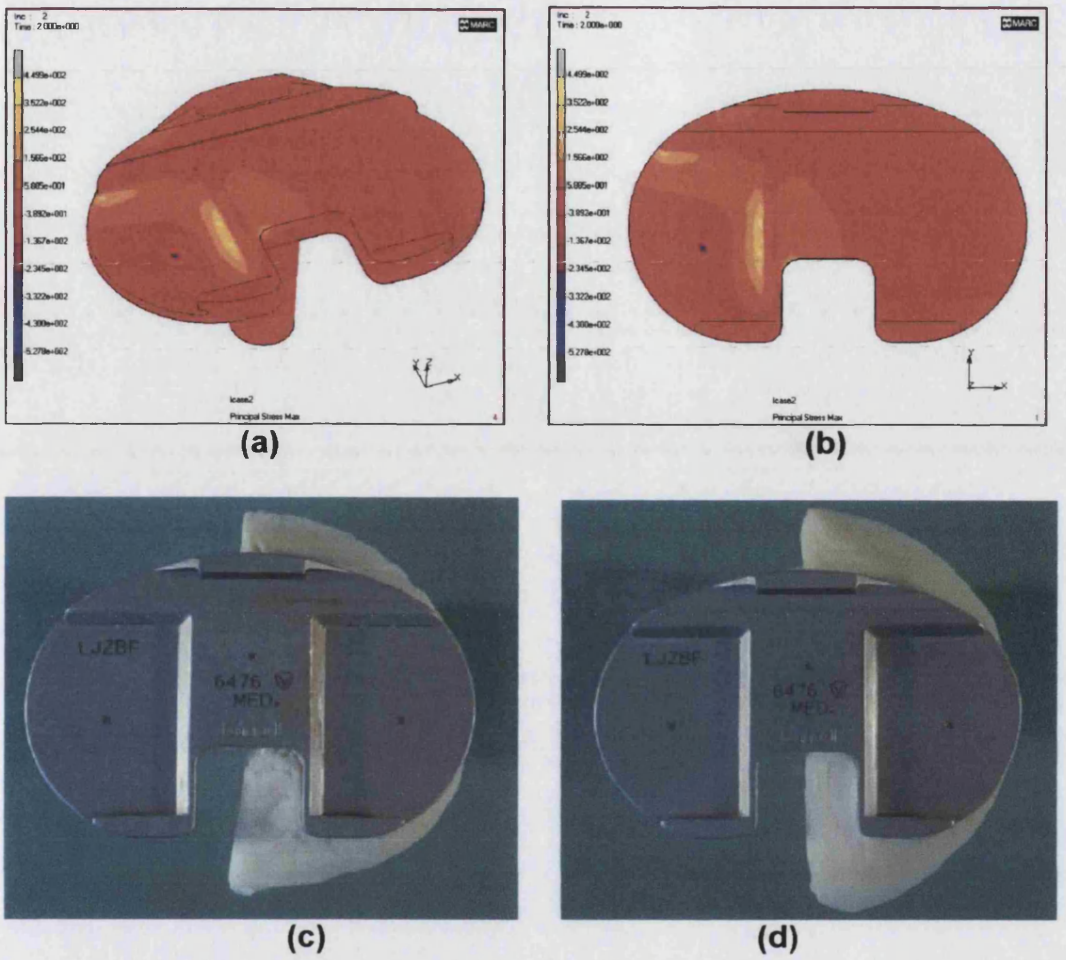

Figure 4.5.14 (a-b) FEA models show that the peak stress for the Kinemax model at 900N is 450 MPa. This is within the fatigue limit for solution heat-treated CoCrMo alloy. (c & d) Survival of both Kinemax trays at 5 million cycles.

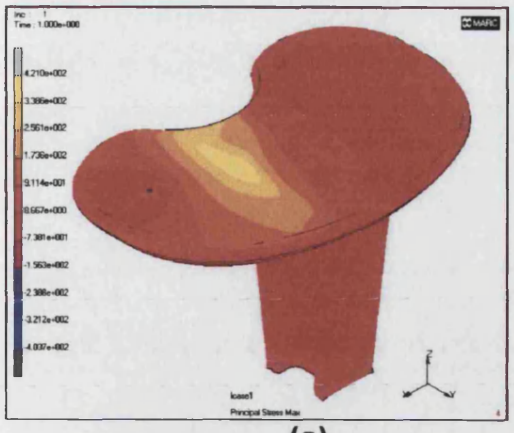

(a)

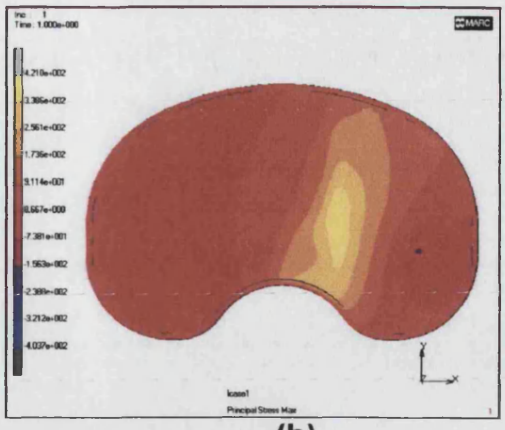

(b)

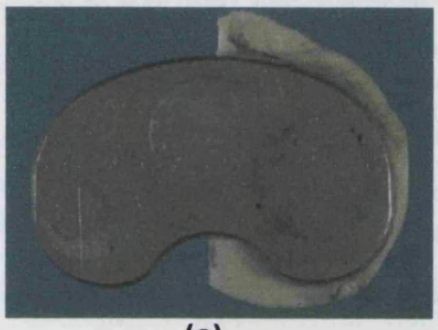

(c)

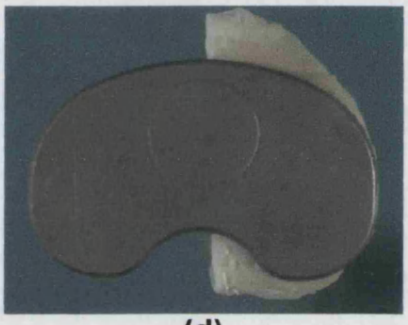

(d)

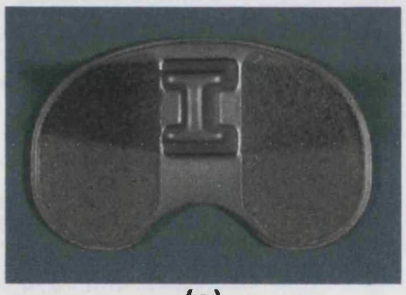

(e)

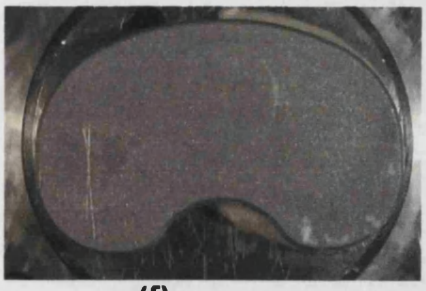

(f)

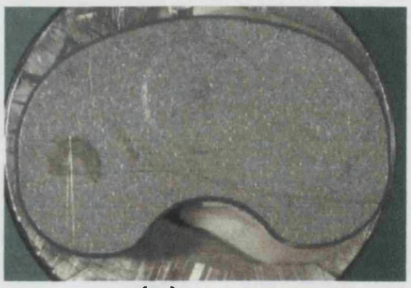

(g)

Figure 4.5.15 (a-b) FEA models show that the peak stress for the AGC model at 900N is 421 MPa. This is higher than the fatigue limit for cast CoCrMo alloy. (c & d) Survival of both AGC trays at 5 million cycles. (e) the undersurface of the porous AGC tray. (f & g) Survival of both porous coated trays at 5 million cycles.

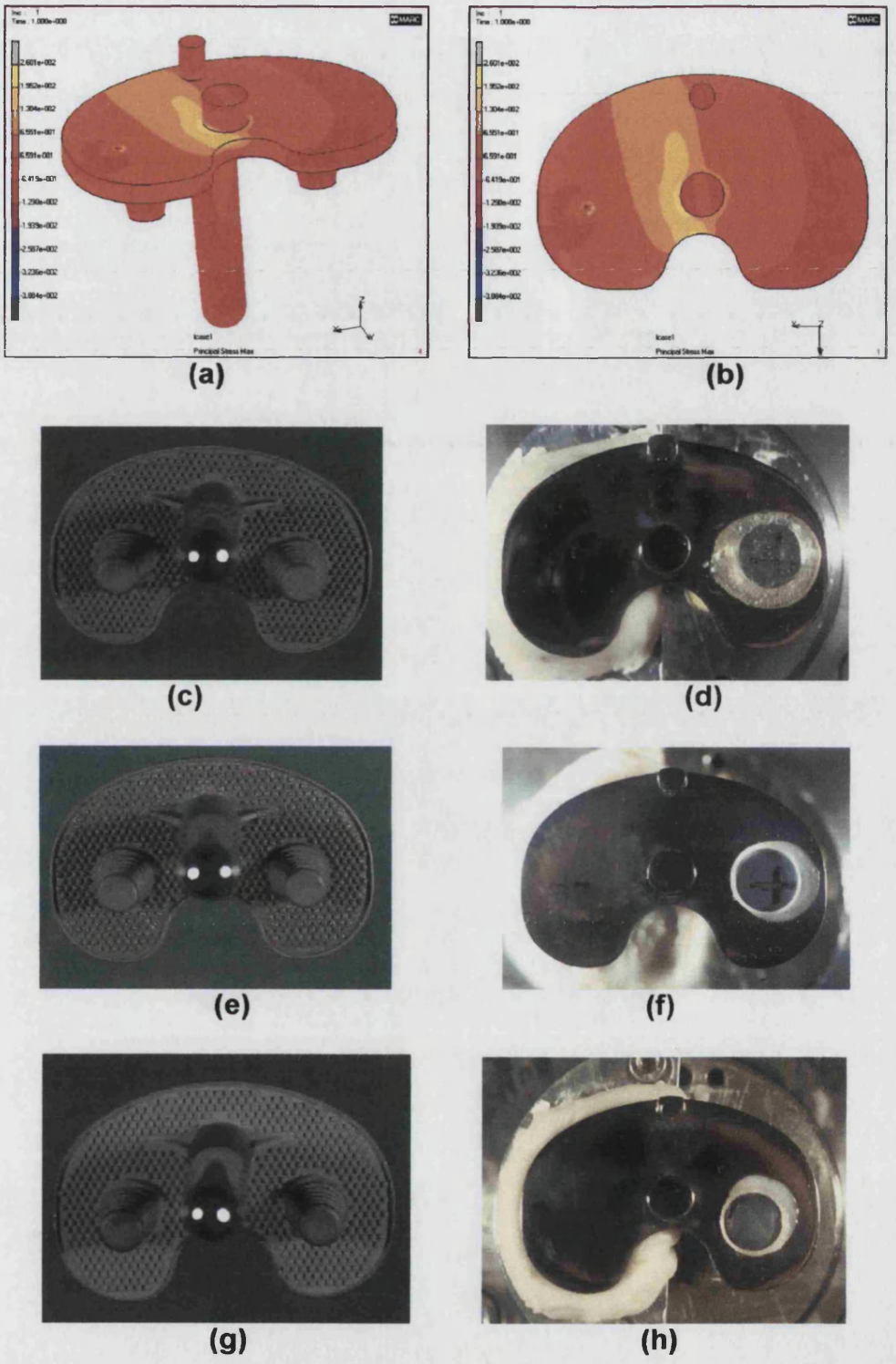

Figure 4.5.16 (a-b) FEA models show that the peak stress for the Rotaglide model at 900N is 260 MPa. This is below the fatigue limit for cast CoCrMo alloy. Upper and lower surfaces of the Rotaglide trays showing survival of (c & d) uncoated (e & f) porous coated (g & h) HA-coated at 5 million cycles.

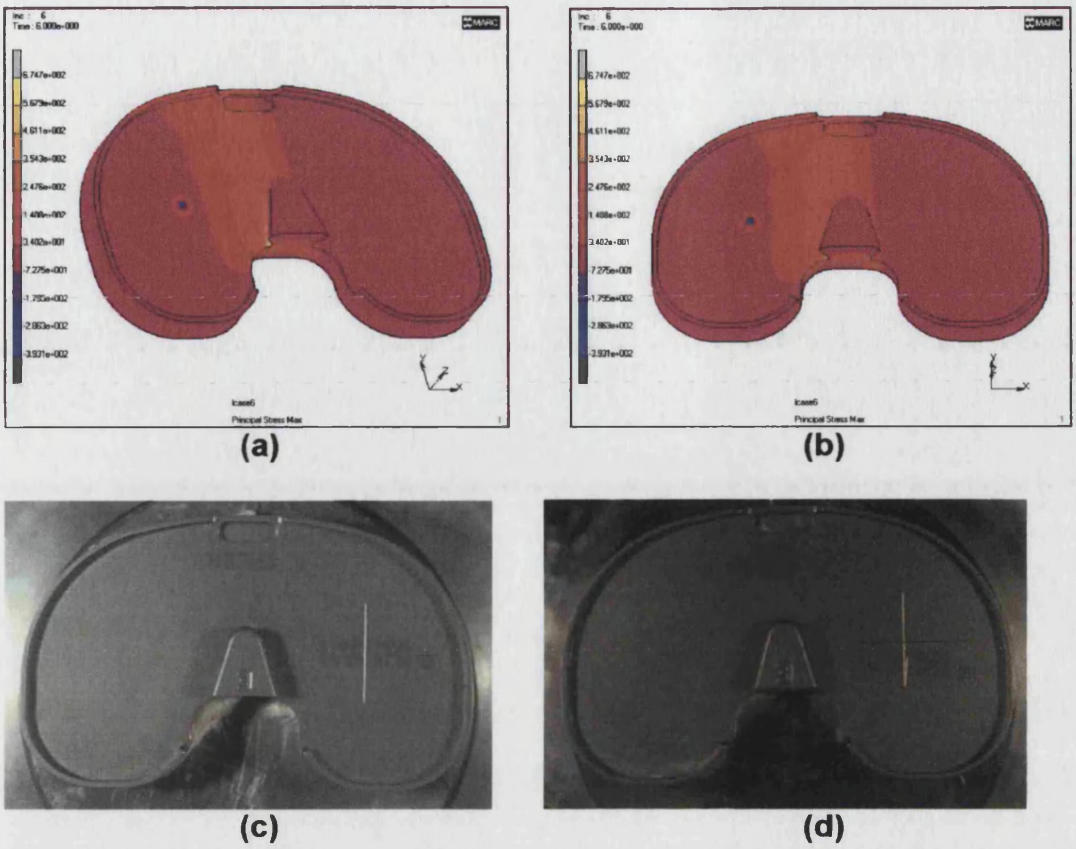

Figure 4.5.17 (a-b) FEA models show that the peak stress for the MG2 model at 900N is 675 MPa. This is higher than the fatigue limit for titanium alloy. (c & d) Survival of both MG2 trays at 5 million cycles.

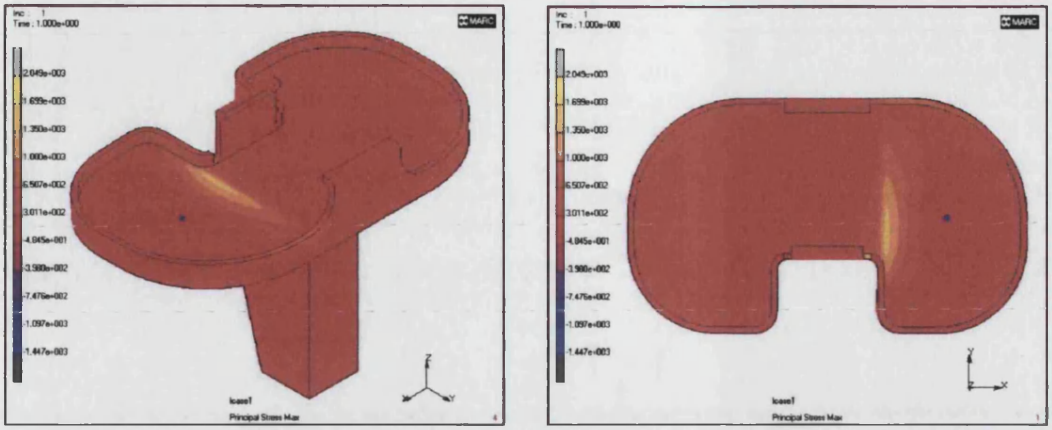

(a) (b)

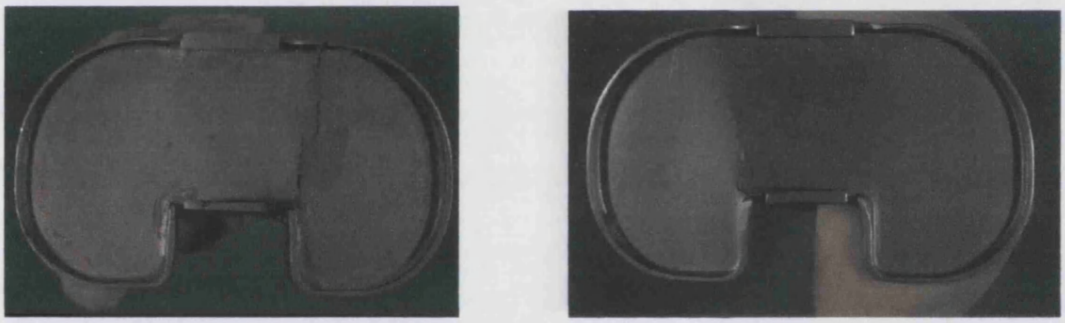

(c) (d)

Figure 4.5.18 (a-b) FEA models show that the peak stress for the Kinematic model at 900N is 2.05GPa. This is significantly higher than the fatigue limit for cast CoCrMo alloy. (c & d) Failure of both Kinematic trays occurred at 154,300 and 485,700 cycles.

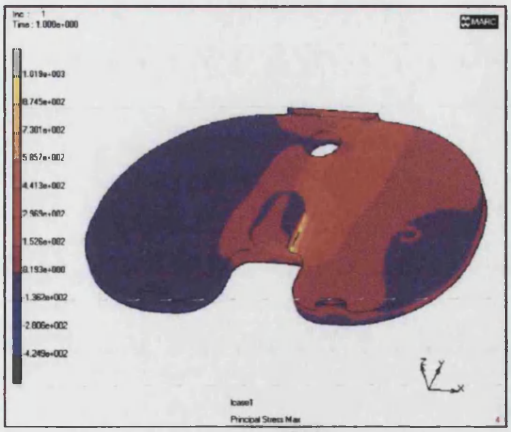

(a)

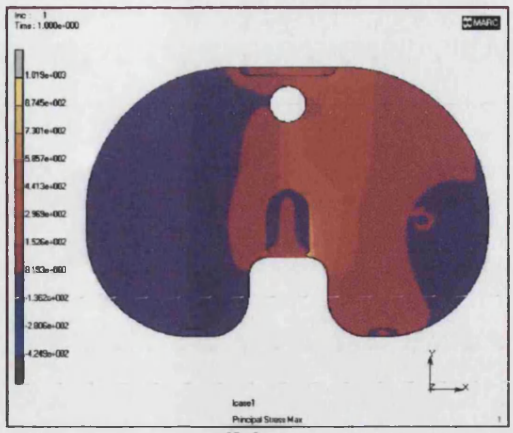

(b)

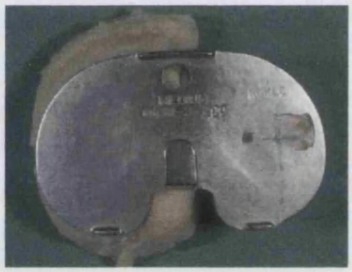

(c) main inset

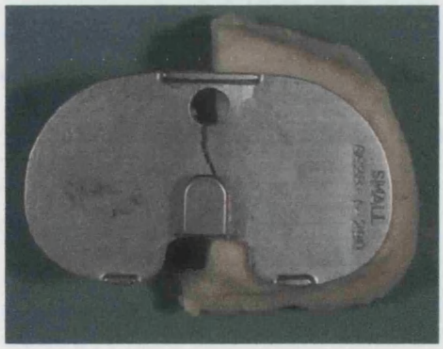

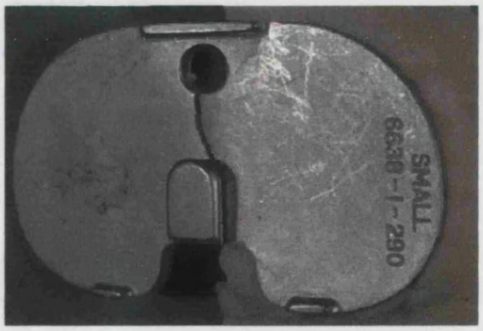

(d) main side view

Figure 4.5.19 (a-b) FEA models show that the peak stress for the PCA model at 900N is 1019 MPa. This is significantly higher than the fatigue limit for cast CoCrMo alloy. (c & d) Failure of both trays at 336,100 and 413,100 cycles.

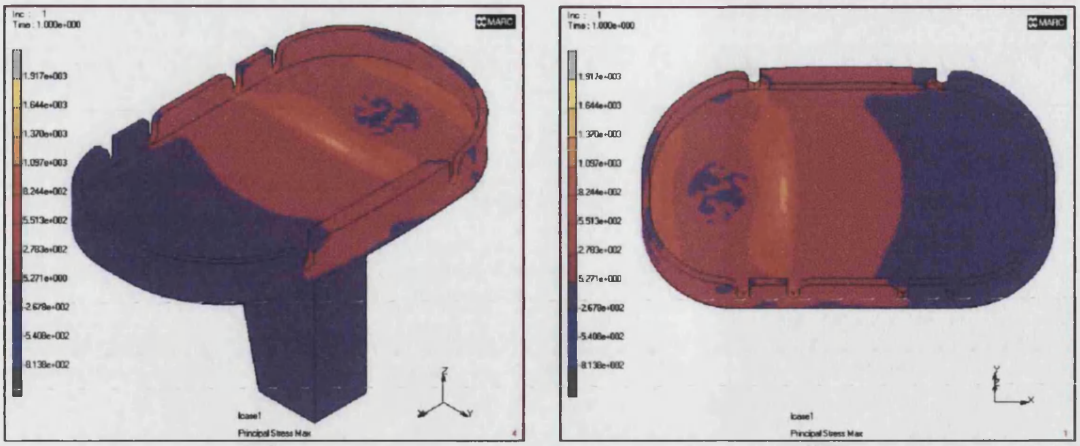

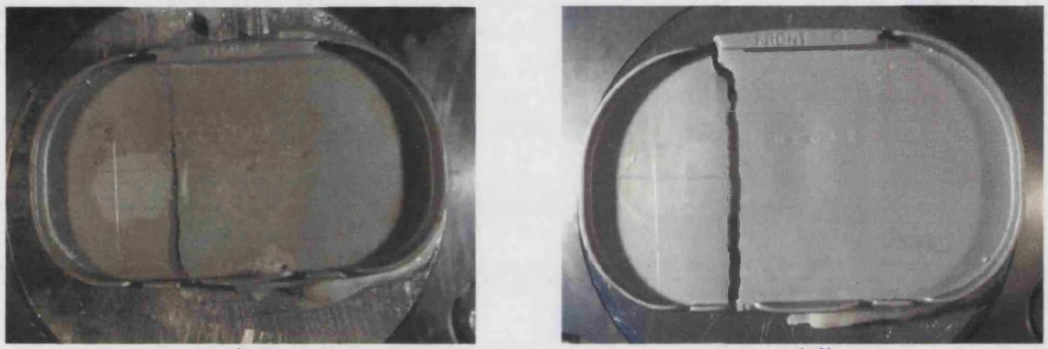

Figure 4.5.20 (a-b) FEA models show that the peak stress for the Total Condylar (type 2) tray at 900N is 1917MPa. This is significantly higher than the fatigue limit for cast CoCrMo alloy. (c & d) Failure of both trays at 527,500 and 848,700 cycles.

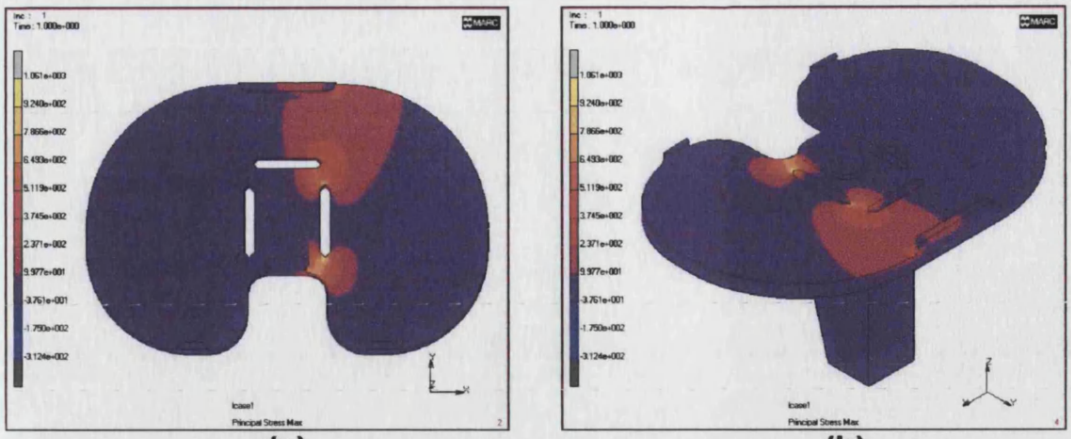

(a) (b)

Figure 4.5.21 (a-b) FEA models show that the peak stress for the Total Condylar (type 1) tray at 900N is 1016 MPa. This stress level is significantly higher than the fatigue limit for cast CoCrMo alloy. There were no samples to test of this component

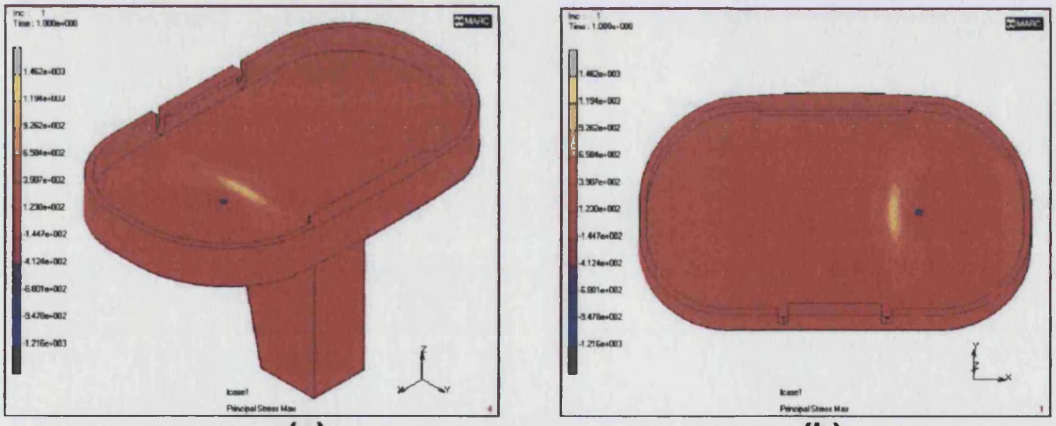

(a) (b)

Figure 4.5.22 (a-b) FEA models show that the peak stress for the revision PCA tray at 900N is 1462 MPa. This is significantly higher than the fatigue limit for cast CoCrMo alloy. For both tray designs no samples were available for testing. There were no samples to test of this component.

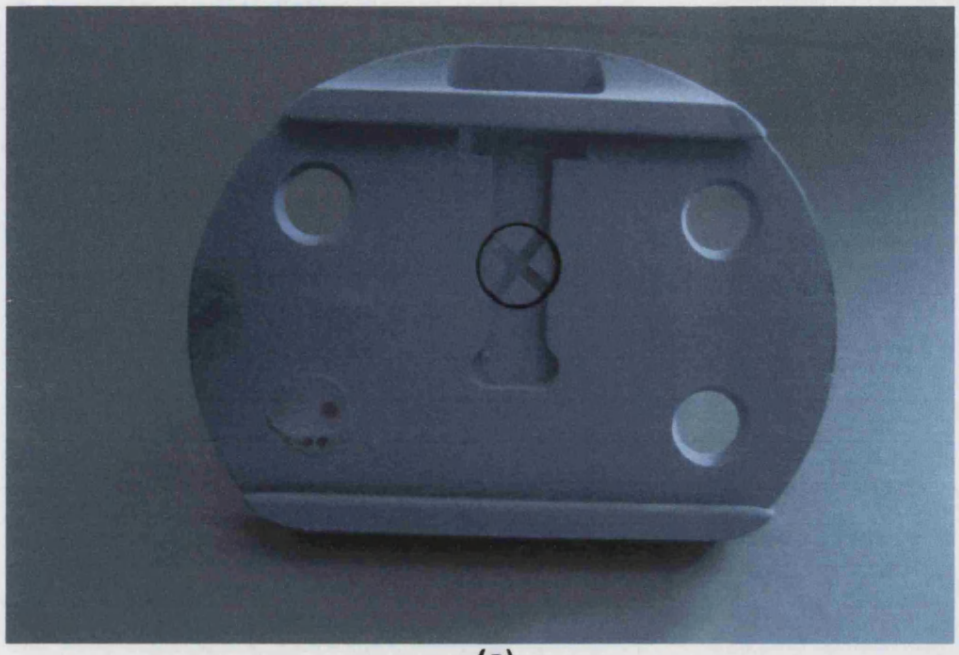

(a)

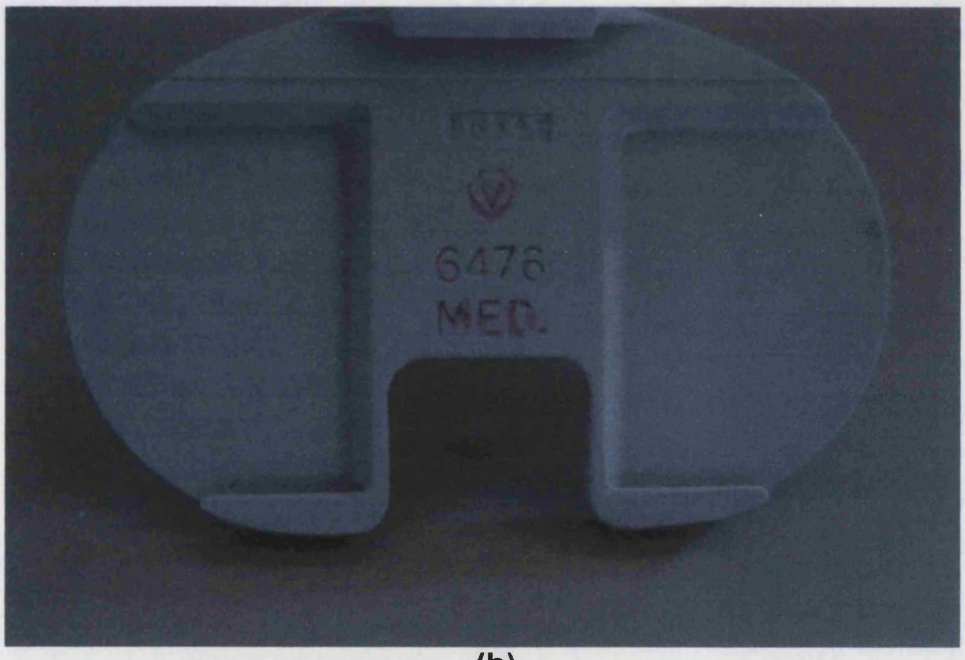

(b)

Figure 4.5.23: Dye penetrant tests for (a) the IB2 and (b) the Kinemax trays tested at 2000N and 1500N respectively.

4.5.3 DISCUSSION

There was a very good correlation between FEA predictions for peak stress and fatigue test results at 2000N and 900N. The only exception was the AGC tray design using a load level of 2000N. At 1500N, the FEA predictions differed from the fatigue test results for the Kinemax, AGC and the Rotaglide tray designs.

There are a number of reasons for the differences between the FEA predictions and fatigue test results. Some samples of the Kinemax, AGC and the Rotaglide survived to five million cycles under fatigue test conditions, when FEA predicted that they would fail (on the basis of fatigue data given by individual manufacturers) at 1500N. Survival of these components may be as a result of two reasons. Firstly, fatigue life is calculated on standard sized bar specimens and not on a particular design. The fatigue limit is calculated by averaging the fatigue life of a large number of individual standard sized bar specimens. These particular designs may have a higher fatigue limit than the standard sized specimens or the fatigue life of the samples tested may deviate from the average standard sized specimens. Secondly, fatigue depends on crack initiation and propagation in the material. The FEA predicts the peak maximum principal stress. This stress value is used to predict crack propagation and not crack initiation. Crack initiation depends on the surface condition. The AGC tray is surface treated by ceramic peening. This work hardens the surface and increases the stress level at which a component is likely to fracture. Surface factors are not available to consider in a linear elastic FEA model as conducted in this study. In addition, ceramic peening reduces grain size on the surface of the tray. Also, the grain size across the surface of the Kinemax, AGC and Rotaglide varied between components as a result of manufacturing techniques. Grain size variation is likely to have an effect on the crack initiation of the material. Additionally, the AGC and Rotaglide trays are made from cast CoCrMo alloys. This technique is prone to casting defects. A manufacturer (Biomet Merck Ltd., UK) believes that one in six, as cast components are likely to have a casting defect. A casting defect is likely to cause early failure by

fatigue. Grain size variation and casting defects may explain the large degree of scatter in the fatigue test results for identical components. It may also explain why some components survived the fatigue test despite FEA predictions of failure.

The results also showed that the stress distributions vary greatly with implant design. Two of the tray designs (the Profix and the IB2) had four screwholes placed in the periphery of the tray. In both cases high stresses were observed around the anterior screwhole by finite element analysis. The purpose of the screwhole is to allow screws into cancellous bone and depending on the patient, extend out towards the cortices so that fixation can be improved. However, with respect to fatigue of tibial trays, screwholes have the potential to be detrimental. In this study, both the Profix and the IB2 are made from titanium alloy that has been net forged, which has a high fatigue limit and hence these tray designs did not experience failure under mechanical test conditions for a load of 2000N.

Many of the tray designs have no changes in the cross-section i.e. they are flat. However, in two early designs, the Kinematic and Total Condylar, the section changes where the stem meets the lower surface of the tray. The cross-section then becomes thinner as it forms the condyles of the tray. For both these tray designs fracture occurred at the junction of the thick part to the thin section. This is because the intensity of stress increases in this region and these high concentrations of stress become positions where cracks initiate and propagate. The Kinemax design (although it has no history of fracture) also exhibits this change in section. This occurs as the tray reduces in cross-section to accommodate the polyethylene insert. At this change in cross-section, small radii occur and this becomes an area of high stress and failure occurs under ISO test conditions. The AGC is another tray design where there is a change in cross-section at the condyles of the tray. This is to allow cement recesses on the undersurface of the tray. Again at the change in cross-section (where the cement recess begins) crack initiation and propagation occurs at the upper surface with high loads.

Small radii in the design of the tray are also an area for stress concentrations. Examples of this occurring in tray design are the PCL cut-out and top corner of the Kinemax, the locking tab of the MG2 and the junction of the tray and the pin used for engaging the polyethylene insert for the Rotaglide tray. In each case crack initiation and propagation occurred in these regions with high loads. Failure of the Kinematic and Total condylar designs *in vivo* has, in addition to changes in cross-section, been attributed to stress concentrating notches in the peripheral rim. It is important that all aspects of tray designs are thoroughly investigated prior to clinical trials and for the development of new tibial tray designs testing methods play a vital role.

Material properties are an important factor for tibial tray designs. Failure of the PCA was attributed to the reduction in fatigue life of cast CoCrMo alloy once it had been sintered. In addition to which, the beaded surface increased notch sensitivity and cracks occurred within the beaded surface. This study shows that titanium alloy trays were able to experience higher stresses and higher loads. Both the Profix and the IB2 survived at 2000N. The exception was the MG2 tray design that has no central stem. It experienced rapid failure at 2000N and 1500N. *In vivo* it is more likely to subside compared with trays that have a central stem so is unlikely to experience the stresses observed under the ISO test conditions. Titanium alloy has a higher fatigue limit but is notch sensitive (due to its high tensile strength) and has a poor bearing surface. This makes the material unusable in mobile bearing applications. CoCrMo alloy has a good bearing surface so can be used for mobile bearing applications even though it has a lower fatigue limit. It can also be cast. The casting process allows intricate details such as fins for the stem on the Kinemax and the cement recesses for the AGC and stem design for AGC. Net forging of titanium is able to produce intricate details but is a more expensive process.

The thickness of the tray is often considered an important factor in tibial tray design. Table 4.5.5 shows the variation in thickness for each tray design. The table shows that the Total Condylar and Kinematic designs have the thinnest cross-section and have a history of clinical failure. The PCA and revision PCA have a thicker dimension (at 3mm) with no change in cross-section but inspite of this clinical failure has been reported for these designs. The reasons for failure of the PCA have been poor material properties for the sintered CoCrMo alloy. The revision PCA has stress concentrating notches that further weaken the structure with respect to fatigue. Comparing the AGC and MG2 designs, the AGC has a thinner cross-section but is able to survive higher loads than the MG2 as a result of a stress concentrating notch at the locking tab for the MG2. The thickest trays are the MBK and the Rotaglide – both are made from cast CoCrMo alloy and are polished to provide a good bearing surface. Polishing will improve the surface finish, resulting in fewer defects (such as scratches) occurring on the surface which experiences the highest tensile stresses. The other two CoCrMo alloy trays (the AGC and the Kinemax) have further treatments: the AGC is ceramic peened and the Kinemax is solution heat-treated. Both treatments increase the fatigue life of the implant. This part of the discussion shows that thickness alone cannot be considered as a sole factor with respect to fatigue of an implant design. The material properties and stress concentrating features also have to be considered when designing implants. Often there is a trade-off between material properties (and their subsequent treatments) and design features and these have to be properly assessed for safe design of tibial trays. Testing methods are, therefore, an important way to make such assessments.

4.6 GENERAL CONCLUSION

The conclusion of this chapter is that the ISO support conditions can reliably, with high repeatability, predict weak points of designs, but a load level is required to distinguish between those trays that are clinically successful and those that have a history of failure. Based on the number of samples available to test for each tray design, only three load levels were selected for study two. If more samples were available it may have been possible to refine the load level further. This chapter has shown that the worst case physiologic load of 2000N is too severe for some clinically successful designs and that a sub-physiologic load is required. Study Two has shown that all trays that are currently used survived a load level of 900N using the ISO test conditions for a femoral-tibial contact position at zero degrees of flexion. All tray designs that had a propensity for failure, identified in the literature, failed at a load level of 900N. The fact that many trays survived a load of 900N and do not have a history of failure clinically (where the trays are subjected to higher physiological loads) is indicative that the support of the tray in the ISO test represents an extreme situation *in vivo* where there is rigid support at one side and complete loss of support on the opposite side. This situation could occur clinically as a result of bone loss due to varus or valgus deformities which are inadequately filled, or where a radiolucent line develops and where most of the load still goes through that side due to undercorrection of the deformity. However, the fact that the ISO test cannot reproduce the range of cracks observed from retrievals, means that further investigations need to be carried out. Chapter three showed a large variety of crack paths for the Kinematic and the PCA tray. There are a number of reasons why this may occur. A variety of support conditions will occur *in vivo* due to different types of deformity. Another reason why crack paths differ from those seen under the ISO test conditions is contact location. Contact positions will vary due to the design of the tibial insert. The point of load application in the ISO test is that predicted for zero degrees flexion, which for the implant design was determined as being the lowest point on the

polyethylene insert. However, *in vivo,* the contact could frequently be more anterior or posterior due to instability, incorrect component placement or inaccurate ligament balancing. Wear of the polyethylene insert may also affect contact location and severe wear as reported by Engh et al. (1992) may result in the femoral component being stuck within the polyethylene insert thereby limiting the contact locations. Appendix B2 has shown that a clinically successful tray design (the MG2) is unable to support a load of 900N for a more posterior contact position. Study one and appendix B2 have shown that for a more posterior contact position some tray designs have been able to survive a load level of 500N. Due to the lack of availability of samples, this was not fully validated. It remains important to understand failure *in vivo* and why different crack paths occur. This is the subject of the following chapters.

CHAPTER FIVE:
FINITE ELEMENT ANALYSIS OF THE IMPLANTED TIBIA

Page

5.1 INTRODUCTION

Finite element analysis has been used to model the natural tibia and the implanted tibia for a number of different implant designs. These models have given an insight into the performance of implant design and the stresses induced in the resected bone. Some studies have compared these results with the stresses induced in the natural tibia (Murase et al., 1982; Vasu et al., 1986; Beaupre et al., 1986).

5.1.1 MATERIAL PROPERTIES OF BONE

The tibia consists of cortical and cancellous bone. The cancellous bone consists of individual trabeculae predominantly arranged in a pattern of axially oriented columns (Hvid and Hansen, 1985). This means that the properties in one direction, the axial direction, are considerably higher than the same parameters measured in the lateral or anteroposterior direction. This pattern characterises cancellous bone to be transversely isotropic. Studies of cortical bone have also defined it to be transversely isotropic (Ashman et al., 1989).

A number of methods have been used to evaluate the mechanical properties of tibial bone. These include tensile studies (Ryan and Williams, 1989), buckling tests (Townsend et al., 1975), ultrasonic evaluation (Ashman and Rho, 1988), finite element analysis (Mente and Lewis, 1987) and three point bending tests (Kuhn et al., 1989). Two alternative methods are compression testing (Goldstein et al., 1983) and penetration tests (Hvid et al., 1984). For compression methods the bone specimen is tested in a uniaxial Instron machine at a strain rate of $0.1\%s^{-1}$. Recordings are made of load versus deformation and curves are created. From these curves, ultimate load and tangent elastic modulus are determined (Goldstein et al., 1983). Penetration tests use a penetrating device that is driven into the bone at a constant velocity. The force of penetration is recorded as a function of the

depth of penetration. A calibration method is then used to relate the resisting force on the probe to the elastic modulus and compressive strength (Hvid, 1988). Results of bone stiffness using both methods show variations in the exact values for bone (Hvid and Hansen, 1985; Goldstein et al., 1983). However, there are consistent patterns with regards to bone strength. These studies regardless of the method used found that the medial condyle is stronger than the lateral, with evidence of a low modulus area, which emanated up from the intercondylar space to the proximal area of the tibia. The highest values for bone strength occurred well within the boundaries of the tibia, with a gradual reduction in strength towards the metaphyseal cortices. Some authors tested the anteroposterior variation of bone strength and found that posteriorly the condyles are of equal strength while centrally and anteriorly the medial condyle is significantly stronger than the lateral. There is also evidence of a decrease in bone strength distally. Hvid and Hansen (1985) found using penetration tests that there was distal weakening of the trabecular bone at both condyles. Hvid and Jensen (1984) found that changes in material properties away from the joint were considerably smaller on the medial side compared to the lateral. Harada et al. (1988) found that below a depth of 5mm cancellous bone weakens and so advocated removal of as little bone as possible proximally. Hvid and Hansen (1985) found that there was a large variation in maximal medial and lateral bone strengths between individuals. Their values are considerably smaller than those reported elsewhere. They found the medial condyle to have an average value of 52.8MPa (ranging from 13.8 to 116.4 MPa) and lateral to have an average of 29.1MPa (ranging from 9.1 to 47.5 MPa). Overall, the tibia is regarded as heterogenous (Goldstein et al., 1983) but Harada et al. (1988) divided the tibial bone into five areas relating to bone strength. They identified the medial and lateral areas of the bone. The intercondylar or central region was the area between the medial and lateral eminentiae. The paramedical and paralateral regions were the intermediate zones (refer to figure 5.1).

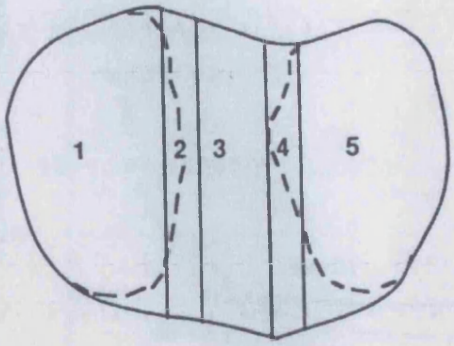

Figure 5.1: The five regions of the tibia: (1) the medial, (2) paramedical, (3) intercondylar or central, (4) paralateral, (5) lateral. (Harada et al., 1988)

Finite Element studies have used a variety of different material properties for the cortical and cancellous bone properties (refer to table 5.1 & 5.2). Some authors have included transversely isotropic values for the cancellous bone (Askew and Lewis, 1981; Rakotomanana et al., 1992 & 1994). Elastic-plastic properties of bone have also been included in some finite element models (Rakotomanana et al., 1992 & 1994; Taylor et al., 1998)

	Bone Stiffness (MPa)	
STUDY	**DIAPHYSEAL**	**METAPHYSEAL**
Askew and Lewis (1981)	15000	-
Hayes et al. (1978)	14400	-
Lewis et al. (1982)	15000	-
Murase et al. (1982)	18000	-
Beaupre et al. (1986)	5000	1000
Vasu et al. (1986)	5000	1000
Rakotomanana et al. (1992 and 1994)	11500	-
Taylor et al. (1998)	17000	5000

Table 5.1: Cortical bone properties used in finite element studies

	Bone Stiffness (MPa)					
STUDY	**1**	**2**	**3**	**4**	**5**	**6**
Askew and Lewis (1981)	600*	180*	360*	60*		
Lewis et al. (1982)	600	180	360	60		
Murase et al. (1982)	400	300	100	200	230	200
Beaupre et al. (1986)	440	320	100			
Vasu et al. (1986)	440	320	100			
Rakotomanana et al. (1992 and 1994)	630*		300*			
Taylor et al. (1998)	400	100	300			

where : * - transversely isotropic properties; 1 is medial
2 is intercondylar 3 is lateral; 4, 5, 6 intermediary zones.

Table 5.2: Cancellous Bone material properties used in finite element studies

Arthritic conditions of the knee result in a reduction in bone strength (Harada et al., 1988). Hvid (1988) used penetration tests in 150 patients that had osteoarthritis (OA) and rheumatoid arthritis (RA). He found that the RA knees had slightly lower bone strength values than the OA knees in the tibia. Wixson et al., (1989) reported bone stiffness values for OA and RA and these results are shown in Table 5.3.

	Elastic Modulus (MPa)			Source
	Medial	**Lateral**	**Anterior**	
Normal	336	183	49	from Goldstein et al., (1983)
OA	187	133	106	Wixson et al., 1989
RA	146	139	58	Wixson et al., 1989

Table 5.3: Comparison of normal osteoarthritic (OA), rheumatoid arthritic (RA) bone

5.1.2 FINITE ELEMENT STUDIES

With regards to design, a number of studies (Bartel et al., 1982; Lewis et al., 1982; Murase et al., 1982; Cheal et al., 1985; Taylor et al., 1998) have compared all-polyethylene to metal–backed tibial components. They all found that all-polyethylene designs had higher stresses in the cement and cancellous bone stresses when compared to metal-backed components. These early studies advocated metal-backed tibial components to address the problem of loosening which was a major problem in the 1970s and 1980s. Now, twenty years later this design change together with improvements in surgical technique has led to a vast reduction in loosening of the tibial component.

Lewis et al. (1982) examined a number of different metal backed designs such as one piece or two piece designs, with either one, two or three posts. They found that one piece designs have lower cement, compressive and tensile tilting stresses beneath the plate. Single metallic post designs have the lowest cement-bone interface tensile stresses followed by two and three posts. Those models without a post reduced tensile tilting stresses further.

Murase et al. (1982) examined the effect of coverage of the tibial component on the resected tibia and found that using either complete coverage or smaller components the difference in results were minor. The effect of the length of central stem on bone stresses has also been investigated (Lewis et al., 1982; Murase et al., 1982). These studies found that the use of a central stem of 35mm was found to produce stress levels in the bone that were similar to those designs that did not have a central stem. Long central fixation posts of 70mm substantially reduced proximal cancellous bone and cement stress levels resulting in unloading of the proximal tibia if adequate distal cement was used. Most primary knee replacements that are used currently have a central stem that is 35mm long. Longer stems are now used in revision cases where proximal cancellous bone may be weak.

Other researchers (Garg and Walker, 1986; Rakotomanana et al., 1992 & 1994; Taylor et al., 1998) compared the performance of cemented and uncemented designs. They found that there was little difference in stresses and displacements between cemented or uncemented fixation. However, other differences in tibial component design led to different parts of the bone being loaded in the resected tibia. The effect of an uneven resected surface was examined by Taylor et al. (1998). They found that stresses in the cancellous bone increased significantly for an uneven surface risking the bone to fatigue failure. Few studies have incorporated a fibrous tissue layer in their FEA models of the tibia. Garg and Walker (1986) found that a 1mm layer of fibrous tissue directly beneath the tibial plateau had the effect of smoothing out the stresses in the bone. They noted that there was a 23% reduction in the peak stress at the cement bone interface for normal bone. In all the FEA studies that were conducted, none of the authors reported on the stresses in the metal baseplate.

The results from these FEA studies vary. This is due to the type of analysis performed. Two dimensional studies (Askew and Lewis, 1981; Beaupre et al., 1986; Garg and Walker, 1986; Vasu et al., 1986; Rakotomana et al., 1992) axisymmetric studies (Hayes et al., 1978; Murase et al., 1982), three dimensional studies (Lewis et al., 1982; Rakotomanana et al., 1994; Cheal et al., 1985; Little et al., 1986) have been conducted. Some studies modelled the interface between the implant and the bone as continuous (Lewis et al., 1981; Beaupre et al., 1986; Vasu et al., 1986) whiles others as discontinous (Rakotomanana et al., 1992 & 1994; Taylor et al., 1998). A continuous interface is simpler to model and does not involve contact analysis. However, the nodal values at the interface are averaged between the cement and bone, which have different material properties leading to inaccuracies. In reality there is a discontinous interface between the implant and bone and therefore it is more accurate to perform a contact analysis, where nodal values are not averaged.

5.1.2 FORCES AT THE KNEE

In the late 1960s Morrison (1969,1970) used a force plate to measure ground reaction for patients carrying out a number of activities. Theoretical calculations were then made for forces at the knee. This knee model was then analysed by Nissan (1980). He found that errors were minor with the most influential factors being the estimates of contact point and joint centre that could result in errors of peak force of 10-15%. Morrison (1970) calculated the peak force for level walking, walking up and down a ramp and walking up and down stairs. He found that the peak force for level walking was the lowest of all the activities. The results are presented in terms of body weight (BW). The peak force during walking ranged from 2-4 (BW) with a mean of 3BW. Taylor et al. (1998a) using telemetry to measure forces directly in a distal femur found similar results to Morrison (1970) and reported forces of 2.4-3BW for level walking. Forces for other activities were higher with a peak force of 5.6BW in one patient for walking down a ramp. Kuster et al. (1997) reported a force of 8BW for downhill walking.

The load levels used in different finite element studies vary. Some studies compare the differences in performance on where the load is applied. This includes applying the load to both condyles and/or just one condyle. A number of authors have used a load of 2000N in their finite element models of the tibia (Lewis et al., 1982; Murase et al., 1982; Vasu et al., 1986; Beaupre et al., 1986) where they had different load cases including a unicondlyar load of 2000N. Rakotomanana et al. (1992 & 1994) used a load of 2000N applied to both condyles and then in a ratio of 66:33 ratio to the medial and lateral condyles respectively. Other studies have used different load levels. Garg and Walker (1986) applied 2500N centrally to the tibia; Little et al. (1986) applied 2450N to their tibia model; Hayes et al. (1978) applied 445N to one compartment; Cheal et al. (1985) applied 1000N to the whole tibia; Taylor et al. (1998) used a load of 2200N which was shared between both condyles and applied as a unicondylar load.

5.2 MATERIALS AND METHOD

Finite element analyses of the implanted tibia were performed using two tray designs: the Kinematic and AGC components. Both the Kinematic and the AGC were modelled with a 2mm layer of cement using Unigraphics (EDS Corp., USA). Finite element models of the two tray designs were created using a hand generated mesh. *Iges* files of the two models developed in Unigraphics were used as a guide, so that all the essential features of the tray design were incorporated into the finite element models. The Kinematic model consisted of 6186 hexahedral elements and 13128 nodes and the cement layer consisted of 4312 elements and 6404 nodes (figure 5.2a & b). The AGC model consisted of 8715 elements and 11383 nodes and the cement layer consisted of 6680 elements and 9531 nodes (figure 5.3a & b).

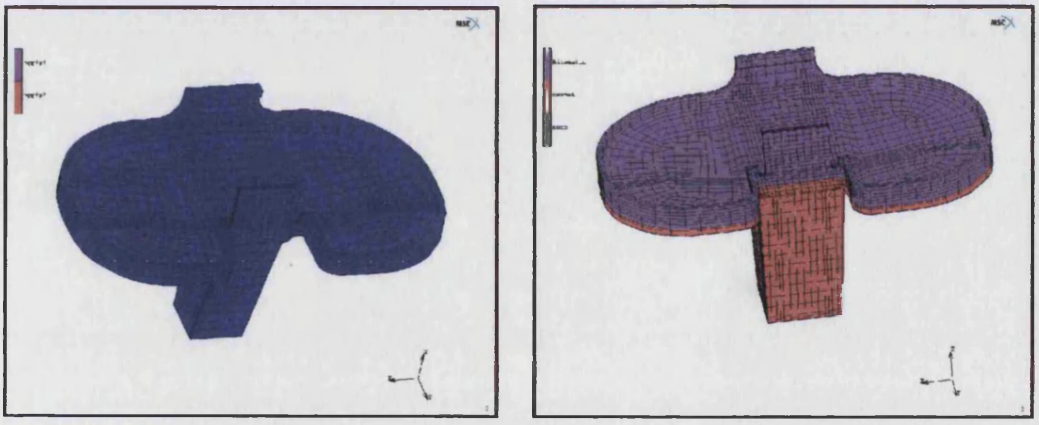

Figure 5.2: Kinematic model (a) without cement layer (b) with cement

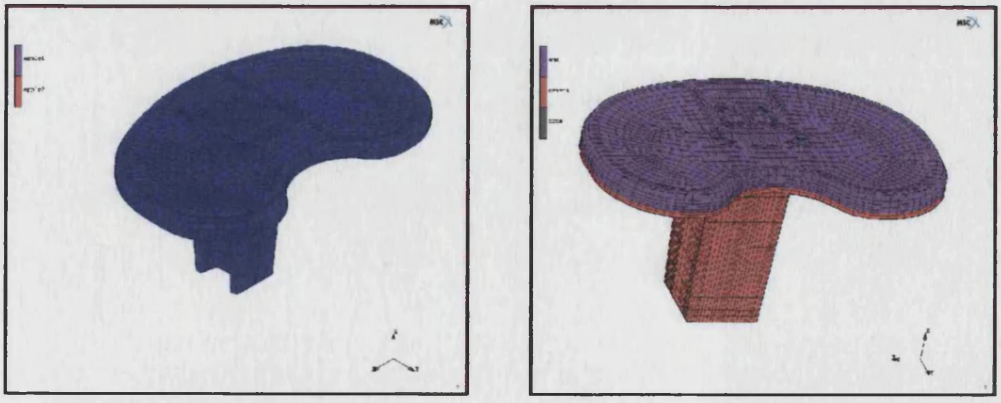

Figure 5.3: AGC model (a) without cement layer (b) with cement

The male CT scans from the Human Visible Project (National Library of Medicine, USA) were used to obtain the geometry for the natural tibia. These scans are 1mm apart. An edge detection software called MIMICS (Materialise, Leuven) was then used to obtain the curves that define outer and inner cortices of the tibia. These curves were then imported into the finite element software MARC (MSC software, USA). By using the set of curves that defined the outer geometry of the tibia a surface mesh consisting of two dimensional triangular elements was created.

The lower surfaces of the implant with cement models were then used to define the upper surface of the resected tibia so that the implants would be correctly aligned. A two dimensional triangular surface was then constructed of this lower surface. Using the two surfaces that defined the implanted tibia an automatic hexahedral mesh was generated using the software capabilities within MARC. For the Kinematic tibia model the bone consisted of 9712 elements and 18097 nodes (figure 5.4a & b). For the AGC tibia model the bone consisted of 12322 elements and 32823 nodes (figure 5.5a & b). The material properties of cast CoCrMo alloy and cement are given in Table 5.4.

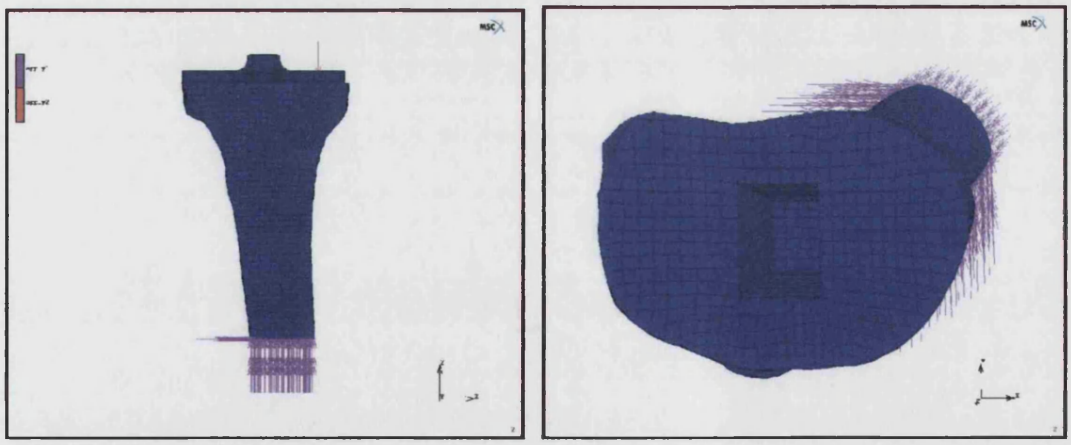

Figure 5.4: The bone model (a) with the implanted Kinematic (b) showing resection.

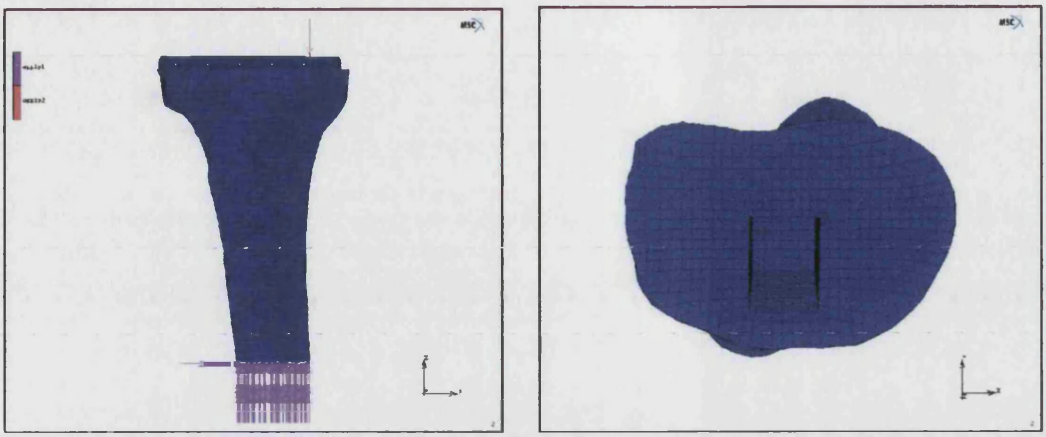

Figure 5.5: The bone model (a) with the implanted AGC (b) showing resection.

	Young's Modulus (MPa)	Poisson's Ratio	References
Cast CoCrMo alloy	220000	0.3	Weinstow & Clemow (1990)
Cement	2000	0.3	Paganelli et al. (1988)

Table 5.4: The material properties for the AGC, Kinematic and cement layers.

The cortical bone was divided into diaphyseal and metaphyseal bone using the edge detection software MIMICS (figure 5.6 a & b). For the cancellous bone the proximal part of the tibia was divided into five regions (figure 5.7a & b) based on the definition provided by Harada et al. (1988) shown in figure 5.1. For the material properties, the data from Goldstein et al. (1983) was taken. Goldstein et al. (1983) took data at various locations in anterior to posterior direction. This data was tabulated in Table 5.5.

Medial		Paramedial	Inter	condylar	Paralateral		Lateral
210	210	143	88	80	105	233	251
296	293	125	32	105	172	183	
	336	134	31	54	122	172	
	305	185	80	49	119		
		112	49	34	52		

Table 5.5: Bone stiffness (MPa) taken from anterior to posterior positions. (from Goldstein et al., 1983)

For OA and RA properties the data from Wixson et al. (1989) was used. Wixson et al. (1989) showed an almost 40% decrease from the normal values to OA conditions. The RA conditions showed a greater decrease on the medial side and a slight increase in the lateral side when compared with the OA properties. The values used for OA and RA bone incorporated the values obtained from Wixson et al. (1989). The paralateral, paramedial and intercondylar values were reduced to correspond for OA and RA bone conditions (table 5.6).

	Medial	Paramedial	Intercondylar	Paralateral	Lateral
Normal	336	185	105	172	251
OA	187	102	58	95	133
RA	146	78	40	74	139

Table 5.6: Cancellous bone stiffness (MPa)

There was no data available regarding the OA and RA properties of cortical bone. However, as OA and RA causes a reduction in the mechanical properties of cancellous bone, it was assumed that there would be a reduction in mechanical properties for OA and RA. For the Kinematic model a further model showing reductions of 50% in cortical bone properties were also analysed (Table 5.7).

	Bone Stiffness (MPa)	
	Diaphyseal	**Metaphyseal**
Normal	15000	5000
OA	13000	4000
RA	12000	3500
Reduced	7500	2500

Table 5.7: Cortical bone stiffness (MPa).

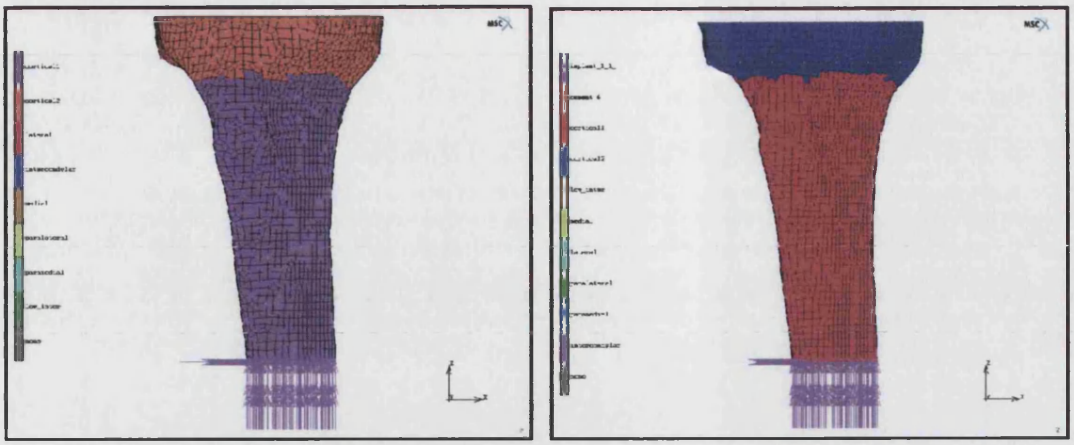

(a) (b)

Figure 5.6: Diaphyseal and metaphyseal bone distribution for the (a) Kinematic and (b) AGC bone models.

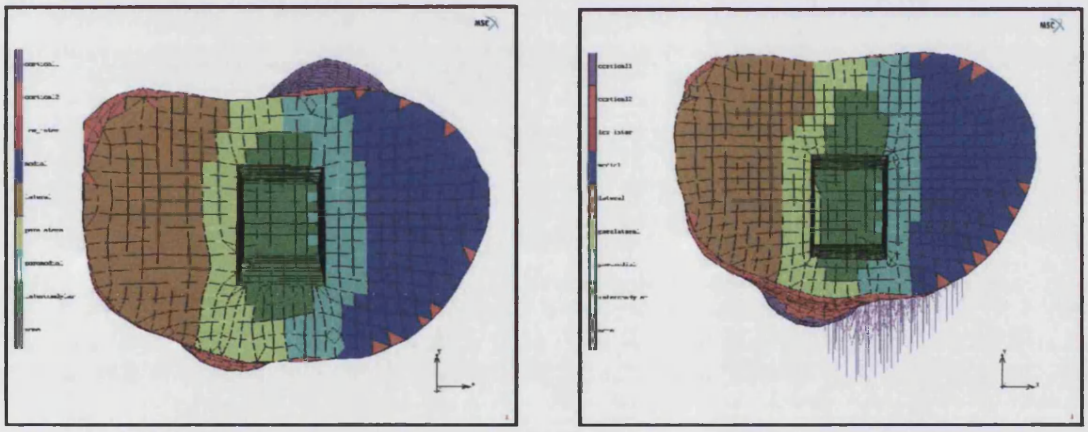

Figure 5.7: Cancellous bone properties for the (a) Kinematic and (b) AGC finite element models.

For OA and RA properties the data from Wixson et al. (1989) was used. Wixson et al. (1989) showed an almost 40% decrease from the normal values to OA conditions. The RA conditions showed a greater decrease on the medial side and a slight increase in the lateral side when compared with the OA properties. These values used for OA and RA bone reported by Wixson et al. (1989) were incorporated into the finite element models.

A 1mm fibrous tissue layer was modelled for normal, OA and RA bone properties using the contact position that had the highest peak stresses in the metal baseplate. The Young's modulus for the fibrous layer was 1MPa and the Poisson's Ratio was 0.495. These values were taken from Garg and Walker (1986) and Paganelli et al. (1988).

A load of 2000N was applied at three defined contact positions. The first contact position used was that defined in the 1996 draft ISO standard (refer to figure 2.2.7). The second contact position was that defined in the 1997 draft standard at zero degrees flexion (refer to figure 2.2.8) and the third was defined medio-laterally in the same position at zero degrees flexion but anteriorly in line with the cruciate cut-out. These contact positions are shown in figure 5.8. The most distal part of the tibia was rigidly fixed.

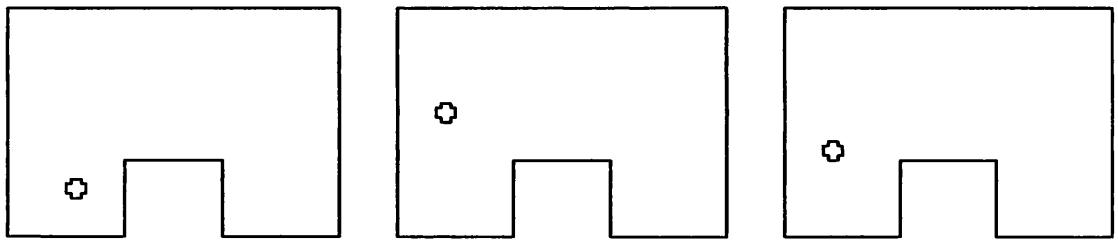

Figure 5.8: Contact locations: (a) first contact position defined in the 1996 draft standard, (b) second contact position defined in the 1997 draft standard (zero degrees flexion), (c) third contact position medio-laterally in the same position at zero degrees flexion but anteriorly in line with the cruciate cut-out.

A contact analysis was then performed to determine the stresses in the bone and metal baseplate using the direct constraint method within the MARC software.

5.3 RESULTS

The results show that for normal, OA and RA bone, the stresses in both metal baseplate designs, the Kinematic and AGC, are lower than the fatigue limit (tables 5.10 and 5.11) of 300MPa (Paganelli et al., 1988). This shows that the metal baseplate would not fail due to fatigue if both tibial trays are well-supported and correctly aligned.

FEA analysis of both tray designs show that the contact position defined in the 1996 draft ISO standard is the most damaging, with the highest stresses induced in the metal baseplate (figures 5.9 and 5.10).

A 1mm layer of fibrous tissue increased the stresses in the metal baseplate. The stresses in the Kinematic tray increased beyond the fatigue limit of cast CoCrMo alloy for all material properties with a layer of fibrous tissue (table 5.10). The stresses in the AGC tray increased but these stresses were below the fatigue limit (table 5.11), indicating that the tray would not fail due to fatigue.

	Peak Tensile (MPa) Stress			
Position	**Normal**	**OA**	**RA**	**Reduced**
1	223.7	269.7	287.3	313.7
2	125.8	146.8	151.5	161.9
3	195.3	226.9	235.6	253.3
For position 1 with fibrous tissue layer	449.5	542.5	614.1	671.8

Table 5.8: Peak stress values (MPa) for three types of bone condition and with a fibrous tissue layer for the Kinematic component.

	Peak Tensile Stress (MPa)		
Position	**Normal**	**OA**	**RA**
1	86.9	118.5	135.6
2	57.3	78.3	83.2
3	73.2	95.4	95.4
With fibrous tissue layer for position 1	178.6	200	212.2

Table 5.9: Peak stress values (MPa) for three types of bone condition and a fibrous tissue layer for the AGC component.

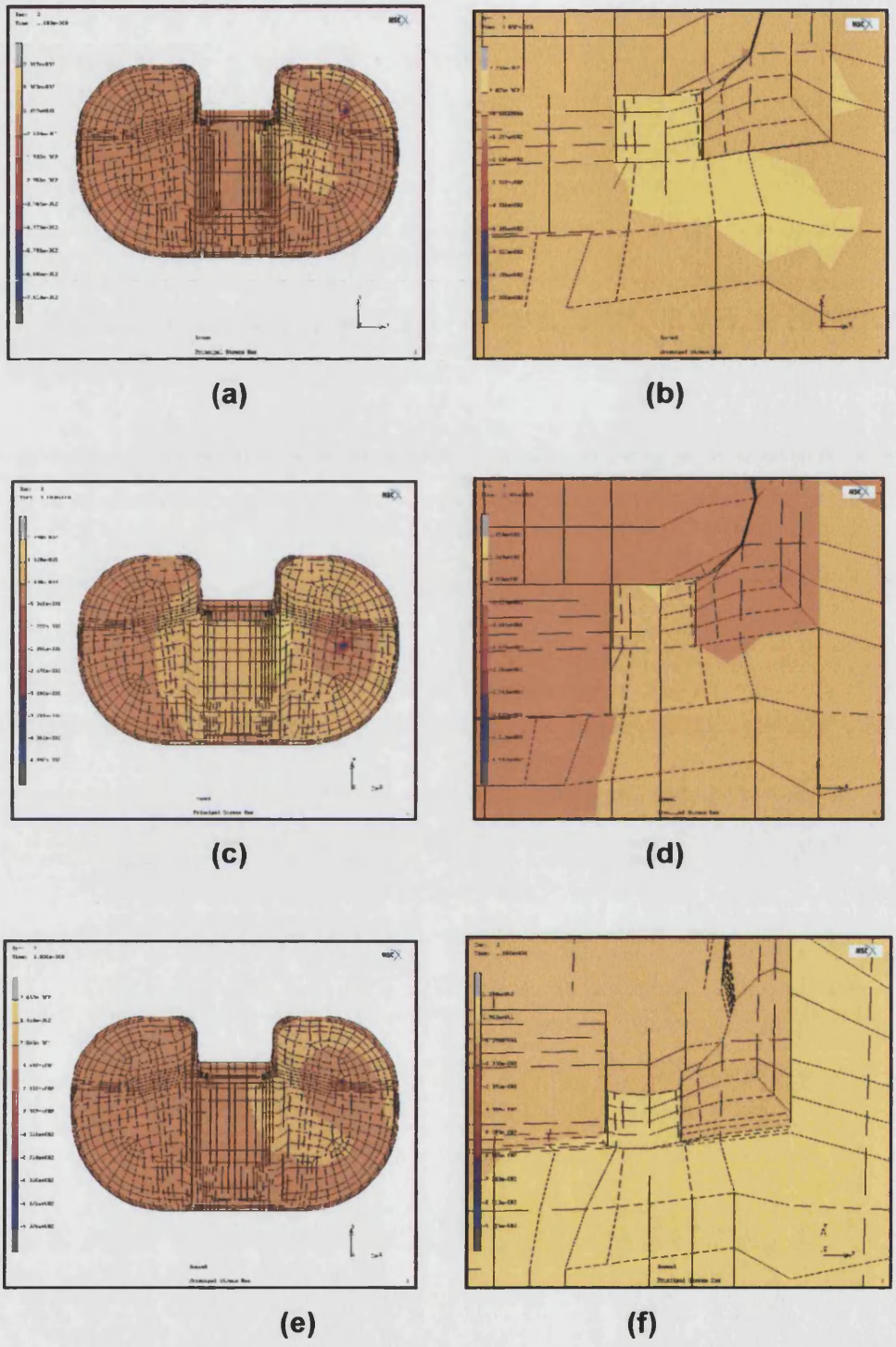

Figure 5.9: Stress distribution for the (a) first contact position, (c) second contact position, (e) third contact position, (b, d, f) showing highest stresses in the notch for all contact positions.

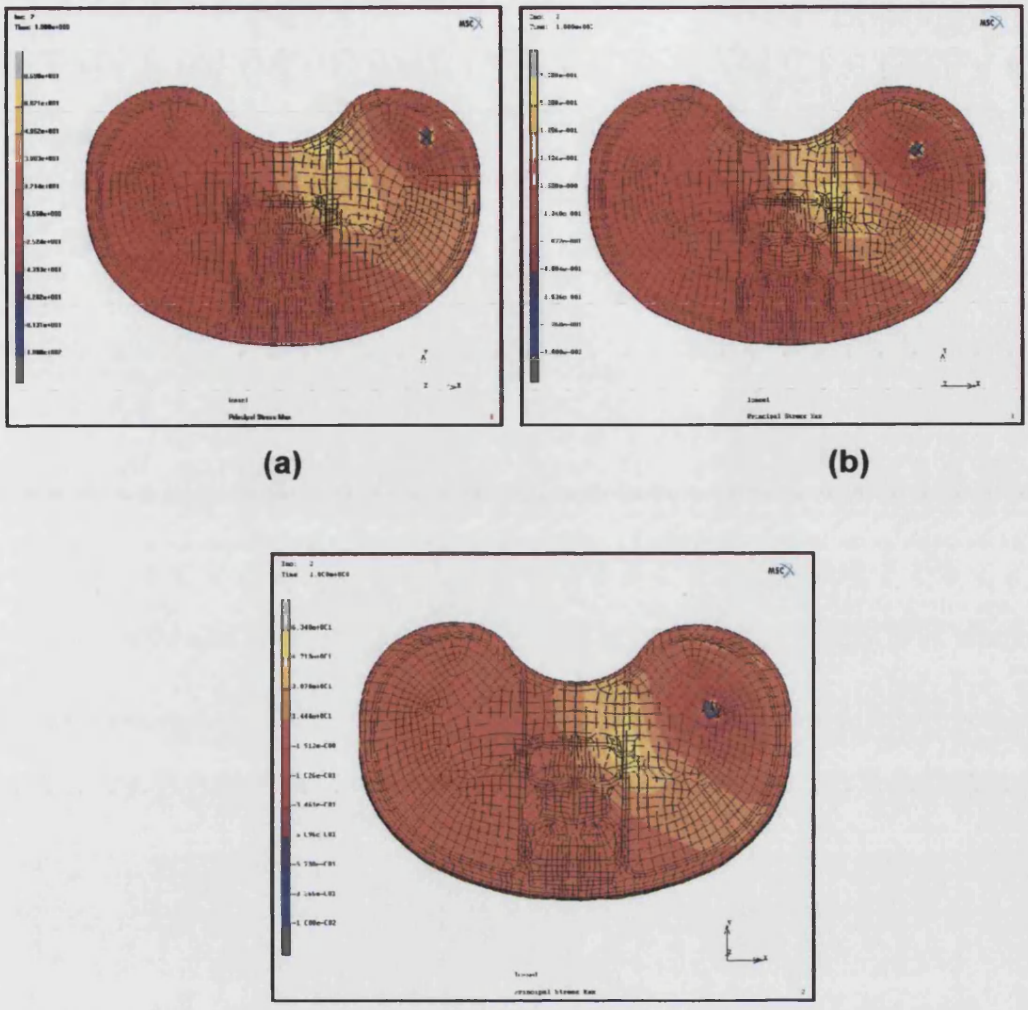

Figure 5.10: Stress distribution for the AGC tray for (a) the first contact position (b) second contact position (c) third contact position

The bone bends in response to the unicondylar load resulting in the highest tensile stresses on the lateral side of the bone with compressive stresses on the medial. The stresses in the bone show peak stresses at the distal end where it is rigidly fixed for all material and loading cases for both tray designs (figure 5.11 and 5.12). Tables 5.12 and 5.13 show the stresses at the distal end with contact location for the Kinematic and AGC respectively. Tables 5.14 and 5.15 show the peak stresses at the resected level for the Kinematic and AGC respectively.

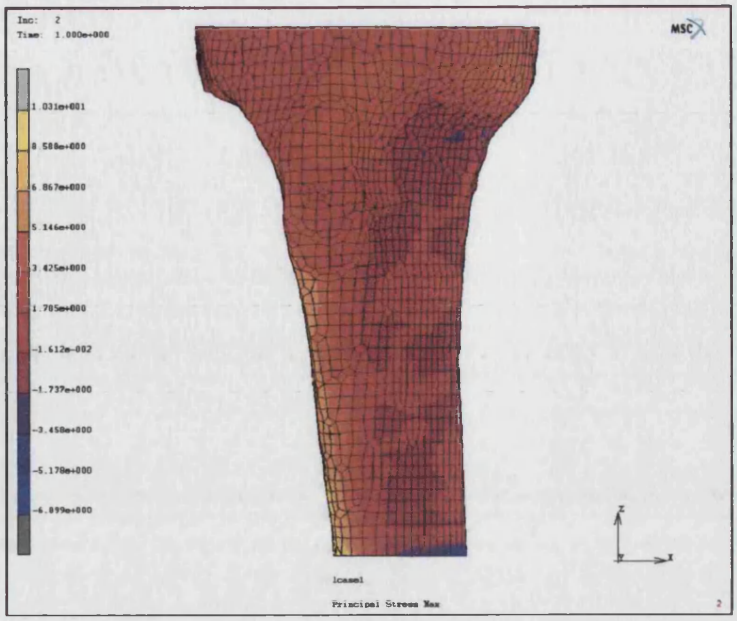

(a)

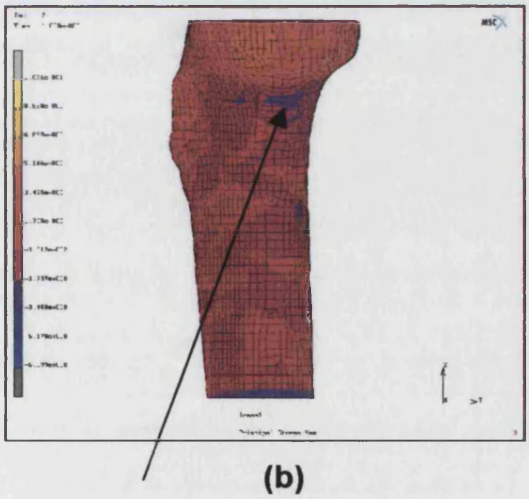

(b)

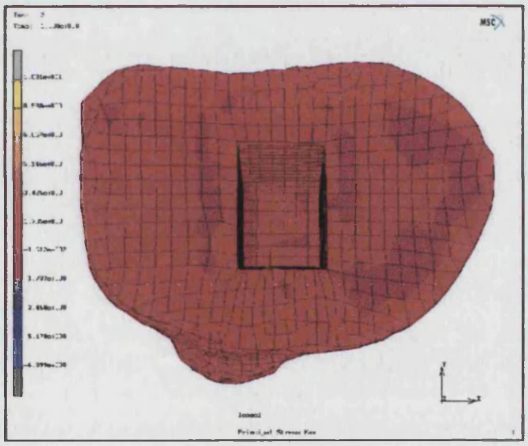

(c)

Compressive stresses under the medial condyle due to the bone bending under the unicondylar load.

Figure 5.11: Stress distribution in the bone for the Kinematic implant.

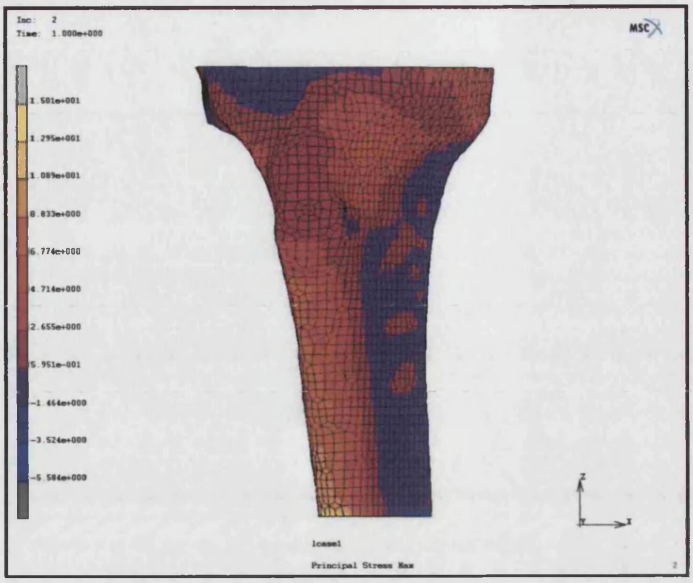

(a)

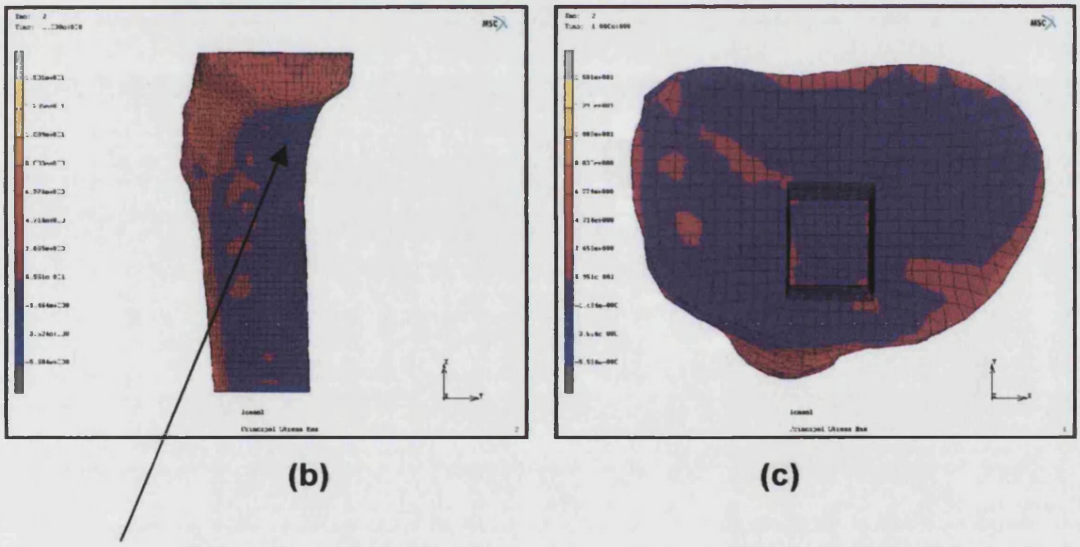

(b) (c)

As a result of bone bending under a unicondylar load, compressive stresses are observed under the medial condyle.

Figure 5.12: Stress distribution in the bone for the AGC implant.

	Peak Compressive (MPa) Stress		
	Position 1	Position 2	Position 3
Normal	4.117	4.567	4.208
OA	4.37	4.27	4.76
RA	5.036	4.265	4.769
Reduced	3.89	4.509	5.036

Table 5.10: Peak compressive stresses at the resected level for cortical bone in the Kinematic model

	Peak Compressive (MPa) Stresses		
	Position 1	Position 2	Position 3
Normal	4.2	5.5	4.1
OA	3.9	4.9	3.7
RA	3.7	4.5	3.5

Table 5.11: Peak stresses at the resected level for cortical bone in the AGC model

Cancellous bone stresses for all the models were tensile on the lateral side of the bone and on the medial side were compressive. These stresses depended on the contact location. For the tensile stresses, the peak stresses were 0.5MPa. The peak compressive stresses were 1.7MPa.

5.4 DISCUSSION

The objective of this chapter was to compare two tibial tray designs: one with a history of clinical failure (the Kinematic) and one that is clinically successful (the AGC). Both trays were implanted in a bone model where the bone properties were varied to represent normal and diseased conditions. The results show that if both the AGC and the Kinematic are correctly aligned and well supported, the trays did not fail due to fatigue, irrespective of bone condition. A 1mm layer of fibrous tissue, under the tray, modelled as compliant increased the stresses in both tray designs. However, the stresses exhibited by the Kinematic increase disproportionally to the extent that they predict fatigue failure, as a result of the presence of fibrous tissue layer under the tray, when compared with the AGC. Hence, the Kinematic tray is more sensitive to fibrous tissue than the AGC. Both trays were subjected to the same support condition and this implies that it is the differences in design that cause the differences in performance. The Kinematic has a stress concentrating notch in its peripheral rim. However, when the tray is well-supported load transfer occurs between the bone and the tray and peak stresses are below the fatigue limit. (A long-term clinical follow-up study of the Kinematic tray showed 97.6% survival at 14 years (Weir et al., 1996).)

In the presence of fibrous tissue the tray becomes loose and the compliant layer allows the tray to bend more and hence increases the stresses in the baseplate. In case studies of fractured baseplates (Maruyama et al., 1994; Abernethy et al., 1996; Clarke and Trousdale, 1999; Altintas et al., 1999) radiolucency was always reported. The fact that the AGC is able to survive in the presence of a 1mm compliant layer shows that design plays an important role. The thicker the tray the less it will bend. The Kinematic is 1.02mm thick compared with 2.533mm for the AGC. Both trays have a change in section (although this is less marked for the AGC) and cement recesses. The thickness of the tray does play a part in the design of tibial baseplates. However, chapter 4 (study 2) showed that it cannot be

considered in isolation and stress concentrating features and material properties must also be considered.

Other factors also affect fixation of the tray. These include wear of the tibial insert. Wear is affected by the design of the tibial insert as well as material properties of the polyethylene. Wear particles are known to induce osteolysis and migration of the wear particles to the bone interface cause fibrous tissue formation. Fibrous tissue layers have been observed to be thicker at the periphery of the tibia. This may also be affected by greater amounts of bending of the tray at the outer edges of the baseplate.

This study only considered three contact locations. The first two have been defined in the ISO standard as contact locations. For all analyses, this study shows that position 1 is the most damaging with higher stresses than the other two positions. Appendix B also showed that under ISO test conditions the first contact location is the most damaging and a lower load level is required to distinguish between clinically successful and unsuccessful designs. The results show that independent of contact location the stresses are highest in the notch region for the Kinematic. For the AGC, peak stresses occur at the PCL cut-out for position 1 and in the middle region of the tray for the other two contact locations. A limitation of this study is the number of contact locations. *In vivo*, the contact locations will vary depending on the design of the tibial insert, wear of the insert, incorrect positioning of the tray, the conditions of the ligaments, and any loss of ligaments. Oakeshott et al. (2003) have shown using video fluoroscopy of patients with mobile bearing posterior cruciate retaining tibal trays, that the contact location varies significantly from anterior to posterior on activity. Under non-weight-bearing conditions, the contact locations were significantly more anterior. They also showed that individual patients exhibited variable motion patterns. In a separate study reported by Dennis et al. (2003) involving 33 different designs of total knee arthroplasty, the highest magnitude of translation was found in the normal and ACL-retaining TKA

groups. Again, substantial variability in kinematic patterns was observed in all groups.

In this study only one condyle was loaded. Other studies have varied the ratio of loading in an 80:20 ratio or 60: 40 ratio. However, it has not been reported scientifically what the ratio is *in vivo*. Based on the fact that the medial condyle is larger than the lateral, it is generally regarded that the majority of the load, is experienced by the medial side. The study conducted by Dennis et al. (2003) demonstrated that patients having posterior-stabilized and posterior cruciate-retaining total knee arthroplasties experienced condylar lift-off. Subjects having a posterior cruciate-retaining total knee arthroplasty predominantly experienced lateral condylar lift-off whereas subjects with posterior-stabilized total knee arthroplasties experienced either medial or lateral condylar lift-off. In this situation the total load would go through one condyle. This justifies the worst case situation simulated in this study with the total load experienced by the tray through one condyle.

The mechanical properties of bone play an important role with regards to the stresses experienced by the baseplate. This chapter shows that a reduction in stiffness causes greater stresses in the baseplate. However, the material properties used in this study have some limitations. The cancellous bone of the tibia is known to be transversely isotropic. It was only modelled as isotropic in this study, primarily for simplicity and the basis of this study was only to perform a direct comparison between two tray designs. However, future studies could incorporate more details with regard to the mechanical properties of bone, as well as increasing the heterogeneity of the cancellous bone and aligning more closely the material properties with those found in the natural tibia. The stiffness values for diseased conditions have only been reported for cancellous bone but not for cortical bone. It would be interesting to investigate the effect of diseased conditions on cortical bone. For this study, a reduction in the stiffness values for cortical bone showed a marked increase in stress for the Kinematic tray. Other conditions that need to be considered are areas of bone erosion beneath the tray. Abernethy et al.

(1999) reported patchy osteoporosis beneath fractured trays and this could be incorporated into future models.

This study shows that tray design has a direct effect on the performance of tibial trays when exposed to the same support conditions. Finite element models can reliably predict the performance of implant design. It shows that finite element models can play an important role in the design and development of tibial trays for the future, especially as knowledge is increased about material properties of bone for normal and diseased conditions as well as soft tissues.

CHAPTER SIX:
DEVELOPMENT OF ALTERNATIVE TESTING METHODS

Page

6.1 INTRODUCTION

The literature has shown that some tibial trays have been prone to fracture due to a deficiency in their design. These include designs such as the Kinematic, Total Condylar, PCA and revision PCA trays. These designs had a thin baseplate, porous coatings (which decreased the fatigue properties of the substrate material) stress concentrating notches, small radii between the tray and its rim, and/or cruciate cut-outs with sharp corners.

Chapter 3 showed that for the Kinematic (figure 3.16) and PCA (figure 3.21) tray designs, crack propagation occurred along a number of different paths. For the Total Condylar (figure 3.19) tray design, there were only two retrieved trays and both had cracks, which propagated in the anterior-posterior direction.

The aim of this chapter was to determine why crack propagation occurred along different paths. It also aimed to ascertain if there was a testing method under which tray designs would experience multiple crack paths.

6.2 DIFFERENT CRACK PATHS

A number of FEA models were created with varying support and loading positions to ascertain the relationship between crack path, amount of support and load position.

6.2.1 MATERIALS AND METHODS

6.2.1.1 Finite Element Analysis

A solid model of the Kinematic tray was created in Unigraphics (EDS Corp., USA). This model was then translated into *iges* format and incorporated into MARC (MSC software, USA) where meshes were generated automatically using higher order tetrahedral elements. Initially a load of 2000N was selected because this is a physiological load value based on theoretical calculation of the peak force during the normal walking cycle (Morrison, 1969). A number of mesh sizes were modelled until subsequent mesh sizes showed peak stresses within 3% of each other. The model was then considered to have converged. For the Kinematic model, the final mesh size at 1.3mm consisted of 32,963 nodes and 53531 elements. Figures 6.2.1– 6.2.4 show the loading position and amount of support applied to each Kinematic model.

6.2.1.2 Mechanical Testing

A mechanical test was performed on the Kinematic tray. It was based on the ISO test but the amount of support on the loaded side of the tray was increased (shown in Figure 6.2.3c). The test was then conducted under the ISO test conditions described previously in chapter 4. An additional mechanical test was performed on the Kinematic tray, which compared the effect of changing contact location using the same ISO support conditions. It is important to study contact location because it may vary *in vivo* due to the

design and wear of the tibial insert (figure 6.2.5). The contact positions used were (a) the contact location defined in the 1996 draft standard (refer to appendix A1 or figure 2.2.7 in chapter2) and (b) the contact location defined in the 1997 draft standard (zero degrees flexion) (refer to appendix A2 or figure 2.2.8 in chapter 2).

6.2.2 RESULTS

Figures 6.2.1(d), 6.2.2(c), 6.2.3(b, c & d), 6.2.4(a &b) show the results of the FEA and fatigue test results. The results show that there is a correlation between amount of support and the loading position and the areas of maximum stress. These areas of maximum tensile stress correspond to the areas of crack propagation observed in the retrievals presented in figures 6.2.1 (e), 6.2.2 (d) and 6.2.3(e).

Figure 6.2.4 shows the results from testing with the ISO test method. The results show that the crack direction although in the anterior-posterior direction varies with its end point. For the more posterior contact location (figure 6.2.4b) the crack extends more laterally.

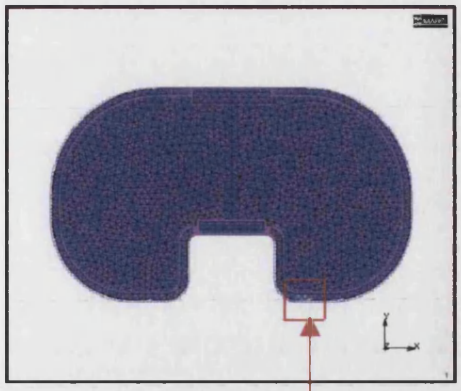

(a)

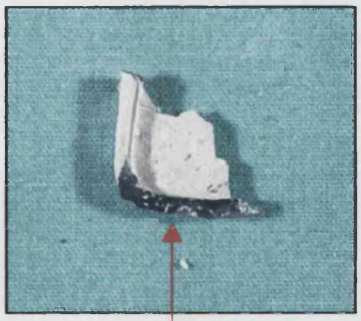

(b)

Point of load application shown by the highlighted green nodes within the red box

Shiny surface indicating rubbing of the femoral component against the tibial tray

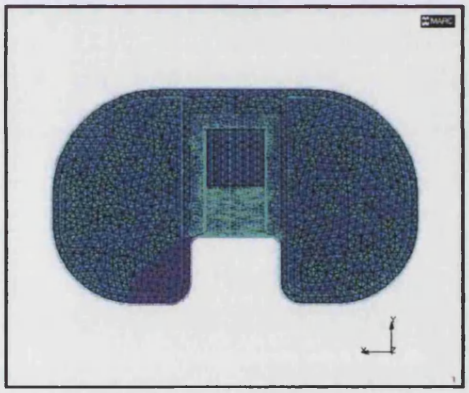

(c)

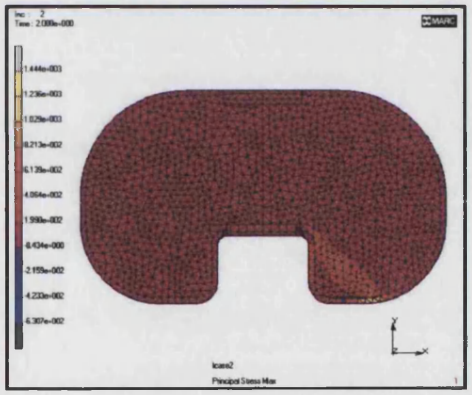

(d)

Figure 6.2.1: (a) FEA model of the Kinematic. The point of load application is based on the shiny surface indicated in (b). The shiny surface represents rubbing of the femoral component against the tibial tray *in vivo* (c) The highlighted green nodes are the area of the tray that is fully supported. The remainder of the tray receives no support. (d) FEA results showing that the areas of maximum stress occur at the boundary of the supported and unsupported areas.

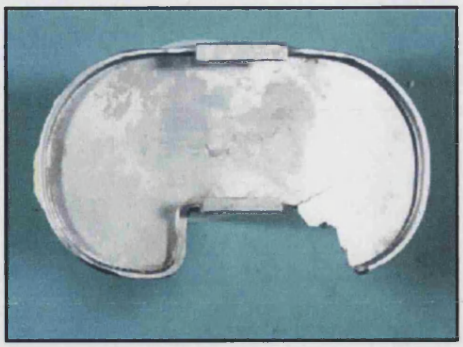

(e)

Figure 6.2.1 (e) Retrieved tray, showing crack formation in the posteromedial part of the tray, consistent with figure 6.2.1 (d)

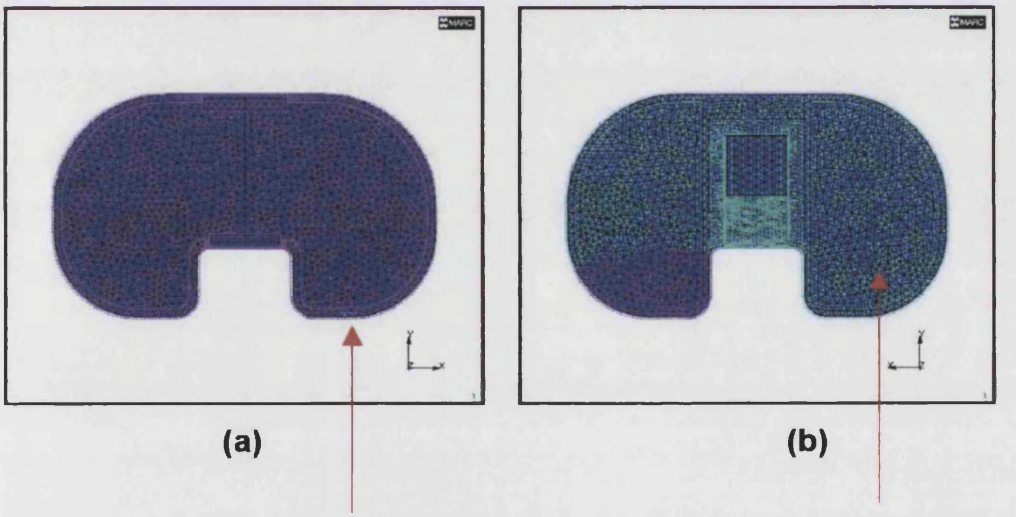

Figure 6.2.2: (a) FEA model of the Kinematic. (b) The highlighted green nodes are the area of the tray that is fully supported. The remainder of the tray receives no support.

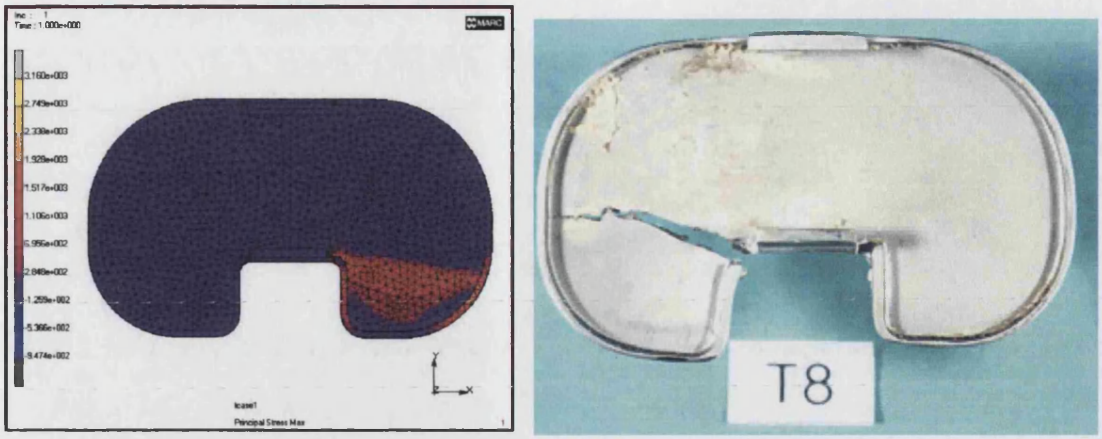

(c) (d)

Figure 6.2.2 (c) FEA results showing that the areas of maximum tensile stress occur at the boundary of the supported and unsupported areas. (d) Retrieved tray showing crack formation in the posteromedial part of the tray.

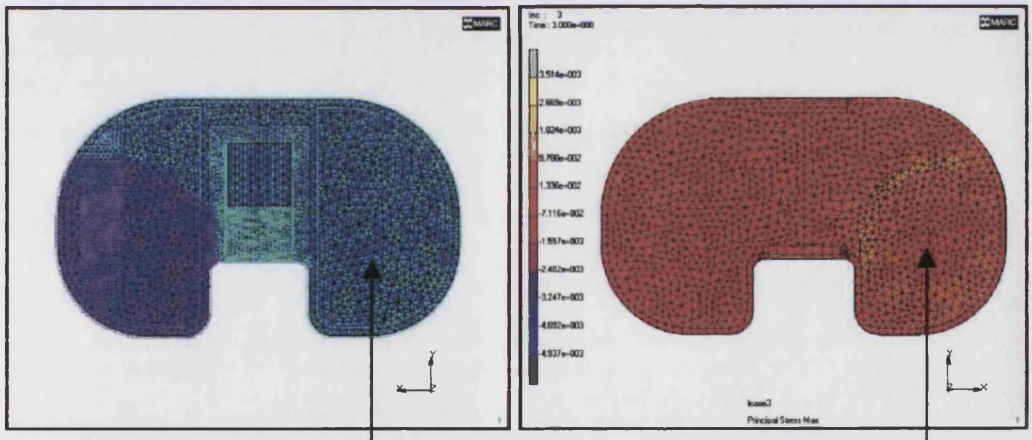

(a) (b)

High lighted green nodes Point of load application

Figure 6.2.3: (a) FEA model of the Kinematic. The highlighted green nodes are the area of the tray that is fully supported. The remainder of the tray receives no support. The point of load application is on the unsupported area (b) FEA results showing that the areas of maximum tensile stress occur at the boundary of the supported and unsupported areas.

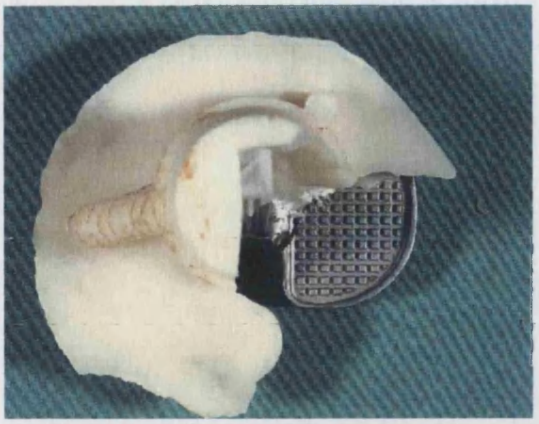

(c)

(d)

(e)

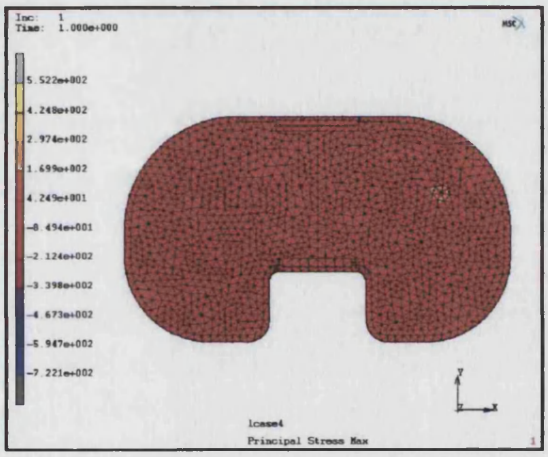

(f)

Figure 6.2.3 (c) Mechanical test performed where the supported region is modelled using cement. The point of load application is on the unsupported side. (d) Fatigue test results of the component showing crack formation at the border of the supported and unsupported region. (e) Retrieved tray showing crack formation that is similar to the FEA and fatigue testing results. (f) FEA study showing that if the point of load application is on the supported region then peak tensile stresses are well below the fatigue limit of the material.

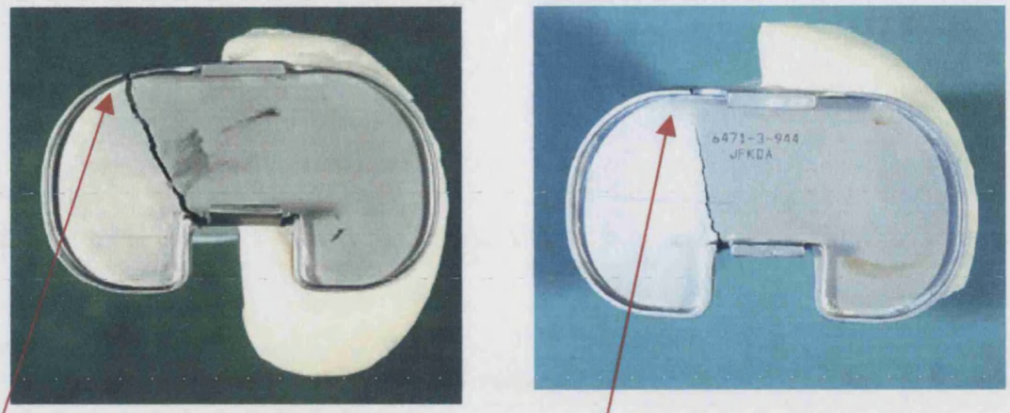

(a) (b)

In (a) the crack end point is more lateral as a result of a more posterior crack position.

Figure 6.2.4 (a) Fatigue test results using the 1996 contact position for the ISO support conditions (b) Fatigue test results using the 1997 contact position for the ISO support conditions. This shows that using the same support conditions (from the ISO test method) but two different contact positions there is a slight variation in crack propagation with (a) showing a more lateral crack path.

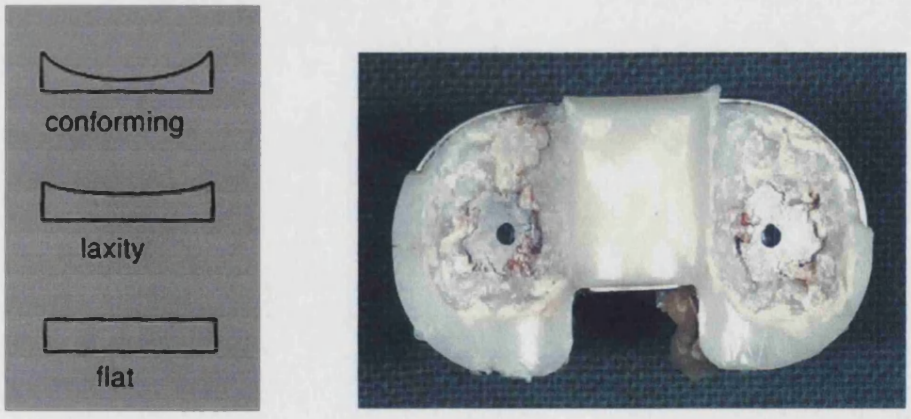

(a) (b)

Figure 6.2.5: Contact position is affected by (a) design of the tibial insert and (b) wear degradation of the tibial insert.

6.2.3 DISCUSSION

Chapter three showed that there were a large number of crack patterns from retrievals of fractured trays. This study has shown that using FEA and mechanical testing, the direction in which a crack grows depends on the amount of support and the position of load application. This finding is consistent with the fact that in clinical conditions the amount of support may vary either at the time of surgery or progressively through the patients lifetime and the contact location may also vary with differences in tibial insert design and as a result of wear degradation.

6.3 ALTERNATIVE TESTING METHODS

The study in 6.2 showed that the way in which crack propagation occurred depended on the amount of support the tray received in addition to the position of loading. A test method that represents failures seen *in vivo* would ideally be able to represent a number of different crack paths. Any standardized test method for tibial trays would have to be simple, relatively inexpensive and easily set-up. The results should also be repeatable so that identical tests could be carried out in a number of different laboratories with identical results. This study investigates the development of an alternative test method with the aim of being able to represent a number of different crack paths as seen *in vivo* retrievals.

Clinical evidence shows that poor bone support is one of the main factors in the fracture process. The literature reveals that with respect to fatigue fracture, each retrieval case with a central fixation post, the stem (or post) was distally well fixed. There were also layers of fibrous tissue present under one or both condyles (figure 6.3.1).

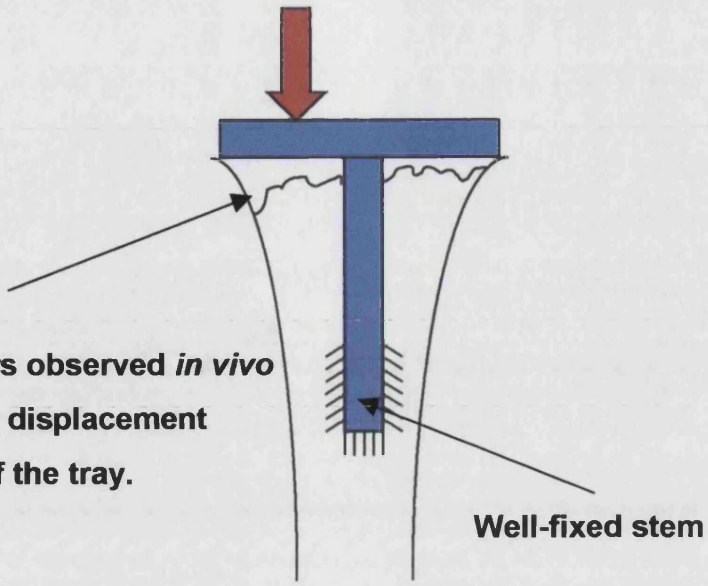

Figure 6.3.1

Fibrous tissue layers observed *in vivo*
Resulting in greater displacement
of the plate of the tray.

6.3.1 MATERIALS AND METHOD

Chapter five showed that using FEA, a Kinematic component that was well supported and correctly aligned in bone does not experience high enough stress levels to cause fracture. When a fibrous tissue layer was incorporated into the finite element model, stress levels within the Kinematic tray design increased to a level where there was a possibility of fatigue fracture. Thus the fibrous tissue layer compromised the fixation of the tibial baseplate, allowing the flat parts of the tray (or condyles) to displace whilst the stem was well fixed.

A new test method was then developed to incorporate a well-fixed stem but allowing the flat parts of the tray to displace. The distal one-third of the stem was well-fixed using cement in a specially made fixture. The component was supported using two blocks of material (figure 6.3.2). The materials for the blocks were titanium, aluminium, delrin and polyurethane (figure 6.3.3). These materials were chosen to study the effects of decreasing the Young's modulus of the supporting material. The properties of the material are defined in Table 6.1. The use of metallic supports was to assess the suitability of a standard material in spite of a high Young's modulus.

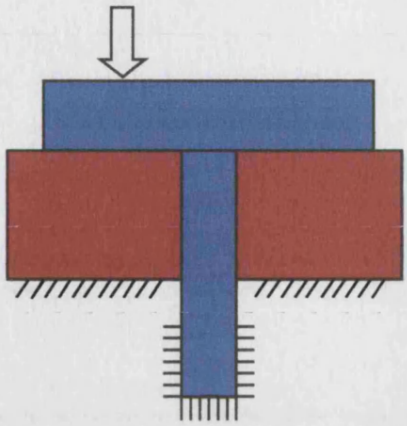

Figure 6.3.2: Alternative testing method: the stem is well fixed and the plate is not cemented to the supporting block allowing greater displacement of the plate of the tibial tray.

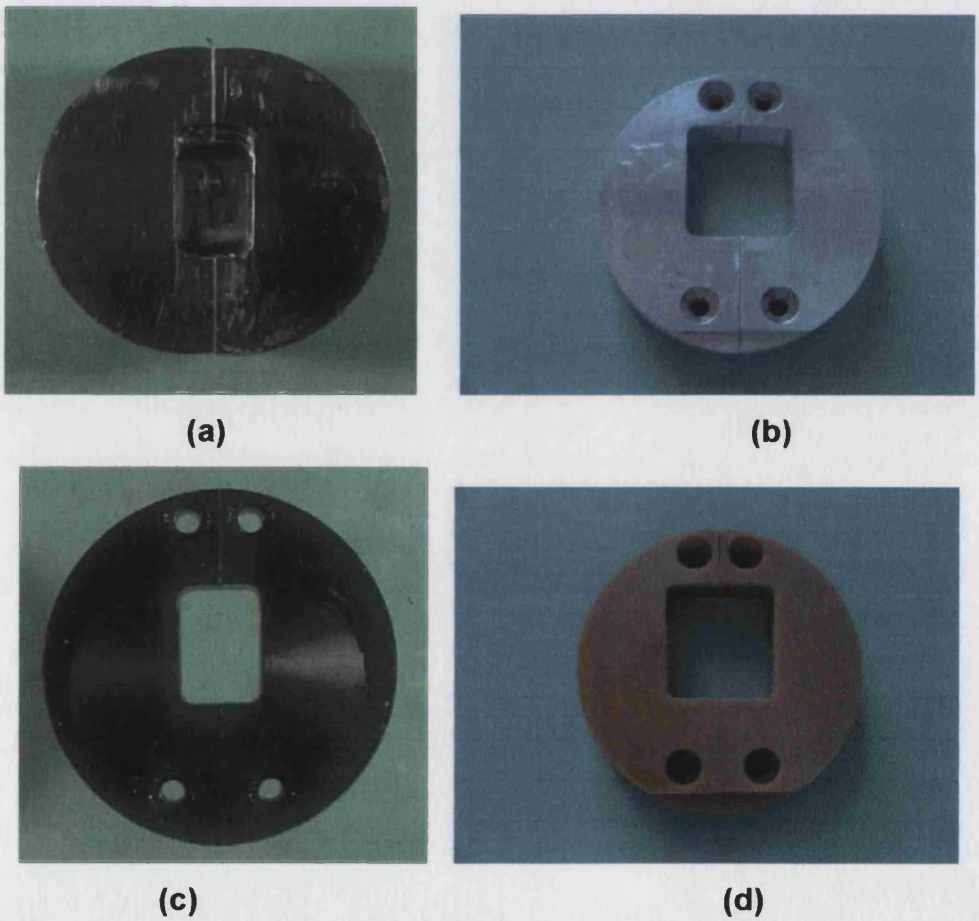

Figure 6.3.3: Support blocks made from (a) titanium (b) aluminium (c) Delrin (d) polyurethane.

Block Material	Young's Modulus (MPa)
Titanium	110000
Aluminum	68000
Delrin	3100
Polyurethane	120

Table 6.1: Properties of the supporting block

A study by Uematsu et al (1987) found that the frequency of fibrous tissue was more common on the medial and lateral sides of the prosthesis (figure 6.3.4). In order to assess the effects of increasing amounts of fibrous tissue in these areas of the tray, partial support blocks were made. These blocks were made from aluminium because of the availability of the material and it was relatively easy to machine. Two types of blocks were manufactured as shown in figure 6.3.5.

A load of 2000N was applied to one condyle at a frequency of 5Hz for five million cycles. Three contact locations were defined. The first was the contact position defined in the 1996 ISO draft standard, the second was the contact position defined in the 1997 draft ISO standard and the final position was defined as being identical to the medio-lateral location at zero degrees flexion but in the anterior-posterior direction it coincided with the posterior location of the cruciate cut-out (figure 6.3.6).

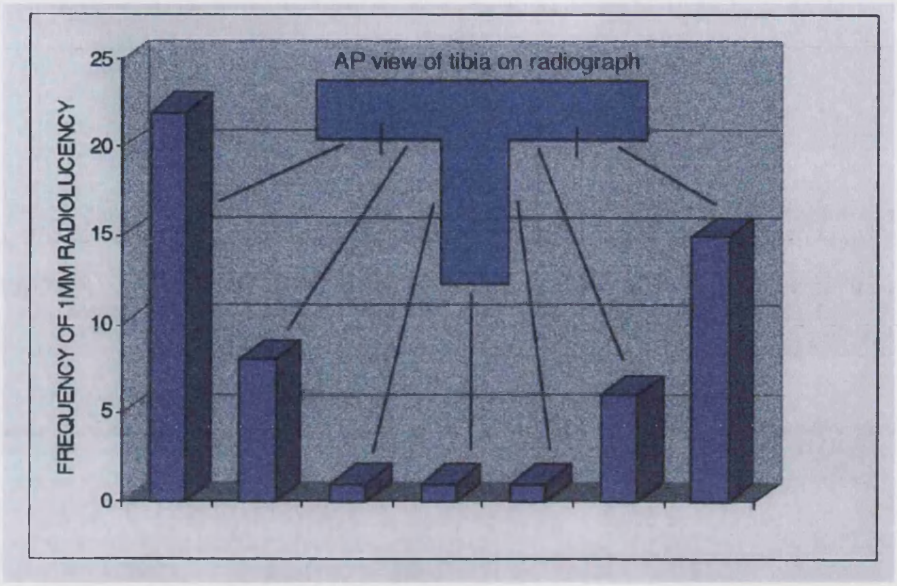

Figure 6.3.4: Frequency of 1mm radiolucency in 7 zones averaged for 616 cases of Kinematic knees followed for mean follow-up of 2.2 years, minimum 6 months. (Uematsu et al., 1987)

(a) partial support block 1

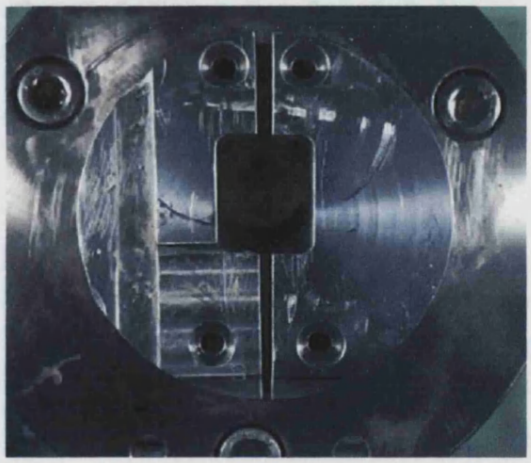

(b) partial support block 2

Figure 6.3.5 (a & b): Aluminium support blocks with cut-outs to show varying partial support.

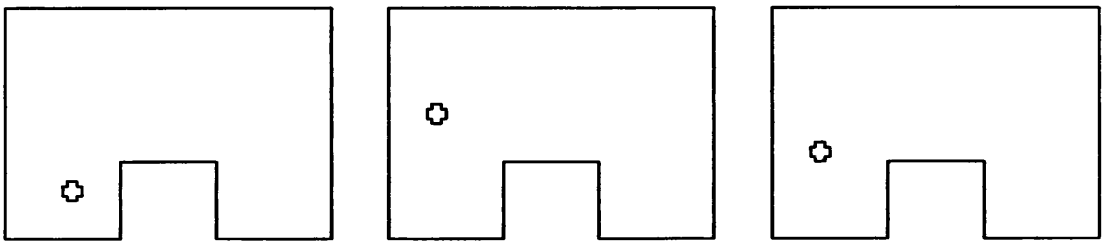

Figure 6.3.6: Contact locations: (a) first contact position defined in the 1996 draft standard, (b) second contact position defined in the 1997 draft standard (zero degrees flexion), (c) third contact position medio-laterally in the same position at zero degrees flexion but anteriorly in line with the cruciate cut-out.

6.3.1 MATERIALS AND METHOD (cont'd)

6.3.1.1 Finite Element Analysis

The finite element analysis was performed using the Kinematic and AGC components. Both the Kinematic and the AGC models were created using a hand generated mesh. Iges files of the two models developed in Unigraphics were used as a guide so that all the essential features of the tray design were incorporated into the finite element model. The Kinematic model consisted of 9962 hexahedral elements and 13282 nodes. The AGC model consisted of 11936 elements and 15522 nodes. For both models, each support block consisted of 5990 hexahedral elements and 7216 nodes. The size of the models reflected the maximum number of elements that could be analysed by the computer for a contact analysis.

The FEA was carried out using blocks made of four materials. The partial support blocks were also analysed. In each case one third of the stem of the component was rigidly fixed. The blocks were also rigidly fixed at the base in all six degrees of freedom. The Kinematic was analysed for all block types. The AGC was analysed for the full support blocks only. Both tray designs were analysed at 2000N for all three contact positions. The AGC was analysed at 4000N for the second contact position.

6.3.1.2 Mechanical Testing

For the Kinematic model, mechanical tests were performed for the partial support blocks and the full support blocks. The AGC was tested using Delrin support blocks only. The Kinemax was also tested using Delrin and polyurethane full support blocks. All the tests were carried out using a maximum compressive load of 2000N at 5Hz until failure or 5 million cycles was achieved.

6.3.2 RESULTS

Table 6.2 and 6.3 show the FEA results for the Kinematic tray subjected to all the different support blocks for all contact positions. The results show that the stresses in the tray are all above the fatigue limit for cast CoCrMo alloy of 300 MPa (Paganelli et al., 1988). These results predict failure by fatigue for the Kinematic tray regardless of supporting block and contact location.

	1st contact	position	2nd contact	position
Block Material	Peak Compressive Stress in block (MPa)	Peak Tensile Stress in Kinematic (MPa)	Peak Compressive Stress in block (MPa)	Peak Tensile Stress in Kinematic (MPa)
Titanium	18.48	1333	18.12	939.8
Aluminum	17.87	1334	17.22	940.1
Delrin	10.50	1337	7.51	942.5
Polyurethane	6.72	1324	2.98	922.7
Aluminum (partial support 1)	43.2	3223	18.0	1264
Aluminum (partial support 2)	51.9	3618	21.3	1564

Table 6.2: Peak stresses in the Kinematic tray for the first and second contact position at load values of 2000N.

	3rd contact	position
Block Material	Peak Compressive Stress in block (MPa)	Peak Tensile Stress in Kinematic (MPa)
Titanium	22.97	842.7
Aluminium	22.23	842.8
Delrin	7.50	845.1
Polyurethane	3.86	828.7
Aluminium (partial support 1)	23.2	1956
Aluminium (partial support 2)	25.6	2220

Table 6.3: Peak stresses in the Kinematic tray for the third contact position.

Results of the FEA using the AGC for different load levels and full support block materials are shown in Table 6.4 and Table 6.5. The FEA results for the AGC show that using a load level of 2000N for any support block material, the peak stress is below the fatigue limit for CoCrMo alloy (300MPa). Interestingly, the peak stress in the tray is virtually independent of the supporting material.

FEA of the AGC component was also carried out at 4000N for the second contact location. Table 6.5 shows that the peak tensile stress predicted by FEA would be 505 MPa. A fatigue test was not carried out as there were no samples of the AGC available. FEA predicted peak tensile stresses of 421 MPa for the AGC tray design for a load level of 900N under the ISO test conditions. For a load level of 1500N the AGC would experience tensile stress levels of 682.9 MPa under the ISO test conditions. Under fatigue test conditions all samples of the AGC survived 900N and 3 out of 4 survived at 1500N. It is highly likely that using a load level of 4000N under the alternative test conditions, the majority of AGC samples would survive.

	1st contact position		**3rd contact position**	
Block Material	Peak Compressive Stress in block (MPa)	Peak Tensile Stress in AGC (MPa)	Peak Compressive Stress in block (MPa)	Peak Tensile Stress in AGC (MPa)
Titanium	40.37	227.8	61.29	154.5
Aluminum	38.03	227.2	52.48	156.1
Delrin	10.87	234.7	13.58	176.1
Polyurethane	4.93	222.5	6.35	168.3

Table 6.4: Peak stresses in the AGC tray for the first and third contact position at load values of 2000N

	2nd contact position using a load of 2000N		2nd contact position Using a load of 4000N	
Block Material	Peak Compressive Stress in block (MPa)	Peak Tensile Stress in AGC (MPa)	Peak Compressive Stress in block (MPa)	Peak Tensile Stress in AGC (MPa)
Titanium	38.03	248.6	96.67	496.1
Aluminum	35.41	247.8	93.01	496.3
Delrin	5.45	252.3	10.86	505.4
Polyurethane	5.37	244.2	10.82	489.3

Table 6.5: Peak stresses in the AGC tray for the second contact position at load values of 2000N and 4000N

Figure 6.3.7.a shows the stress distribution of the Kinematic tray supported on a titanium block. The peak stress indicated that the Kinematic would fail. Using the titanium block, crack initiation occurred. The crack began to propagate but after 100,000 cycles the metal tray stopped displacing and the crack did not propagate further.

Figure 6.3.8 shows the stress distribution in the Kinematic tray using a partial aluminium support. The FEA predicted that the peak stress in the Kinematic would be above the fatigue limit. Under mechanical test conditions, crack initiation occurred and the crack began to propagate but after 100,000 cycles the metal tray stopped displacing and crack did not propagate further.

FEA predicted that using a Delrin support block that the Kinematic tray would fail due to fatigue for all three contact positions. The stress distribution for these contact locations is shown in Figure 6.3.9.

Fatigue testing of the Kinematic component using Delrin showed crack paths in the medio-lateral and anterior-posterior directions (figure 6.3.10). Indentation of the block occurred figure 6.3.10(a). These cracks emanated from the area below the contact location. Figure 6.3.10 shows that by varying the contact location different crack patterns occur (compare b with c, d, & e). For the second contact position, three components were tested. The results show very similar crack formation to the retrieval (figure 6.3.10 c, d and e) represented in figure 6.3.10 f).

FEA predicted that the AGC would survive at 2000N for all three contact positions using a Delrin support block. The stress distribution for these contact locations is shown in Figure 6.3.11. Under fatigue test conditions, the AGC was tested for the second and third contact locations and all survived to five million cycles (figure 6.3.12). The Kinemax component was also tested using Delrin supports for two contact locations. All samples survived to five million cycles (figure 6.3.13).

Figure 6.3.14 shows the stress distribution, predicted from FEA, in the Kinematic and the polyurethane supporting block. Peak stresses of 627MPa are observed on the undersurface of the Kinematic directly below the contact location. A mechanical test performed on the Kinematic tray showed multiple crack formation around the contact location propagating in both A-P and M-L directions (figure 6.3.15a). The component was removed from the test at 1,360,800 cycles. As there were no samples of the AGC to use, the Kinemax was subjected to fatigue test conditions. It survived to five million cycles for the second contact position.

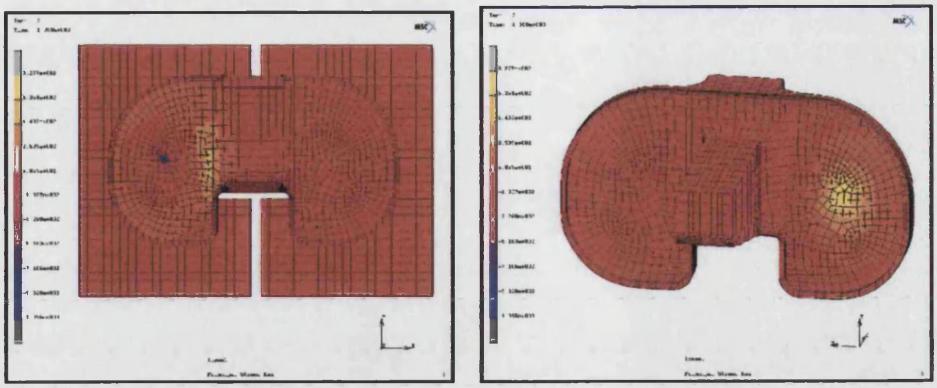

(a) (b)

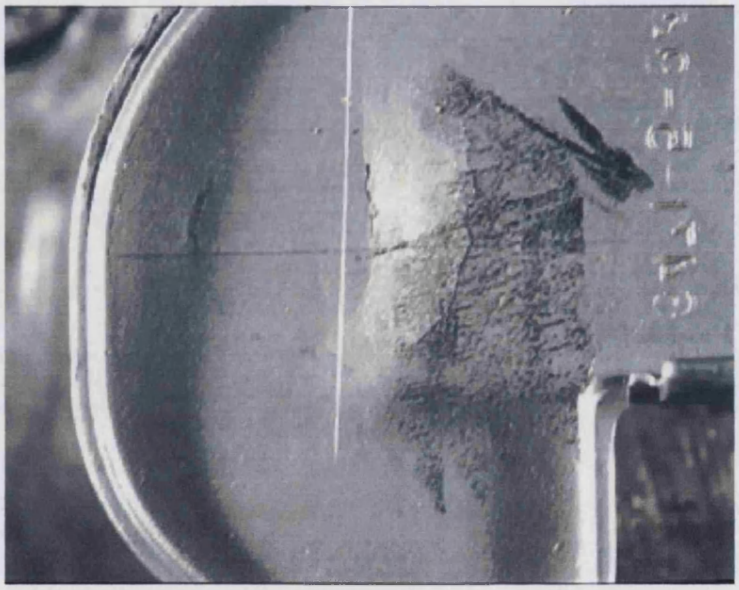

(c)

Figure 6.3.7: (a) Tensile stress distribution for the Kinematic component supported on titanium blocks. (b) Close–up view showing high tensile stresses in the notch of the Kinematic component. (c) Fatigue test results of the Kinematic component using titanium support blocks.

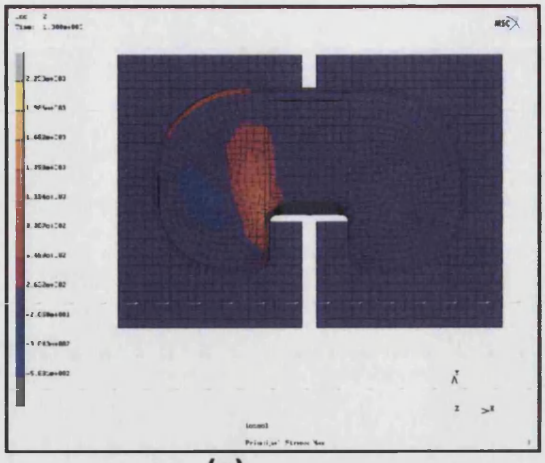

(a)

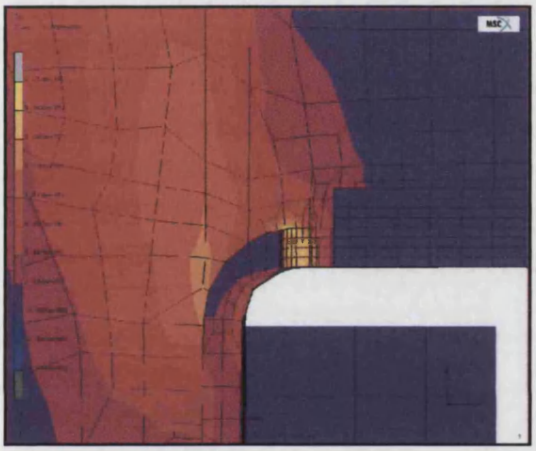

(b)

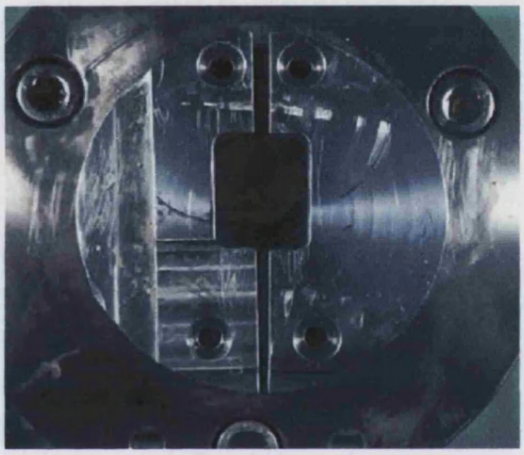

(c)

(d)

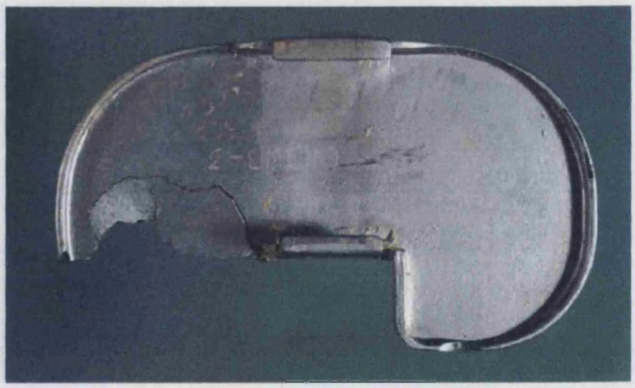

(e)

Figure 6.3.8: (a & b) FEA results of the Kinematic component supported on a partial aluminum support. (c) Aluminum partial support block. (d) Fatigue test result of the Kinematic component using support block in (c). (e) Kinematic retrieval.

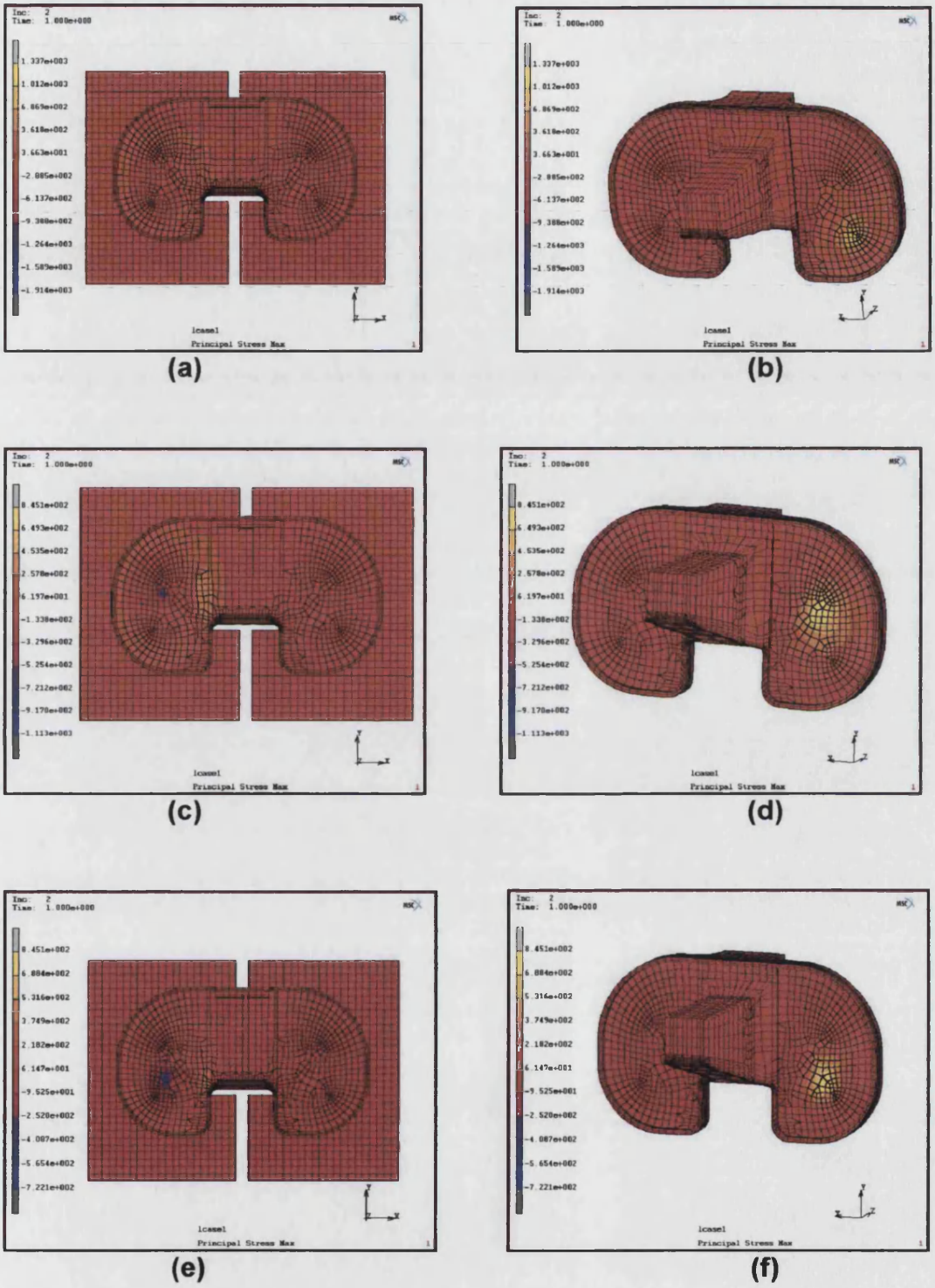

Figure 6.3.9: FEA results of the Kinematic component using Delrin support blocks for (a-b) 1st contact positions (c-d) 2nd contact position (e-f) 3rd contact position.

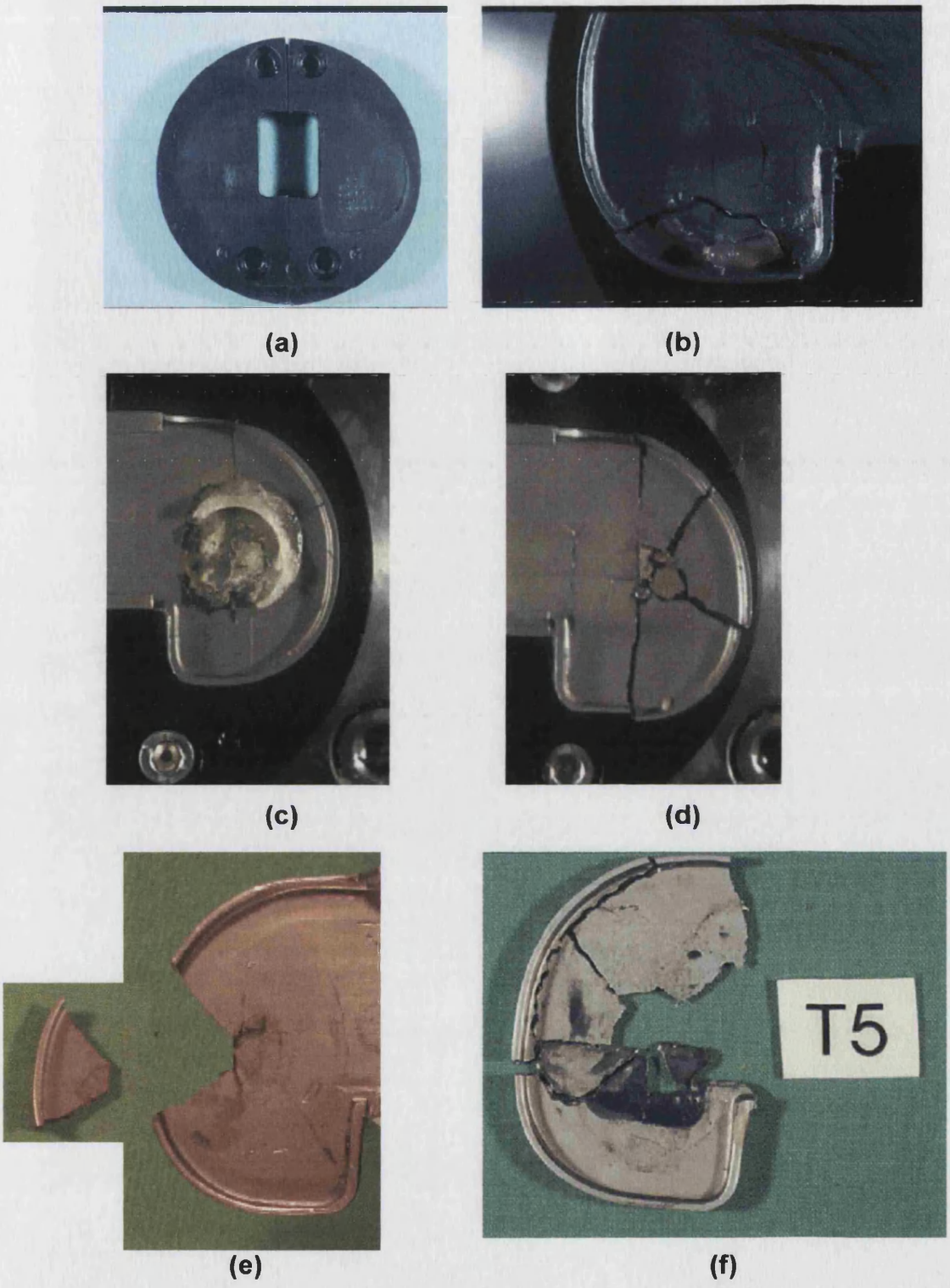

Figure 6.3.10: (a) Delrin support showing indentation as predicted by the FEA. (b) Failure of the Kinematic using a posterior contact position. (c), (d), and (e) Failure of the Kinematic component for the 2nd contact position with very similar crack formation. (f) Retrieval Kinematic component.

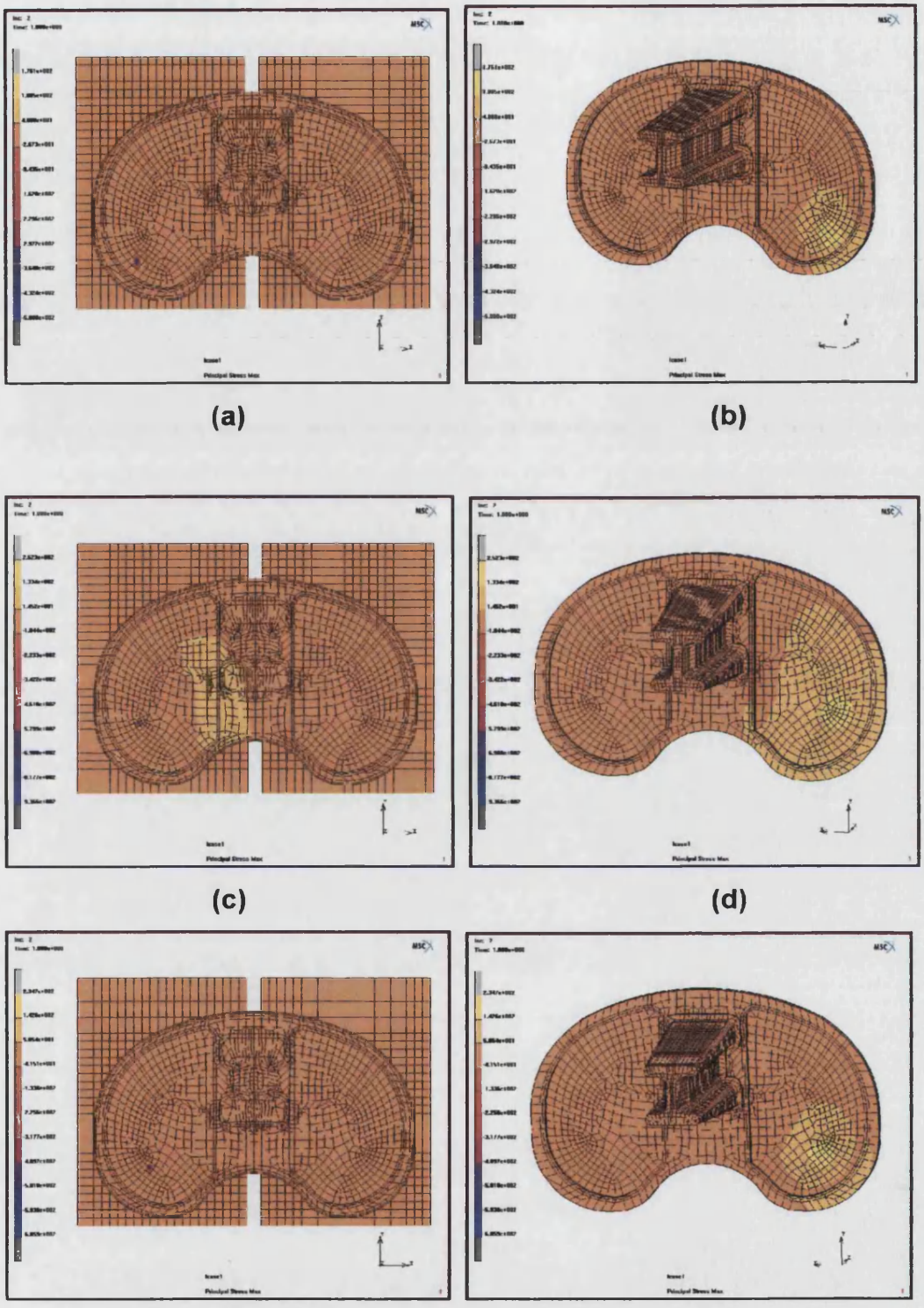

Figure 6.3.11: FEA results of the AGC component using Delrin support blocks for (a-b) 1st contact positions (c-d) 2nd contact position (e-f) 3rd contact position.

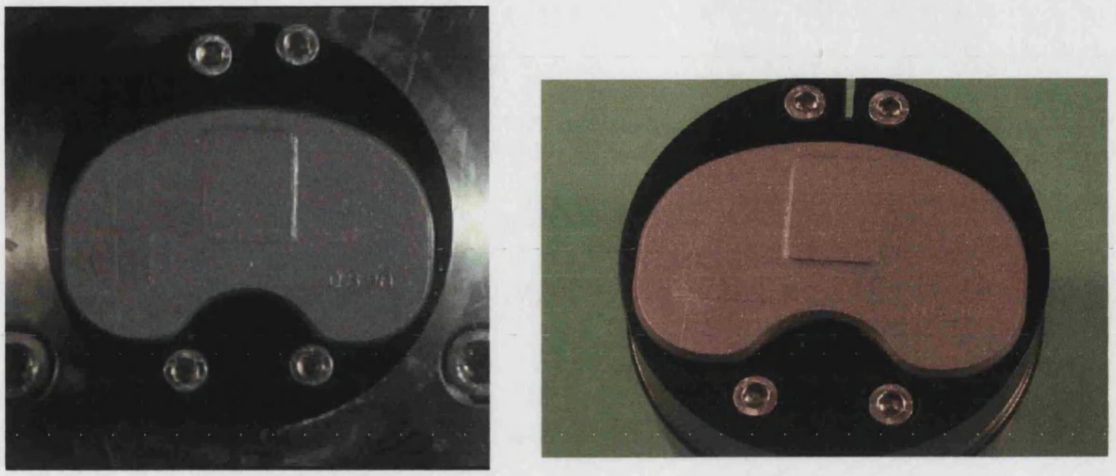

(a) (b)

Figure 6.3.12: Survival of the AGC component using Delrin support blocks to five million cycles (a) 2nd contact position (b) 3rd contact position.

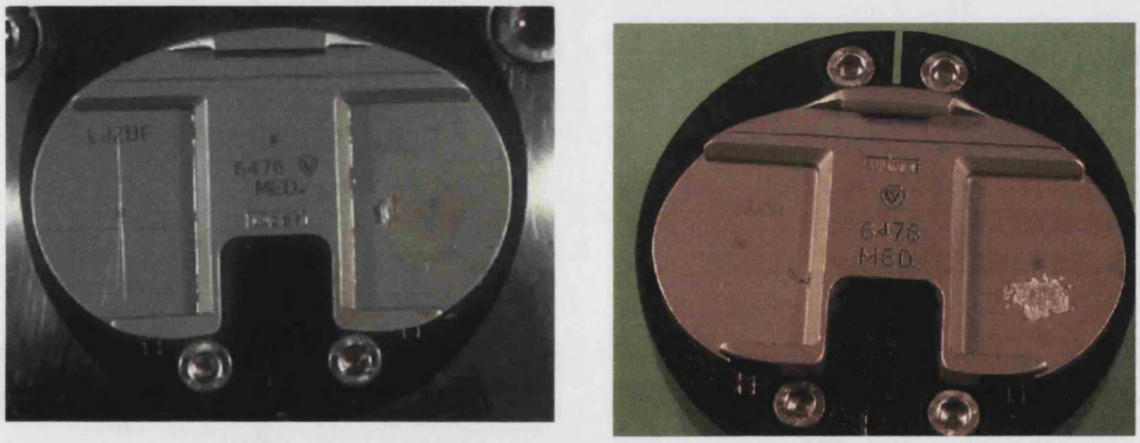

(a) (b)

Figure 6.3.13: Survival of the Kinemax component using Delrin support blocks to five million cycles (a) 2nd contact position (b) 3rd contact position.

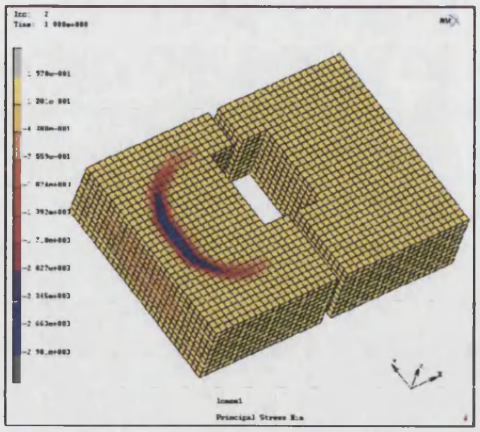

(a)

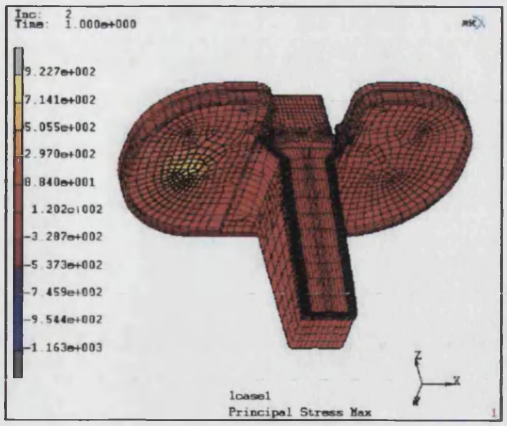

(b)

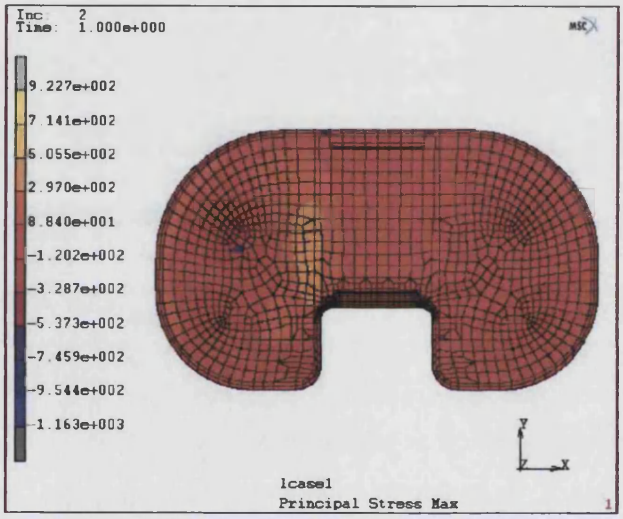

(c)

Figure 6.3.14: (a) Results of the Kinematic tray supported on two blocks of polyurethane material. (b-c) Results show the peak stress in the tray and material.

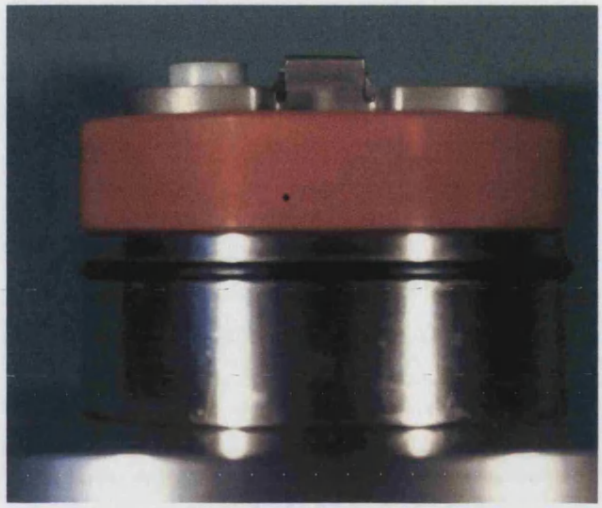

(a)

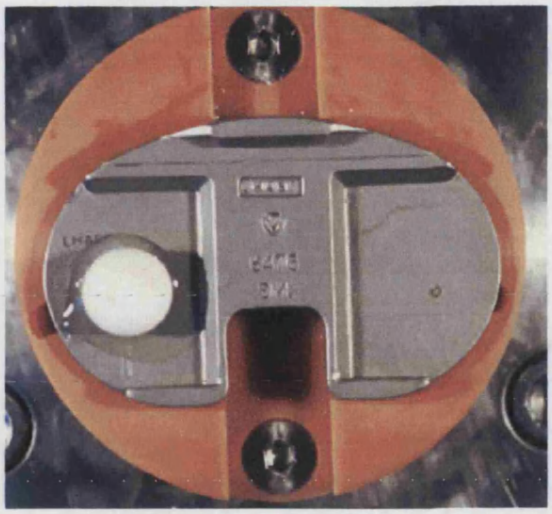

(b)

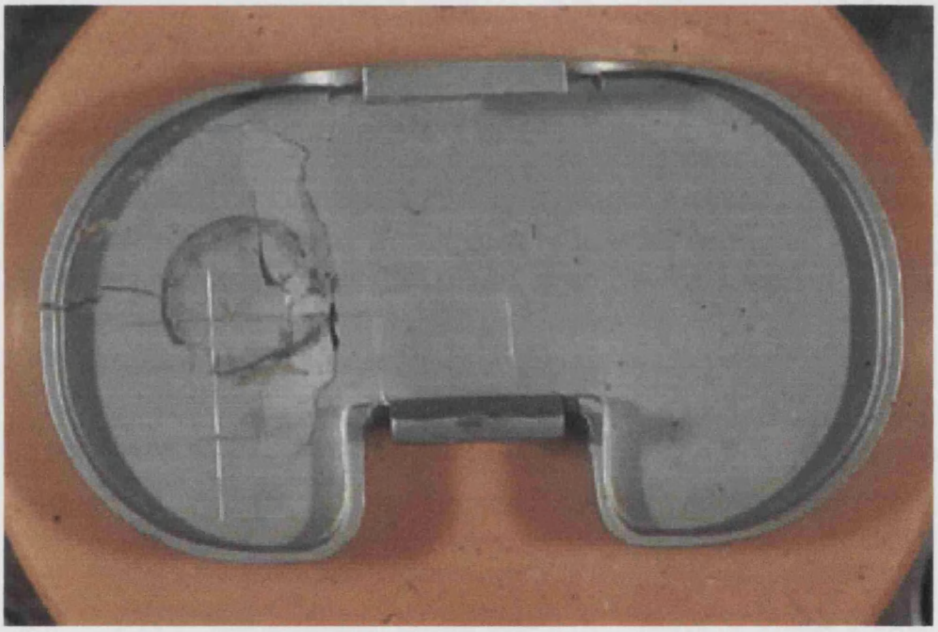

(c)

Figure 6.3.15: (a) Kinematic tray supported on polyurethane blocks. (b) Survival of the Kinemax component to five million cycles. (c) Failure of the Kinematic component with multiple crack paths.

6.4 DISCUSSION

The material analysis showed that using a metallic support whether it was titanium or aluminium with full or partial support resulted in adhesion between the metal support and the metal tray. The prediction by FEA of failure and the expected amount of crack propagation was limited by this adhesion.

Microscopically, a surface is not smooth; the irregularities consist of peaks and valleys. When two irregular surfaces contact, the peaks of the irregular surfaces adhere or "weld" to each other. In addition, the peaks may adhere to the valleys of the opposite surface. The real area of contact is consequently very small and the real pressure at the contact asperities is high. As a result, friction is required to overcome the force of attraction, or adhesion, between the two metals. Hodgson et al. (1999) used ultrasound techniques to measure the interface stiffness between two highly polished aluminium blocks that were brought into contact with each other. They found that the interface stiffness was 8.6MPa. Wimmer et al. (2001) reported on the stick phenomena on metal on metal hips after resting periods. They compared metal heads articulating against metal cups with metal heads articulating against polyethylene cups for a set of defined resting periods. They found that metal heads and cups rigidly adhered to each other and the coefficient of friction between metal on metal was much higher when compared with metal on polyethylene in vitro. A study of retrievals showed evidence of the femoral head and cup adhering to each other. They reported that resting periods might interrupt motion and influence the tribology of metal on metal hips as a result of interlocking between surface discontinuities. (i.e. protruding carbides from the metal matrix, environmental precipitation). These phenomena may increase the frictional torque and may cause particle and ion release due to the disruption of the protective layers on the metal surfaces.

Using either Delrin or polyurethane material for the support block resulted in higher stresses in the tray designs. The loaded condyle of the tray was able to displace without adhesion and resulted in a range of crack paths dependent of the position of contact. A load of 2000N could be used to distinguish between the Kinematic, AGC and Kinemax tray designs. This test method showed that a physiological load level could be used to distinguish between clinically unsuccessful and successful tray designs with a physiological load level. Repeatability of the crack patterns for the Kinematic tray and survival of the AGC and Kinemax trays was also shown. In addition, the results from the Kinematic tray showed similar fracture patterns to those seen in retrievals.

The limitations of this alternative testing method are that there are a wide number of material specifications for polyurethane. Therefore, Delrin may be a more suitable material to choose. However, there may be difficulties in obtaining Delrin worldwide. Another limitation would be that the test could not be used for those tray designs without a central stem. The testing in this study showed that for each contact location using the different materials for support – a set of crack patterns could be obtained. The current testing was unable to reproduce all the crack patterns seen in retrievals especially those observed using the ISO test method.

The question remains whether it is important to use a physiologic load level and whether all crack patterns seen on retrieved trays are required to be reproduced. The crack patterns from this study always revealed the same design faults as the ISO test, namely that the Kinematic tray has a thin baseplate with a stress concentrating notch in the periphery of the tray.

CHAPTER 7:
DISCUSSION AND CONCLUSIONS

7.0 GENERAL DISCUSSION

The aim of this study was to investigate and develop clinically relevant testing methods to avoid fracture of new metallic tibial component designs of total knee replacements. The main objective was to determine if the test proposed by the International Standards Organisation was clinically relevant, and if so, to define the value of the load used as this is not done in the standard. Clinical relevance was defined as being representative of failures seen *in vivo*. Although the reported incidence of fracture was infrequent, it is a catastrophic method of failure that results in loss of function and pain for the patient, requiring a revision operation. An examination of the literature revealed that there are a number of factors that contribute to this failure mechanism. The main reason for fracture was increased stresses in the baseplate, due to lack of bone support particularly under one condyle of the tray in conjunction with a rigidly fixed stem. Design also played a part in the fracture process. Design features that resulted in stress concentration, inadequate thickness of the baseplate and poor material properties were contributing factors. Other factors were patient weight and activity levels, malalignment and coverage of the tibial plateau.

The International Standards Organisation had proposed a test method for determining the fatigue performance of total knee tibial trays. This test method had been in existence for many years in its draft form. The test specified that the tibial tray should be rigidly fixed on one half of the component so that one condyle receives total support and the other condyle receives no support. The gap under the unsupported condyle should be greater than 5mm. Only the unsupported condyle is loaded. The contact location for this load was first defined in 1996 at a known position with respect to the A-P and M-L dimensions. In 1997, this contact location was redefined as being the contact position at zero degrees flexion. The magnitude of the load had not been defined but the duration of the test was specified as five million cycles.

Clinically unsuccessful designs were identified from the literature. Clinically successful designs were selected so that they represented the design range currently available. The work by Morrison (1969) showed that the peak force during the walking cycle is three times body weight, which is about 2000N. However the studies carried out in Chapter 4 showed that using a load level of 2000N was too severe for some clinically successful designs. Further analyses and experiments showed that a sub-physiological load level of 900N at the contact position at zero degrees flexion, was found to be applicable to be used to distinguish between clinically successful and unsuccessful tray designs.

Examining the fracture patterns of those trays that had failed *in vivo* showed that for the Kinematic, there was only one retrieval from eleven (held by the Centre for Biomedical Engineering, Stanmore, UK) that had failed in the same manner *in vivo* as under ISO test conditions. For the Total Condylar (type I) design all of the four retrievals obtained had failed in the same manner as under ISO test conditions. However, there were a number of Kinematic trays, PCA and revision PCA identified either within the Centre of Biomedical Engineering or in the literature that had different crack paths than those predicted using the ISO test conditions.

To understand why trays failed with different crack paths, it was decided first to examine the performance of two tibial tray designs *in vivo*. Chapter 5 used FEA to examine the performance of the Kinematic and the AGC, when placed in bone with material properties representing normal and arthritic conditions. This study showed that when correctly supported both the Kinematic and the AGC although subjected to a physiological load of 2000N did not experience stress levels near their fatigue limits for three different contact positions. Fibrous tissue was modelled as a 1mm compliant interface between the cement layer and bone, increased the stress levels in the Kinematic to an extent that failure by fatigue was possible within the tray. For the AGC tray a 1mm layer of fibrous tissue did not compromise fixation.

However, these models did not explain why cracks propagate in different ways.

In chapter 6 study one, a series of tests using FEA and fatigue testing showed that by varying the amount of support and the contact position, there was a direct relationship with the manner in which crack paths occur. *In vivo*, the amount of support the tray receives will vary from patient to patient as a result of bony deficiencies prior to surgery or during the lifetime of the patient. Contact positions can also vary, as a result of tibial insert design and wear. This explains why retrievals of trays that have fractured *in vivo* show a large variation in crack patterns.

The criticism that the ISO test method receives from clinicians, orthopaedic scientists and the orthopaedic industry is that the test is too simplistic, does not use a physiological load level and is unable to reproduce failure modes seen *in vivo*. However, by the same token the orthopaedic industry require a test method that is simple, easily set-up, where the results are reproducible so that they can be compared amongst different laboratories. To address the criticism of the ISO test, an alternative testing method was developed. The basis of this test, described in chapter 6 study two, is that the incidence of fracture is associated with a lack of bony support. In retrieval cases, the condyle/s of the tray are able to bend, either as a result of fibrous tissue layers beneath the tibial component or as a result of bone deficiency. In addition, a well-fixed stem was always identified for those trays with a central fixation post.

The alternative test method involved rigidly fixing the lower one-third of the stem by embedding it in acrylic cement held in a specially made fixture. The condyles of the tray were then simply supported using different support materials. These materials were titanium, aluminium (standard materials that are easily available with consistent material properties), delrin and polyurethane (the young's modulus is closer to that of bone). Three contact positions were defined. A load of 2000N was then applied to the three

contact positions varying from a posterior position through to the most anterior position defined at zero degrees flexion. The analyses were performed using FEA and fatigue testing. In spite of the FEA results, under mechanical test conditions the results showed that when using a metallic support, adhesion would occur between the support and the tray. This minimised displacement of the tray condyles and this resulted in the crack being unable to propagate beyond initiation. With polymeric materials such as polyurethane and Delrin, displacement of the tray occurred and failure was observed with multiple crack paths for the Kinematic tray. Survival of the AGC and Kinemax trays was observed at 2000N to five million cycles. This test method showed that a physiological load level could be used to distinguish between clinically successful and unsuccessful tray designs with a physiological load level. Repeatability of the crack patterns for the Kinematic tray and survival of the AGC and Kinemax trays was also shown.

The advantages of the alternative test method are that a physiological load level of 2000N can be used to distinguish between clinically successful and unsuccessful tray designs. Using this test, a clinically unsuccessful design, the Kinematic, produced a range of crack paths with repeatability. The limitations of this alternative testing method are that there are a wide number of material specifications for polyurethane. Therefore, Delrin may be a more suitable material to choose. However, there may be difficulties in obtaining Delrin worldwide. Another limitation would be that the test could not be used for those tray designs without a central stem. In addition, the alternative test is also unable to produce a crack path as seen under the ISO test. The study shows that any test method that is used would only be able to produce a defined number of crack paths and not the entire range seen *in vivo*.

Therefore, the requirement of any test method for fatigue fracture would be to identify weaknesses in the design of tibial tray particularly under conditions which are representative of poor bone support. If this is the case, then clinical relevance would need to be redefined so that instead of being defined

in terms of types of crack paths seen *in vivo,* it refers to failure seen under conditions experienced *in vivo.*

If a standardised test method is to be developed, it should either specify one such clinical condition or identify a number of support conditions, which a tibial tray would have to survive. For each support condition, different load values may have to be defined. The contact location would also have to be considered. It is clear from the results of appendix B that using the same support conditions but a different contact location, that different load values would have to be used to distinguish between clinically successful and unsuccessful tray designs. Appendix B showed that for the first contact position, a lower value would have to be used, than that defined for the position at zero degrees flexion. More samples would have to tested to validate and to establish if this lower value of 500N is suitable. Clearly some load positions are more damaging than others.

A comprehensive testing method would require a series of tests that have different support conditions and different contact locations with different load levels. The problems of time and expense then arise. The industry wants to be able to carry out tests quickly and cheaply and one possibility is that a worse case scenario test or one defined test should be advocated. This would mean that the worst support conditions and the worst contact location, with an appropriate load level would have to be defined.

A subject for further debate is increasing the length of testing time to ten million cycles and so representing 5 to 7 years of *in vivo* use. However, this increases testing time and cost. One solution may be to accelerate the testing method. This is advocated by Brown and Gregson (2001) who showed that the ISO test can be accelerated for CoCrMo alloys tray designs. The test method remains the same but the frequency of the test is increased to 10Hz and the test is run to 750,000 cycles using a higher load level of 1500N with agreement of the results obtained in chapter 4. If 1.5 million

cycles were run then the test would represent ten million cycles. This reduces the total time taken to carry out the test and reduces cost.

The future development of tibial trays has to look at improvements in design and material properties. The elimination of stress concentrating features is of critical importance. It is clear from this study that some designs are able to survive even higher load levels than 900N under the ISO test conditions. This would indicate that for severe bone conditions as represented in the ISO test, the tibial baseplate would be able to sustain higher loads *in vivo* prior to fracture. Publications of this work would hopefully encourage new designs to be created so that they are able to survive higher load levels at zero degrees flexion so that the incidence of failure *in vivo* can be further reduced.

The final conclusion of this study is that the ISO test is easily set-up, highly repeatable, able to identify weaknesses in design. The only material requirements are acrylic cement, which is easily available to the Orthopaedic industry and Orthopaedic research community. The work performed in this thesis has shown that the ISO test method is a clinically relevant testing method and should be used with a load level of 900N for a contact location at zero degrees of flexion for five million cycles.

CHAPTER EIGHT:
FUTURE WORK

8.0 FUTURE WORK

Following on from this study, the following work should be carried out:

(I) The current project relies on the fatigue testing of a small number of samples of each design. For further validation of this work, a larger number of samples needs to be tested. This data can then be incorporated into finite element packages that simulate fatigue (as these models rely on the S-N curve data). This would give credence to the further development and accuracy of fatigue finite element simulations. However, samples would still need to be tested, as current fatigue finite element simulations would be unable to give predictions about porosity or other casting defects.

(2) Working more closely with the ISO and ASTM committees with regards to recommendations for updating the standard testing method, especially by the specification of forces, the method of fixation of the tibial tray and the number of cycles the test should run for.

(3) The optimisation of current designs with respect to the PCL cut-out. Small radii increase stress concentrations and these may be positions for fatigue initiation. Guidelines could be created with respect to shape and size of the cut-out region.

(4) Optimisation of the locking mechanisms. Some designs have features at the locking mechanism for the plastic insert which are positions of the highest tensile stress under the ISO loading regime. In addition, the effectiveness of the locking mechanism with respect to backside wear in both fixed and mobile bearing knees has been raised as an issue of some concern.

(5) Minimally-invasive procedures are now being investigated and some designers are considering inserting modular trays through small incisions. It is important to investigate whether current standard tests are suitable for such devices.

(6) It is important to apply standardised testing to modular trays (where the stem and plate are modular) as modularity could be introducing significant weaknesses in the design.

(7) Development of more comprehensive bone models with regards to bone adaptive remodelling and the formation of fibrous tissue. This could be used as a predictive tool for new implant designs.

Appendix A1:
1996 draft ISO standard

Ed. 1 received from G Rhodes 15 February 1996
Project leader: G Rhodes
Based on ISO/WD 14879-1 Ed. 3

Implants for surgery - Total knee joint prostheses -

Part 1:
Determination of endurance properties of knee tibial trays

1 Scope

This part of ISO 14879 describes a test method for determining the endurance properties, under specified laboratory conditions, of tibial trays used in knee joint prostheses. It applies to tibial trays which cover the medial and lateral plateaux of the tibia.

The test method does not apply to tibial components manufactured solely from plastics materials.

This part of ISO 14879 does not cover methods of examining and reporting the final condition of the test specimen; these should be agreed between the test laboratory and the parties submitting the specimen for test.

2 Normative references

The following standards contain provisions which, through reference in this text, constitute provisions of this International Standard. At the time of publication, the editions indicated were valid. All standards are subject to revision, and parties to agreements based on this International Standard are encouraged to investigate the possibility of applying the most recent editions of the standards indicated below. Members of IEC and ISO maintain registers of currently valid International Standards

Secretariat note: The need for this clause will be checked at final draft.

ISO 4965: 1979, *Axial load fatigue testing machines - Dynamic force calibration - Strain gauge technique*

ISO 5834-2: 1985, *Implants for surgery - Ultra-high molecular weight polyethylene. Part 2: Moulded forms*

ISO 7207-1: 1994, *Implants for surgery - Components for partial and total knee joint prostheses. Part 1: Classification, definitions and designation of dimensions*

ISO 7500-1: 1986, *Metallic materials - Verification of static uniaxial testing machines. Part 1: Tensile testing machines*

3 Definitions

For the purposes of this International Standard, the following definitions apply.

Secretariat note: The need for this clause will be checked at final draft.

3.1 anteroposterior centreline: Line which passes through the centre of the tibial tray, parallel to the sagittal plane and perpendicular to the line of load application.

3.2 mediolateral centreline: Line which passes through the centre of the tibial tray, parallel to the coronal, or frontal, plane and perpendicular to the line of load application.

3.3 moment arm, 'd_{ml}': Perpendicular distance between the anteroposterior centreline of the tibia component and the line of load application.

3.4 moment arm, 'd_{ap}': Perpendicular distance between the mediolateral centreline of the tibia component and the line of load application.

4 Principle

Mounting of the test specimen in a test rig and fixed such that it is mounted as a cantilever beam. Application of a cyclic load through an ultra-high-molecular-weight-polyethylene (UHWPE) spacer on the unsupported condyle perpendicular to the undeflected superior surface of the tibial tray at a defined distance from the anteroposterior and mediolateral centreline. Cyclic load applied until the test specimen exhibits failure or until the chosen number of cycles has been attained. Subsequent examination of the specimen for defects caused by the loading regime.

5 Apparatus

5.1 Mechanical or hydraulic testing machine, having the following characteristics:

a) dynamic loading waveform: sinusoidal

b) instrumentation to monitor the values of the maximum and minimum loads and the vertical deflection (optional) of the tibial tray test specimen to an accuracy of $\pm$ 2 % and to record the number of cycles.

c) error in applied load: not greater than $\pm$ 2 % at the maximum load (see ISO 7500-1 and ISO 4965).

5.2 Means of fixturing the test specimen, to allow:

a) the test specimen to be held as a cantilever beam;

b) fixing the inferior surface or clamping the superior surface of the unsupported test specimen tray away from the mid line, to reduce the stress concentration at the centre line;

c) the load axis to be perpendicular to the undeflected superior surface of the test specimen;

5.3 Ultra-high molecular-weight polyethylene spacer to place between the test specimen and the load applicator to distribute the loading and reduce fretting fatigue.

NOTE. Recommended spacer dimensions are 13 mm diameter and 6 mm thickness.

5.4 Means of transmitting the load, a spherical indentor, diameter 32 mm.

6 Procedure

6.1 Determine overall AP and ML dimensions in accordance with ISO 7207-1, figure 2 and figure 3 (dimensions *w* and *d*)

6.2 Mount the test specimen in accordance with figure 1 or 2.

If asymmetrical the test specimen should be fixed so that the bending moment is a maximum at the junction of the tray with the keel, or at the division between the medial and lateral compartments if no keel is present'.

6.3 Position the test specimen such that the load axis is perpendicular to the undeflected superior surface of the tray since the tray surface sill not remain perpendicular to the load axis during loading. The point of load application will be located at a known distance from the anteroposterior centreline (d_{ml}) and from the mediolateral centreline (d_{ap}).

6.4 Fix the test specimen (5.2) in the test rig.

6.5 Place the spacer (5.3) between the test specimen and the load applicator (figures 1 or 2).

6.6 Start the testing machine and adjust it so that a load, R_{value} of 10, is applied to the test specimen using a spherical indentor (5.4) at a frequency of 30 Hz where

R_{value} is the ratio of the minimum load to the maximum load.

6.7 Continue the test until one of the following events occurs:

a) fracture of the tray;

b) the occurrence of cracks when inspected visually;

c) there is a vertical deflection of χ % $\pm$ y %, if required by the party submitting the specimen for test;

d) 1 x 10^6 cycles duration achieved.

6.8 Examine the test specimens using the methods requested by the party that submitted the specimen for testing.

7 Test Report

The test report shall include the following information:

7.1 A reference to this part of ISO 14879.

7.2 The identity of the test specimens, as stated by the party submitting the specimen for test including tibial tray thickness, diameter, size, ML and AP dimensions and material.

7.3 Identify the test conditions, including spacer diameter, d_{ml}, d_{ap}, fixation method and maximum load.

7.4 A statement of results including number of cycles applied and location of fracture (if fractured), description of test specimens at the end of the test, and the results of examination requested by the party submitting the specimen for test.

8 Disposal of test specimens

Test prostheses shall not be used for clinical purposes after testing. Care should be exercised in the use of the specimens for further mechanical test, because the loading regime may have altered the mechanical properties.

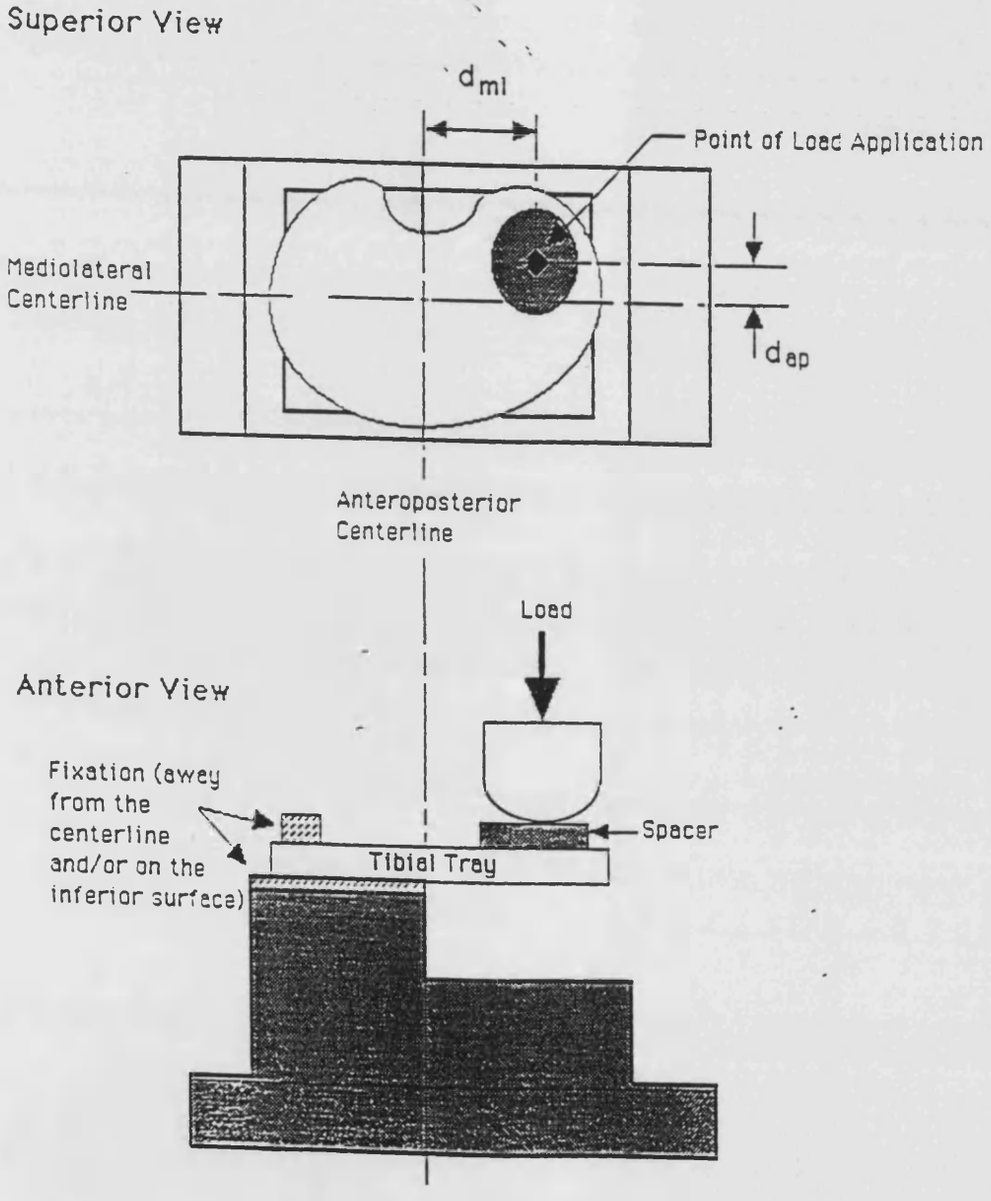

Figure 1 - Schematic of the test set-up for tibial trays without a central keel

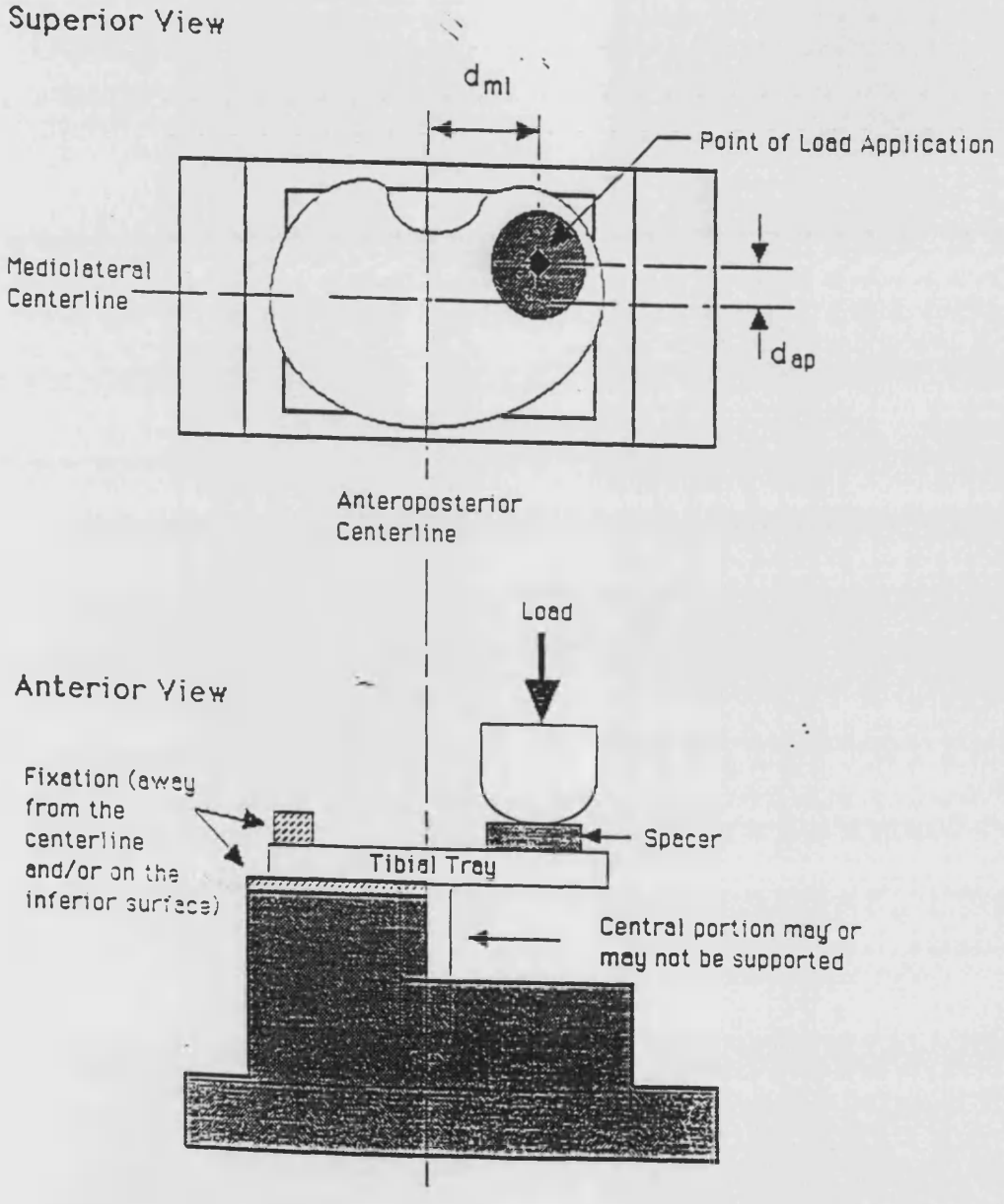

Figure 2 - Schematic of the test set-up for tibial trays with a central keel

Appendix A2:
1997 draft ISO standard

ISO/TC 150/SC 4 N 210

Date: 1997-10-03

ISO/CD 14879-1.3

ISO/TC 150/SC 4/WG

Secretariat: BSI

Implants for surgery — Total knee joint prostheses — Part 1: Determination of endurance properties of knee tibial trays

—

Document type: International Standard
Document subtype: Not applicable
Document stage: (30) Committee
Document language: E

J:\SECTN-H1\BROOMESM\ISO\150\SC4NDOCS\SC4N210.DOC ISOSTD ISO Template Version 3.0 1997-02-07

Implants for surgery — Total knee joint prostheses — Part 1: Determination of endurance properties of knee tibial trays

1 Scope

This part of ISO 14879 specifies a test method for determining the endurance properties, under specified laboratory conditions, of tibial trays used in knee joint prostheses. It applies to tibial trays which cover the medial and lateral plateaux of the tibia.

The test method does not apply to tibial components manufactured solely from plastics materials.

This part of ISO 14879 does not cover methods of examining and reporting the final condition of the test specimen; which are the subject of agreement between the test laboratory and the parties submitting the specimen for test.

2 Normative references

The following normative documents contain provisions which, through reference in this text, constitute provisions of this International Standard. For dated references, subsequent amendments to, or revisions of, any of these publications do not apply. However, parties to agreements based on this International Standard are encouraged to investigate the possibility of applying the most recent editions of the normative documents indicated below. For undated references, the latest edition of the normative document referred to applies. Members of ISO and IEC maintain registers of currently valid International Standards.

ISO 4965 : 1979, *Axial load fatigue testing machines - Dynamic force calibration - Strain gauge technique*

ISO 5834-2 : 1985, *Implants for surgery - Ultra-high molecular weight polyethylene. Part 2: Moulded forms*

ISO 7207-1 : 1994, *Implants for surgery - Components for partial and total knee joint prostheses. Part 1: Classification, definitions and designation of dimensions*

ISO 7500-1 : 1986, *Metallic materials - Verification of static uniaxial testing machines. Part 1: Tensile testing machines*

3 Definitions

For the purposes of this part of ISO 14879, the definitions given in ISO 7207-1 apply together with the following:

3.1 anteroposterior centreline
line which passes through the centre of the tibial tray, parallel to the sagittal plane and perpendicular to the axis of load application.

3.2 contact point
centroid of the femorotibial contact area for a given pair of femoral/tibial components.

3.3 mediolateral centreline
line which passes through the centre of the tibial tray, parallel to the coronal, or frontal, plane and perpendicular to the axis of load application.

3.4 moment arm, 'd_{ml}'
perpendicular distance between the anteroposterior centreline of the tibial component and the axis of load application.

3.5 moment arm, 'd_{ap}'
perpendicular distance between the mediolateral centreline of the tibial component and the axis of load application.

3.6 radii intersection point
intersection of the AP radius and the ML radius on the tibial plateau for biconcave tibial designs.

4 Principle

The test specimen is placed in a test rig and fixed so that it is mounted as a cantilever beam. A cyclic load is applied through an ultra high molecular weight polyethylene (UHMWPE) spacer on the unsupported condyle perpendicular to the undeflected superior surface of the tibial tray. The cyclic load is applied until the test specimen exhibits failure or until the chosen number of cycles has been attained. The specimen is examined subsequently for defects caused by the loading regime.

5 Apparatus

5.1 Testing machine, with the following characteristics:

a) a sinusodial dynamic loading waveform;

b) an error in applied load not greater than ± 2 % at the maximum load (see ISO 7500-1 and ISO 4965;

c) instrumentation to monitor the values of the maximum and minimum loads on the tibial tray test specimen to an accuracy of ± 2 %;

d) instrumentation to record the number of cycles.

5.2 Means of fixing the test specimen, to allow:

a) the test specimen to be held as a cantilever beam;

b) fixing the inferior surface or clamping the superior surface of the unsupported test specimen tray away from the mid line, to reduce the stress concentration at the centre line;

c) the tibial tray to be supported up to the center line (see figures 1 and 2). NOTE If the tray includes a central stem or other prominence these may be supported in the same manner.

d) the load axis to be perpendicular to the undeflected superior surface of the test specimen.

5.3 Ultra-high molecular-weight polyethylene spacer to be placed between the test specimen and the load applicator to distribute the loading and reduce fretting. The grade in accordance with ISO 5834-2. The spacer dimensions are 13 mm ± 0,5 mm diameter and 6 mm ± 0,5 mm thickness.

NOTE The spacer should be replaced if its thickness is reduced to 3 mm or if it fragments.

The spacer diameter and/or shape may be modified to accommodate the tibial tray design being tested but any deviations from the specified dimensions shall be included in the test report.

5.4 Means of transmitting the load, an indentor with a spherical end, diameter 32 mm ± 1 mm. It is recommended that the indentor be manufactured from a steel or cobalt-chrome alloy.

6 Procedure

6.1 Determine the overall ML and AP dimensions in accordance with ISO 7207-1, figures 2 and 3.

6.2 Fix the test specimen in the test rig in accordance with 5.2 (c) If asymmetrical ensure the test specimen is fixed so that the bending moment is a maximum at the junction of the tray with the stem, or at the division between the medial and lateral compartments if no stem is present. Ensure the level of fixation under the loaded compartment is at least 5 mm below the bottom surface of the tibial tray and does not contact any part of the loaded side of the tray during testing.

6.3 Position the test specimen so that the load axis is perpendicular to the undeflected superior surface of the tray since the tray surface will not remain perpendicular to the load axis during loading.

NOTE 1 The point of load application will be located at a distance from moment arm of the anteroposterior centre line d_{ml}, and from the moment arm of the mediolateral centre line d_{ap}, in a manner similar to where it is expected to be loaded *in vivo* at 0° flexion.

Use one of the following methods to determine the loading point.

a) **For femoral/tibial components**, for the contact point at 0° flexion corresponding to the ML and AP location on the tibial tray use the loading point.

NOTE 2 The contact point may be determined using pressure-sensitive film, removable dye, etc.

b) **For biconcave tibial designs**, for the radii intersection point corresponding to the ML and AP location on the tibial tray use the loading point.

NOTE 3 The radii intersection point is a natural position in which the femoral component sits on the tibial plateau.

6.4 Place the spacer (5.3) between the test specimen and the load applicator (figures 1 or 2).

6.5 Start the testing machine and adjust it so that it applies the maximum load F_{max}, using the spherical indentor (5.4), with an R_{value} of 10, at a frequency not greater than 10 Hz ± 0,1 Hz.

NOTE 1 R_{value} is the ratio of the maximum load F_{max} to the minimum load F_{min}.

NOTE 2 The value of F_{max} is given by the party that submitted the specimen for testing.

6.6 Continue the test until one of the following occurs:

a) fracture of the tray;

b) cracks are observed when the tray is inspected under normal or corrected vision;

c) 5×10^6 cycles test duration is achieved;

d) the test machine fails to maintain the specified load range (5.1 b).

6.7 At the end of the test:

a) record the number of cycles of loading when the test was terminated; and

b) examine the test specimens using the methods requested by the party that submitted the specimen for testing.

7 Test report

The test report shall include the following information:

a) a reference to this part of ISO 14879;

b) the identity of the test specimens, as stated by the party submitting the specimen for test, including tibial tray thickness, size, d and w defined in ISO 7207-1, and materials of construction.

c) details of the test conditions, including spacer diameter and thickness (including any deviations in diameter or shape), d_{rd}, d_{ap}, fixation method, frequency, and maximum load.

d) a statement of results including number of cycles applied and location of fracture (if fractured), description of test specimens at the end of the test, and the results of examination requested by the party submitting the specimen for test.

8 Disposal of test specimens

Test prostheses shall not be used for clinical purposes after testing. Care should be exercised in the use of the specimens for further mechanical test, because the loading regime may have altered the mechanical properties.

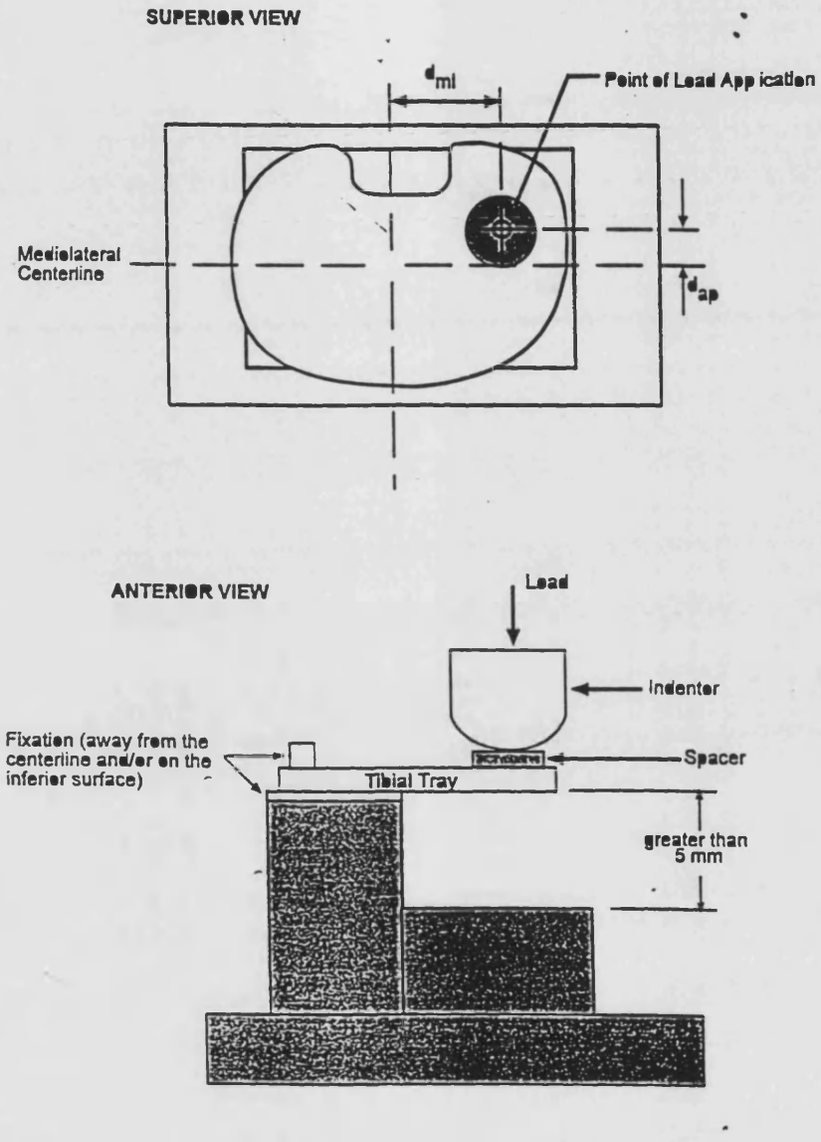

Figure 1 – Schematic diagram of the test set-up for tibial trays without a central stem

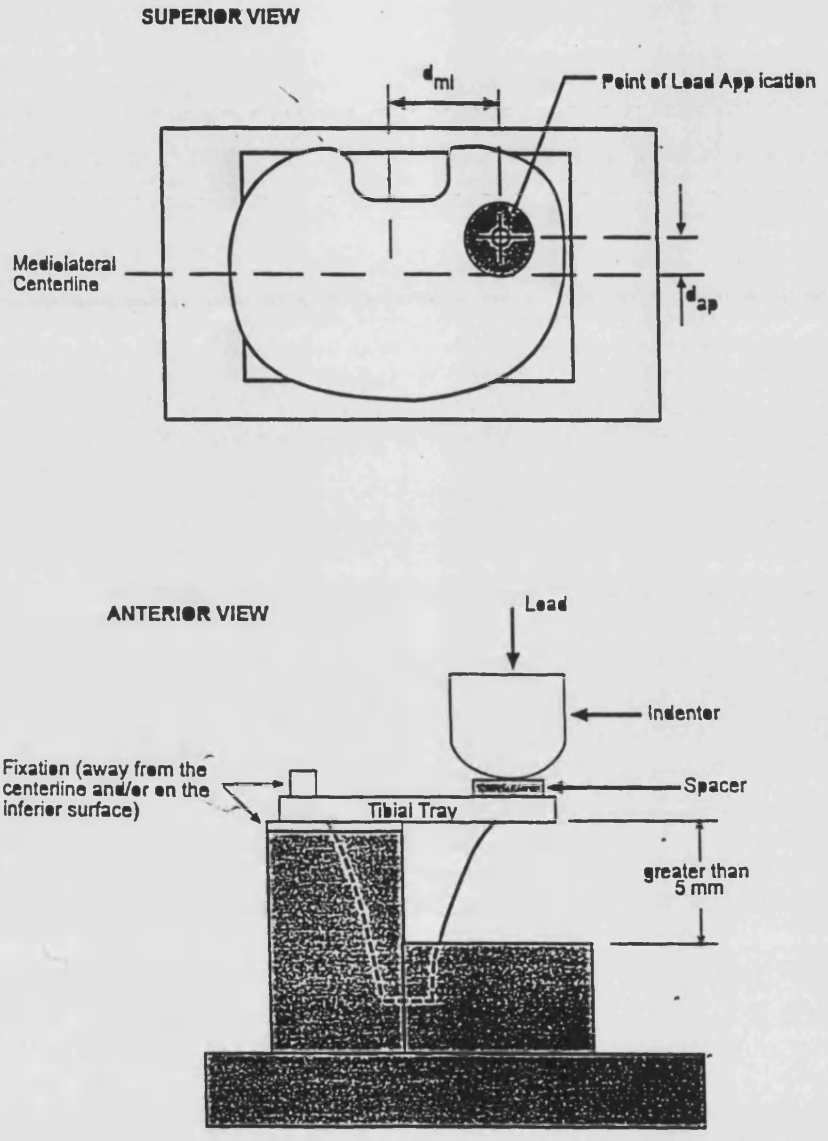

Figure 2 – Schematic diagram of the test set-up for tibial trays with a central stem.

Appendix B1:
INVESTIGATION OF THE EFFECT OF CEMENT

B1.1 INTRODUCTION

The aim of this study was to investigate the effect of the cement layer on tibial trays. Under test conditions the tray is supported using a layer of acrylic cement. This study examined four components: the AGC, the Kinemax, the IB2, the Kinematic.

B1.2 MATERIALS AND METHOD

Solid models of each design were created in Unigraphics (EDS, USA) with a layer of support on one half of the component. These models were then translated into iges format and incorporated into MARC (MSC software, USA). Surface meshes of the metallic component were modeled first. This was then used to form the surface mesh of the cement layer. Then meshes were generated automatically using lower order tetrahedral elements. The individual meshes of the implant and cement were then merged. This enabled the material properties of the cement and implant to be allocated correctly. The combined mesh was then converted to a higher order tetrahedral mesh. A number of mesh sizes were modelled until the maximum the computer could solve was achieved. The final mesh sizes are shown in Table B1.1. The final mesh sizes are shown in Figures B1.1 - 1.4 (a and b).

B1.3 RESULTS

Table B1.2 shows the differences between the implant only models and the implants with a layer of cement. Figures B1.5-1.8 (a and b) show pictorially the stress distribution in each implant with and without a layer of cement. The results show that the stress distribution with and without cement are essentially the same.

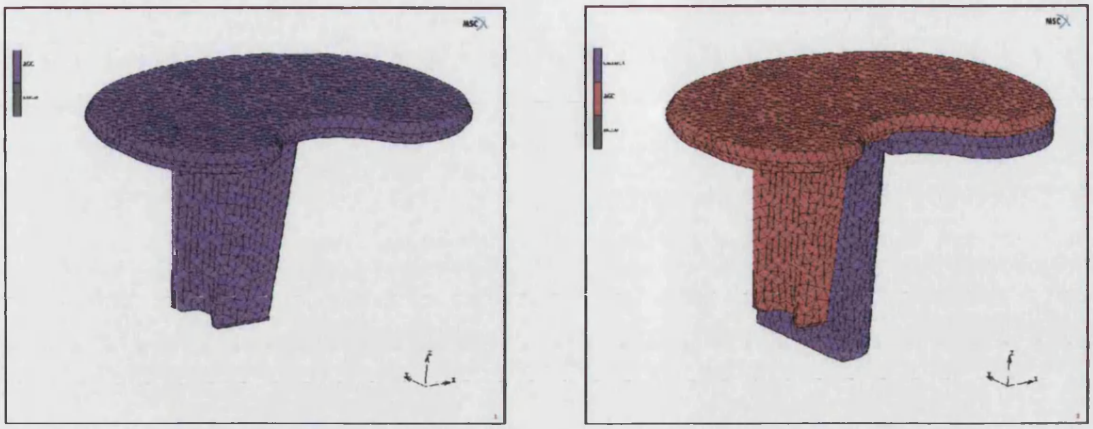

(a) (b)

Figure B1.1 Mesh of the (a) AGC (b) AGC and cement

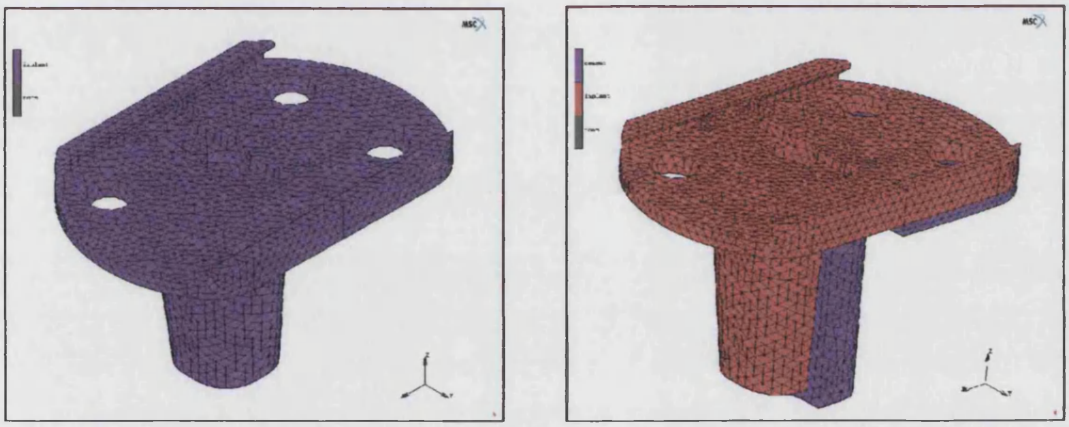

(a) (b)

B1.2 Mesh of the (a) IB2 (b) IB2 with cement

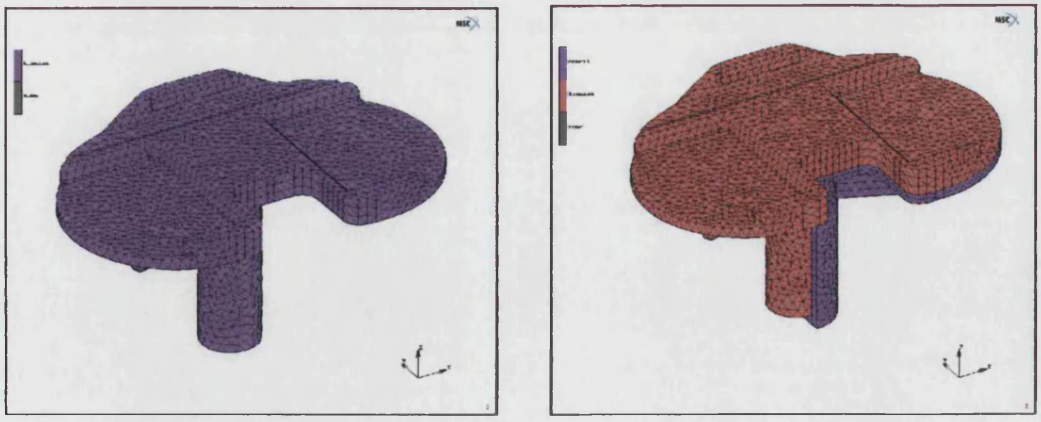

(a) (b)

B1.3 Mesh of the (a) Kinemax (b) Kinemax with cement

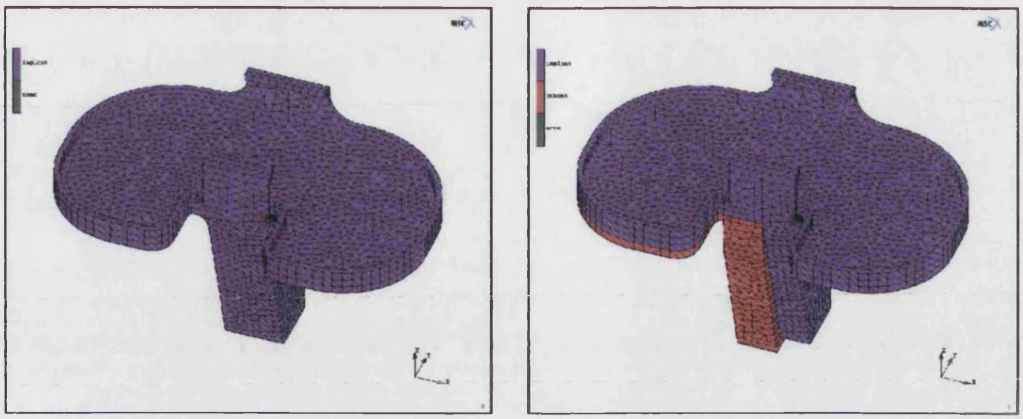

(a) (b)

B1.4 Mesh of the (a) Kinematic (b) Kinematic with cement

	Implant	Only	Cement	Layer
	Elements	Nodes	Elements	Nodes
Kinemax	30925	48573	10126	17792
IB2	34967	55566	12313	21119
AGC	26578	42319	19319	25914
Kinematic	26562	43511	9804	17167

Table B1.1: Final mesh sizes for the four components with and without cement layer.

	Peak	Stress (MPa)
	Implant only	Implant with Cement layer
AGC	910.6	926.8
IB2	947.1	943.6
Kinemax	999.0	1003.0
Kinematic	4062	4088

Table B1.2: Comparison of the peak stress with out and with a cement layer in four tibial tray designs

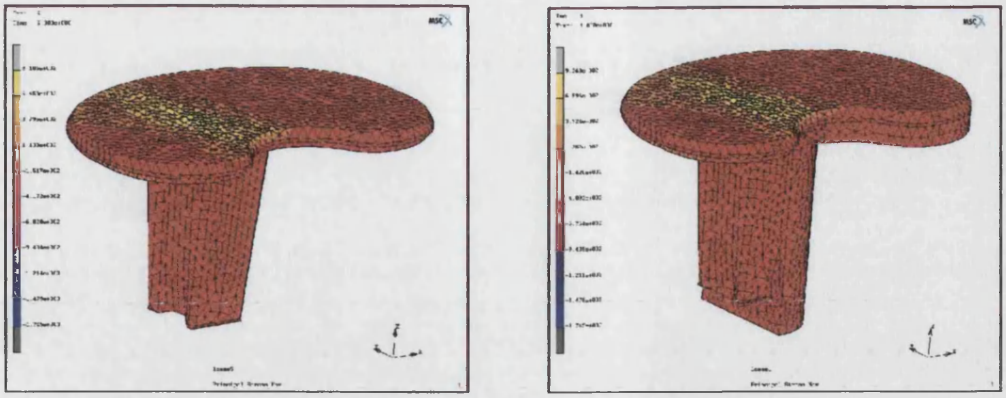

(a) (b)

Figure B1.5 Results showing the stress distribution in the (a) AGC (b) AGC with cement

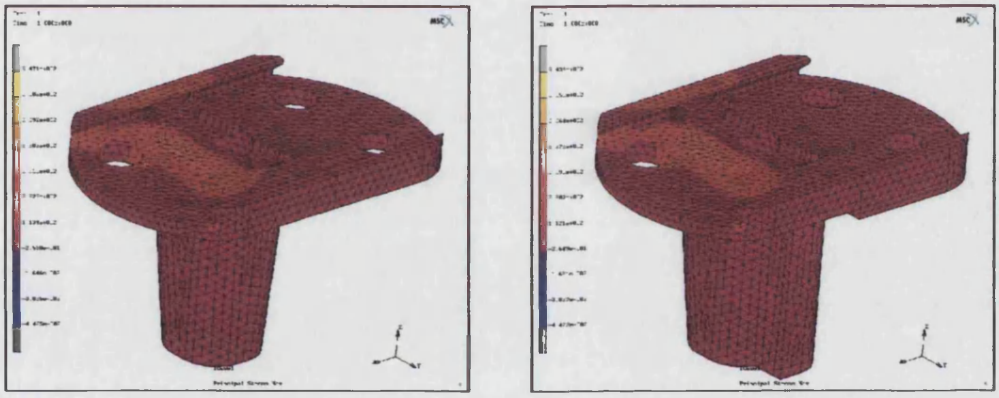

(a) (b)

Figure B1.6 Results showing the stress distribution in the (a) IB2 (b) IB2 with cement

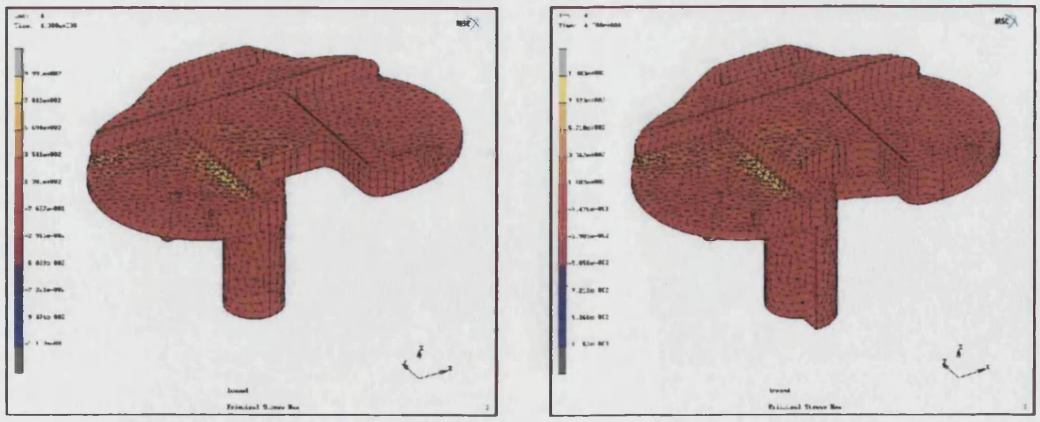

(a) (b)

Figure B1.7 Results showing the stress distribution in the (a) Kinemax (b) Kinemax with cement

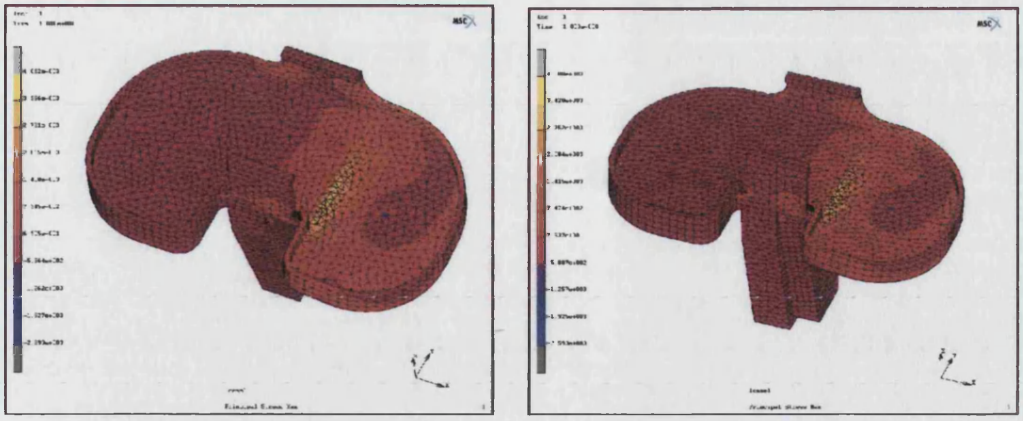

(a) (b)

Figure B1.8 Results showing the stress distribution in the (a) Kinematic (b) Kinematic with cement

B1.4 DISCUSSION

The results show that the differences between each implant with and without a layer of cement is small. Therefore the results that were represented in chapter 4 (though modelled without a layer of cement) can be considered as accurate and that the cement layer has very little effect on the stresses in the implant for the ISO test conditions. Primarily this is because the cement layer is on the unsupported side of the tray which is largely unstressed.

Appendix B2:
THE FIRST CONTACT POSITION

B2.1 INTRODUCTION

Study one examined the difference in results for two trays designs using the first and second contact points. The aim of this study is to determine the load level that can be used for the first contact point for a number of tray designs.

B2.2 MATERIALS AND METHOD

B2.2.1 Finite Element Analysis

Models that were previously created for studies in chapter 4 were used again for this study. The trays selected were the Kinematic, MG2, MBK and AGC. The FEA models were identical to those described in 4.4.1.1 except that the contact position was changed to that defined in the draft standard defined in 1996 (appendix A1 and figure 2.2.7). The FEA was used to find the load for which the Kinematic, MG2 and AGC failed using the position defined in the 1996 draft standard. The FEA study was used to find the load at which the MBK survived using the position defined in the 1996 draft standard.

B2.2.2 Mechanical Testing

Two samples of each component were set-up according to the ISO test procedure. One half of the component was rigidly held with specifically made fixtures and using acrylic cement. A gap of at least five millimetres separated the base of the fixture and the undersurface of the tray being tested. The fixed part of the component was then clamped. A maximum cyclic load was then applied at 5Hz through a polyethylene spacer in a multi-channel pneumatically loaded fatigue testing machine until crack formation, or 5 million cycles was achieved (refer to figure 4.3.3). The Kinematic was subjected to a maximum compressive load of 500N. The MG2 was subjected to a maximum compressive load of 900N. The MBK was subjected to a maximum compressive load of 1400N. The AGC was subjected to a maximum compressive load of 2000N.

B2.3 RESULTS

The results are represented pictorially in figures B2.1-2.4. The finite element results show that the AGC failed at a load level of 2000N for the first contact point. This prediction was validated by mechanical testing. The MBK was able to survive a load of 1400N and this was also validated by mechanical testing. The MG2 failed using a load level of 900N for the FEA and mechanical testing. FEA using a load level of 500N showed that the tray may survive using this load level. However, there were no samples available to validate this result. Using a load level of 500N the Kinematic failed for the FEA and mechanical testing.

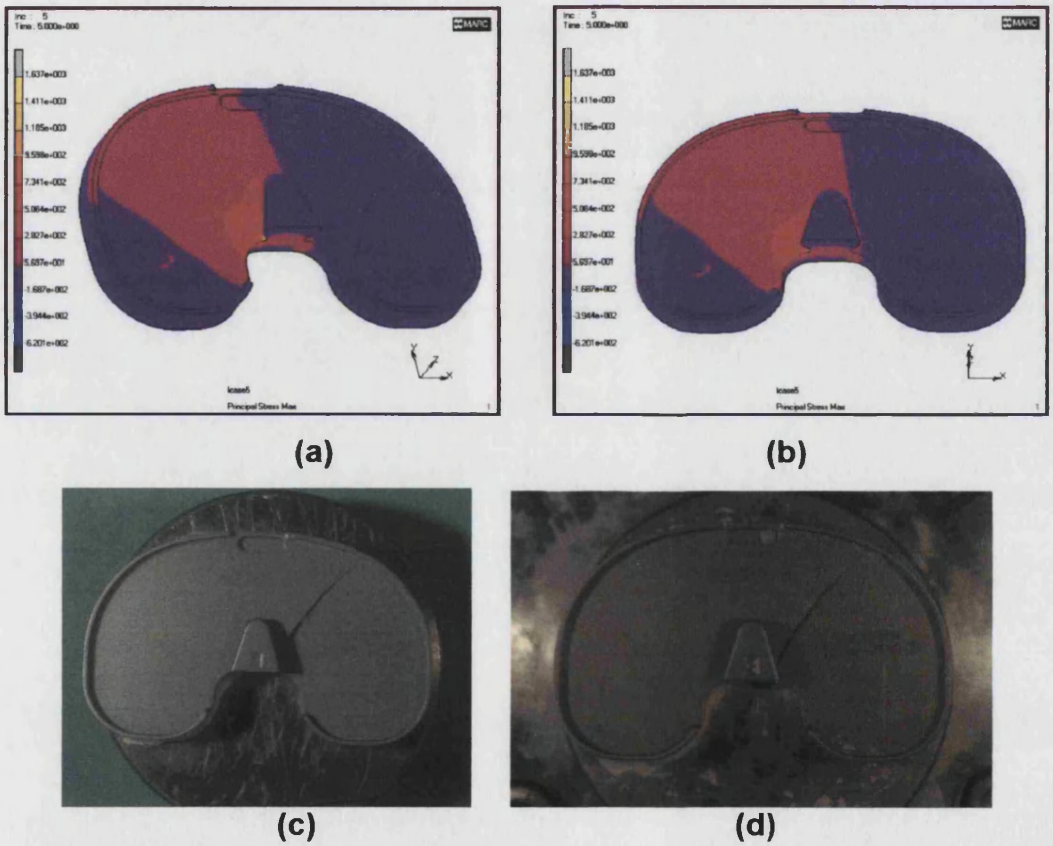

Figure B2.1: (a-b) FEA of the MG2 under the ISO test conditions at 900N. (c-d) Failure of two samples of the MG2 at 900N.

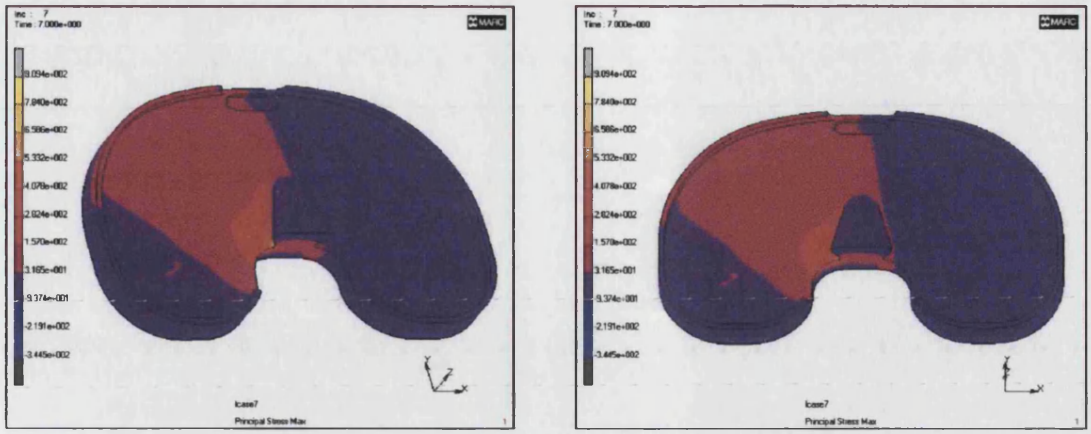

(e) (f)

Figure B2.1 (e-f): FEA of the MG2 under the ISO test conditions at 500N showing stress values above the fatigue limit.

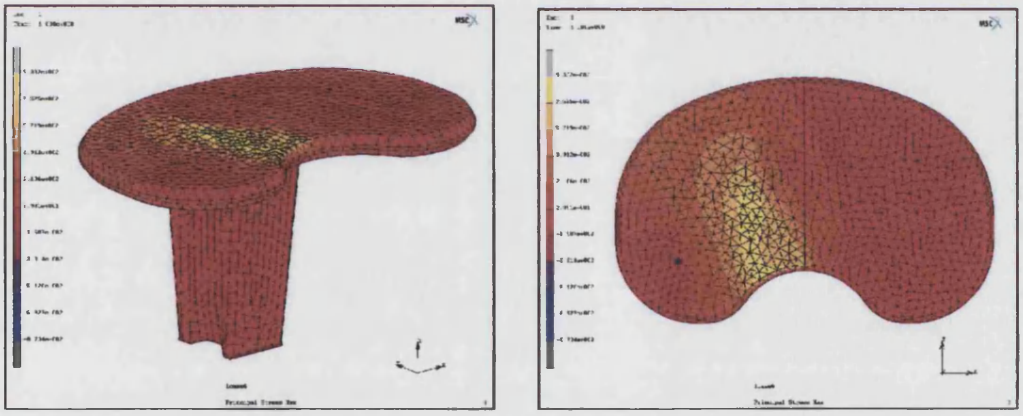

(a) (b)

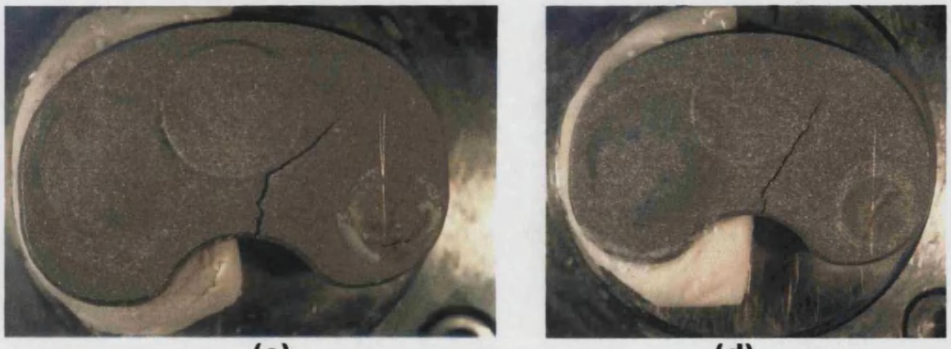

(c) (d)

Figure B2.2 (a & b): FEA results of the AGC (c & d) Mechanical test results showing failure at 2000N for two samples.

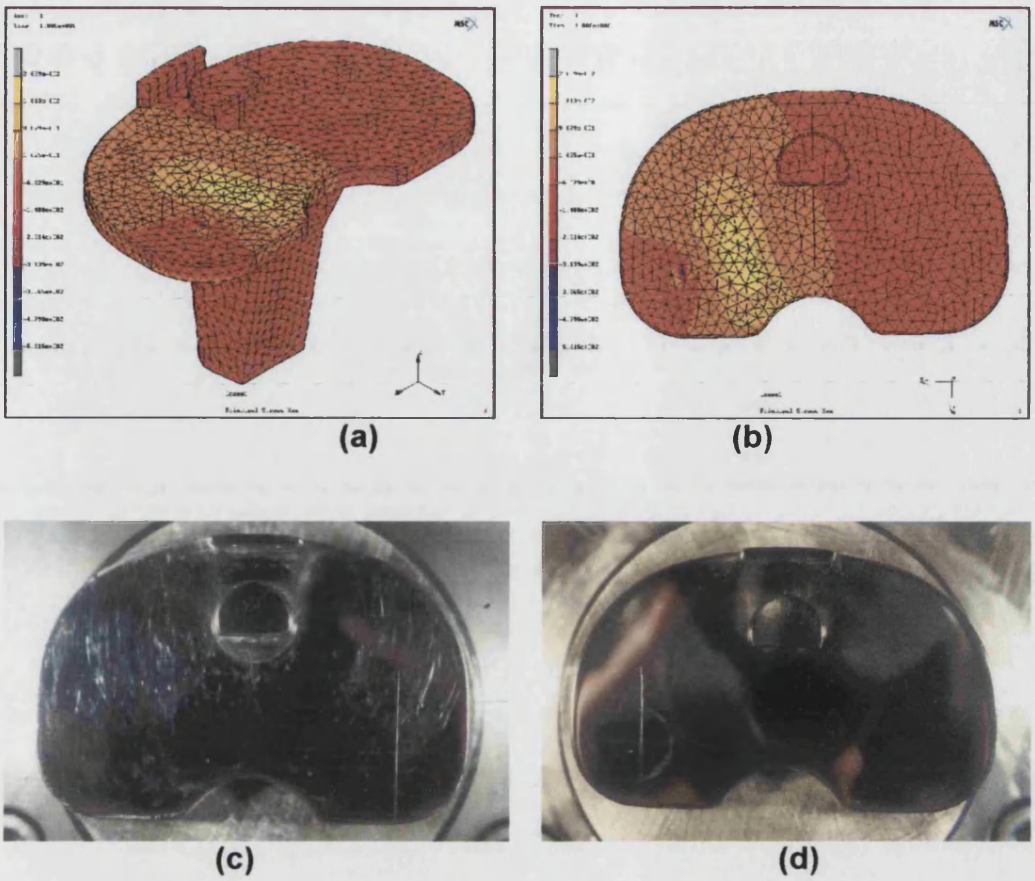

Figure B2.3: (a & b) FEA results of the Kinematic (c & d) Mechanical test results showing survival at 1400N for two samples to five million cycles.

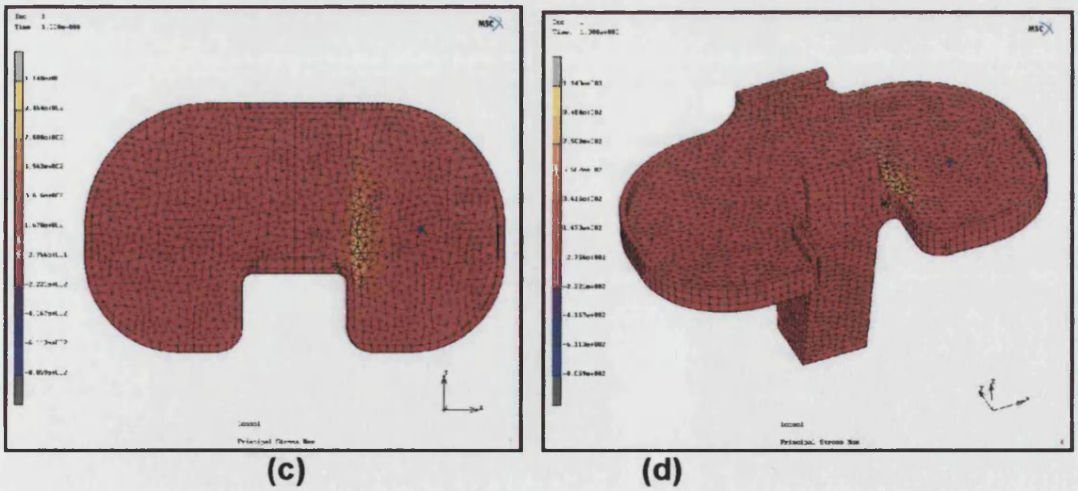

Figure B2.4: (a and b) FEA results of the Kinematic

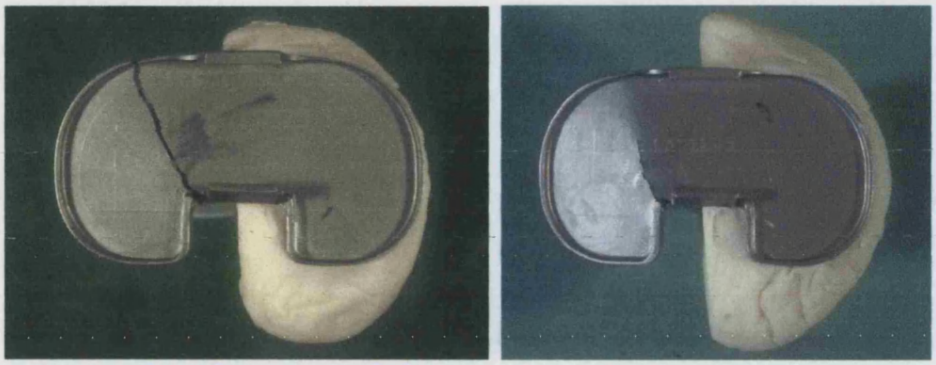

(c) (d)

Figure B2.4:(c and d) Mechanical test results showing failure at 500N for two samples.

B2.4 DISCUSSION

The conclusion of this study is that 900N would be too severe a load level for the first contact point defined in the 1996 draft standard. A lower load level of 500N may be suitable but this would require further validation using mechanical testing.

APPENDIX C:
RETRIEVED TIBIAL TRAYS

APPENDIX C1.0: RETRIEVED KINEMATIC COMPONENTS

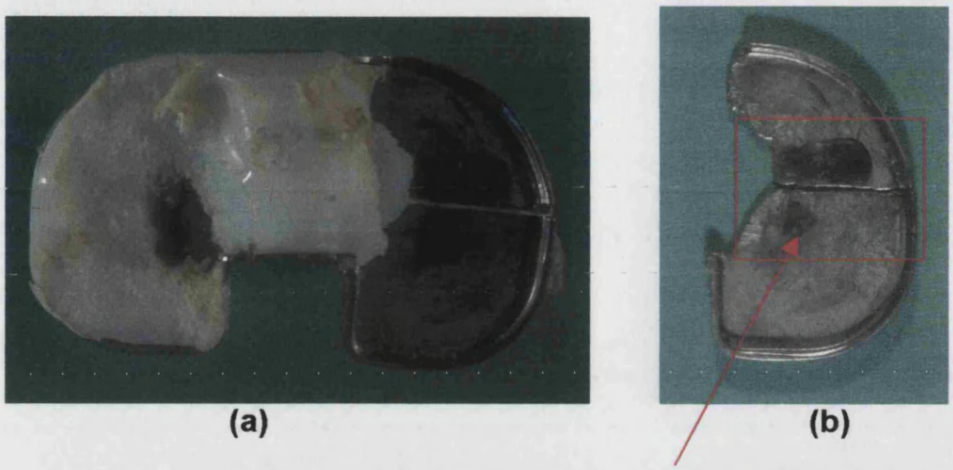

Figure C1.1: COMPONENT C: A retrieved Kinematic in a left knee showing medial compartment failure at 6 years and 6 months

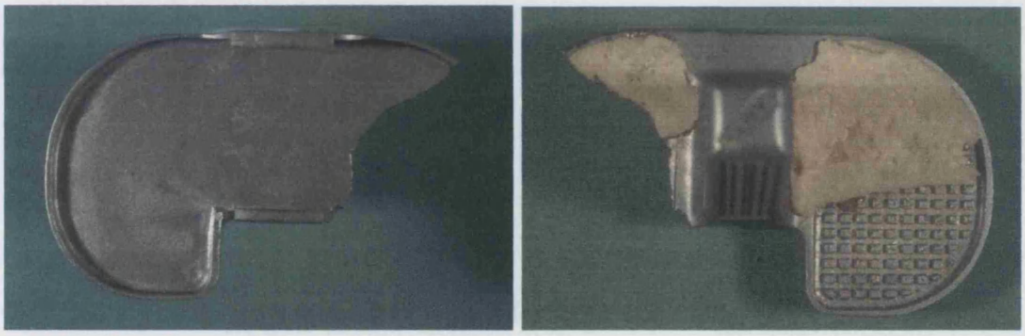

Figure C1.2: COMPONENT D: Failure of a Kinematic knee in the medial compartment of a left knee at 5 years 2 months.

(a) (b)

(c) (d)

shiny surface on rim of fractured piece

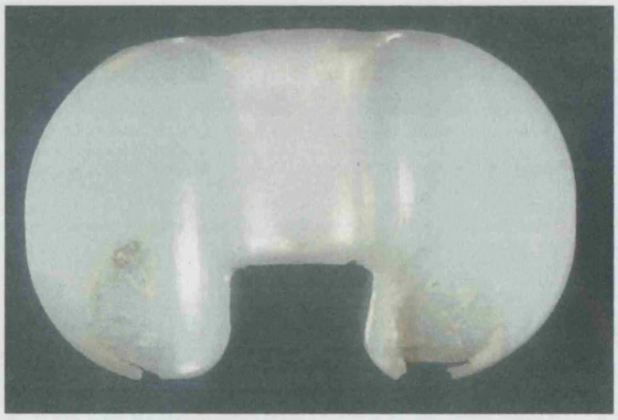

(e)

Figure C1.3: COMPONENT E: Failure of a Kinematic knee in one of the compartments as a result of polyethylene wear and malalignment. Fractured tibial tray (a) top view (b) from below (c) tibial baseplate (d) fractured portion showing shiny surface (e) tibial insert with wear more marked in same location as fracture of the baseplate.

(a) (b)

Figure C1.4 (a & b): COMPONENT F: Medial compartment fracture of a Kinematic tibial tray of a right knee in a patient two years post-operatively.

(a) (b)

Figure C1.5 (a & b): COMPONENT G: No records were available for this fractured Kinematic tibial tray

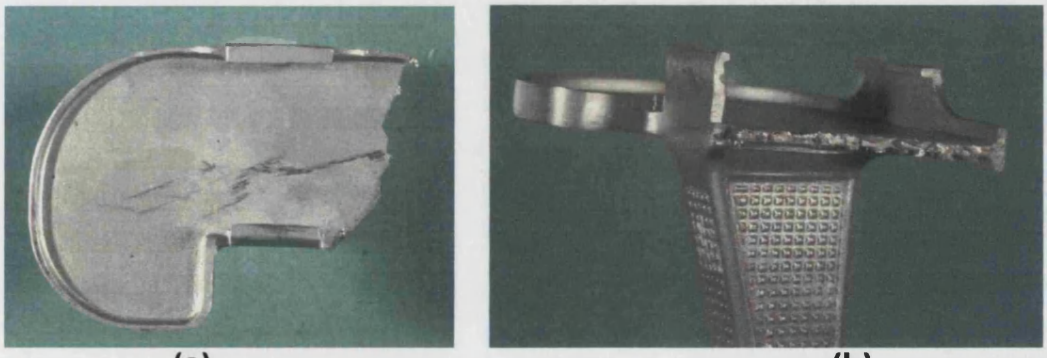

(a) (b)

Figure C1.6 (a & b): COMPONENT H: Medial compartment failure in a left knee for a Kinematic tray. The tray was retrieved at 13 years.

(a) (b)

Figure C1.7 (a & b): COMPONENT I: Lateral compartment fracture of a Kinematic tibial tray for the right knee of a male patient. The tray was retrieved 4 years after implantation.

Figure C1.8: COMPONENT J: No records were available for this tray.

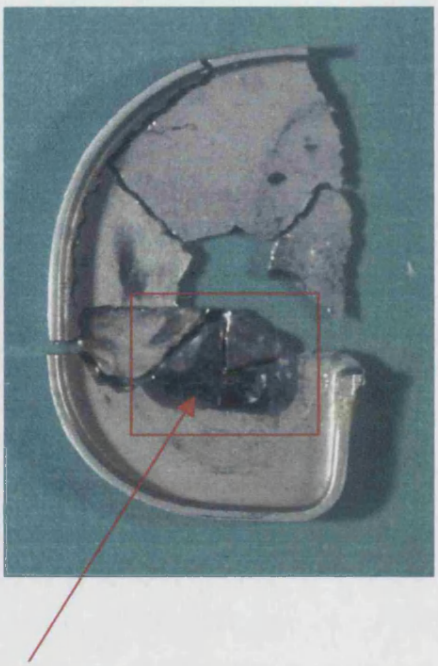

Shiny surface on upper part of fractured portion of tray

Figure C1.9: COMPONENT K: No records were available for this tray.

APPENDIX C2.0: RETRIEVED TOTAL CONDYLAR COMPONENTS

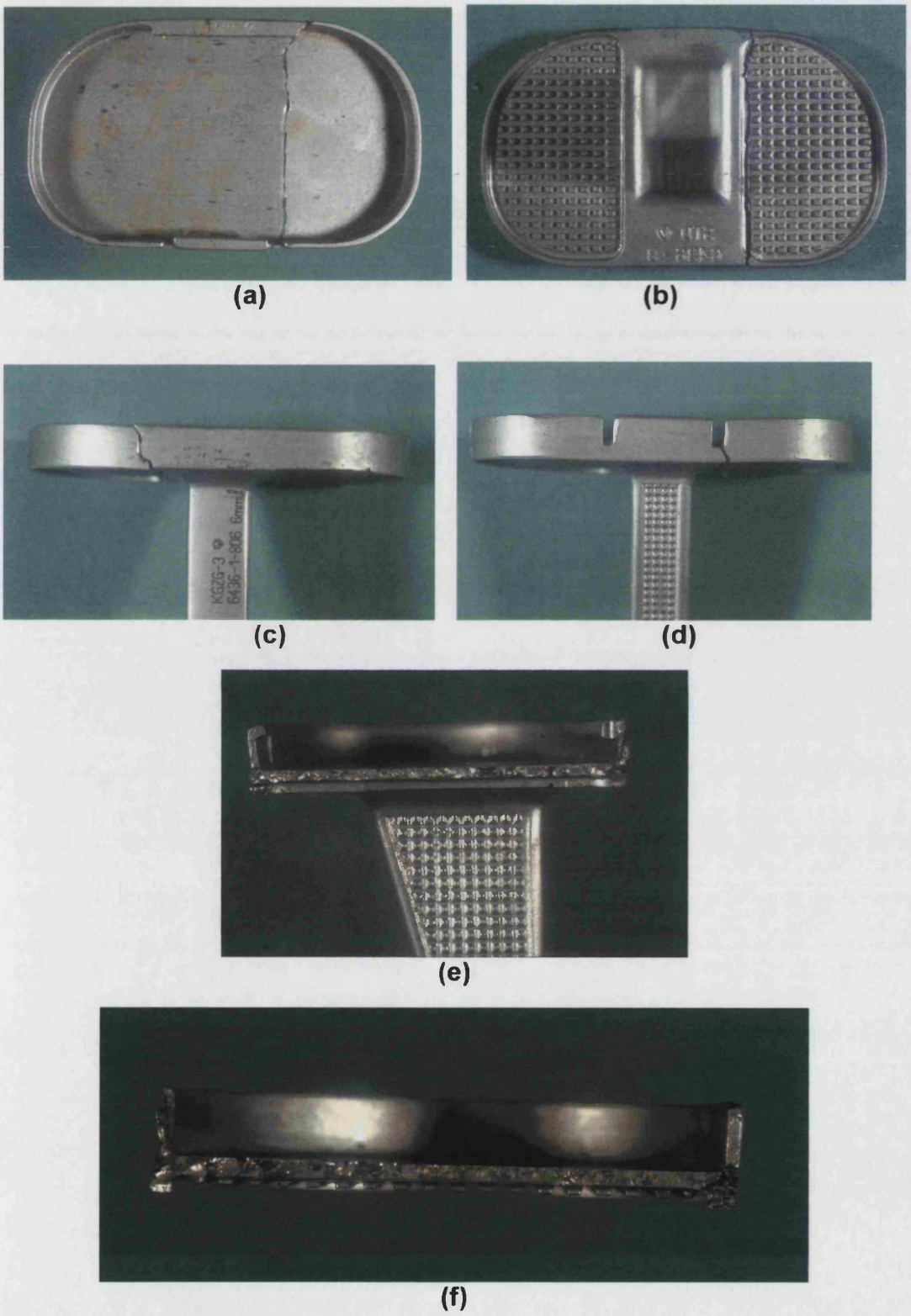

(a) (b) (c) (d) (e) (f)

Figure C2.1: COMPONENT M: (a-f): No records were available for fracture of this Total Condylar design.

(a)

(b)

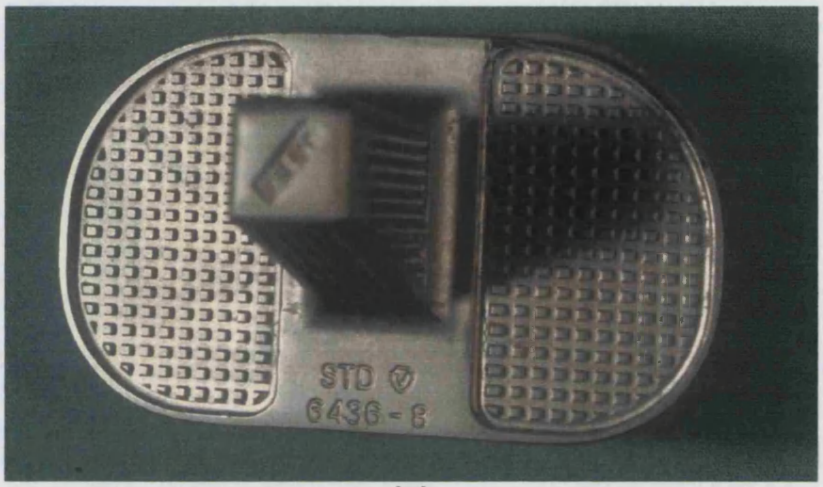

(c)

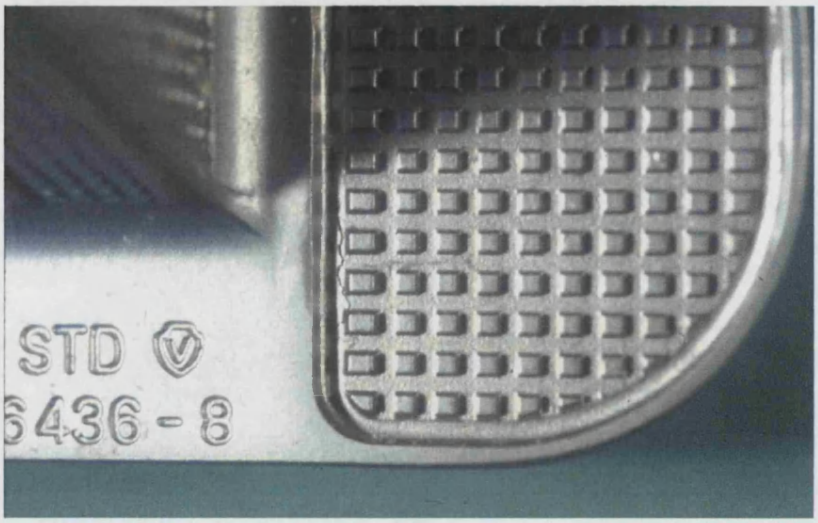

(d)

Figure C2.2: COMPONENT N(a-d): Fracture of a Total Condylar design. The fracture began at the anterior side at one of the grooves within the design. The tray was removed prior to the fracture reaching the other side of the tray.

APPENDIX C3.0: RETRIEVED PCA COMPONENT

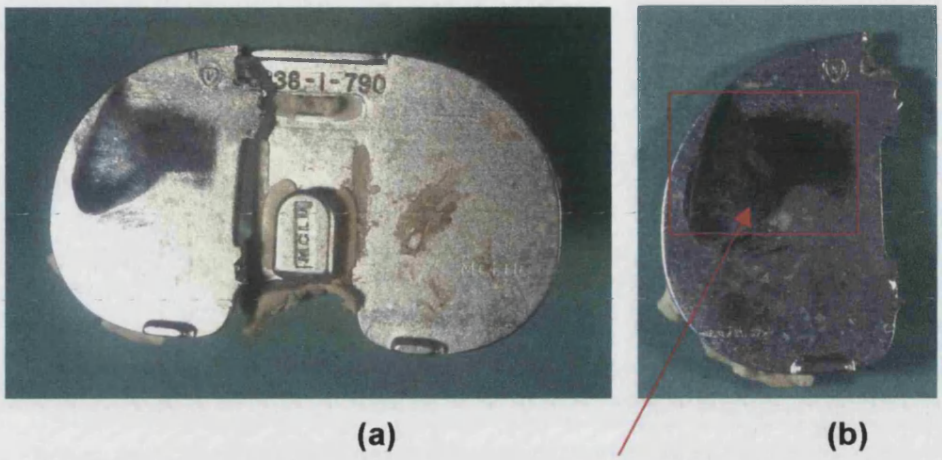

Figure C3.1 COMPONENT 0: (a –b): Fracture of a PCA tray design. (c-d): The fracture surfaces of both parts of the tray (e-f): close up views of (c).

REFERENCES

Abernethy PJ, Robinson CM, Fowler RM. Fracture of the metal tibial tray after Kinematic total knee replacement. *J Bone Joint Surg:* 78B(2):220-225 (1996)

Abraham W, Buchanan JR, Daubert H, Greer RB. Should the patella be resurfaced in total knee arthroplasty? Efficacy of patellar resurfacing. *Clin Orthop:* 236:128-34 (1988)

Ahir SP, Blunn GW, Haider H, Walker PS. Evaluation of a testing method for the fatigue performance of total knee tibial trays. Journal of Biomechanics 32: 1049-1057 (1999)

Albrektsson BJ, Ryd L, Carlsson LV, Freeman MAR, Herberts P, Regner L, Selvik G. The effect of a stem on the tibial component of knee arthroplasty. *J Bone Joint Surg:* 72B(2):252-257 (1990)

Altintas F, Sener N, Ugutmen E. Fracture of the tibial tray after total knee arthroplasty. *J Arthroplasty*: 14(1):112-114 (1999)

Argenson J, O'Connor JJ. Polyethylene wear in meniscal knee replacement: a one to nine year retrieval analysis of the Oxford knee. *J Bone Joint Surg:* 74B(2):228-32 (1992)

Askew MJ, Lewis JL. Analysis of model variables and fixation post length effects on stresses around a prosthesis in the proximal tibia. *J Biomech Eng.* 103:239-245 (1981)

Ashman RB, Rho JY, Turner CH. Anatomical variation of orthotropic elastic moduli of the proximal human tibia. *J Biomech*: 22: 895-900 (1989)

Baldwin JL, El-Saied MRA, Rubinstein RA. Uncemented total knee arthroplasty: report of 109 titanium knees with cancellous–structured porous coating. *Orthopaedics:* 19(2):123-129 (1996)

Bardos DI. Titanium and titanium alloys. In: *Concise Encyclopaedia of Materials & Dental Materials*, Williams D (ed). Pergamon Press Oxford 360-365 (1990)

Bargren JH, Day WH, Freeman MAR, Swanson SAV. Mechanical tests on the tibial components of non-hinged knee prosthesis. *J Bone Joint Surg:* 60B(2):256-261 (1978)

Bargren JH, Blaha JD, Freeman MAR. Alignment in total knee arthroplasty: correlated biomechanical and clinical observation. *Clin Orthop:* 173:178-183 (1983)

Bartel DL, Burstein AH, Santavicca EA, Insall JN. Performance of the tibial component in total knee replacement. *J Bone Joint Surg:* 64B(7):1026-33 (1982)

Bartel DL, Bicknell VL, Wright TM. The effect of conformity, thickness and material on stresses in Ultra High Molecular Weight components for total joint replacements. *J Bone Joint Surg:* 68A(7):1041-1051 (1986)

Bauer TW, Saltarelli M, McMahon JT, Wilde AH. Regional dissemination of wear debris from a total knee prosthesis. *J Bone Joint Surg:* 75A(1):106-111 (1993)

Beaupre GS, Vasu R, Carter DR, Schurman DJ. Epiphyseal-based designs for tibial plateau components II.stress analysis in the sagittal plane. J Biomech 19(8): 663-673 (1986)

Bell CJ. Variability, oxidation resistance and wear of 'medical grade' ultra-high molecular weight polyethylene. University College London, PhD Thesis (1999)

Berry DJ, Rand JA. Isolated patellar component revision of total knee arthroplasty. *Clin Orthop*: 286:110-115 (1993)

Bindeglass DF, Chen JL, Dorr LD. Patellar tilt and subluxation in total knee arthroplasty: relationship to pain, fixation and design. *Clin Orthop:* 286:103-109 (1993)

Bloebaum RD, Rhodes DM, Rubman MH, Hofmann AA. Bilateral tibial components of different cementless designs and materials: microradiographic, backscattered imaging, and histologic analysis. *Clin Orthop:* 268:179-187 (1991)

Bloebaum RD, Rubman MH, Hofmann AA. Bone ingrowth into porous-coated tibial components implanted with autograft bone chips: analysis of ten consecutively retrieved implants. *J Arthroplasty:* 7(4):483-493 (1992)

Blunn GW, Joshi AB, Minns RJ, Lidgren L, Lilley P, Ryd L, Englebrecht E, Walker PS. Wear in retrieved condylar knee arthroplasties: a comparison of wear in different designs of 280 retrieved condylar knee prosthesis. *J Arthroplasty:* 12(3): 281-290 (1997)

Bourgeault ST, Charaeancholvanich C, Lew K, Bechtold W, Gustilo RB. Does a central stem affect bone strain and the stability of a cemented tibial tray in primary and revision TKA? *Trans Orthop Res Soc*, 635 (1997)

Brach del Prever E, MacPherson IS, Freeman MAR, Samuelson KM. Clinical experience with the Freeman-Samuelson knee arthroplasty. *Italian J Orthop Traum:* 13(4):411-424 (1987)

Brand MG, Daley RJ, Ewald FC, Scott RD. Tibial tray augmentation with modular metal wedges for tibial bone stock deficiency. *Clin Orthop:* 248:71-79 (1989)

Brooks PJ, Walker PS, Scott RD. Tibial component fixation in deficient tibial bone stock. *Clin Orthop:* 184:302-308 (1984)

Brown M, Gregson PJ. Accelerated fatigue testing of knee tibial trays. *DTI CAM 2 Final Technical Report, Unpublished* (2001)

Bryan RS, Rand JA. Revision total knee arthroplasty. *Clin Orthop:* 170:116-122 (1982)

Buechel FF. LCS mobile bearing knee replacement: 20 year experience. *Trans 11th Annual Symposium International Soc Tech Arthroplasty (ISTA),* 106 (1998)

Buechel FF, Pappas MJ. The New Jersey Low Contact Stress knee replacement system: biomechanical rationale and review of the first 123 cemented cases. *Arch Orthop Trauma Surg:* 105:197-204 (1986)

Cadambi A, Engh GA, Dwyer KA, Vinh TN. Osteolysis of the distal femur after total knee arthroplasty. *J Arthroplasty:* 9(6):579-594 (1994)

Callaghan JJ, Dysart SH, Savory CG. The uncemented porous-coated anatomic total hip prosthesis: two year results of a prospective consecutive series. *J Bone Joint Surg:* 70A(3):337-346 (1988)

Callaghan JJ, Dennis DA. Orthopaedic knowledge update: hip and knee reconstruction. *AAOS,* 269-276 (1995)

Cameron HU, Hunter GA. Failure in total knee arthroplasty: mechanisms, revisions and results. *Clin Orthop:* 170:141-146 (1982)

Carr A, Keyes G, Miller R, O'Connor JJ, Goodfellow J. Medial unicompartmental arthroplasty. A survival study of the Oxford meniscal knee. *Clin Orthop:* 295:205-213 (1993)

Cates HE, Ritter MA, Keating EM, Faris PM. Intramedullary versus extramedullary femoral alignment systems in total knee replacement. *Clin Orthop:* 286:32-39 (1993)

Cheal EJ, Hayes WC, Lee CH, Snyder BD, Miller J. Stress analysis of a condylar knee tibial component: influence of metaphyseal shell properties and cement injection depth. *J Orthop Res*: 3(4): 424-434 (1985)

Chen F, Krackow KA. Management of tibial defects in total knee arthroplasty. *Clin Orthop:* 305:249-257 (1994)

Cheng CL, Gross AE. Loosening of the porous coating in total knee replacement. *J Bone Joint Surg:* 70B(3):377-381 (1988)

Chillag KJ, Barth E. An analysis of polyethylene thickness in modular total knee components. *Clin Orthop:* 273:261-263 (1991)

Churchill DL, Incavo SJ, Jewell RP, Beynnon BD. A comparison of patellofemoral contact loads in the normal knee and total knee arthroplasty. *Trans Orthop Res Soc*, 652 (1997)

Clarke HD, Trousdale RT. Component fracture in total knee arthroplasty. *The Knee:* 6:261-267 (1999)

Collier JP, Sperling DK, Currier JH, Sutula LC, Saum KA, Mayor MB. Impact of gamma sterilization on clinical performance in the knee. *J Arthroplasty*: 11(4):377-389 (1996)

Cook SD, Thomas KA. Fatigue failure of noncemented porous-coated implants: a retrieval study. *J Bone Joint Surg:* 73B(1):20-25 (1991)

Cooke TDV, Chir B, Collins A, Wevers H. Failure of a knee prosthesis accelerated by shedding of beads from the porous metal surface. *Clin Orthop:* 258:204-208 (1990)

Cooper MB, Anthony ME, Salehi AB, Holbrook JA. Fatigue integrity test of a modular tibial stem extension. In: *Modularity of orthopaedic implants*, Marlowe DE, Parr JE, Mayor MB. American Society for Testing and Materials ASTM STP 1301, 137-145 (1997)

Dannenmeier WC, Haynes DW, Nelson CL. Granulomatous reaction and cystic bony destruction associated with high wear rate in a total knee prosthesis. *Clin Orthop:* 198:224-230 (1985)

Davis PF, Bocell JR, Tullos HS. Disassociation of the tibial component in total knee replacement. *Clin Orthop*: 272:199-204 (1991)

Dennis DA. Removal of well-fixed cementless metal-backed patella components. *J Arthroplasty:* 7(2):217-220 (1992)

Dennis DA. Primary knee replacement: isolated patellofemoral arthritis. *Orthopaedics:* 18(9):893-895 (1995)

DesJardins JD, Walker PS, Haider H, Perry J. The in vitro measurement of TKR and soft tissue shear reaction forces during gait. *Trans Orthop Res Soc*, 437 (2000)

DesJardins JD, Walker PS, Haider H, Perry J. The in vitro measurement of walking cycle kinematics for multiple TKR designs. *Trans Orthop Res Soc*, 430 (2000)

Dobbs HS, Robertson JLM. Heat treatment of cast CoCrMo for orthopaedic implant use. *J Mater Sci:* 18:391-401 (1983)

Doerr T, Eckhoff DG. Lateral patellar burnishing in total knee arthroplasty following medialisation of the patellar button. *J Arthroplasty:* 10(4):540-542 (1995)

Ducheyne P, Kagan A, Lacey JA. Failure of total knee arthroplasty due to loosening and deformation of the tibial component. *J Bone Joint Surg:* 60A(3):384-391 (1978)

Elloy MA, Manning MP, Johnson R. Accuracy of intramedullary alignment in total knee replacement. *J Biomed Eng: 14*:363-370 (1992)

Emmerson KP, Moran CG, Pinder IM. Survivorship analysis of the Kinematic stabiliser knee replacement: a 10 to 14 year follow-up. *J Bone Joint Surg:* 78B(3): 441-445 (1996)

Engel L, Klingele H. *An Atlas of Metal Damage.* Wolff Publishing Ltd. (1981)

Engh GA, Dwyer KA, Hanes, CK. Polyethylene wear of metal-backed tibial components in total and unicompartmental knee prosthesis. *J Bone Joint Surg:* 74B(1):9-17 (1992)

Engh GA, Parks ML, Ammeen DJ. Tibial osteolysis in cementless total knee arthroplasty: a review of 25 cases with and without tibial component revision. *Clin Orthop:* 309:33-43 (1994)

Engh GA, Loucini, S, Anand RR, Collier, MB. In vivo deterioration of tibial baseplate locking mechanisms in contemporary modular knee components. *J Bone Joint Surg*: 83A(11):1660-1665 (2001)

Escobedo J, Mendez J, Cortes D, Gomez J, Mendez M, Mancha H. Effect of nitrogen on the microstructure and mechanical properties of a CoCrMo alloy. *Mater Design*: 17(2):79-83 (1996)

Ezzet KA, Garcia R, Barrack RL. Effect of component fixation method on osteolysis in total knee arthroplasty. *Clin Orthop:* 321:86-91 (1995)

Fehring TK, Peindl RD, Humble RS, Harrow ME, Frick SL. Modular tibial augmentations in total knee arthroplasty. *Clin Orthop:* 327:207-217 (1996)

Feng EL, Stulberg SD, Wixson RL. Progressive subluxation and polyethylene wear in total knee replacements with flat articular surfaces. *Clin Orthop:* 299:60-71 (1994)

Figgie HE, Goldberg VM, Heiple KG, Moller HS, Gordon NH. The influence of tibial-patellofemoral location on function of the knee in patients with the posterior stabilized condylar knee prosthesis. *J Bone Joint Surg:* 68A(7):1035-1040 (1986)

Flivik G, Ljung P, Rydholm U. Fracture of the tibial tray of the PCA knee: a case report of early failure caused by improper design. *Acta Orthop Scand:* 61(1):26-28 (1990)

Furman BD, Furman GL, Li S. Effect of resin type on the oxidation of UHMWPE. *Fifth World Boimaterials Congress* II, 188 (1996)

Furman BD, Awad JN, Chastain KE, Li S. Material and performance differences between retrieved machined and molded Insall-Burstein type total knee arthroplasties. *Trans Orthop Res Soc*, 643 (1997a)

Furman, BD, Ritter, MA, Perone JB, Furman, GL, Li S. Effect of resin type and manufacturing method on UHMWPE oxidation and quality at long aging and implant times. *Trans Orthop Res Soc*, 92 (1997b)

Gabriel SA, Dennis DA. Back-side polyethylene wear in total knee replacement components: effects of metal-backing surface finish and relative motion. *Trans Europ Orthop Soc*, 109 (1997)

Garg A, Walker PS. The effect of the interface on the bone stresses beneath tibial components. *J Biomech* 19(12): 957-967 (1986)

Georgette FS, Davidson JA. The effect of HIPing on the fatigue and tensile strength of a cast, porous-coated CoCrMo alloy. *J Biomed Mater Res:* 20: 1229-1248 (1986)

Gerdes G, Gysler A, Lutjering G. *Fatigue crack threshold concepts.* Davidson DL, Suresh S (ed) American Society of Mechanical Engineers, 465-478 (1979)

Gilbert JL, Piehler HR. Grain egression: a new mechanism of fatigue-crack initiation in Ti6Al4V. *Metallurg Trans:* 20A: 1715-1725 (1989)

Gilbert JL, Piehler HR. Grain egression: a new mechanism of fatigue-crack initiation in Ti6Al4V. *Metallurg Trans:* 24: 669-680 (1993)

Goldstein SA, Wilson DI, Sonstegard DA, Matthews LS. The mechanical proerties of human tibial trabecular bone as a function of metaphyseal location. *J Biomech* 16(12): 965-969 (1983)

Goodfellow JW, O'Connor JJ. The mechanics of the knee and prosthesis design. *J Bone Joint Surg:* 60B(3):358-369 (1978)

Goodfellow JW, Kershaw CJ, Benson MK, O'Connor JJ. The Oxford knee for unicompartmental osteoarthritis: the first 103 cases. *J Bone Joint Surg:* 70B(5):692-701 (1988)

Grace JN, Rand JA. Patella instability after total knee arthroplasty. *Clin Orthop:* 237:184-189 (1988)

Gradisar IA, Hoffman ML, Askew MJ. Fracture of a fenestrated metal backing of a tibial knee component: a case report. *J Arthroplasty:* 4(1):27-30 (1988)

Grosskreutz, JC, Shaw GG. Fine subgrain structure adjacent to fatigue cracks. *Acta Metallurgica:* 20(4):523-528 (1972)

Haider H, Walker PS, Blunn GW, Bell CJ. The sensitivity of total knee replacement kinematics to misaligned installation. *Trans Orthop Res Soc*, 1097 (2001)

Hailey JL, Fisher J, Dowson D, Sampath SA, Johnson R, Elloy M. A tribological study of a series of retrieved Accord knee explants. *Med Engng Physics:* 16:223-228 (1994)

Hamelynck KJ. 15 years' experience with the Low Contact Stress (LCS) total knee prostheses in osteoarthritis and rheumatoid arthritis. *Proc International Conference on Knee Replacements 1974-2024*, Institution of Mechanical Engineers, UK, 30-33 (1999)

Harada Y, Wevers HW, Cooke TDV. Distribution of bone strength in the proximal tibia. *J Arthroplasty* 3(2): 167-175 (1988)

Harwin S. Patellofemoral complications in symmetrical total knee arthroplasty. *Proc International Conference on Knee Replacements 1974-2024*, Institution of Mechanical Engineers, UK, 37-46 (1999)

Hayes WC, Swenson LW, Schurman DJ. Axisymmetric finite element analysis of the lateral tibial plateau. *J Bomech*: 11:21-33 (1978)

Healy WL, Wasilewski SA, Takei R. Patellofemoral complications following total knee arthroplasty: correlation with implant design and patient risk factors. *J Arthroplasty:* 10(2):197-201 (1995)

Hearn EJ. *Mechanics of Materials*, Volume 1 Pergammon Press. (1985)

Hearn EJ. *Mechanics of Materials*, Volume 2 Pergammon Press. (1985)

Higgins RA. *Properties of Engineering Materials.* Edward Arnold (1977)

Hodgson K, Dwyer-Joyce RS, Drinkwater BW. Ultrasonic reflection to measure engineering contacts. *Mission of tribology research 8.* Proc Instn Mech Engrs, 1-5 (1999)

Hofmann AA, Bachus KN, Wyatt WB. Effect of the tibial cut on subsidence following total knee arthroplasty. *Clin Orthop:* 269:63-69 (1991)

Hofmann AA. The cementless alternative to total knee arthroplasty. *Orthopaedics:* 19(9):789-791 (1996)

Hsu H, Luo Z, Rand JA, An K-A. Influence of patellar thickness on patellar tracking and patellofemoral contact characteristics after total knee arthroplasty. *J Arthroplasty:* 11(1):69-80 (1996)

Hungerford DS, Kenna RV. Preliminary experience with a total knee prosthesis with porous coating used without cement. *Clin Orthop:* 176:95-107 (1983)

Hvid I. Trabecular bone strength at the knee. *Clin Orthop*: 227: 210-221 (1988)

Hvid I, Jensen J. Cancellous bone strength at the proximal human tibia. *Eng in Med.* 13: 21-5 (1984)

Hvid I, Hansen SL. Trabecular bone strength patterns at the proximal tibial ephiphysis. *J Orthop Res*: 3: 464-472 (1985)

Hvid I, Andersen K, Olesen S. Cancellous bone strength measurements with the osteopenetrometer. *Eng in med.* 13(2):73-78 (1984)

Insall JN. Presidential address to the knee society; choices and compromises in total knee arthroplasty. *Clin Orthop:* 226:43-48 (1988)

Insall JN. Knee arthroplasty: then, now and tomorrow. *Orthopaedics:* 18(9):889-892 (1995)

Insall JN. Extensor mechanism complications. *Orthopaedics:* 19(9):809-811 (1996)

Insall JN, Dethmers DA. Revision of total knee arthroplasty. *Clin Orthop:* 170:123-129 (1982)

Insall JN, Tria AJ, Scott N. The Total Condylar knee prosthesis: the first five years. *Clin Orthop:* 145:68-77 (1979)

Insall JN, Bnazzi R, Soudry M, Mestriner LA. Total knee arthroplasty. *Clin Orthop:* 192:13-22 (1985)

Incavo SJ, Ronchetti PJ, Howe JG, Tranowski JP. Tibial plateau coverage in total knee arthroplasty. *Clin Orthop:* 299:81-85 (1994)

Jahan MS, Thomas DE, Trieu HH, Haggard WO, Conta RL, Parr JE. Investigation of free radicals in shelf aged polyethylene tibial components. *Fifth World Biomaterials Congress* I:298, (1996)

Jeffery RS, Orton MA, Denham RA. Wedged tibial components for total knee arthroplasty. *J Arthroplasty:* 9(4):381-387 (1994)

Johnson DP, Eastwood DM. Lateral Patellar release in knee arthroplasty: effect on wound healing. *J Arthroplasty:* 7 Supplement:427-431 (1992)

Johnson R, Walker CR, Harvey IA, Barry GK, Elloy MA. Five to eight year results of the Johnson-Elloy (Accord) total knee arthroplasty. *J Arthroplasty:* 8(1):27-32 (1993)

Kavolus CH, Ritter MA, Keating EM, Faris PM. Survivorship of cementless total knee arthroplasty without tibial plateau screw fixation. *Clin Orthop:* 273:170-176 (1991)

Khaw FM, Kirk LMG, Gregg PJ. Eleven–year survival analysis of cemented PFC total knee arthroplasty. *Proc International Conference on Knee Replacements 1974-2024,* Institution of Mechanical Engineers, UK, 34-36 (1999)

Kilner T, Laanemae WM, Pilliar R, Weatherly GC, MacEwan SR. Static mechanical properties of cast and sinter-annealed cobalt-chromium surgical implants. *J Mat Sci:* 21:1349-1356 (1986)

Kitsugi T, Gustilo RB, Bechtold JE. Results of nonmetal-backed high-density polyethylene biconvex patellar prosthesis: a 5-7 follow-up evaluation. *J Arthroplasty:* 9(2):151-162 (1994)

Knight JL, Gorai PA, Atwater RD, Grothaus L. Tibial polyethylene failure after Porous Coated Anatomic total knee arthroplasty. *J Arthroplasty:* 10(6):748-757 (1995)

Knutson K, Lindstrand A, Lidgren L. Survival of knee arthroplasties: a nationwide multicentre investigation of 8000 cases. *J Bone Joint Surg:* 68B(5):795-803 (1986)

Koeneman JB, Johnson RH, Weinstein AM, Dupont JA. Failure of metal tibial trays. *Trans 12th meeting Society Biomaterials*, 146 (1986)

Kraemer WJ, Harrington IJ, Hearn TC. Micromotion secondary to axial, torsional and shear loads in two models of cementless tibial components. *J Arthroplasty:* 10(2):227-235 (1995)

Kuhn JL, Goldstein SA, Choi K, London M, Feldkamp LA, Matthews LS. Comparison of thetrabecular and cortical tissue moduli from human iliac crests. *J Orthop Res*: 7(6): 876-884 (1989)

Kurtz SM, Rimnac CM, Li S, Bartel DL. A bilinear material model for UHMWPE in total joint replacements. *Trans Orthop Res Soc*, 289 (1994)

Kuster MS, Wood GA, Stachowiak GW, Gachter A. Joint load considerations in total knee replacement. *J Bone Joint Surg*: 79B: 109-113 (1997)

Landy MM, Walker PS. Wear of Ultra High Molecular Weight Polyethylene components of 90 retrieved knee prosthesis. *J Arthroplasty:* 3 Supplement: S73-85 (1988)

Lee RW, Volz RG, Sheridan DC. The role of fixation and bone quality on the mechanical stability of tibial knee components. *Clin Orthop:* 273:177-183 (1991)

Leverant GR, Langer BS, Yuen A, Hopkins SW. Surface residual stresses, surface topography and the fatigue behaviour of Ti6Al4V. *Metallurg Trans A*: 104(2):251-257 (1979)

Levitsky KA, Harris WJ, McManus JRN, Scott RD. Total knee arthroplasty without patellar resurfacing: clinical outcomes and long-term follow-up evaluation. *Clin Orthop:* 286:116-122 (1993)

Lewis, JL, Askew MJ, Jaycox DP. A comparative evaluation of tibial component designs of total knee prosthesis. *J Bone Joint Surg:* 64A(1):129-135 (1982)

Lewis P, Rorabeck CH, Bourne RB, Devane P. Posteromedial tibial polyethylene failure in total knee replacements. *Clin Orthop:* 299:11-17 (1994)

Lewis PL, Rorabeck CH, Bourne RB. Screw osteolysis after cementless total knee replacement. *Clin Orthop:* 321:173-177 (1995)

Little RB, Wevers HW, Siu D, Cooke TDV. A three dimensional finite element analysis of the upper tibia. *J Biomech Eng*: 108: 111-119 (1986)

Liu A, Jasty M, Bragdon CR, Elder J, Biggs SA, Harris WH. Radiation damage in polyethylene acetabular components is not inevitable. *Trans Orthop Res Soc*, 21 (1996)

Long M, Rack HJ. Titanium alloys in total joint replacement – a materials science perspective. *Biomaterials:* 19(18):1621-1639 (1998)

Malkani AL, Rand JA, Bryan RS, Wallrichs SL. Total knee arthroplasty with the Kinematic condylar prosthesis: a ten year follow up study. *J Bone Joint Surg:* 77A(3): 423-431 (1995)

Maruyama M, Terayama K, Sunohara H, Adachi T, Suzuki S, Fukuzawa T. Fracture of the tibial tray following PCA knee replacement: a report of two cases. *Arch Orthop Traum Surg:* 113:330-333 (1994)

Mason MD, Ewald FC, Wright J, Thomas WH, Poss R, Sledge CB, Walker PS. 10-13 year review of a non-constrained cruciate retaining total knee. *Orthopaedic Proc:* 17:1091 (1994)

McPherson EJ, Vince KG. Breakage of a total condylar III knee prosthesis: a case report. *J Arthroplasty:* 8(5):561-563 (1993)

Mendes DG, Brandon D, Galor L, Roffman M. Breakage of the metal tray in total knee replacement. *Orthopaedics:* 7(5):860-862 (1984)

Mente PL, Lewis JL. Elastic modulus of calcified cartilage is an order of magnitude less than that of subchondral bone. *J Orthop Res:*12(5): 637-647 (1994)

Messersmith PB, Cooke FW. Stress enhancement and fatigue susceptibility of porous coated Ti6Al4V implants: an elastic analysis. *J Biomed Mater Res:* 24:591-604 (1990)

Miller J. Fixation in total knee arthroplasty. In: Insall JN (Ed.), *Surgery of the Knee.* Churchill Livingstone, chapter 22, p717- (1984)

Miura H, Whiteside L, Easley JC, Amador DD. Effects of screws and a sleeve on initial fixation in uncemented total knee tibial components. *Clin Orthop:* 226:49-64 (1990)

Moran CG, Pinder IM, Lees TA, Midwinter MJ. Survivorship analysis of the uncemented porous coated anatomic knee replacement. *J Bone Joint Surg:* 73A(6):848-857 (1991)

Moreland JR. Mechanisms of failure in total knee arthroplasty. *Clin Orthop:* 226:49-64 (1988)

Morrey BF, Chao EYS. Fracture of the porous-coated metal tray of a biologically fixed knee prosthesis: report of a case. *Clin Orthop:* 228:182-189 (1988)

Morrison JB. Function of the knee joint in various activities. *Biomed Eng:* 4: 573-580 (1969)

Morrison JB. The mechanics of the knee joint in relation to normal walking. *J Biomech*: 3: 51-61 (1970)

Murase K, Crowinshield RD, Pedersen DR, Chang T. An analysis of tibial component design in total knee arthroplasty. *J Biomech:* 16:13-22 (1982)

Nafei A, Kristensen O, Knudsen HM, Hvid I, Jensen J. Survivorship analysis of cemented Total Condylar knee arthroplasty. *J Arthroplasty:* 11(1):7-10 (1996)

Nagamine R, Whiteside L, Otani T, White SE, McCarthy DS. Effect of medial displacement of the tibial tubercle on patellar position after rotational malposition of the femoral component in total knee arthroplasty. *J Arthroplasty:* 11(1):104-110 (1996)

Nelissen RG, Brand R, Rozing PM. Survivorship analysis in Total Condylar knee arthroplasty. *J Bone Joint Surg:* 74A(3):383-389 (1992)

Nissan M. Review of some basic assumptions in knee biomechanics. *J Biomech*: 13: 375-381 (1980)

Oonishi H, Yamamoto M, Ishimaru H, Tsuji E, Kushitani S, Aono M, Ukon Y. The effect of hydroxyapatite coating on bone growth into porous titanium alloy implants. *J Bone Joint Surg:* 71B(2):213-221 (1989)

Paganelli JV, Skinner HB, Mote CD. Prediction of fatigue failure of a total knee replacement tibial plateau using finite element analysis. *Orthopaedics:* 11(8):1161-1167 (1988)

Pagnano MW, Trousdale RT, Rand JA. Tibial wedge augmentation for bone deficiency in total knee arthroplasty. *Clin Orthop:* 321:151-155 (1995)

Parton VZ. *Fracture mechanics from theory to practice.* Gordon and Breach Science Publishers, (1982)

Paul JP. Strength requirements for internal and external prostheses. *J Biomechanics:* 32(4):381-393 (1997)

Picetti GD, McGann WA, Welch RB. The patellofemoral joint after total knee arthroplasty without patellar resurfacing. *J Bone Joint Surg:* 72A(9):1379-1382 (1990)

Pilliar RM. Powder metal-made orthopaedic implants with porous surface for fixation by tissue ingrowth. *Clin Orthop:* 176:42-51 (1983)

Polineni UK, Wang A, Essner A, Sun DC, Stark C, Dumbleton JH. Effect of gamma–irradiation induced oxidation and crosslinking on the wear performance of UHMWPE acetabular cups. *Symposium on characterization and properties of Ultra High Molecular Weight Polyethlyene (UHMWPE)* sponsored by ASTM Committee F-4 on Medical and Surgical Materials and Devices, New Orleans, (1996)

Polyzoides J. Brooks S, Tsakonas A, Tuke M. Design characteristics, experimental work and ten year clinical experience with a fully conforming mobile bearing knee prosthesis. *Proc International Conference on Knee Replacements 1974-2024,* Institution of Mechanical Engineers, UK, 47-49 (1999)

Rakotomanana RL, Leyvraz PF, Curnier A, Heegaard JH, Rubin PJ. A finite element model for evaluation of tibial prosthesis-bone interface in total knee replacement. *J Biomech*: 25(12):1413-1424 (1992)

Rakotomanana RL, Leyvraz PF, Curnier A, Meister JJ, Livio JJ. Comparison of tibial fixations in total knee arthroplasty: an evaluation of stress distribution and interface micromotions. *The Knee*: 1: 91-99 (1994)

Rand JA. Augmentation of a total knee arthroplasty with a modular metal wedge. *J Bone Joint Surg:* 77A(2):266-268 (1995)

Ranawat CS, Johanson NA, Rimnac CM, Wright TM, Schwartz RE. Retrieval analysis of porous-coated components for total knee arthroplasty: a report of two cases. *Clin Orthop:* 209:244-248 (1986)

Ranawat CS, Flynn WF, Saddler S, Hansraj KK, Maynard MJ. Long-term results of the Total Condylar knee arthroplasty: a 15 year survivorship study. *Clin Orthop:* 286:94-102 (1993)

Regner L, Carlsson L, Karrholm J, Herberts P. Ceramic coating improves tibial component fixation in total knee arthroplasty. *J Arthroplasty:* 13(8):882-889 (1998)

Rhoads DD, Noble PC, Reuben JD, Mahoney OM, Tullos HS. The effect of femoral component position on patellar tracking after total knee arthroplasty. *Clin Orthop:* 260:43-51 (1990)

Ries M, Rose R, Greer J, Weaver K, Sauer W, Beals N. Sterilisation induced effects on UHMWPE performance properties. *Trans Orthop Res Soc*, 757 (1995)

Ritter MA, Worland R, Saliski J, Helphenstine JV, Edmondson KL, Keating EM, Faris PM, Meding JB. Flat-on-flat, nonconstrained, compression molded polyethylene total knee replacement. *Clin Orthop:* 321:79-85 (1995)

Rorabeck CH. Mechanisms of knee implant failure. *Orthopaedics:* 18(9):915-918 (1995)

Rostoker W, Chao EYS, Galante JO. Defects in failed stems of hip prostheses. *J Biomedical Mater Res:* 12:635-651 (1978)

Rubash HE, Berger RA, Britton CA, Nettrour WS, Seel MJ. Avoiding neurologic and vascular injuries with screw fixation of the tibial component in total knee arthroplasty. *Clin Orthop:* 286:56-63 (1993)

Ryan SD, Williams JL. Tensile testing of rodlike trabeculae excised from bovine femoral bone. *J Biomech*: 22(4): 351-5 (1989)

Sathasivam S, Walker PS. A computer model with surface friction for the prediction of total knee kinematics. *J Biomech*: 30(2): 177-184 (1997)

Schai PA, Thornhill TS, Scott RD. Total knee arthroplasty with the PFC system: results at a minimum of ten years and survivorship analysis. *J Bone Joint Surg:* 80B(5):850-858 (1998)

Scott RD. Bone loss: prosthetic and augmentation methods. *Orthopaedics:* 18(9): 923-926 (1995)

Scott RD, Ewald FC, Walker PS. Fracture of the metal tray following total knee replacement. *J Bone Joint Surg:* 66A(5):780-782 (1984)

Scott CE, Heiner J, Worzola FJ, Vanderby R. Condylar failure of the Lacey rotating-hinge total knee. *J Arthroplasty:* 11(2):214-216 (1996)

Scuderi GR, Insall JN, Windsor RE, Moran MC. Survivorship of cemented knee replacements. *J Bone Joint Surg:* 71B(5):798-803 (1989)

Shaw JA, Murray DG. Knee joint simulator. *Clin Orthop:* 94:15-23 (1973)

Shoji H, Shimozaki E. Patellar clunk syndrome in total knee arthroplasty without patellar resurfacing. *J Arthroplasty:* 11(2):198-201 (1996)

Silverton C, Rosenberg AO, Barden RM, Sheintop MB, Galante JO. The prosthesis-bone interface adjacent to tibial components inserted without cement. *J Bone Joint Surg:* 78A(3):340-347 (1996)

Skinner HB, Mabey MF, Pagannelli JV, Meagher JM. Failure analysis of PCA revision total knee replacement tibial component: a preliminary study using the finite element method. *Orthopaedics:* 10:581-584 (1987)

Skolnick ND, Coventry MB, Ilstrup DM. Geometric total knee arthroplasty: a two year follow-up study. *J Bone Joint Surg:* 58A(6):749–753 (1976)

Soudry M, Mestrimer LA, Binazzi R, Insall JN. Total knee arthroplasty without patella resurfacing. *Clin Orthop:* 205: 166-170, (1986)

Steinbrink K. Long term results of the hinged prosthesis (two decades of Endo-Klinik experience). *Proceedings of the International Conference on Knee Replacements 1974-2024,* Institution of Mechanical Engineers, UK, 47-49 (1999)

Stubbington CA, Bowen AW. Improvements in the fatigue strength of Ti6Al4V through microstructure control. *J Mat Sci:* 9:941-947 (1974)

Stulberg SD. Extensor Mechanism complications after total knee arthroplasty. *Orthopaedics:* 18(9):919-920 (1995)

Sun DC, Stark C, Dumbleton JH. Development of an accelerated aging method for evaluation of long term irradiation effects on UHMWPE implants. *Polymer preprints*: 35(2):960-970 (1994)

Taylor M, Tanner KE, Freeman MAR. Finite element analysis of the implanted proximal tibia: a relationship between the initial cancellous bone stresses and implant migration. *J Biomech*: 31:303-310 (1998)

Taylor SJG, Walker PS, Perry J, Cannon SR, Woledge R. The forces in the distal femur and the knee during walking and other activities measured by telemetry. *J Arthroplasty:*13(4); 428-437 (1998a)

Townley CO. Total knee arthroplasty: a personal retrospective and prospective review. *Clin Orthop:* 236:8-22 (1988)

Townsend PR, Rose RM, Radin EL. Buckling studies of single human trabeculae. *J Biomech*: 8(4):199-201 (1975)

Trieu HH, Paxson RD. The oxidized surface layer in shelf-aged UHMWPE tibial inserts. *Trans Orthop Res Soc*, 758 (1995)

Trieu HH, Buchanan DJ, Needham DA, Rouleau JP, Morris LH, Haggard WO, Parr JE. Accelerated fatigue wear of gamma sterilized UHMWPE tibial components. *Trans Europ Orthop Res Soc* 106, 1997

Tsao A, Mintz L, McRae CR, Stulberg SD, Wright T. Failure of the Porous Coated Anatomic prosthesis in total knee arthroplasty due to severe polyethylene wear. *J Bone Joint Surg:* 75A(1):19-26 (1993)

Uematsu O, Hsu HP, Kelley KM, Ewald FC, Walker PS. Radiologic study of Kinematic total knee arthroplasty. *J Arthroplasty*: 2(4):317-326 (1987)

Unwin PS, Walker PS, Briggs TW, Cannon SR, Carter SR, Cobb J, Grimer RJ, Blunn GW. Rotating hinged, hydroxyapatite coated versus fixed hinged, uncoated distal femoral replacements. *International Symposium on Limb Salvage*, p15 (1999)

Unwin PS. The recent advancements in bone and joint implant technology. Cost-effective titanium component technology for leading edge performance. Institution of Mechanical Engineers, UK, *Seminar Publication,* 15-28, Edited by M. Ward-Close (2000)

Vasu R, Carter DR, Schurman DJ, Beaupre GS. Epiphyseal-based desgigns for tibial plateau components I. Stress analysis in the frontal plane. *J Biomech* 19(8):647-662.

Vince KG, Johnson JA, Krygier JJ, Miller JE, Chan KH. Tibial component tilting in total knee arthroplasty. *Trans Orthop Res Soc*, 360 (1986)

Volz RG, Nisbet JK, Lee RW, McMutry MG. The mechanical stability of various noncemented tibial components. *Clin Orthop:* 226:38-42 (1988)

Walker PS. Preclinical prediction of failure modes in total knee replacement. *SERC, IMechE Conference Report "Failure of Joint Prostheses"*, 15-18 (1994)

Walker PS. Design and performance of joint replacement. In: Insall, JN, Scott WN, (eds) *Surgery of the knee.* Churchill Livingstone, New York, chapter 100, 2573-2628 (2000).

Walker PS, Blunn GW. Modern design of total knee replacement. In: *Reconstruction of the knee joint*, 129-142. Edited by: S Niwa, S Yoshino, M Kurosaka, K Shino, S Yamamoto. Springer-Verlag, Tokyo, (1997)

Walker PS, Sathasivam S. Design forms of total knee replacement. *Proc Instn Mech Engrs, Part H:* 214(1):101-119 (2000)

Walker PS, Ranawat C, Insall J. Fixation of the tibial components of condylar replacement knee prostheses. *J Biomechanics:* 9(4):269-275 (1976)

Walker PS, Greene D, Reilly D, Thatcher J, Ben-Dov M, Ewald FC. Fixation of tibial components of knee prosthesis. *J Bone Joint Surg:* 63A(2): 258-267 (1981)

Walker PS, Thatcher J, Ewald FC, Hilden J. Variables affecting the fixation of tibial components. *Eng in Med:* 11(2): 83-87 (1982)

Walker PS, Blunn GW, Perry JS, Gregson PJ. Lifetime prediction tests for the fatigue performance of knee tibial trays. *Unpublished* (1996)

Wang A, Polineni VK, Stark C, Dumbleton JH. Effect of femoral head surface roughening on the wear of unirradiated and gamma irradiated UHMWPE acetabular cups. *Trans Orthop Res Soc,* 473 (1996)

Wang A, Polineni VK, Essner A, Sun DC, Stark C, Dumbleton JH. Effect of shelf aging on the wear of UHMWPE acetabular cups: a 10 million cycle hip simulator study. *Trans Orthop Res Soc,* 139 (1997)

Wasielewski CR, Galante JO, Leighty R, Natarajan R, Rosenberg HG. Wear patterns on retrieved polyethylene tibial inserts and their relationship to technical considerations during total knee arthroplasty. *Clin Orthop:* 299:31-43 (1994)

Weaver JK, Derkash RS, Greenwald AS. Difficulties with bearing dislocation and breakage using a movable bearing total knee replacement system. *Clin Orthop:* 290: 244-252 (1993)

Weinstein AM, Clemow AJT. Cobalt-based Alloys. In: *Concise Encyclopaedia of Materials & Dental Materials*, Williams D (ed). Pergamon Press Oxford 106-112. (1990)

Weir DJ, Moran CG, Pinder IM. Kinematic condylar total knee arthroplasty: 14 year survivorship analysis of 208 consecutive cases. *J Bone Joint Surg:* 78B(6):907-911 (1996)

Werner F, Foster D, Murray DG. The influence of design on the transmission of torque across knee prostheses. *J Bone Joint Surg:* 60A(3):342-348 (1978)

Wevers HW, Simurda M, Griffin M, Tarrel J. Improved fit by asymmetric tibial prosthesis for total knee arthroplasty. *Med Engng Physics:* 16:297-300 (1994)

Whiteside LA, Fosco DR, Brooks JG. Fracture of the femoral component in cementless total knee arthroplasty. *Clin Orthop:* 286:71-77 (1993)

Whiteside LA. Four screws for fixation of the tibial component in cementless total knee arthroplasty. *Clin Orthop:* 299:72-76 (1994)

Williams IR, Mayor MB, Collier JP, Bargmann BC, Bargmann LS, Currier JH. Clinical damage in retrieved mobile bearings. *Proc International Conference on Knee Replacements 1974-2024,* Institution of Mechanical Engineers, UK, 225-228 (1999)

Wimmer IR, Nassutt R, Kunze J, Loos J, Artelt D, Schneider E, Fischer A, Tager G. Stick phenomena in metal-on-metal hip joints after resting periods. *Combined Orthopsedic Research Society*, 219 (2001)

Windsor, RE, Scuderi GR, Moran MC, Insall JN. Mechanisms of failure of the femoral and tibial components in total knee arthroplasty. *Clin Orthop:* 248:15-19 (1989)

Wixson, RL, Elasky N, Lewis J. Cancellous bone material properties in osteoarthritic and rheumatoid total kene patients. *J Orthop Res* 7:885-892 (1989)

Woods GW, Lionberger DR, Tullos HS. Failed total knee arthroplasty: revision and arthrodesis for infection and noninfectious complications. *Clin Orthop:* 173:184-190 (1983)

Wright TM, Rimnac CM, Stulberg SD, Mintz L, Tsao A, Klein RW, McCrae C. Wear of polyethylene in total joint replacements: observations from retrieved PCA knee implants. *Clin Orthop:* 276:126-134 (1992)

Yoshida K, Asada K, Sakane H. Intra-operative measurement of tibial component micromovement in total knee arthroplasty. *Micromovements in orthopaedics*, 124-139, Turner (ed) Clarendon Press, Oxford, (1993)

Yoshii I, Whiteside LA, Anouchi YS. The effect of patellar button placement and femoral component design on patellar tracking in total knee arthroplasty. *Clin Orthop:* 275:211-219 (1992a)

Yoshii I, Whiteside LA, Milliano MT, White SE. The effect of a central stem and stem length on micromovement of the tibial tray. *J Arthroplasty:* 7-Suppl:433-438 (1992b)

Zahavi E, Torbillo V. Cyclic stress-strain and plastic deformation aspects of fatigue crack growth. *Fatigue Design: Life expectancy of machine parts*. A Solomon Press Book, American Society for Testing and Materials, STP 637 (1977)

Zhuang LZ, Langer EW. Effects of the range of the stress intensity factor on the appearance of localised fatigue fracture in cast CoCrMo alloy used for surgical implants. *Mater Sci Engng:* A102: L9-L12 (1988)

Zhuang LZ, Langer EW. Observations on the faceted fatigue fracture of cast CoCrMo alloy used for surgical implants. *Metallurg Trans A:* 20A:99-103 (1989a)

Zhuang LZ, Langer EW. Study on fatigue threshold behaviour and fatigue crack propagation in a cast CoCrMo alloy used for surgical implants. *Fatigue Fracture Engineering Material Structure:* 12(4):283-293 (1989b)

Zhuang LZ, Langer EW. Determination of cyclic strain hardening behaviour produced during fatigue crack growth in cast CoCrMo alloy used for surgical implants. *Mater Sci Engng:* A108:247-252 (1989c)

Zhuang LZ, Langer EW. Effects of alloy additions on the fatigue properties of cast CoCrMo alloy used for surgical implants. *J Mats Sci:* 25:683-689 (1990)

ISO/CD 14879-1 draft standard (1997). Implants for surgery - total knee joint prostheses. Part 1: Determination of endurance properties of knee tibial trays. Secretariat, British Standards Institute, 389 Chiswick High Road, London W4 4AL.

ASTM Draft Standard - January (1997). Standard test method for cyclic fatigue testing of metal tibial tray components of total knee joint replacements.